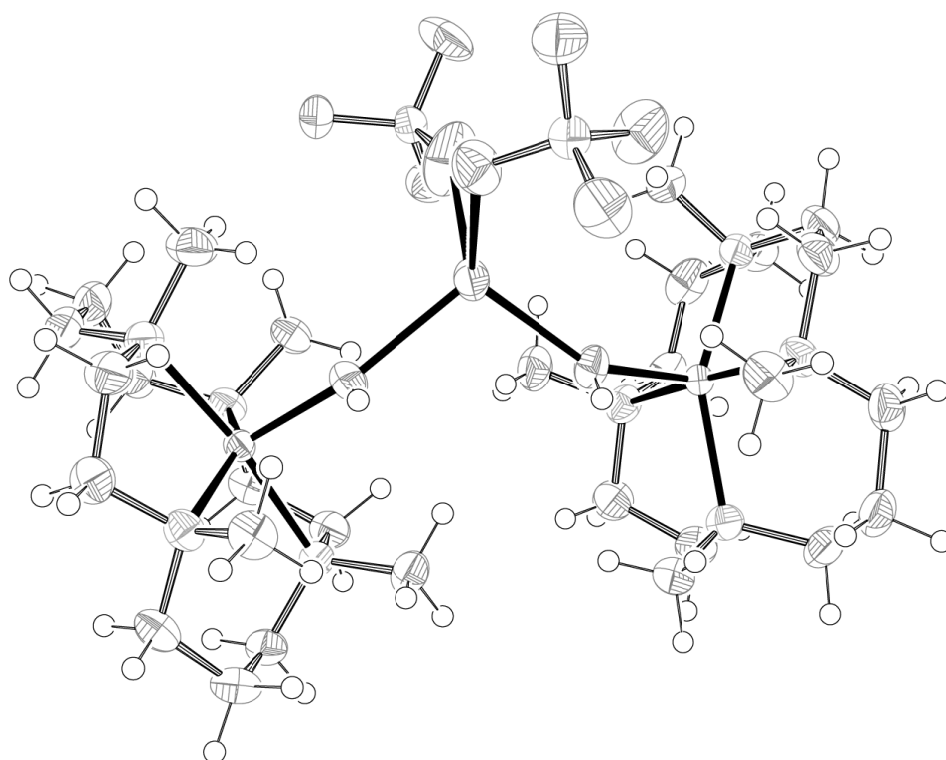




Justus-Liebig-Universität Gießen

Institut für Anorganische und
Analytische Chemie



Synthesis, Characterization and Reactivity of Nickel Complexes with N-Donor, Olefinic and Macrocyclic Ligands

Inaugural-Dissertation zur Erlangung des Doktorgrades der
Naturwissenschaften im Fachbereich Biologie und Chemie
der Justus-Liebig-Universität Gießen

von

Lars Valentin

aus

Gießen

Justus-Liebig-Universität Gießen
Fachbereich Biologie und Chemie
Institut für Anorganische und Analytische Chemie

Erstgutachter:	Prof. Dr. S. Schindler
Zweitgutachter:	Prof. Dr. R. Göttlich
Vorgelegt von:	Lars Valentin
Abgabe der Dissertation im Prüfungsamt:	30.09.2014

Eidesstattliche Erklärung

Ich erkläre hiermit, dass ich diese Dissertation selbstständig ohne Hilfe Dritter und ohne Benutzung anderer als der angegebenen Quellen und Hilfsmittel verfasst habe. Alle den benutzten Quellen wörtlich oder sinngemäß entnommenen Stellen sind als solche einzeln kenntlich gemacht.

Diese Arbeit ist bislang keiner anderen Prüfungsbehörde vorgelegt worden und auch nicht veröffentlicht worden.

Ich erkläre: Ich habe die vorgelegte Dissertation selbstständig und ohne unerlaubte fremde Hilfe und nur mit den Hilfen angefertigt, die ich in der Dissertation angegeben habe. Alle Textstellen, die wörtlich oder sinngemäß aus veröffentlichten Schriften entnommen sind, und alle Angaben, die auf mündlichen Auskünften beruhen, sind als solche kenntlich gemacht. Bei den von mir durchgeführten und in der Dissertation erwähnten Untersuchungen habe ich die Grundsätze guter wissenschaftlicher Praxis, wie sie in der „Satzung der Justus-Liebig-Universität Gießen zur Sicherung guter wissenschaftlicher Praxis“ niedergelegt sind, eingehalten.

Ich bin mir bewusst, dass eine falsche Erklärung rechtliche Folgen haben wird.

Gießen, den 30.09.2014

Lars Valentin

Danksagung

Mein erster Dank gilt Herrn Prof. Dr. Siegfried Schindler für die gegebene Möglichkeit meine Dissertation in seiner Arbeitsgruppe durchzuführen sowie für die vielseitigen wissenschaftlichen Anregungen und die stets gewährte Unterstützung während meiner Arbeit. Des Weiteren bedanke ich mich bei allen Kollegen und ehemaligen Kollegen des AK Schindler für die gute Zusammenarbeit und den stets freundschaftlichen Umgang miteinander: Dr. Alexander Beitat, Dr. Thomas Nebe, Dr. Jörg Müller, Dr. Sabrina Schäfer, Dr. Christian Würtele, Dr. Sandra Kisslinger, Dr. Jennifer Blank, Dr. Manfred Steinbach, Dr. Sabine Becker, Jonathan Becker, Janine Will, Melanie Jopp, Stefan Schaub, Tobias Hoppe, Andreas Miska, Frank Mehlich, Miriam Wern, Natascha Kempf, Cornelius Brombach, Steffen Müller, Florian Ritz und Nico Fischer.

Besonderer Dank gilt hierbei Stefan Schaub und Tobias Hoppe, die mir immer mit Rat und Tat zur Seite standen und stets eine große Unterstützung waren. Dr. Sabine Becker, Jonathan Becker und Dr. Christian Würtele danke ich für die Mühe und Hilfe bei den Einkristallmessungen.

Ebenfalls bedanke ich mich bei allen ehemaligen Kommilitonen für die gute Zusammenarbeit und Unterstützung während des gesamten Studiums, besonders bei Dr. Halit Aydin und Dr. Christoph Bachmann.

Der größte Dank gilt meiner Familie, die mich über die Jahre stets unterstützt hat und ein großer Rückhalt für mich war.

“Es spielt keine Rolle wie langsam Sie gehen, so lange Sie nicht anhalten.”

(Konfuzius)

Für meine Familie

Table of Ligands

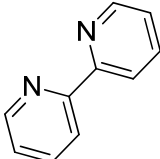
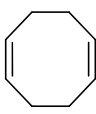
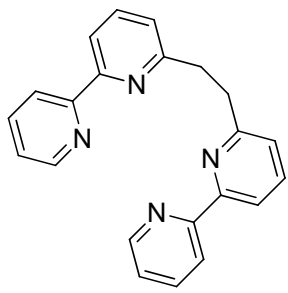
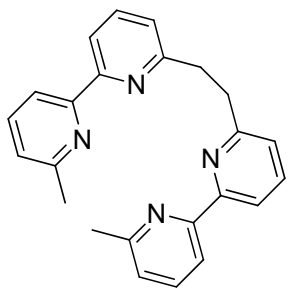
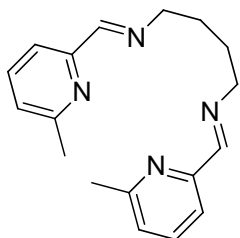
Name	Abbr./ Formula	Structure	Molar mass [g/mol]
2,2'-bipyridine	bipy $C_{10}H_8N_2$		156.2
1,5-cyclooctadiene	COD C_8H_{12}		108.2
1,2-bis(2,2'-bipyridine-6-yl)ethane	O-BPy $C_{22}H_{18}N_4$		338.4
1,2-bis(4'-methyl-2,2'-bipyridine-4-yl)ethane	Me-BPy $C_{24}H_{22}N_4$		366.5
<i>N,N'</i> -bis((6-methylpyridine-2-yl)methylene)butane-1,4-diamine	mpmbd $C_{18}H_{22}N_4$		294.4

Table of Ligands

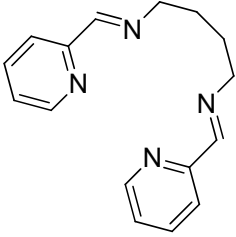
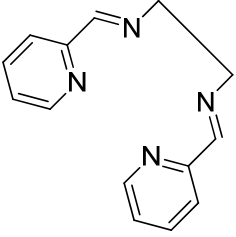
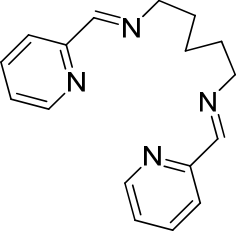
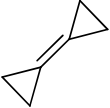
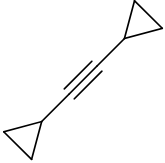
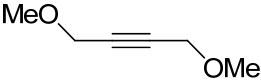
<i>N,N'</i> -bis(pyridine-2-ylmethylene)butane-1,4-diamine	pmbd C ₁₆ H ₁₈ N ₄		266.3
<i>N,N'</i> -bis(pyridine-2-ylmethylene)ethane-1,2-diamine	pmed C ₁₄ H ₁₄ N ₄		238.3
<i>N,N'</i> -bis(pyridine-2-ylmethylene)ethane-1,2-pentane	pmpd C ₁₇ H ₂₀ N ₄		280.4
bicyclopropylidene	bcp C ₆ H ₈		80.1
1,4-dicyclopropylacetylene	dcpa C ₈ H ₁₀		106.1
1,4-dimethoxy-2-butyne	dmbu C ₆ H ₁₀ O ₂		114.1

Table of Ligands

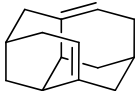
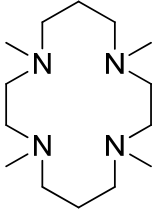
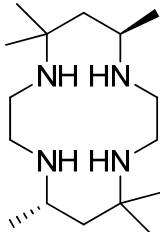
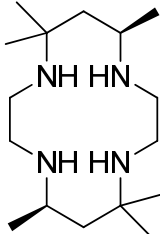
tetracyclo [7.3.1.1 ^{4,12} .0 ^{2,7}]tetradeca- 6,11-diene	tctd C ₁₄ H ₁₈		186.0
1,4,8,11-tetramethyl- 1,4,8,11- tetraazacyclotetradecane	14-tmc C ₁₄ H ₃₂ N ₄		256.4
(7 <i>S</i> ,14 <i>R</i>)-5,5,7,12,12,14- hexamethyl-1,4,8,11- tetraazacyclotetradecane	tetA C ₁₆ H ₃₆ N ₄		284.5
(7 <i>R</i> ,14 <i>R</i>)-5,5,7,12,12,14- hexamethyl-1,4,8,11- tetraazacyclotetradecane	tetB C ₁₆ H ₃₆ N ₄		284.5

Table of Abbreviations

e.g.	for example (latin: exempli gratia)
i.e.	that is (latin: id est)
IR	infrared
RT	room temperature
UV-Vis	ultraviolet and visible (light)
NMR	nuclear magnetic resonance
TMS	tetramethylsilane
d	doublet
m	multiplet
s	singlet
t	triplet
THF	tetrahydrofuran
DMF	dimethylformamide

Table of Contents

Table of Ligands.....	I
Table of Abbreviations	IV
Table of Contents.....	V
1 Introduction	1
1.1 The Element Nickel.....	1
1.2 Application.....	2
1.3 Motivation.....	3
1.4 Nickel(0)-Catalyzed Reactions.....	4
1.4.1 Cyclooligomerization of Alkenes	4
1.4.1.1 Cyclooligomerization of Cyclopropenes	4
1.4.1.2 Cyclooligomerization of 1,3-Butadiene.....	6
1.4.2 Cyclooligomerization of Alkynes	9
1.4.2.1 Cyclooligomerization of Acetylene	9
1.4.3 Carboxylation of 1,3-Dienes.....	11
1.5 Biochemistry of Nickel.....	15
1.5.1 Methyl-Coenzyme M Reductase.....	15
1.5.2 Superoxide Dismutase.....	18
1.5.3 Dioxygen Activation by Nickel	21
1.5.3.1 Ni-O _x Species with Ni(II) and Hydrogen Peroxide	21
1.5.3.2 Ni-O _x Species with Ni(0) and Dioxygen	22
1.5.3.3 Ni-O _x Species with Ni(I).....	22
1.6 Research Goals	25
a) Reactivity of Ni(0) and Cu(I) Complexes Towards Alkenes and Alkynes.....	25
b) Ni(0) and Cu(I) Complexes with the Adamantane Ligand tctd	26
c) Ni(0) and Cu(I) Complexes with the Ligand System O-BPy and Derivatives.....	26
d) Reactivity of Nickel Complexes with Macrocyclic Ligands	27

Table of Contents

2	Reactivity of Ni(0) and Cu(I) Complexes Towards Alkenes and Alkynes.	29
2.1	Introduction.....	29
2.2	Nickel (0) Complexes with bcp, dcpa and dmbu	31
2.2.1	Molecular Structures.....	32
2.2.1.1	[Ni(bipy)(bcp)].....	32
2.2.1.2	[Ni(bipy)(dcpa)].....	33
2.2.1.3	[Ni(bipy)(dmbu)]	33
2.2.2	Mechanistic Studies	34
2.2.2.1	[Ni(bipy)(bcp)].....	35
2.2.2.2	[Ni(bipy)(dcpa)].....	38
2.2.2.3	[Ni(bipy)(dmbu)]	40
2.3	Copper(I) Complexes with bcp and dcpa	46
2.3.1	Molecular Structures.....	46
2.3.1.1	[Cu(bipy)(bcp)]PF ₆	46
2.3.1.2	[Cu(bipy)(dcpa)]PF ₆	47
2.3.2	Reactivity Towards Dioxygen.....	48
2.4	Experimental	49
2.4.1	Material and Reagents.....	49
2.4.2	Kinetic Measurements.....	49
2.4.3	Synthesis of the Complexes.....	50
2.4.3.1	[Ni(COD) ₂].....	50
2.4.3.2	[Ni(bipy)(COD)]	50
2.4.3.3	[Ni(bipy)(dmbu)]	50
3	Ni(0) and Cu(I) Complexes with the Adamantane Ligand tctd.....	51
3.1	Introduction.....	51
3.2	Copper(I) Complexes with tctd	53
3.2.1	Molecular Structure of [Cu ₂ (bipy) ₂ (tctd)](PF ₆) ₂	53
3.2.2	Molecular Structure of [Cu ₂ Cl ₂ (CH ₃ CN)(tctd)]	54
3.3	Synthesis of Ni(0) Polymers with tctd.....	57
3.4	Experimental	58
3.4.1	Materials and Reagents.....	58
3.4.2	Crystallography	58
3.4.3	Synthesis of tctd	59
3.4.4	Synthesis of [Cu ₂ Cl ₂ (CH ₃ CN)(tctd)]	59

3.4.5	Synthesis of $[\text{Ni}_x(\text{tctd})_y]_n$	59
4	Ni(0) and Cu(I) Complexes with the Ligand O-BPy and Derivatives.....	61
4.1	Introduction.....	61
4.2	Results.....	66
4.2.1	Ligands	67
4.2.1.1	O-BPy.....	67
4.2.1.2	Mpmbd	69
4.2.1.3	Pmed, pmbd, pmpd	72
4.2.1.4	Me-BPy	74
4.2.2	Ni(0) Complexes	75
4.2.2.1	$[\text{Ni}(\text{O-BPy})]$	75
4.2.2.2	$[\text{Ni}_2(\text{O-BPy})(\eta^2\text{-C}_4\text{H}_6)_2]$	78
4.2.2.3	$[\text{Ni}(\text{pmbd})]$	78
4.2.2.4	$[\text{Ni}(\text{mpmbd})]$	81
4.2.2.5	$[\text{Ni}(\text{pmed})]$ and $[\text{Ni}(\text{pmpd})]$	84
4.2.2.6	$[\text{Ni}(\text{Me-BPy})]$	84
4.2.3	Cu(I) Complexes with O-BPy and Derivatives.....	84
4.2.3.1	$[\text{Cu}(\text{COD})_2]^+$	86
4.2.3.2	$[\text{Cu}_2(\text{O-BPy})_2]^{2+}$	88
4.2.3.3	$[\text{Cu}(\text{O-BPy})]^{2+}$	91
4.2.3.4	$[\text{Cu}_2(\text{O-BPy})(\text{COD})_2](\text{SO}_3\text{CF}_3)_2$	93
4.2.3.5	$[\text{Cu}_2(\text{O-BPy})(\text{C}_4\text{H}_6)_2](\text{SO}_3\text{CF}_3)_2$	96
4.2.4	UV-Vis Spectroscopy	98
4.2.4.1	$[\text{Ni}(\text{O-BPy})]$ vs. $[\text{Ni}_2(\text{O-BPy})(\eta^2\text{-C}_4\text{H}_6)_2]$	98
4.2.4.2	$[\text{Ni}(\text{pmbd})]$	100
4.2.4.3	$[\text{Ni}(\text{mpmbd})]$	101
4.2.4.4	$[\text{Ni}(\text{pmed})]$	102
4.2.4.5	$[\text{Ni}(\text{pmpd})]$	103
4.2.4.6	$[\text{Ni}(\text{Me-BPy})]$	104
4.3	Experimental	105
4.3.1	Materials and Reagents.....	105
4.3.2	Crystallography	105
4.3.3	NMR Spectroscopy	105
4.3.4	UV-Vis Spectroscopy	105

Table of Contents

4.3.5	IR Spectroscopy	106
4.3.6	Synthesis of the Ligands	106
4.3.6.1	O-BPy.....	106
4.3.6.2	Me-BPy	106
4.3.6.3	Mpmbd, pmbd, pmed, pmpd	106
4.3.7	Synthesis of the Ni(0) Complexes	107
4.3.7.1	[Ni(COD) ₂].....	107
4.3.7.2	[Ni(O-BPy)]	107
4.3.7.3	[Ni ₂ (O-BPy)(η^2 -C ₄ H ₆) ₂]	108
4.3.7.4	[Ni(pmbd)]	108
4.3.7.5	[Ni(mpmbd)]	108
4.3.7.6	[Ni(pmed)]	108
4.3.7.7	[Ni(pmpd)].....	109
4.3.7.8	[Ni(Me-BPy)]	109
4.3.8	Synthesis of the Cu(I) Complexes	109
4.3.9	[Cu(COD) ₂] ⁺	109
4.3.9.1	[Cu ₂ (O-BPy) ₂](BF ₄) ₂	109
4.3.9.2	[Cu(O-BPy)](BF ₄) ₂	110
4.3.9.3	[Cu ₂ (O-BPy)(COD) ₂](SO ₃ CF ₃) ₂	110
4.3.9.4	[Cu ₂ (O-BPy)(C ₄ H ₆) ₂](SO ₃ CF ₃) ₂	110
5	Reactivity of Nickel Complexes with Macrocyclic Ligands.....	111
5.1	Introduction.....	111
5.2	Results.....	114
5.2.1	Synthesis and Reactions of Nickel Complexes bearing 14-tmc.....	114
5.2.1.1	Ligand 14-tmc.....	114
5.2.1.2	Synthesis of [Ni(14-tmc)] ²⁺	115
5.2.1.3	Synthesis of [Ni(14-tmc)]ClO ₄	120
5.2.1.4	Reaction of [Ni(14-tmc)]ClO ₄ with Nitrous Oxide	120
5.2.1.5	[Na(14-tmc)]ClO ₄	121
5.2.1.6	[Ni(14-tmc)(OH)]ClO ₄	124
5.2.1.7	Reaction of [Ni(14-tmc)]SO ₃ CF ₃ and Nitrous Oxide	129
5.2.1.8	Reaction of [Ni(14-tmc)] ²⁺ with Peroxides and Superoxides.....	131

Table of Contents

5.2.2	Synthesis and Reactions of Nickel Complexes bearing tetB.....	135
5.2.2.1	Ligand tetB	135
5.2.2.2	[Ni(tetB)](ClO ₄) ₂	137
5.3	Experimental	142
5.3.1	Materials and Reagents.....	142
5.3.2	Crystallography	142
5.3.3	NMR Spectroscopy	142
5.3.4	UV-Vis Spectroscopy	143
5.3.5	IR Spectroscopy	143
5.3.6	Synthesis of the Ligands	143
5.3.6.1	14-tmc.....	143
5.3.7	Synthesis of the Nickel Complexes	144
5.3.7.1	[Ni(14-tmc)] ²⁺	144
5.3.7.2	[Ni(tetB)](ClO ₄) ₂	144
5.3.7.3	[Ni(14-tmc)] ⁺	144
5.3.7.4	Reaction of [Ni(14-tmc)] ⁺ and Nitrous Oxide	144
5.3.7.5	Reaction of [Ni(14-tmc)](ClO ₄) ₂ and H ₂ O ₂	145
5.3.7.6	Reaction of [Ni(tetB)](ClO ₄) ₂ and H ₂ O ₂ /Et ₃ N	145
5.3.7.7	Reaction of [Ni(14-tmc)](ClO ₄) ₂ /[Ni(tetB)](ClO ₄) ₂ and Na ₂ O ₂	145
5.3.7.8	Reaction of [Ni(tetB)](ClO ₄) ₂ and KO ₂	145
6	Summary/Zusammenfassung.....	147
6.1	Summary	147
6.2	Zusammenfassung.....	153
7	List of Figures	161
8	List of Tables	171
9	Bibliography.....	173
A.	Curriculum Vitae	187

1 Introduction

1.1 The Element Nickel

The metal nickel has already been used 1700 - 1400 b. C. as a component of new silver or cupronickel which are alloys mainly consisting of copper, nickel and traces of other transition metals. Chinese used new silver to manufacture articles of daily use as well as ancient Greeks who were the first to use cupronickel in the production of their coins. Thereby, an amount of $\geq 15\%$ of nickel is already sufficient to give the alloy its silver color. Nickel salts were also used later on in the middle ages for dyeing glasses green. The name nickel originates from medieval miners who tried to extract copper from niccolite, a red mineral resembling copper-ore but consisting of nickel and arsenic. They blamed a mischievous spirit, Nickel for enchanting the copper and named it "Kupfernickel" (false copper).

In 1751 nickel was finally discovered by the Swedish mineralogist and chemist Baron Axel Fredrik Cronstedt. Attempting to extract copper from the found mineral he instead obtained a white colored metal with completely different properties and named it after the spirit. 1775 the pure metal could be isolated and further characterized by Torbern Bergman.[1, 2]

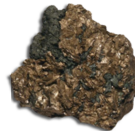
Native nickel is rarely found on Earth's surface due to its reactivity towards oxygen. Its abundance in Earth's crust is about 0.01 %. Most of the native nickel is found in combination with iron because of nickel-iron meteorites that contain 5-25 % nickel. The most important ores are garnierite, niccolite, millerite, pentlandite and nickelskutterudite (see Figure 1.1). Here, nickel mainly occurs in combination with arsenic and sulfur. The biggest production sites are in Canada and Russia.



Garnierite
 $\text{NiMg}(\text{SiO}_4)_x$



Niccolite
 NiAs



Millerite
 NiS



Pentlandite
 $(\text{Ni}, \text{Fe})_9\text{S}_8$



Nickelskutterudite
 $(\text{Ni}, \text{Fe}, \text{Co})\text{As}_3$

There are several procedures to purify nickel, mainly roasting, which are adapted to the respective ore. The most known technique to obtain highly pure nickel is the Mond process (see Figure 1.2).

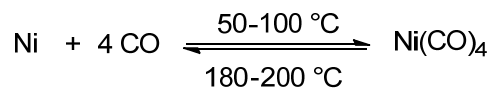


Figure 1.2: Equation for the Mond process.

It was developed in 1890 by the chemist Ludwig Mond and is based on the reversible formation of tetracarbonylnickel(0) which was also the first isolated metal carbonyl complex. Thereby, reduced impure nickel is reacting with carbon monoxide at 50-100 °C to form the volatile carbonyl complex which can be subsequently decomposed on heating to 180-200 °C to give nickel metal with a purity of 99.9 %.[4] This unique reaction is utilized even today as the industrial refining method of metallic nickel.

1.2 Application

Nickel is a hard and corrosion resistant metal and therefore has various applications in metallurgy, coinage or batteries. The biggest part of the global nickel production (about 2 million tons in 2012) is used for making nickel steels, non-ferrous alloys and electroplating.[5] Besides these applications, the metallic properties of nickel make it interesting for chemical catalysis. About 70 % of all industrial chemicals have involved the use of a catalyst at some point during their manufacturing process which highlights the paramount importance of catalysis in chemistry.[6] In general, catalysts can be heterogeneous or homogeneous. In heterogeneous catalysis the phase of the catalyst differs from that of the reactants during the chemical reaction. Most of the time these catalysts are solids which act on substrates in a liquid or gaseous reaction mixture and accelerate the reaction. Thereby, the surface area of the catalyst is critical since it determines the availability of catalytic sites. A common approach to maximize the surface area is to use catalyst supports to which the catalysts are affixed. With the help of this technique surface areas can be enlarged, e. g. some mesoporous silicates have surface areas of 1000 m²/g. The big advantage of heterogeneous

1.3 Motivation

catalysis is the fact that the catalyst can be separated and recovered from the reaction mixture easily which is an important consideration for industrial manufacturing processes.[4]

In homogenous catalysis the catalyst is in the same phase as the substrate during the reaction. Because of the wide use of organometallic compounds, homogeneous catalysis is also the success story of organometallic chemistry. Due to usually milder reaction conditions, such as lower reaction temperatures and pressures as well as higher yields and selectivity, homogeneous catalysis has many advantages compared to heterogeneous catalysis. The far better mechanistic understanding of the micro processes (catalytic cycles) allows the possibility of influencing both steric and electronic properties of the defined catalysts. Thus, it is possible to tailor optimized catalysts to the particular problem involved, by adapting their chemical and structural basis.[7] However, a disadvantage of homogeneous catalysis is the complicated and expensive recycling of the catalyst due to the fact that all components are in the same phase.

Only since the 1950s homogeneous catalysis has been established as a field of organometallic chemistry thanks to discoveries of Roelen, Ziegler, Natta et al.[7] The discovery of the Reppe-catalyst in 1940 and of nickelocene in 1953 finally triggered the enormous commercial and industrial interest in the organometallic chemistry of nickel.[8]

1.3 Motivation

The most common metals used in homogeneous catalysis are palladium and platinum. Besides these two metals nickel also shows a wide variety of organometallic compounds which makes it so interesting for catalysis. Furthermore, nickel has a much higher production with about 2 million tons per year and is about ten to fifty times cheaper than palladium and platinum. This leads to the endeavor replacing palladium and platinum catalysts with nickel. Today many organic syntheses can only be carried out with high yields by the use of organic nickel compounds.[9–11] A great amount of catalysts are Ni(0) complexes which are highly sensitive towards oxygen but the current state of chemical technology allows successful handling of these complexes.[7, 10, 11]

1.4 Nickel(0)-Catalyzed Reactions

In the following, Ni(0) complexes and their catalytic properties concerning cyclooligomerization of alkenes and alkynes as well as the fixation of carbon dioxide, an inexhaustible and cheap resource, in form of carboxylation of 1,3-dienes will be described briefly.[8, 12, 13]

1.4.1 Cyclooligomerization of Alkenes

Nickel-catalyzed cyclooligomerization reactions of alkenes and alkynes are cornerstones of the organic chemistry of transition metals and have been first discovered by Reppe et al. in the late 1940s. Even today they belong to the most studied reactions. In cyclooligomerization reactions strained molecules such as cyclopropenes, methylenecyclopropanes or norbornadiene are often used as reactive substrates. Thereby, either weakened carbon-carbon π -bonds, as in the case of many cyclooligomerization and cycloisomerization reactions, or strained carbon-carbon bonds are cleaved to obtain new carbon-carbon σ -bonds. Unstrained alkenes usually form mainly linear oligomers in the presence of nickel catalysts.[9]

1.4.1.1 Cyclooligomerization of Cyclopropenes

Cyclopropenes are highly strained carbocyclic compounds with strain energies up to $54.5 \text{ kcal} \cdot \text{mol}^{-1}$ (cyclopropene).[16] In presence of nickel(0) catalysts cyclopropenes undergo cyclooligomerization reactions.

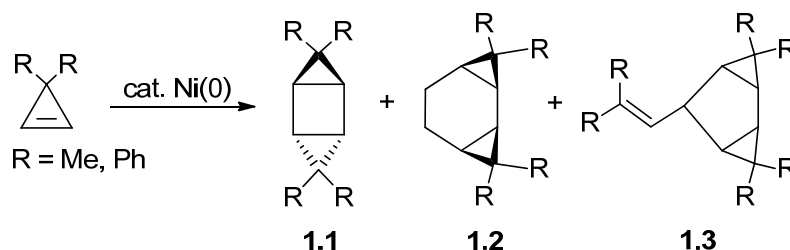


Figure 1.3: Cyclodimerization and cyclotrimerization products of cyclopropene.

As an example, the cyclodimerization and cyclotrimerization products of 3,3-dimethylcyclopropene are shown in Figure 1.3.[17, 18] The postulated cata-

1.4 Nickel(0)-Catalyzed Reactions

lytic cycle for this reaction is shown in Figure 1.4.[9] At first, the nickel(0) complex interacts with the π -bond of the cyclopropene and forms a Ni(0)- η^2 -olefin complex **1.4**. This complex reacts with another cyclopropene to a nickellacyclopentane **1.5**. Subsequently, the cyclobutane derivative **1.1** is formed by reductive elimination of **1.5** and recovery of the Ni(0) complex **1.4** as the product of the cyclodimerization (*path A*).

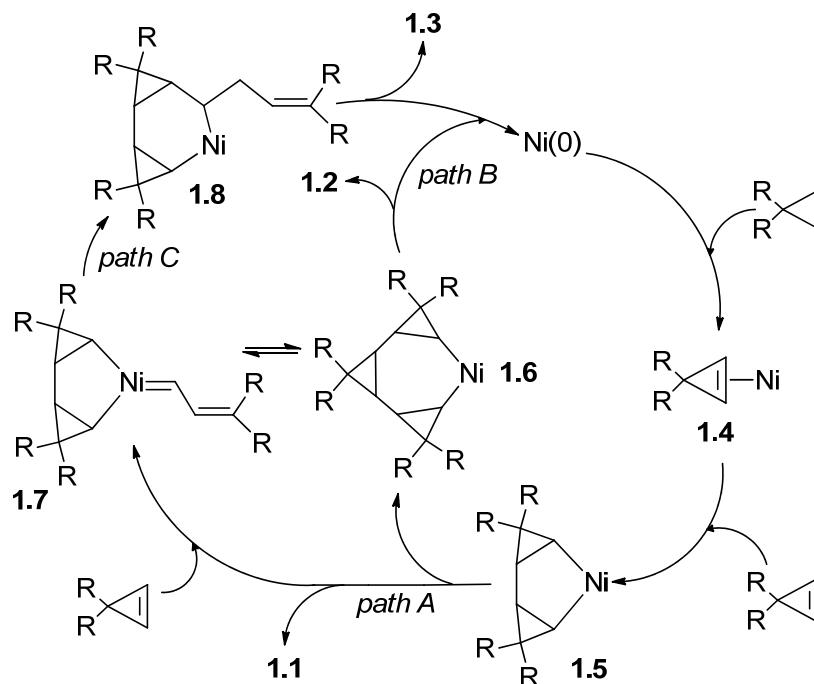


Figure 1.4: Catalytic cycle for the nickel-catalyzed cyclooligomerization of cyclopropenes.

By the insertion of another molecule of cyclopropene the seven-membered nickellacycle **1.6** is formed which undergoes reductive elimination to give the product of cyclotrimerization **1.2** (*path B*). The carbene complex **1.7** can either be formed by the reaction of **1.5** with cyclopropene or stepwise by the isomerization of **1.6**. After insertion of the carbene carbon into the Ni-C(α) bond the six-membered metallacycle **1.8** is obtained. Finally, reductive elimination of **1.8** forms the vinylcyclopentane **1.3** as the third product of the cyclooligomerization of cyclopropene. (*path C*). Bipyridyl complexes **1.9** [19, 20] and **1.10** [21, 22] which have close structural similarity to the intermediates proposed in the catalytic cycle (see Figure 1.4) could be isolated and structurally characterized by X-ray diffraction. These Ni(0) cyclopropene complexes could be obtained by the reaction of 3-tertbutyl-1-cyclopropene-1,2-dicarboxylate **1.9** and by oxidative

addition of two molecules of 3,3-Dimethylcyclopropane **1.10** with $[\text{Ni}(\text{bipy})(\text{COD})]$. The molecular structures of the complexes are shown in Figure 1.5.

Furthermore, palladium complexes are also capable of catalyzing the cyclooligomerization of cyclopropenes.[23–25]

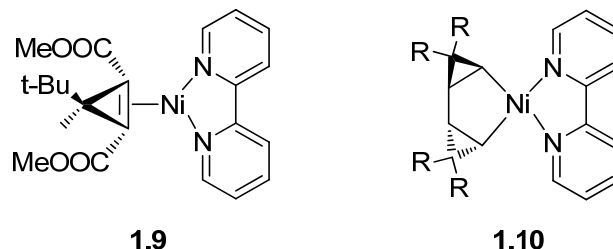


Figure 1.5: Molecular structures of analogue Ni(0) complexes of reactive intermediates proposed in Figure 1.4 determined by X-ray analysis.

1.4.1.2 Cyclooligomerization of 1,3-Butadiene

In 1954 the first nickel-catalyzed cyclodimerization and cyclotrimerization of 1,3-butadiene was reported by Reed.[26] Wilke further investigated the polymerization of 1,3-butadiene extensively by using Ziegler catalysts prepared from nickel acetylacetonate and $\text{Al}(\text{OEt})\text{Et}_2$ in 1959.[6, 27] They both obtained a mixture of products containing 4-vinylcyclohexene (VCH) **1.11**, (*E,E*)-1,5-cyclooctadiene (COD) **1.12** and (*E,E,E*)-1,5,9-cyclododecatriene (CDT) **1.13** as well as other oligomers (see Figure 1.6).[8, 26, 27]

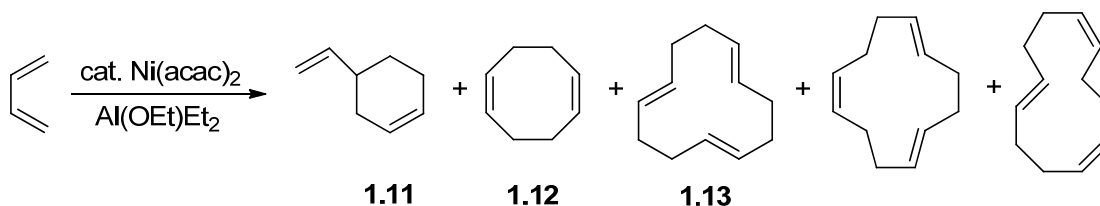


Figure 1.6: Products of the nickel-catalyzed cyclooligomerization of 1,3-butadiene.

These studies contributed to a better understanding of the reaction mechanism involved. A generally accepted mechanism for the cyclodimerization and cyclotrimerization of 1,3-butadiene is shown in Figure 1.7.[9, 27] At first, the

1.4 Nickel(0)-Catalyzed Reactions

Ni(0) species reacts with two molecules of 1,3-butadiene and forms a nickellacycle via oxidative cyclization **1.16**.

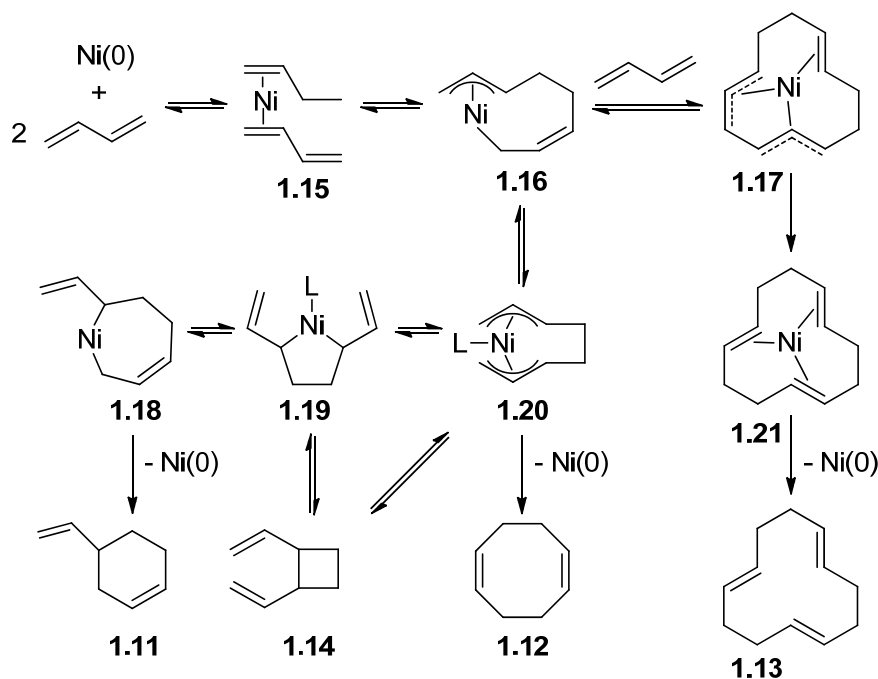


Figure 1.7: Reaction pathway of the nickel-catalyzed cyclooligomerization of 1,3-butadiene.

In presence of a phosphine ligand (R_3P), one coordination site is blocked for 1,3-butadiene and the complex isomerizes to various nickellacycles **1.18-1.20**. Subsequently, these intermediates form the cyclodimerized products **1.11**, **1.12** and **1.14** by reductive elimination. In case of a low phosphine to nickel ratio the intermediate **1.17** is formed and the cyclotrimerized product **1.13** is isolated as the major product. The intermediates **1.15-1.20** could be isolated and characterized using NMR-spectroscopy.[30–32] Detailed computational mechanistic studies have also been carried out to support the proposed mechanism.[29, 30]

Table 1.1: Reaction of 1,3-butadiene with nickel acetylacetonate and Al(OEt)Et₂; control of oligomerization using R₃P ligands. Conditions: 30 °C, 5 bar.[6]

Product	(C ₆ H ₁₁) ₃ P [%]	(Ph-C ₆ H ₄ O) ₃ P [%]	without [%]
4-Vinylcyclohexene 1.11	39.6	3.1	10
1,5-Cyclooctadiene 1.12	41.2	96.5	25
1,5,9-Cyclododecatriene 1.13	14.4	0.2	65
Higher oligomers	4.8	0.2	-

Therefore, the formation of the major products does not only depend on temperature and pressure, but on the addition of the ligand R₃P as well. The ratio of **1.11** : **1.12** : **1.13** could be varied by the addition of different R₃P ligands (see Table 1.1).[6, 35]

The nickel-catalyzed synthesis of 1,5-cyclooctadiene and 1,5,9-cyclooctadodecatriene is also of industrial interest and thus used by chemical companies, e.g. the corporation Evonik Industries.

CDT is one of the most important starting materials for cyclic and linear compounds with 12 carbon atoms. Due to its triple unsaturated character it permits a wide range of chemical reactions. It serves as a raw material in the manufacture of Polyamid-12 (VESTAMID®), which for example is used in functional elements of sport shoes and premium textiles, as well as in the manufacture of brominated flame retardants used in plastics (polystyrene).[36, 37]

COD serves as an important starting material for the synthesis of cyclic C8 compounds. It is used as a stabilizer in the manufacture of the semicrystalline rubber VESTENAMER®, as a component of catalysts in several production processes and also in the production of fragrances due to its pungent odor.[37, 38]

1.4.2 Cyclooligomerization of Alkynes

A variety of transition metals such as Ni, Co, Pd and Rh catalyze cyclooligomerization reactions of alkynes. The first nickel-catalyzed cyclotrimerization and cyclotetramerization of acetylene yielding benzene and cyclooctatetraene was discovered by Reppe.[9] This also marks the first example of a transition metal-catalyzed cyclooligomerization reaction of alkynes.

1.4.2.1 Cyclooligomerization of Acetylene

Walter Reppe and co-workers set a milestone in nickel organic chemistry in 1948. They investigated nickel-catalyzed cyclooligomerization reactions of acetylene by using a mixture of $\text{Ni}(\text{CN})_2$ and CaC_2 . [39–42] The postulated reaction mechanism is shown in Figure 1.8.

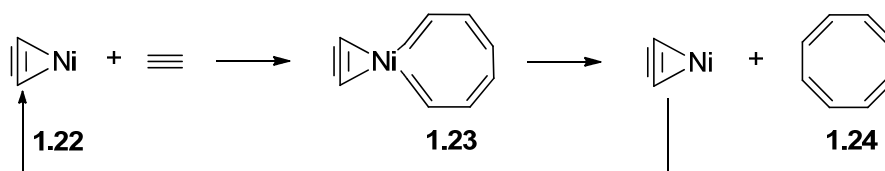


Figure 1.8: Reaction mechanism of the cyclotetramerization of acetylene; Reppe et al.

The precise mechanism was not clear so he assumed that four molecules of acetylene bind to an intermediary formed nickelacetylide **1.22** to give a nickellacyclononatetraene **1.23**. This complex further decomposes into the starting compound **1.22** and cyclooctatetraene **1.24**. [40] In the following, several research groups investigated this reaction. Wilke et al. showed that the cyclotetramerization of acetylene is catalyzed by Ni(0) complexes. [41–45] With subsequent detailed mechanistic studies by Eisch and co-workers more insight into the reaction mechanism was achieved (see Figure 1.9). [46] It could be shown that the reactive nickelacyclopentene **1.25** and nickelacyclopentene **1.26** are crucial intermediates in the cyclotrimerization as well as in the cyclotetramerization of acetylene. If the trimerization product **1.27** or the tetramerization product **1.28** is formed, depends on whether **1.26** reacts with another molecule of acetylene or if it undergoes autodimerisation.

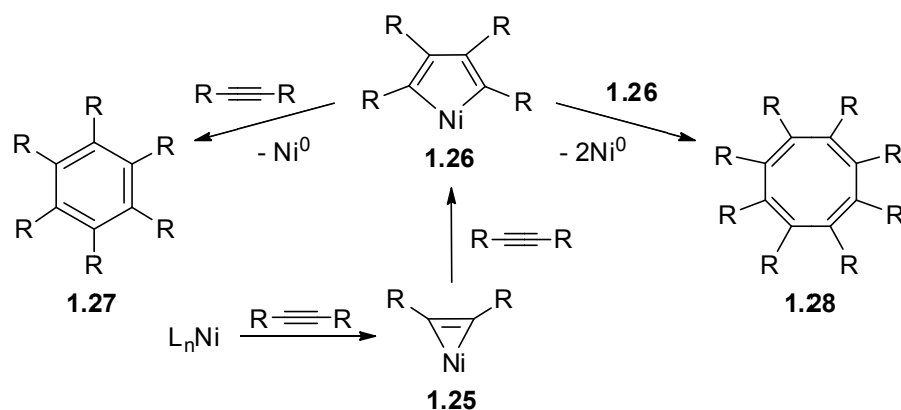


Figure 1.9: Reaction scheme for the cyclooligomerization of acetylene; Eisch et al.

A single crystal structural X-ray analysis of an isolated nickellacyclopropene complex supported the postulated mechanism by Eisch et al (see Figure 1.10).[46]

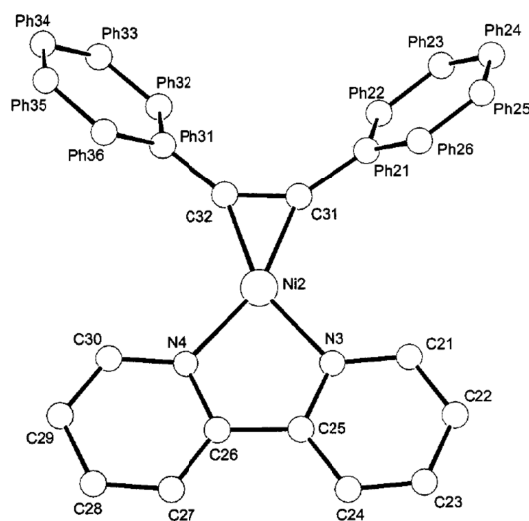


Figure 1.10: Molecular structure of 2,2-bipyridyl(η^2 -diphenylacetylene)nickel.[46]

The varying prevalence of trimerization or tetramerization depends upon the ligands L_n on nickel and the substituents R on the acetylene monomer. $Ni(0)$ complexes with electron-donating ligands tend to form benzene rings while cyclooctatetraenes are formed if weakly coordinating ligands are used.[9, 46]

1.4.3 Carboxylation of 1,3-Dienes

The fixation of carbon dioxide and its use in synthetic organic chemistry is a fascinating and important process. The growing interest of CO₂ as C1 building block relies on its low-cost, lack of toxicity, high abundance and tremendous potential as a renewable carbon source.[47]

It is well known that it can be activated by coordinating to transition metals and particularly strongly to nickel.[9] However carbon dioxide only binds in a few ways. There are two major possible coordination modes, a η^2 -side-on coordination and a η^1 -C-on coordination. A further η^1 -end-on coordination has also been proposed by calculations (see Figure 1.11).[48, 49]

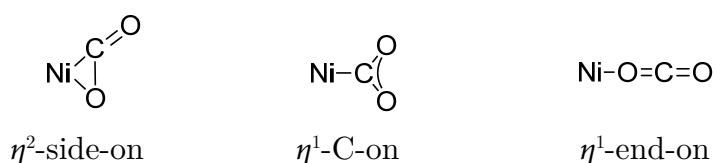


Figure 1.11: Possible coordination modes of carbon dioxide to nickel.

The first isolated and structurally characterized metal carbon dioxide complex [Ni(CO₂)(PCy₃)₂] was reported in 1975.[50] It could be obtained under very mild reaction conditions. Treatment of [Ni(PCy₃)₂] with CO₂ at room temperature in toluene afforded orange crystals of the complex with a η^2 -side-on coordinated carbon dioxide (see Figure 1.12). However, most of the characterized metal carbon dioxide complexes are too stable and not reactive towards substrates.

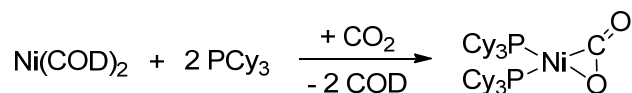


Figure 1.12: Reaction of bis(1,5-cyclooctadiene)nickel(0) with tricyclohexylphosphine and carbon dioxide.

According to this only a few catalytic reactions with carbon dioxide and transition metals are known. In general, a stoichiometric quantity of the nickel complex is required, mainly because the formed oxanickelacycle is stable. Nevertheless, many investigations have been carried out varying substrates as well as catalysts to obtain new reactions leading to the formation of C–H, C–N, C–O as

well as C–C bonds.[51–56] Especially the C–C formation is one of the most central problems of metal organic chemistry.

Electron-rich Ni(0) complexes with electron-donating ligands are reactive species which allow the reaction of carbon dioxide with unsaturated compounds, such as 1,3-dienes, to form new C–C bonds.[57–60] Oxidative coupling of the diene and CO₂ using nickel complexes provides a π -allylnickel complex which has been successfully characterized by X-ray crystallography.[57] As an example the reaction of 2,3-dimethyl-1,3-butadiene **1.29** and CO₂ using a nickel(0) complex is shown in Figure 1.13.[61, 62]

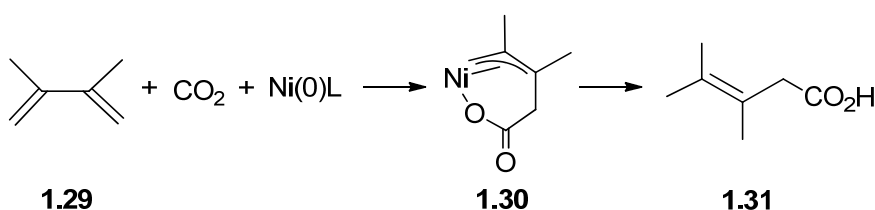


Figure 1.13: Reaction of 2,3-Dimethyl-1,3-butadiene and CO₂ using a nickel(0) complex.

Acidic treatment of the obtained π -allylnickel complex **1.30** affords 3,4-dimethyl-3-pentenoic acid **1.31**.

The reaction of 1,3-butadiene and carbon dioxide in presence of [Ni(COD)₂] and the ligand tetramethylethylenediamine (TMEDA) provides the nickelacarboxylate **1.32** which is in an equilibrium with σ -oxanickelaheptene **1.33** and σ -oxanickelacyclopentane **1.34** (see Figure 1.14).[61, 62]

Further reaction with CO₂ gives a nickeladicarboxylate complex **1.35** and treatment with MeOH/HCl affords the cis-dicarboxylic acid ester **1.36**.

1.4 Nickel(0)-Catalyzed Reactions

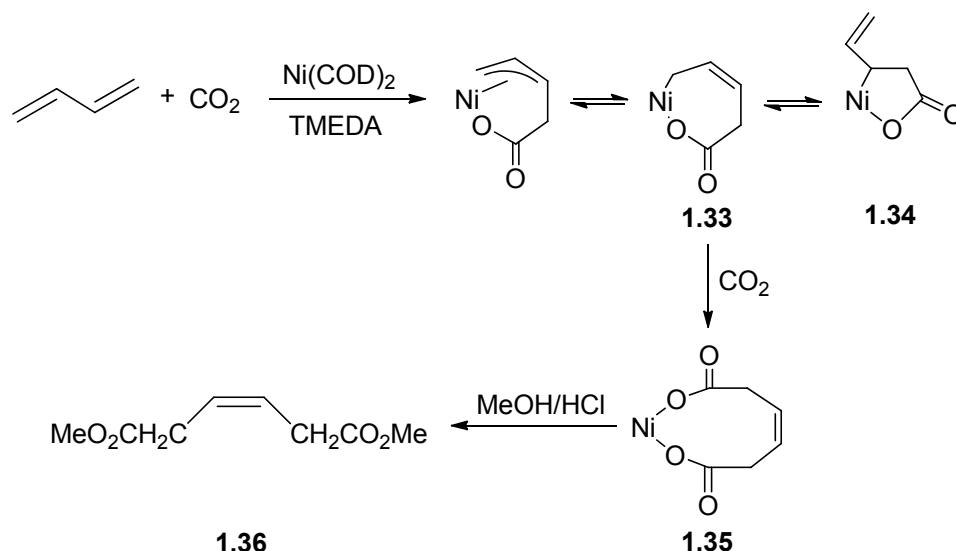


Figure 1.14: Reaction of 1,3-butadiene and CO₂ using [Ni(COD)₂]/TMEDA.

Although these reactions need a stoichiometric quantity of the nickel complex the nickelacarboxylates obtained can be used in preparative chemistry and as model complexes of catalytic reactions. However, the catalytic formation of linear carboxylic acids with butadiene and carbon dioxide using Pd complexes has already been achieved.[65] Nevertheless, there are many investigations on nickel(0)-mediated C-C coupling reactions using carbon dioxide and the cyclooligomerization of 1,3-diene and CO₂ is one of the most extensively studied transition metal-catalyzed CO₂ fixation processes.[9]

The type of ligand, monodentate or multidentate and its electronic and steric effects, as well as the solvent used, play an important role. Since multidentate ligands lead only to stoichiometric reactions a series of monodentate phosphine ligands were examined to obtain carboxylic acids catalytically.[64, 65] A functionalized cyclopentanecarboxylic acid could be obtained from the reaction of butadiene and carbon dioxide using [Ni(COD)₂] and a triisopropyl phosphite ligand (see Figure 1.15).[67] Heating a mixture of butadiene, the catalyst and the ligand in DMF to 60 °C in an autoclave affords 2-methylene-3-vinylcyclopentanecarboxylic acid **1.37** in high yield.

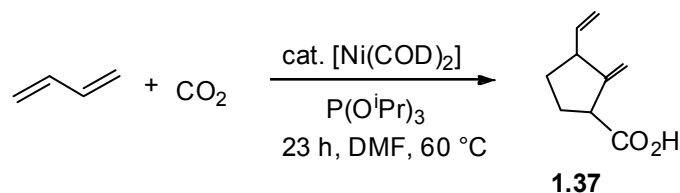


Figure 1.15: Catalytic reaction of 1,3-butadiene and CO_2 using $[\text{Ni}(\text{COD})_2]/\text{P}(\text{O}^i\text{Pr})_3$.

Under these conditions the carboxylic acid can be prepared catalytically; the achieved turnover of Ni is 30. The proposed reaction course for the catalytic cycle is shown in Figure 1.16. The catalysis is initiated by the dimerization of butadiene on the $\text{Ni}(0)\text{L}$ system to give the π -allylnickel complex **1.38**.

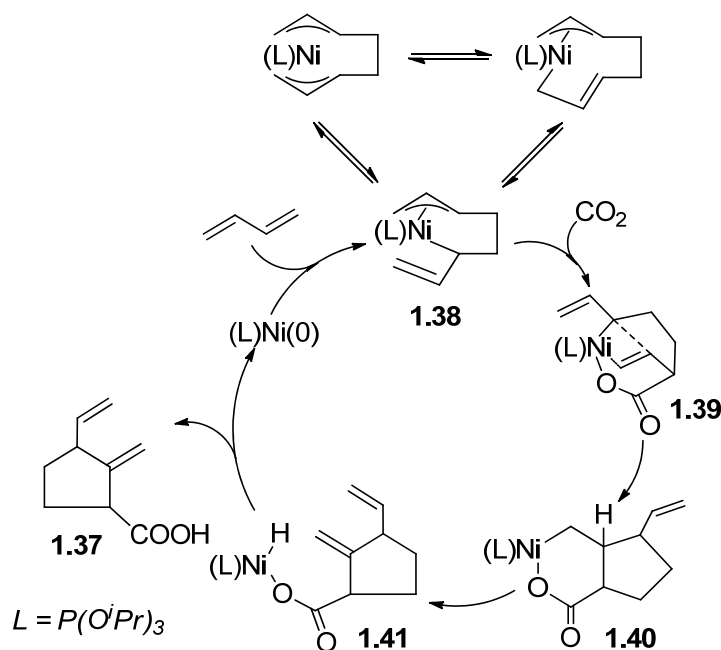


Figure 1.16: Proposed reaction course for the catalytic formation of 2-methylene-3-vinylcyclopentanecarboxylic acid.

The carbon-oxygen bond is inserted into the carbon-nickel bond **1.39** and further insertion of the double bond into the nickel-carbon bond gives **1.40**. Subsequent β -hydrogen elimination forms complex **1.41** and reductive elimination finally gives the cyclopentanecarboxylic acid **1.37** by regenerating the starting nickel(0) compound.

1.5 Biochemistry of Nickel

The biological importance of nickel has not been recognized until the discovery of nickel in the active site of jack bean urease in 1975.[68]

This can be attributed, amongst others, to the uncharacteristic light absorption of nickel(II) ions coordinated to physiologically relevant ligands. Furthermore, most of the time nickel is only part of complex, several coenzymes containing enzymes, e.g. next to Fe/S clusters in the acetyl-CoA synthase. Today several nickel-containing enzymes have been detected and isolated (see Table 1.2).

Table 1.2: Nickel-containing enzymes.

Enzyme	Source	Composition
Urease[68–70]	Plants, bacteria	2 Ni/subunit
Hydrogenases[71–74]	Bacteria	Ni, Fe/S clusters
Methyl-coenzyme M reductase [75–77]	Methanogenic bacteria	Ni tetrahydro- corphin (F430)
Acetyl-CoA synthase[78–81]	Acetogenic and meth- anogenic bacteria	Ni, Zn, Fe/S clusters
Nickel superoxide dismutase[82–85]	Bacteria	Square planar Ni(II), square pyramidal Ni(III)
Acireductone dioxygenase[86–88]	Bacteria, plants	Ni(II) or Fe(II)
Glyoxalase I[89–91]	Bacteria (e. coli)	Ni(II) or Zn(II)

In the following, the role of nickel in the methyl-coenzyme M reductase and superoxide dismutase will be described briefly.

1.5.1 Methyl-Coenzyme M Reductase

Methanogenic archaeobacteria, such as *methanobacterium thermoautotrophicum* catalyze the reaction of carbon dioxide with hydrogen to form methane and water (see Figure 1.17). This eight-electron reduction of CO₂ gains amounts in

free energy up to 130 kJ/mol.[92] The reduction of the C1-unit is carried out in a stepwise manner, i.e. the substrate is transferred from one cofactor/enzyme to the next in course of the reaction.

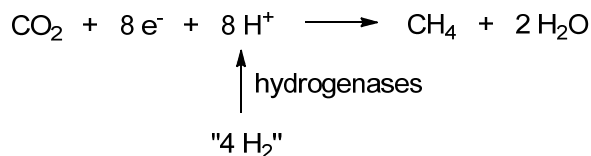


Figure 1.17: Overall equation for the reaction of CO₂ with H₂ affording methane.

The last and key step in the generation of CH₄ is the reaction of the C1-carrier thioether dimethyl-2,2'-dithiobis(ethanesulfonate) **1.42** (methyl-CoM) and N-7-mercaptoheptanoyl-O-phospho-L-threonine **1.43** (HS-HTP) (see Figure 1.18). This exergonic cleavage of **1.42** forms methane and the mixed disulfide CoM-SS-HTP **1.44** and is catalyzed by the enzyme methyl-CoM reductase.

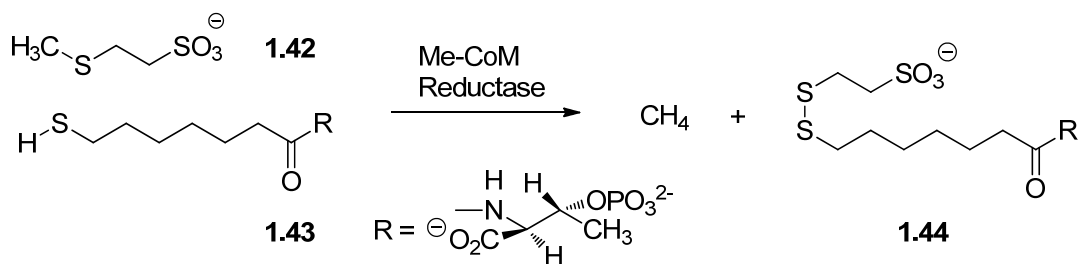


Figure 1.18: Formation of methane by the methyl-coenzyme M reductase.[92]

About 10⁹ tons of methane are produced per year by this reaction. Part of it acts as a potent greenhouse gas by escaping to the atmosphere.[75] Methanogenic bacteria can be found in every habitat in which anaerobic biodegradation of organic compounds occurs, including digestive and intestinal tracts of animals as well as anaerobic waste digesters. Utilized substrates as carbon sources can be, amongst others, CO₂, formate, methanol, ethanol and acetate.[77]

Methyl-CoM reductase was first discovered by Ellefson and Wolfe and consists of three different subunits.[93] The hexameric protein contains two molecules of the coenzyme F430 in the active site. F430 is a nickel-containing macrocyclic tetrapyrrole of unique structure (see Figure 1.19). The ring system has only five double bonds and is the most reduced tetrapyrrole in nature. Due to its lack of

conjugated double bonds F430 appears yellow, in contrast to systems with more unsaturated tetrapyrroles (e.g. heme) which have a red color. Until now it is the only nickel tetrapyrrole coenzyme discovered. Its properties and structure have been determined by the groups of Eschenmoser and Thauer.[88, 89] The active form of F430, often referred to as MCR_{redI} , [96] is a paramagnetic nickel(I) complex and therefore sensitive towards oxygen. The name F430 derives from its intensive absorbance maxima at 430 nm.

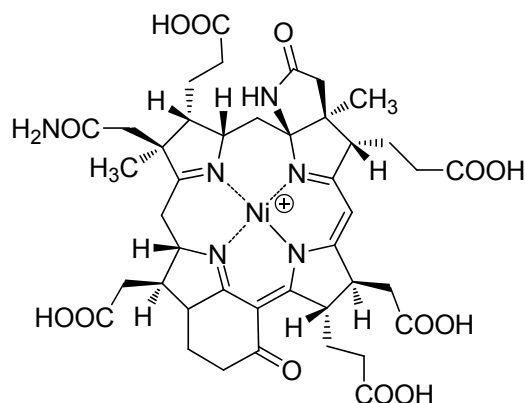


Figure 1.19: Structure of the coenzyme F430.

The exact reaction mechanism for the nickel center in the cofactor F430 is still discussed. Figure 1.20 shows one possible reaction scheme for the formation of methane. The reduction of the Ni(II) center is coupled to the oxidation of S-HTP suggested by electrochemical results on the oxidation of thioethers, thiols and thiolate anions.[91, 92] This forms F430 (Ni^{I}) **1.45** and the thiyl radical **1.46**. This radical can then couple with methyl-CoM, affording the sulfuranyl radical **1.47**. Demethylation of the sulfuranyl radical generates the nickel-methyl species **1.49** and the mixed disulfide CoM-SS-HTP **1.48**. Following protonation of the nickel-methyl compound finally gives methane and F430 (Ni^{II}) which can start the next catalytic cycle.[92]

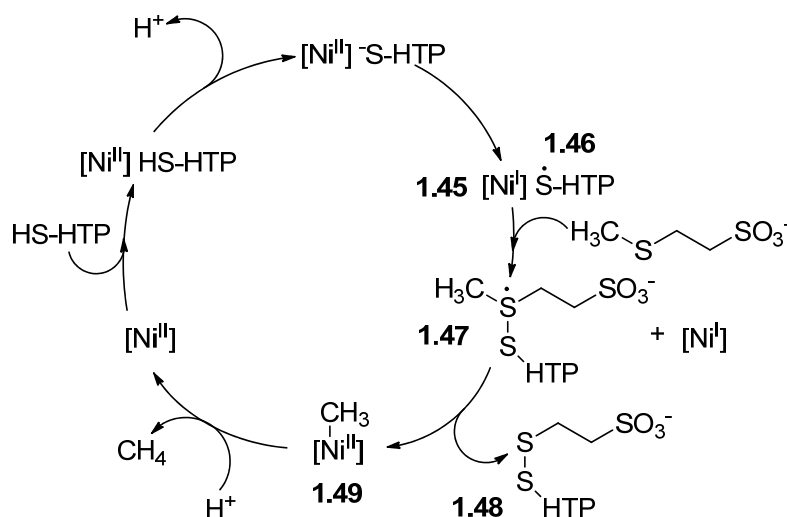


Figure 1.20: Proposed mechanism of methyl-coenzyme M reductase.[92]

1.5.2 Superoxide Dismutase

Superoxide dismutases (SODs) are ubiquitous metalloenzymes that catalyze the disproportionation of superoxide to peroxide and molecular oxygen as part of a cellular defense system against reactive oxygen species generated by various reactions associated with aerobic metabolism.[99, 100] Superoxide has been implicated as an active compound in the aging process, inflammatory diseases and a number of pathological conditions.[101–103]

The dismutation reaction requires the presence of a redox-active metal center and proceeds via a mechanism wherein the metal is first reduced and then reoxidized by superoxide (see Figure 1.21).[104, 105]

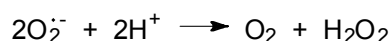
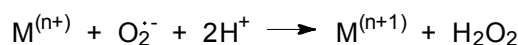
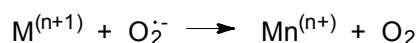


Figure 1.21: Equations for the dismutase reaction catalyzed by SODs.

There are two well-known and extensively characterized classes of SODs, the Cu,Zn-SOD and the Fe-SOD or Mn-SOD. Cu,Zn-SOD contains a dinuclear metal site with a catalytic active copper ion and zinc determining the structure of the enzyme. They are homodimeric or monomeric β -barrel proteins[106] and

1.5 Biochemistry of Nickel

most commonly found in eukaryotes. Mn-SOD and Fe-SOD are homologous homodimeric or homotetrameric proteins which contain an iron or manganese center coordinated by histidine residues and aspartic acid. They most commonly occur in prokaryotes and protists, as well as in mitochondria.

A third and completely different class of SODs, discovered several years ago, contains nickel. Originally isolated from *Streptomyces*, [103, 104] the Ni-SOD gene (*sodN*) has also been found in cyanobacteria [83, 108], marine gammaproteobacteria [110] and a marine eukaryote. [111] The amino acid sequence and structure of the active site of Ni-SODs have no significant homology with Fe-SOD, Mn-SOD or Cu,Zn-SOD. The Ni-SOD biological unit consists of a hexameric assembly of 4-helix bundles with a nickel ion in the active site bound to an N-terminal "nickel hook" which consists of a 12-amino acid sequence providing all of the essential interactions for metal binding (see Figure 1.22). [85, 112] As shown in the figure, the six nickel ions are arranged in an octahedral geometry about an empty cavity whereas the catalytic metal sites within the hexamer do not interact.



Figure 1.22: Ni-SOD: A hexameric assembly of 4-helix bundles. Ni ions displayed in dark gray. [85]

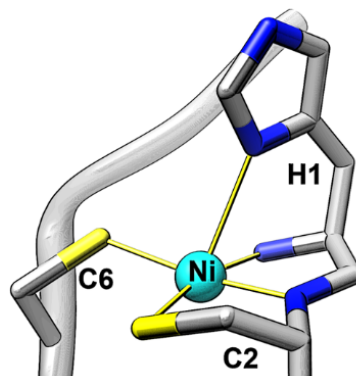


Figure 1.23: Structure of the active site of Ni-SOD (oxidized state, Ni^{III}). [99]

Spectroscopic and computational studies showed that the geometry and the oxidation state of the active site switches between a diamagnetic square planar Ni(II) and a paramagnetic square pyramidal Ni(III) center. [111, 112] In the reduced form the amino group nitrogen of His-1, the backbone nitrogen of Cys-2 and the thiolates of Cys-2 and Cys-6 build the coordination environment for the

Ni(II) ion. Figure 1.23 shows the nickel hook coordinating Ni(III) (Ni-SOD_{ox}) with the imidazole side chain of His-1 acting as additional fifth axial ligand.[98, 110]

Based on experimental studies[85, 112–115] the proposed mechanism for the Ni-SOD reaction (see Figure 1.24)[85] involves the binding of superoxide to the Ni(II) center after passing an electrostatic channel to the active site **1.50**, generating a Ni(II)-peroxo species **1.51**. This intermediate undergoes proton and electron transfer to generate H₂O₂ and the oxidized square pyramidal Ni(III) complex **1.52**. Binding of a second superoxide generates the Ni(III)-peroxo intermediate **1.53** which reduces the Ni(III) center to liberate dioxygen and re-generates the starting Ni(II) state.[99]

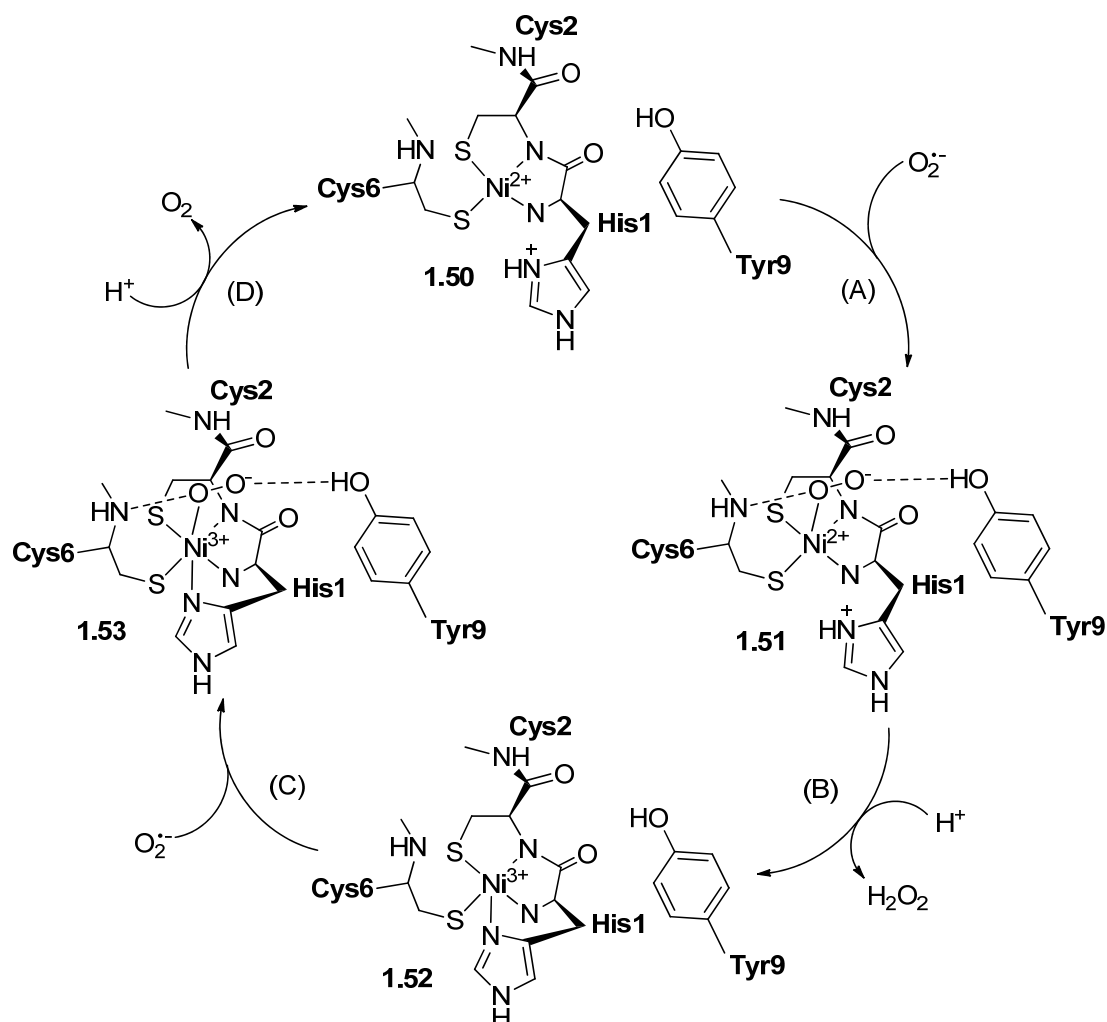


Figure 1.24: Proposed catalytic mechanism for Ni-SOD.[85]

1.5.3 Dioxygen Activation by Nickel

Mononuclear transition metal-dioxygen adducts are key intermediates in the activation of O_2 by metalloenzymes and biomimetic compounds and have attracted the attention of chemists for decades. This includes the oxygen transport in aerobic respiration, superoxide dismutation, biological oxidation or oxygenation of organic compounds as well as numerous stoichiometric and catalytic transformations of organic substrates in industrial processes.[116–122] Synthesized model metal- O_2 complexes, mainly copper and iron, have been investigated extensively to gain a better understanding of the structural and chemical properties of reactive oxygen intermediates that are short-lived and thus difficult to study in enzymatic reactions.[123–125].

The idea of using dioxygen as a primary oxidant (aerobic oxidation) is also very attractive because it is cheap and ecologically benign, but still difficult to control in a broad range of synthetic systems.[126]

Although nickel-dioxygen intermediates have been suggested to be highly active, so far there is little knowledge on these complexes. This has to be inevitably linked to the fact that nature has neglected nickel for aerobic oxidation catalysis. However, recent biological incentive for nickel-dioxygen chemistry originates from the discovery of the enzymes nickel dioxygenase and nickel superoxide dismutase which utilize dioxygen and its reduced form, superoxide (see 1.5.2).

1.5.3.1 Ni- O_x Species with Ni(II) and Hydrogen Peroxide

Since Ni(II) complexes are generally inert towards dioxygen, there are two common approaches to obtain Ni- O_2 compounds. One involves the reaction of hydrogen peroxide with Ni(II)-hydroxo complexes affording bis- μ -oxo-nickel complexes (see Figure 1.25).[127–131]

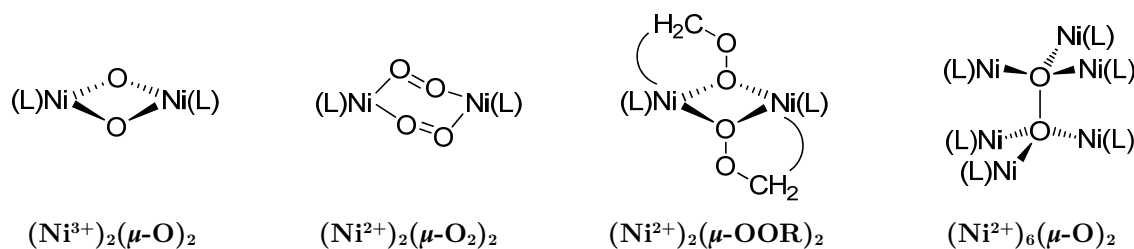


Figure 1.25: Ni- O_x structure types obtained from Ni(II) complexes and H_2O_2 . [128]

1.5.3.2 Ni–O_x Species with Ni(0) and Dioxygen

An alternative to the synthesis of nickel-peroxo complexes is the two-electron reduction of O₂ by Ni(0) complexes which has been pursued in the late 1960s and 70s.[132–134] While investigating the metal-catalyzed oxygenation of isocyanide to isocyanate, Otsuka et al. obtained the side-on Ni(II)-peroxo complex [Ni(O₂)(t-BuNC)₂] which was formed via oxidative addition of dioxygen to [Ni(t-BuNC)₄].

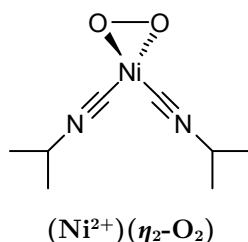


Figure 1.26: Side-on Ni(II)-peroxo complex obtained from the reaction of Ni(t-BuNC)₄ and dioxygen.[134]

1.5.3.3 Ni–O_x Species with Ni(I)

The monovalent oxidation state of nickel is suggested to be essential in nickel-containing enzymes for small molecule activation among hydrogenases, carbon oxide dehydrogenase and methyl-S-coenzymeM reductase (as described above). With a d⁹ valence electronic configuration these complexes are synthetically attractive as one-electron reducing agents. Isolable and stable monovalent nickel precursors also grant access to higher oxidation states of nickel-dioxygen adducts. Therefore, ligand design is of significant importance in stabilizing the lower valent oxidation state and directing the course of the reactions with dioxygen, due to their effect on the coordination mode of O₂ and the electronic structure of the Ni–O₂ adduct.

Today several mononuclear Ni–O₂ complexes with tripodal thioether, chelating monoanionic β-diketiminate and macrocyclic ligands have been obtained by one-electron reduction of O₂ and the respective Ni(I) precursors at low temperatures. Riordan and co-workers reported the purple bis-μ-oxo-nickel complex [(PhTt^{tBu})Ni]₂(μ-O)₂] afforded by the reaction of the nickel(I) complex [(PhTt^{tBu})Ni(CO)] (PhTt^{tBu} = phenyltris((*tert*-butylthio)methyl)borate) and dioxygen at low temperatures. By using the structurally similar ligand PhTt^{Ad}

(PhTt^{Ad} = phenyltris((1-ada-mantylthio)methyl)borate) it was possible to obtain the side-on superoxo-Ni(II) intermediate [(PhTtAd)Ni(O₂)] and sterically preclude the bis- μ -oxo dimer formation (Figure 1.27). The monomeric side-on dioxygen adduct could be characterized spectroscopically supported by DFT calculations.[135]

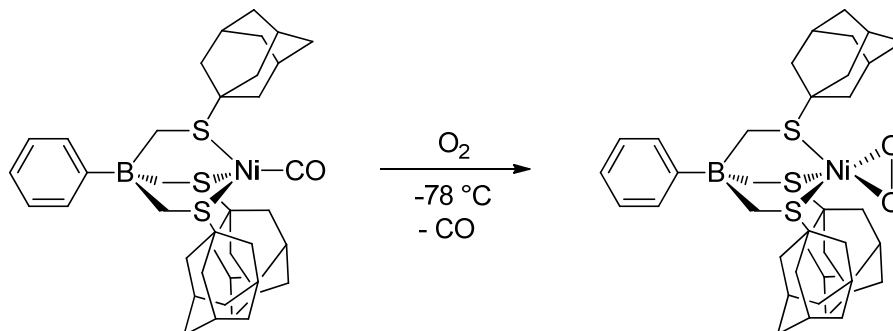


Figure 1.27: Reaction scheme for the oxygenation of [(PhTt^{Ad})Ni(CO)] at -78 °C affording [(PhTt^{Ad})Ni(O₂)]. [135]

The first room temperature stable superoxo-nickel complex structurally characterized by a single-crystal X-ray diffraction analysis was reported by Driess and co-workers.[126] Exposure of a solution of β -diketiminato-(toluene)nickel(I) in toluene to dry dioxygen led to an immediate color change from red-brown to green to form the Ni(II)–O₂ complex (Figure 1.28). The dioxygen adduct complex has a square-planar tetracoordinate Ni(II) center and an unpaired electron localized on the superoxo ligand (Figure 1.29).

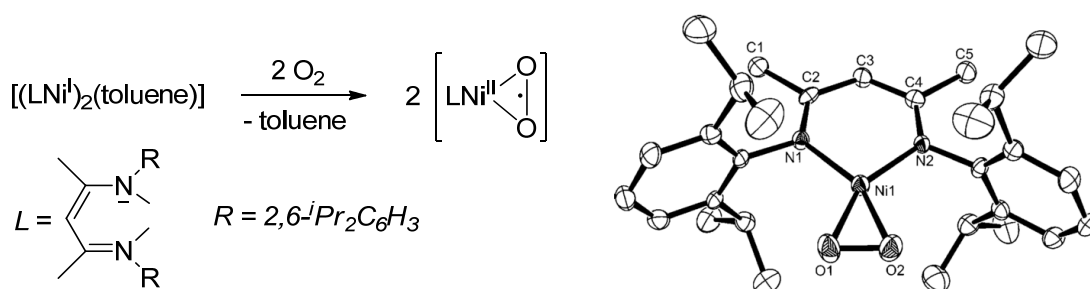


Figure 1.28: Formation of a side-on superoxo-nickel(II) complex from β -diketiminato-(toluene)nickel(I).

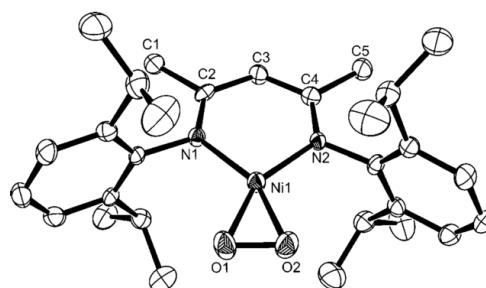


Figure 1.29: Molecular structure of a β -diketiminato-supported Ni–O₂ complex. [126]

The influence of the ligand system on the coordination mode of O_2 can also be observed in the reaction of Ni(I) with the tetradentate tetraaza macrocyclic ligands 12-tmc (12-tmc = 1,4,7,10-tetramethyl-1,4,7,10-tetraazacyclodecane) and 14-tmc (14-tmc = 1,4,8,11-tetramethyl-1,4,8,11-tetraazacyclotetradecane) which have different ring sizes. The $[\text{Ni(12-tmc)O}_2]^+$ complex, reported by Cho et al.,[136] afforded the first reported and structurally characterized mononuclear side-on Ni(III) -peroxo complex (Figure 1.30), whereas the $[\text{Ni(14-tmc)O}_2]^+$ complex, reported by Kieber-Emmons et al.[137], has been characterized as end-on superoxo species (Figure 1.31).

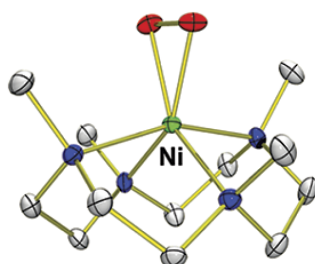


Figure 1.30: Molecular structure of $[\text{Ni(12-tmc)O}_2]^+$. [136]

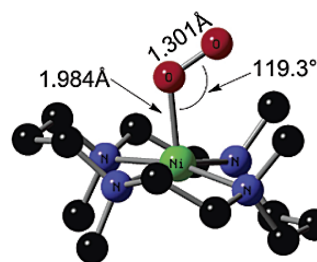


Figure 1.31: DFT optimized structure of $[\text{Ni(14-tmc)O}_2]^+$. [137]

Elimination of the vacant cis-coordination sites on the metal enforces an end-on dioxygen coordination and precludes over-reduction to the thermodynamically favorable bis- μ -oxo-dinickel complexes.[128]

Further possibilities to obtain Ni-O_2 species are to activate small molecules like nitrous oxide (N_2O) and ozonides. Therefore, the metal precursor complex should react with N_2O or metal-ozonides to form mononuclear metal-oxo complexes releasing nitrogen or dioxygen if heated or activated by light. Such complexes are regarded as extremely powerful oxidants and could be used for selective oxidations in situ.[124]

1.6 Research Goals

As discussed above most of the industrial chemicals have involved the use of a metal catalyst at some point during their manufacturing process. Thereby, palladium and platinum are the most common metals used as homogeneous catalysts. Nickel, with its wide variety of organometallic compounds, is a less expensive alternative to palladium and platinum catalysis.[11]

Detailed investigations on the reactivity of Ni(0) complexes are still lacking due to the difficult handling of these complexes. Therefore, new insights need to be achieved for new developments in the field of catalytic organonickel chemistry. With this background, the topic of this thesis is a detailed study on reactions and properties of Ni(0) and Ni(I) complexes with the aim of better understanding their reactivity and thus to develop new catalysts.

Parts of this research are based on results of earlier work done in the Schindler research group in the theses of C. Geyer[138, 139], H. Weiß[140], M. Leibold[141], L. Römmling[142] and A. Henß[143].

a) Reactivity of Ni(0) and Cu(I) Complexes Towards Alkenes and Alkynes

Nickel(0) complexes with the alkene bcp[142] and the alkynes dcpa[143] and dmbu should be synthesized and structurally characterized (see Figure 1.32).

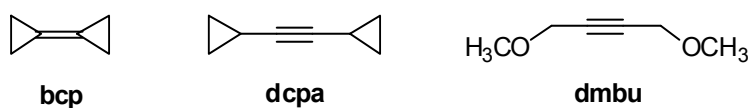


Figure 1.32: Structures of bicyclopropylidene (bcp), dicyclopropylacetylene (dcpa) and dimethoxybutyne (dmbu).

To gain a better understanding of the formation mechanism of these complexes kinetic investigations using “stopped-flow” techniques should be performed on the substitution reaction of [Ni(bipy)(COD)] and the respective ligands (see Figure 1.33).[142, 143]

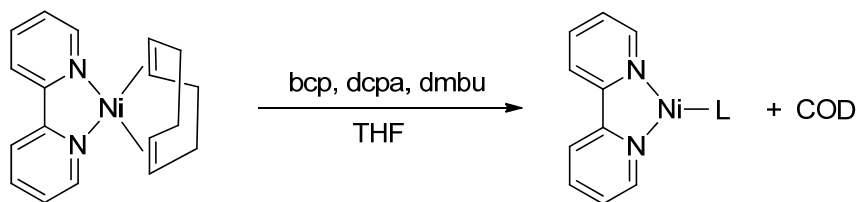


Figure 1.33: Scheme for the reaction of $[\text{Ni}(\text{bipy})(\text{COD})]$ with the unsaturated ligands bcp, dcpa and dmbu.

Due to the extreme sensitivity of nickel(0) complexes towards traces of dioxygen and difficulties in handling and characterization of these compounds, the isoelectronic copper(I) complexes $[\text{Cu}(\text{bipy})(\text{bcp})]\text{PF}_6$ [143] and $[\text{Cu}(\text{bipy})(\text{bcp})]\text{PF}_6$ [143] should be synthesized and characterized as well.

b) Ni(0) and Cu(I) Complexes with the Adamantane Ligand tctd

In collaboration with the research group of Prof. P. R. Schreiner (JLU Gießen, Institute for Organic Chemistry) it was the goal to synthesize nickel(0) coordination polymers with the adamantane derivative tetracyclo[7.3.1.1^{4,12}.0^{2,7}]tetradeca-6,11-diene (tctd) (see Figure 1.34).

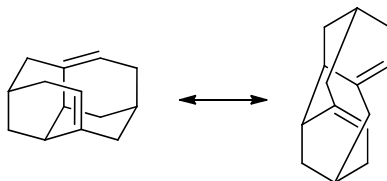


Figure 1.34: Structure of tetracyclo[7.3.1.1^{4,12}.0^{2,7}]tetradeca-6,11-diene (tctd).

c) Ni(0) and Cu(I) Complexes with the Ligand System O-BPy and Derivatives

Studies on ligand exchange reactions of the nickel(0) complex bis(cyclooctadiene)nickel(0) ($[\text{Ni}(\text{COD})_2]$) and the tetradentate ligand 1,2-bis(2,2'-bipyridine-6-yl)ethane (O-BPy) afforded the complex $[\text{Ni}_2(\text{O-BPy})(\eta^2\text{-C}_4\text{H}_6)_2]$ by the cleavage of the COD ligand (see Figure 1.35).[141]

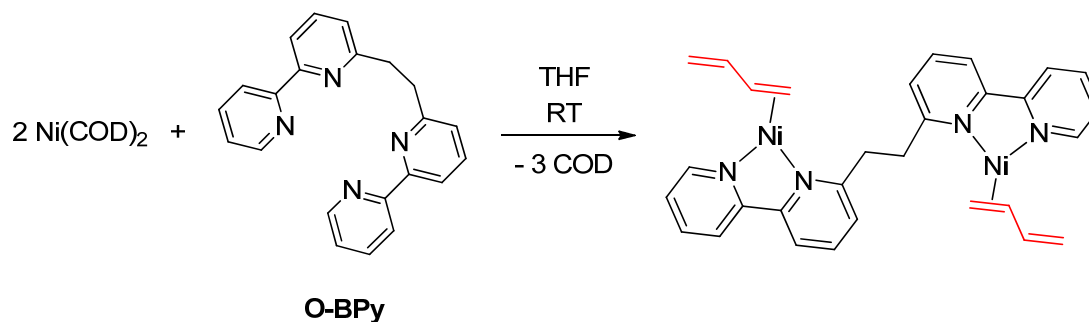


Figure 1.35: Reaction scheme for the synthesis of $[\text{Ni}_2(\text{O-BPy})(\eta^2\text{-C}_4\text{H}_6)_2]$. [141]

In collaboration with the research group of Prof. M. C. Holthausen (Goethe University Frankfurt am Main, Institute for Inorganic and Analytical Chemistry), which performed DFT calculations, this reaction should be further investigated. Additionally, Ni(0) complexes with derivatives of the ligand system O-BPy should be synthesized and structurally characterized in regard to the formation of binuclear complexes and the cleavage of COD.

Due to the extreme sensitivity of the nickel(0) complexes towards dioxygen and therefore difficulties in handling and characterization, again isoelectronic copper(I) complexes with O-BPy and derivatives should be synthesized and characterized as well.

d) Reactivity of Nickel Complexes with Macrocyclic Ligands

Catalytic and selective oxidation reactions of organic substrates play an important role in the field of chemistry and represent a challenging task whereupon selective oxidation using air or O_2 is very important. Comparable to nature, it is the aim to develop metal complexes (containing mainly iron and copper) which model the function and catalytic reactivity of enzymes. Research in this field has been ongoing in the research group of Prof. Schindler for years. Based on recent interesting findings of Nam and co-workers about macrocyclic transition metal-dioxygen adducts, macrocyclic nickel complexes and their reactivity should be investigated. [144]

Nickel(II) and nickel(I) complexes bearing the macrocyclic ligands 1,4,8,11-tetramethyl-1,4,8,11-tetraazacyclotetradecane (14-tmc) and *rac*-5,5,7,12,12,14-

hexymethyl-1,4,8,11-tetraazacyclotetradecane (tetB) (Figure 1.36) should be synthesized.

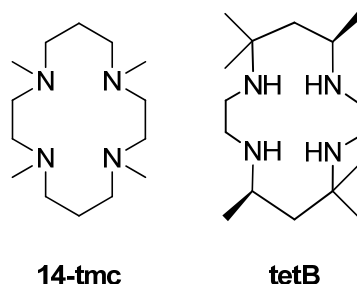


Figure 1.36: Structures of the ligands 1,4,8,11-tetramethyl-1,4,8,11-tetraazacyclotetradecane (14-tmc) *rac*-5,5,7,12,12,14-hexamethyl-1,4,8,11-tetraazacyclotetradecane (tetB).

The reactivity of the nickel(II) complexes towards oxidants (e.g. hydrogen peroxide, etc.) should be investigated and obtained nickel-dioxygen adducts should be characterized. Furthermore, the reactivity of the nickel(I) complex $[\text{Ni}(\text{14-tmc})]^+$ towards nitrous oxide should be examined with the aim of characterizing a “nickel-oxo” species according to procedures reported in literature (see Figure 1.37). [124, 145]

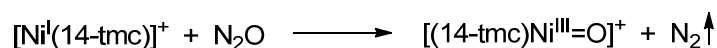


Figure 1.37: Proposed scheme for the reaction of $[\text{Ni}(\text{14-tmc})]^+$ with nitrous oxide.

2 Reactivity of Ni(0) and Cu(I) Complexes Towards Alkenes and Alkynes

2.1 Introduction

In organometallic chemistry unsaturated compounds such as bicyclopropylidene (bcp)[146], 1,4-dicyclopropylacetylene (dcpa)[147] and 1,4-dimethoxy-2-butyne (dmbu) (Figure 2.1) play an important role as molecular building blocks in various transition metal-catalyzed reactions[148–150] as well as in the design of unusual molecular assemblies with remarkable physical and chemical properties.[143, 144] In that regard, octacyclopropylcubane and some of its isomers with an impressive overall strain energy and kinetic stability have been synthesized successfully.[153]

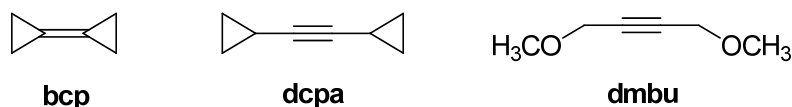


Figure 2.1: Structures of bicyclopropylidene (bcp), 1,4-dicyclopropylacetylene (dcpa) and 1,4-dimethoxy-2-butyne (dmbu).

Due to the nucleophilic character and novel reactions of these unsaturated compounds, transition metal complexes with bcp, dcpa and dmbu as ligands are assumed to have interesting properties and should be investigated in more detail. In collaboration with the research group of Prof. A. de Meijere (University of Göttingen, Institute for Organic Chemistry) who performed investigations on nickel-catalyzed cocyclizations of bcp and alkynes[154] it was interesting to investigate the according Ni(0) complexes of these compounds. Up to date, only three transition metal complexes containing bcp as ligand in η^2 -coordination have been synthesized and structurally characterized.[147, 148, 157] The first transition metal complex with bcp was obtained by the reaction of a bis(cyclopentadienyl)-bis(trimethylphosphine)titanium(II) precursor and bcp in pentane (see Figure 2.2).

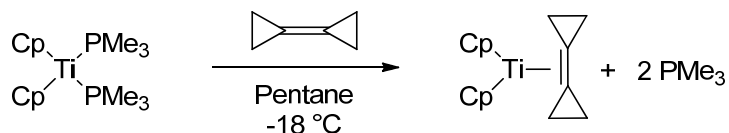


Figure 2.2: Synthesis of the first Ti complex of bcp.[155]

A second bcp complex was prepared by reacting ((2-(di-tert-butylphosphanyl)-P-ethyl)cyclopentadienyl)chloridocobalt(II) with sodium amalgam and bcp (see Figure 2.3). The substituted Cp ligand prevents oligomerization reactions by blocking one coordination site of cobalt with its phosphine arm and therefore, the complexation of another bcp molecule and reaction with the existing bcp ligand.

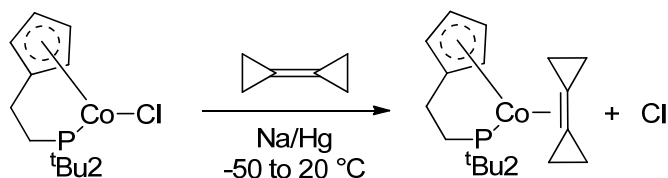


Figure 2.3: Synthesis of the first Co complex of bcp.[156]

The third and last bcp complex [Pt(bcp)(dppp)] (dppp = 1,3-bis(diphenylphosphino)propane) was afforded by the reaction of a diphosphine platinum precursor complex [Pt(C₂H₄)(dppp)] and bcp in benzene.[157]

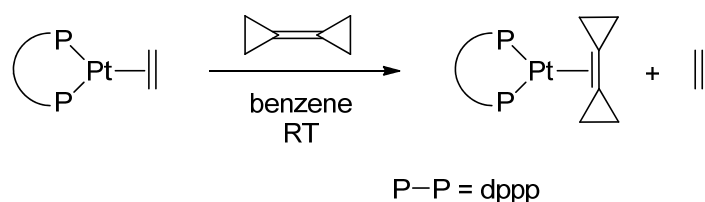


Figure 2.4: Synthesis of the first Pt complex of bcp.[157]

To gain a better understanding of the coordination ability of these ligands and in regard to further possible applications of the corresponding complexes as catalysts we were interested in preparing and investigating metal complexes not only with bcp, but also with dcpa and dmbu. Prior to the investigations pre-

2.2 Nickel (0) Complexes with bcp, dcpa and dmbu

sented herein, bcp and dcpa complexes with Ni(0) and Cu(I) were successfully synthesized and characterized in the Schindler research group.[150, 151]

2.2 Nickel (0) Complexes with bcp, dcpa and dmbu

The Nickel(0) complexes with the ligands bcp, dcpa and dmbu were synthesized by a substitution reaction of the precursor complex $[\text{Ni}(\text{bipy})(\text{COD})]$ (bipy = 2,2'-bipyridine, COD = 1,5-cyclooctadiene) with the respective ligand to give $[\text{Ni}(\text{bipy})(\text{bcp})]$, [142] $[\text{Ni}(\text{bipy})(\text{dcpa})]$ [143] and $[\text{Ni}(\text{bipy})(\text{dmbu})]$ (see Figure 2.5).

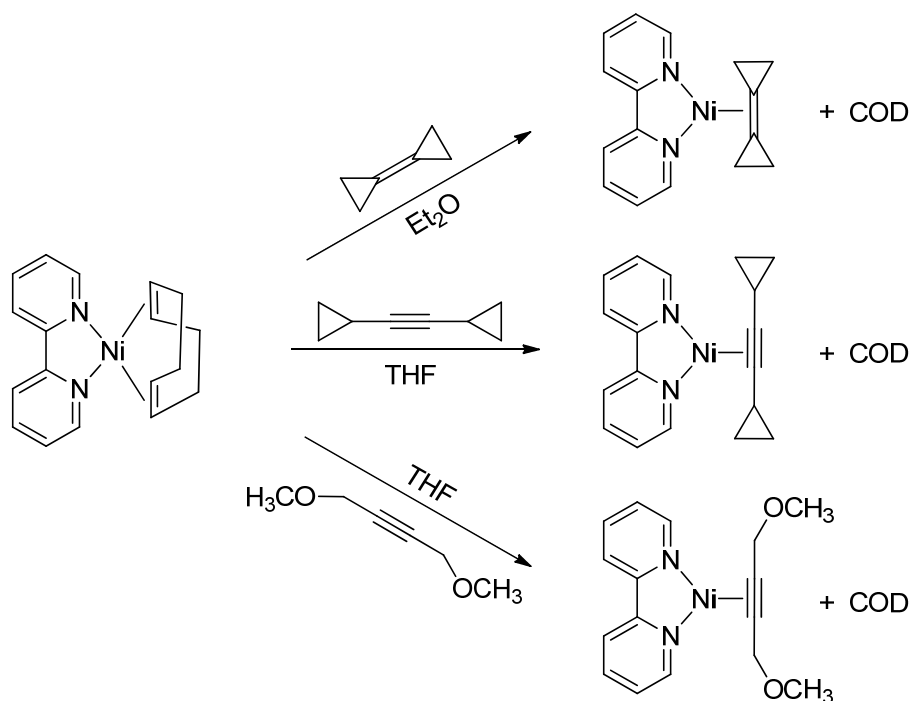


Figure 2.5: Reaction scheme for the synthesis of the Ni(0) complexes $[\text{Ni}(\text{bipy})\text{bcp}]$, $[\text{Ni}(\text{bipy})\text{dcpa}]$ and $[\text{Ni}(\text{bipy})\text{dmbu}]$.

$[\text{Ni}(\text{bipy})\text{bcp}]$ and $[\text{Ni}(\text{bipy})\text{dcpa}]$ were structurally characterized by X-ray studies. The formation of all three complexes could be investigated by UV-Vis spectroscopy using “stopped-flow” techniques.

2.2.1 Molecular Structures

2.2.1.1 [Ni(bipy)(bcp)]

The complex [Ni(bipy)(bcp)] was synthesized by a substitution reaction of [Ni(bipy)(COD)] and bicyclopropylidene in diethyl ether. The course of the reaction was traceable by the change of the deep purple colored solution to green. Diffusion of n-pentane into a THF solution of the complex resulted in dark-green crystals suitable for crystallographic studies. The determined molecular structure of [Ni(bipy)(bcp)] is shown in Figure 2.6.[142]

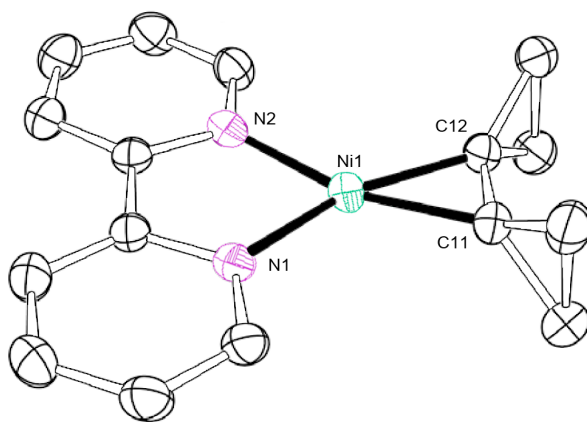


Figure 2.6: ORTEP plot of [Ni(bipy)(bcp)], hydrogen atoms are omitted for clarity. Ellipsoids are drawn at 50 % probability level.[142]

The structure of the complex shows a trigonal planar Ni(0) geometry with nickel being coordinated by the two nitrogen atoms (N1/N2) of bipyridine and the double bond of bcp (C11/C12). The Ni–N bond lengths range between 1.925(2) Å and 1.937(2) Å, the Ni–C bond lengths between 1.883(2) Å and 1.895(2) Å. Corresponding to data published by Helmut Weiß for a similar cyclopropene nickel(0) complex [Ni(bipy)L₁] (see 2.2.2.1),[19] the C–C double bond of bcp (1.422(2) Å) is enlarged compared to the uncoordinated olefin and the cyclopropane rings of the previously planar bcp molecule are angled to the C–C double bond attached to the nickel centre. Both can be explained by the partial change of the hybridization of the olefin double-bond from sp² to sp³.

2.2 Nickel (0) Complexes with bcp, dcpa and dmbu

2.2.1.2 [Ni(bipy)(dcpa)]

For the synthesis of the complex [Ni(bipy)(dcpa)], the nickel(0) precursor complex [Ni(bipy)(COD)] was mixed with an excess amount of dicyclopropylacetylene in THF obtaining yellow crystals suitable for diffraction studies.[143] The determined structure of [Ni(bipy)(dcpa)] corresponds with a previously reported Ni(0) complex by John J. Eisch et al., 2,2-bipyridyl-(η^2 -diphenylacetylene)-nickel(0).[46] The structure of the complex is shown in Figure 2.7. [Ni(bipy)(dcpa)] also shows a characteristic trigonal planar Ni(0) geometry with the nickel centre being coordinated by bipyridine and the triple bond (C11/C15) of dicyclopropylacetylene.

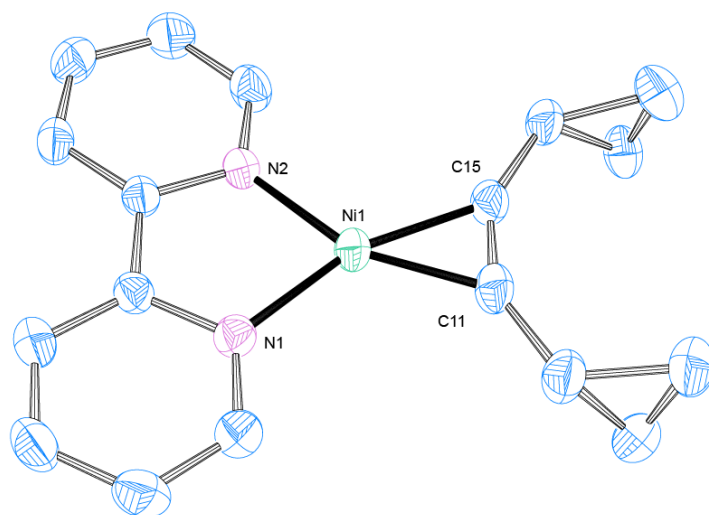


Figure 2.7: ORTEP plot of [Ni(bipy)(dcpa)], hydrogen atoms are omitted for clarity. Ellipsoids are drawn at 50 % probability level.[143]

The average of the Ni-C_{alkyne} distances of 1.85(2) Å is similar to Ni-C bonds involving sp²-hybridized carbon centers.[46, 158] Due to this acetylenic C-C distance of 1.28(3) Å, the presence of a C-C double bond is more likely than a triple bond.

2.2.1.3 [Ni(bipy)(dmbu)]

The complex [Ni(bipy)(dmbu)] was synthesized by a substitution reaction of [Ni(bipy)(COD)] and 1,4-dimethoxy-2-butyne in THF. By mixing the nickel(0) precursor complex with the ligand the solution turned from deep purple to dark

red. Evaporation of the solvent led to a dark green oil of the complex. Diffusion of n-pentane into a THF solution did not result in crystals suitable for X-ray diffraction. So far, this complex could not be characterized. A proposed structure of the complex is shown in Figure 2.8 (Universal force field (UFF) optimized[159]).

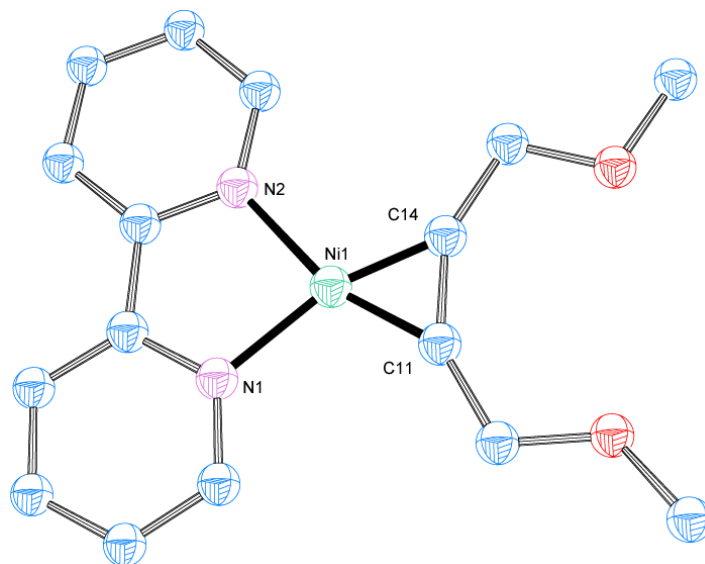


Figure 2.8: Proposed molecular structure for $[\text{Ni}(\text{bipy})(\text{dmbu})]$ (UFF optimized), hydrogen atoms are omitted for clarity.

2.2.2 Mechanistic Studies

There are several kinetic investigations about substitution reactions of $[\text{Ni}(\text{bipy})(\text{COD})]$ and olefin ligands that had been performed in the research group of Prof. Schindler.[19, 140, 139] In regard to better understand the reactivity of these complexes, kinetic studies have been performed on the formation mechanism. Therefore, the reactions of the Ni(0) precursor $[\text{Ni}(\text{bipy})(\text{COD})]$ with the ligands bcp, dcpa and dmbu have been followed by UV-Vis spectroscopy using “stopped-flow” techniques.

Mechanistic studies of such reactions are quite difficult due to the extreme sensitivity of dilute solutions of nickel(0) complexes towards traces of dioxygen and to autocatalytic reactions. However, in the past we successfully managed to overcome these difficulties by using special techniques for handling the samples.

2.2.2.1 [Ni(bipy)(bcp)][142]

The time-resolved UV-Vis spectra for the reaction of [Ni(bipy)(COD)] with the ligand bcp in THF at -20 °C is shown in Figure 2.9. The decrease of the absorbance maxima at 354 and 561 nm indicates the decomposition of the educt complex, whereas the increase of the band at 430 nm shows the formation of the bcp complex. Additionally isosbestic points at 390 and 478 nm could be observed.

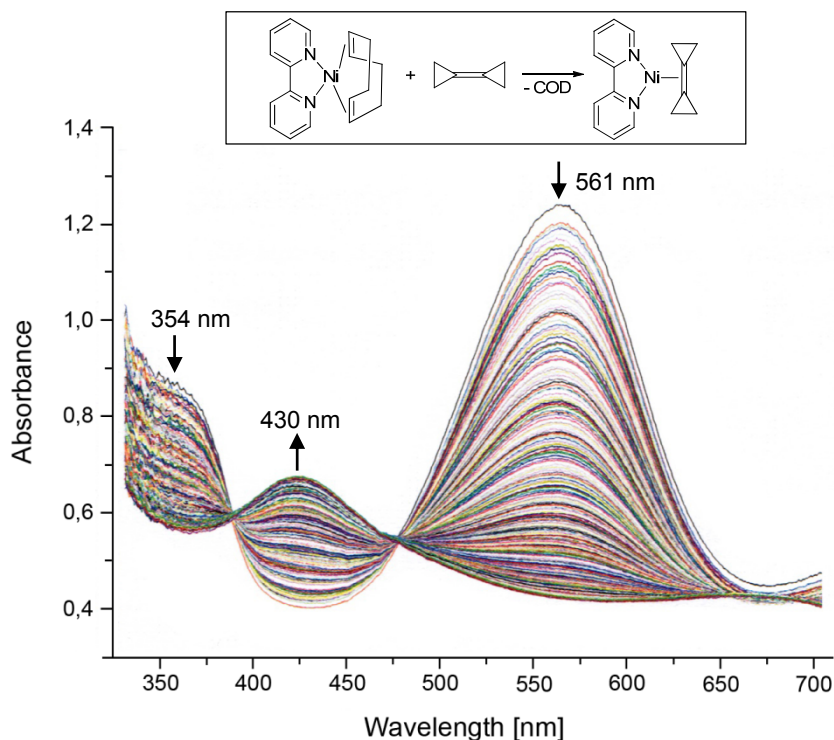


Figure 2.9: Time-resolved UV-Vis spectra of the reaction of [Ni(bipy)(COD)] with bicyclopropylidene in THF; [Ni(bipy)(COD)] = 0.25 mM, [bcp] = 30 mM, xs COD; T = -20.2 °C, t = 299.5 s, Δt = 1 s.[142]

The use of an excess amount of the ligand bcp ensured conditions of pseudo first-order. The dependence of the observed rate constant k_{obs} on the bcp concentration at 561 nm was linear and no intercept was obtained which indicates a completely irreversible reaction (see Figure 2.10). To determine the second-order rate constant k the following mathematical equations were considered:

$$\begin{aligned}
 -\frac{d[\text{Ni}(\text{bipy})(\text{COD})]}{dt} &= k \cdot [\text{Ni}(\text{bipy})(\text{COD})] \cdot [\text{bcp}] \\
 -\frac{d[\text{Ni}(\text{bipy})(\text{COD})]}{dt} &= k_{obs} \cdot [\text{Ni}(\text{bipy})(\text{COD})] \\
 k_{obs} &= k \cdot [\text{bcp}]
 \end{aligned}$$

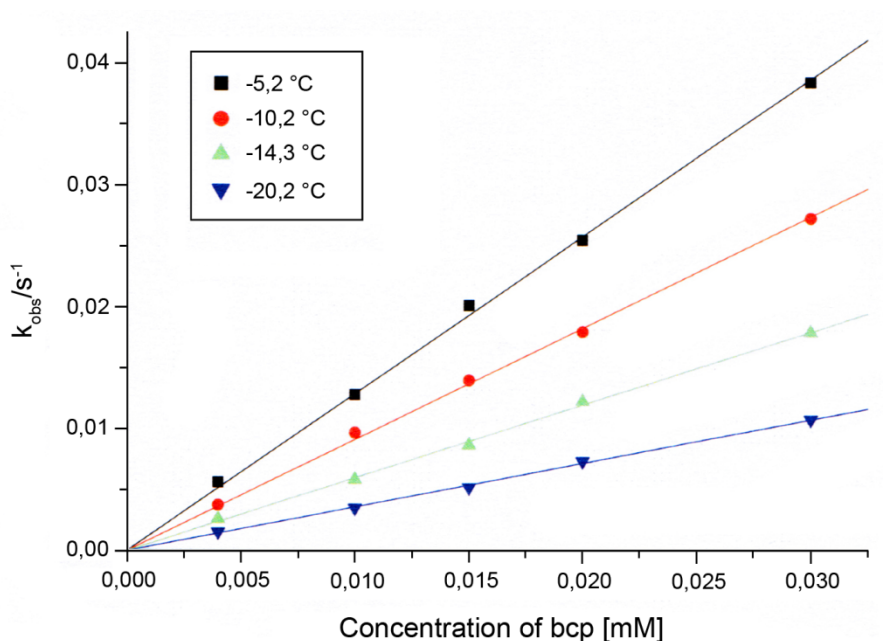


Figure 2.10: k_{obs} vs. bcp-concentration at four different temperatures at 561 nm; $[\text{Ni}(\text{bipy})(\text{COD})] = 0.25 \text{ mM}$. [142]

An Eyring plot of the reaction allowed the determination of the activation parameters ΔH^\ddagger and ΔS^\ddagger (see Table 2.1).

Table 2.1: Activation parameters for the reaction of $[\text{Ni}(\text{bipy})(\text{COD})]$ with bcp. [142]

ΔH^\ddagger	$47 \pm 3 \text{ kJ/mol}$
ΔS^\ddagger	$-68 \pm 9 \text{ J/K} \cdot \text{mol}$

Surprisingly, a negative entropy of activation ($-68 \pm 9 \text{ J/K} \cdot \text{mol}$) was obtained that indicated an associative mechanism for the substitution reaction. This agreed with previously published results by C. Geyer and H. Weiß [19, 140, 139] which also obtained negative values for ΔS^\ddagger for reactions with other olefinic ligands. However, they proposed dissociative mechanisms because of the tetrahedral structure of $[\text{Ni}(\text{bipy})(\text{COD})]$. It is well-known that tetrahedral nickel(0) complexes undergo dissociative substitution reactions. [160] A dissociative mechanism is also supported by the fact that nickel(0) olefin complexes decompose in separation of metallic nickel. [161] Due to these examples a dissociative mechanism was also proposed for the substitution reaction of $[\text{Ni}(\text{bipy})(\text{COD})]$ with

2.2 Nickel (0) Complexes with bcp, dcpa and dmbu

bicyclopropylidene despite negative entropy of activation. The postulated mechanism for the reaction is shown in Figure 2.11.

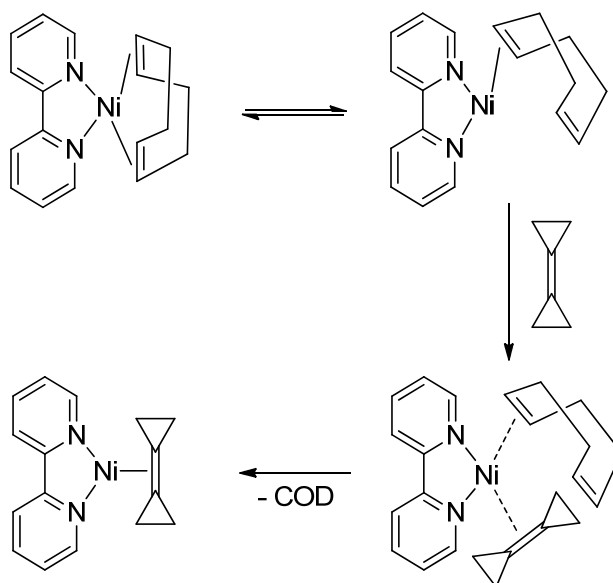


Figure 2.11: Postulated reaction mechanism for the reaction of $[\text{Ni}(\text{bipy})(\text{COD})]$ with bicyclopropylidene.[142]

The reaction of $[\text{Ni}(\text{bipy})(\text{COD})]$ with 3,3-dimethylcyclopropene-1,2-dicarboxylate (L_1) investigated by Helmut Weiß (see Figure 2.12) showed that the values for enthalpy and entropy of activation are higher for reactions with bicyclopropylidene than with L_1 .

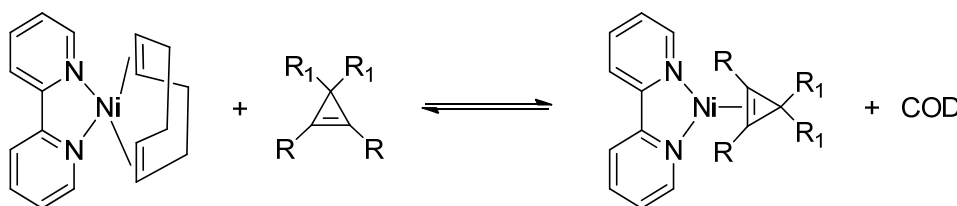


Figure 2.12: Reaction of $[\text{Ni}(\text{bipy})(\text{COD})]$ and L_1 ; $\text{R} = \text{CO}_2\text{Me}$, $\text{R}_1 = \text{CH}_3$. [140]

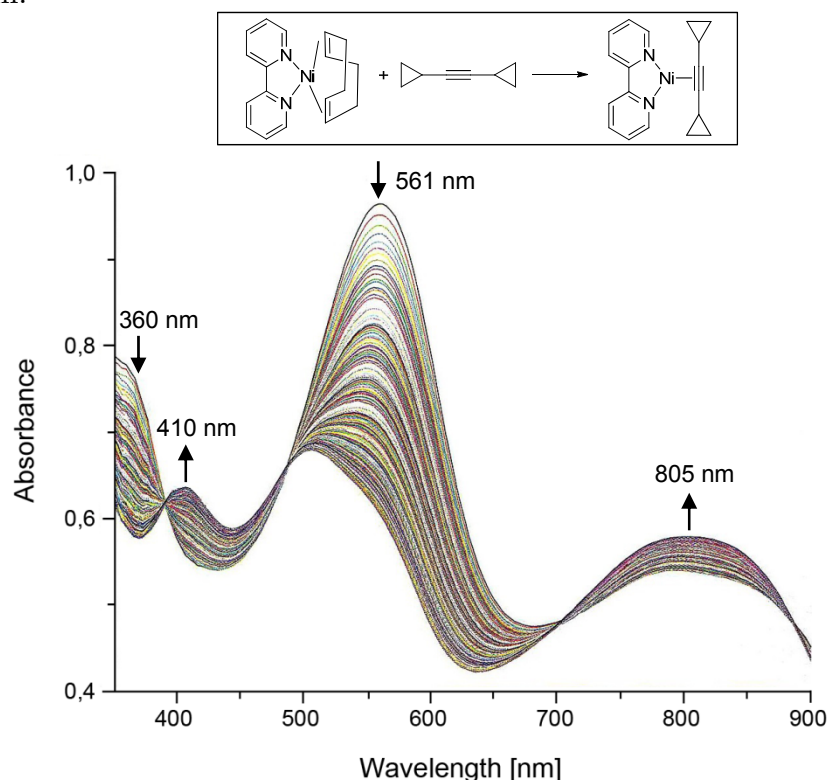
This also correlates with the much smaller second-order rate constant at -20°C for the reaction of the complex with bicyclopropylidene (see Table 2.2) which can be traced back to the electronic properties of L_1 . Due to the electron-withdrawing effects of the CO_2Me substituents, the double bond is electron-deficient and therefore reacts faster with the nucleophilic $\text{Ni}(0)$ complex.

Table 2.2: Activation parameters and reaction rate constants for the formation of [Ni(bipy)(bcp)][142] and [Ni(bipy)(L₁)] [140]

	[Ni(bipy)(bcp)]	[Ni(bipy)(L ₁)]
ΔH^\ddagger [kJ/mol]	47 ± 3	28 ± 2
ΔS^\ddagger [J/K · mol]	-68 ± 9	-128 ± 6
k (-20 °C) [$s^{-1} \cdot M^{-1}$]	$0.36 \pm 0,01$	37.2 ± 0.8

2.2.2.2 [Ni(bipy)(dcpa)][143]

Figure 2.13 shows the time-resolved spectra for the reaction of [Ni(bipy)(COD)] with the ligand dicyclopropylacetylene (dcpa) in THF at 20.1 °C. The decrease of the two bands at 360 and 561 nm shows the decomposition of [Ni(bipy)(COD)] and the increase of the absorbance at 410 and 805 nm the formation of the nickel dcpa complex. Isosbestic points were observed at 390 nm and 485 nm.

**Figure 2.13:** Time-resolved UV-Vis spectra of the reaction of [Ni(bipy)(COD)] with dicyclopropylacetylene in THF; [Ni(bipy)(COD)] = 0.25 mM, [dcpa] = 30 mM, xs COD; T = 20.1 °C, t = 51.3 s, Δt = 1 s.[143]

2.2 Nickel (0) Complexes with bcp, dcpa and dmbu

To ensure conditions of pseudo first-order an excess of dcpa was used. Due to previous investigations it was supposed, that the reaction follows a simple rate law such as:

$$\begin{aligned} -\frac{d[Ni(bipy)(COD)]}{dt} &= k \cdot [Ni(bipy)(COD)] \cdot [dcpa] \\ -\frac{d[Ni(bipy)(COD)]}{dt} &= k_{obs} \cdot [Ni(bipy)(COD)] \\ k_{obs} &= k \cdot [dcpa] \end{aligned}$$

The observed dependence of the rate constants k_{obs} on the dcpa concentration at different temperatures is shown in Figure 2.14. In contrast to the reaction with bcp an intercept was obtained which indicates a reversible reaction. Due to this and to decomposition reactions of the nickel complex, exact fittings to the single exponential functions could not be obtained. Thus, a nonlinear dependence of k_{obs} on the concentration of dcpa was observed which made a more detailed kinetic investigation impossible.

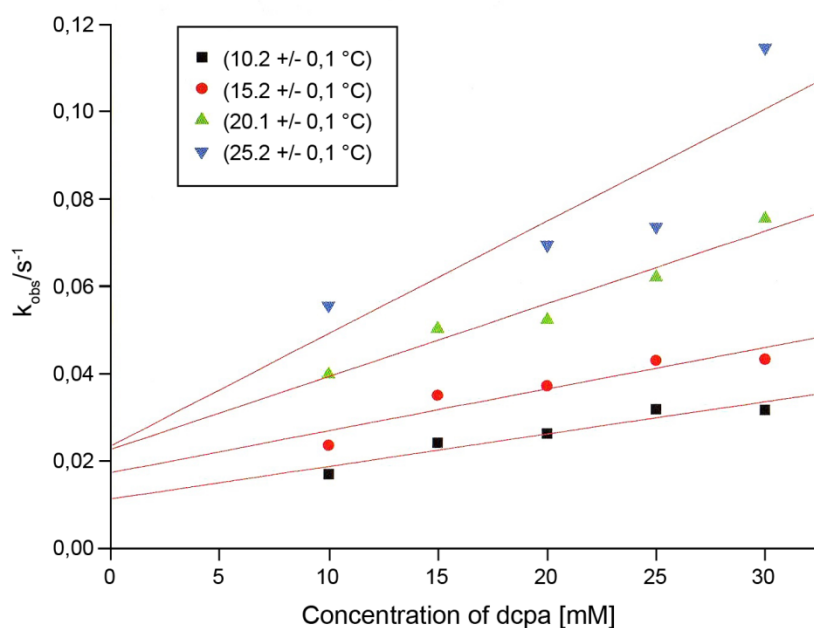


Figure 2.14: k_{obs} vs. dcpa-concentration at four different temperatures at 561 nm; $[Ni(bipy)(COD)] = 0.25$ mM.[143]

Nevertheless, the reaction rate was significantly slower compared to the related reactions of $[Ni(bipy)(COD)]$ with bcp or 3,3-dimethylcyclopropene-1,2-dicarboxylate. Hence, we can conclude that the coordination of dcpa is inhibited kinetically.

2.2.2.3 [Ni(bipy)(dmbu)]

Based on the previous results of the reaction of [Ni(bipy)(COD)] and the ligand dcpa we further investigated substitution reactions of Ni(0) complexes and alkynes using 1,4-dimethoxy-2-butyne. Detailed kinetic studies of this reaction will be presented in the following.

The time-resolved spectra for the reaction of [Ni(bipy)(COD)] and dmbu at 20.2 °C in THF are shown in Figure 2.15. The decrease of the two absorbance maxima at 360 and 561 nm indicates the decomposition of the educt complex and the increase of the bands at 420 and 675 nm shows the formation of the product complex [Ni(bipy)(dmbu)].

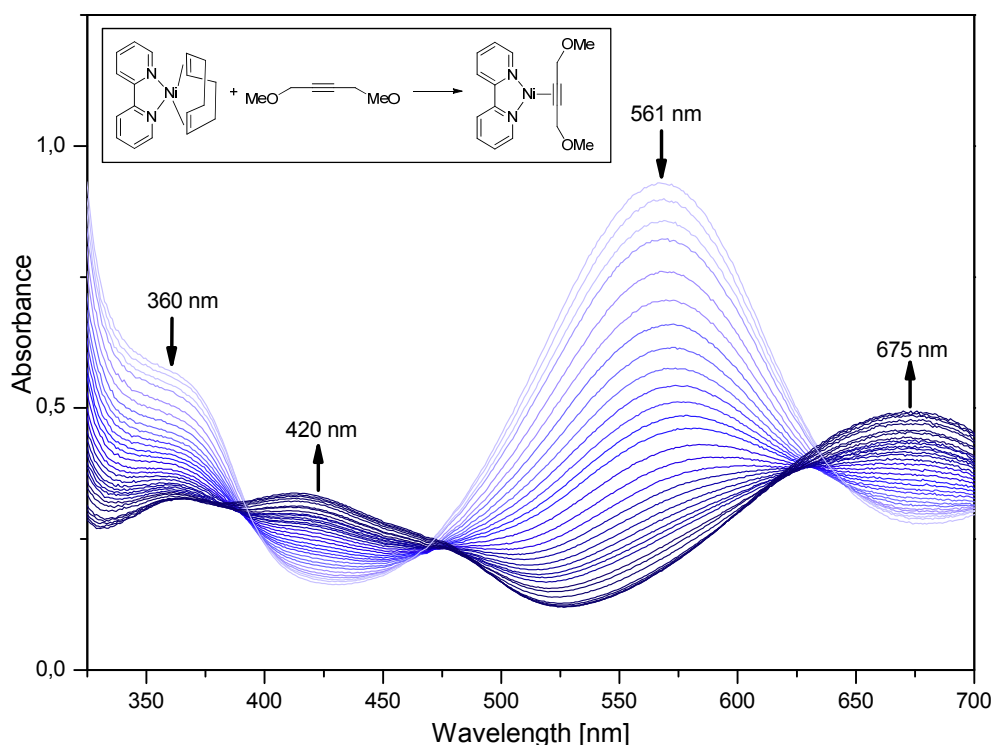


Figure 2.15: Time-resolved UV-Vis spectra of the reaction of [Ni(bipy)(COD)] with 1,4-dimethoxy-2-butyne in THF; [Ni(bipy)(COD)] = 0.25 mM, [dmbu] = 25 mM, xs COD; T = 20.2 °C, t = 45 s, Δt = 1 s.

Two isosbestic points were observed at 385 and 475 nm. Unfortunately, these points are not really precise due to the relative high temperatures applied, which speed up the decomposition of the highly diluted Ni(0) complex. To suppress this reaction an excess amount of COD was used.

2.2 Nickel (0) Complexes with bcp, dcpa and dmbu

Figure 2.16 shows the time trace for the reaction at 561 nm. The obtained data could be fitted to a single one-exponential function and the rate constants of pseudo first-order k_{obs} could be determined by variation of the dmbu concentration and reaction temperatures (see Table 2.3).

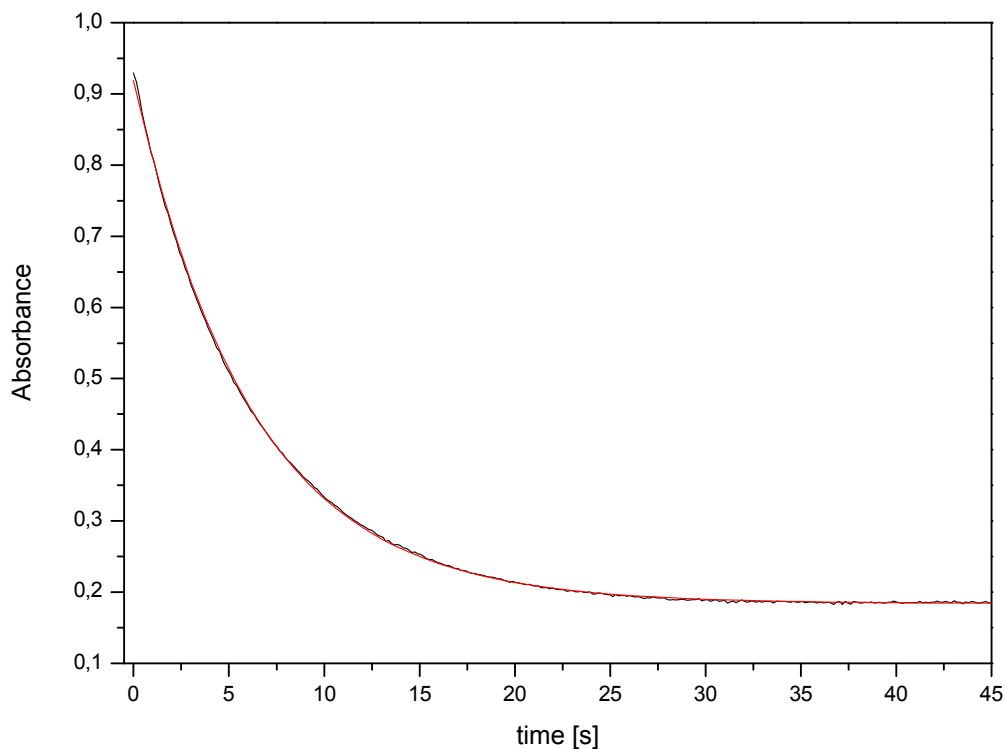


Figure 2.16 Absorbance vs. time for the reaction of $[\text{Ni}(\text{bipy})(\text{COD})]$ with 1,4-dimethoxy-2-butyne at 561 nm and fit to a single exponential function; $[\text{Ni}(\text{bipy})(\text{COD})] = 0.25 \text{ mM}$, $[\text{dmbu}] = 25 \text{ mM}$, xs COD; $T = 20.2 \text{ }^{\circ}\text{C}$.

Table 2.3: Measured reaction rates of the reaction of $[\text{Ni}(\text{bipy})(\text{COD})]$ with dmbu in THF; $[\text{Ni}(\text{bipy})(\text{COD})] = 0.25 \text{ mM}$.

$k_{obs} \cdot 10^{-2} [\text{s}^{-1}]$				
dmbu [mM]	20.2 $^{\circ}\text{C}$	25.3 $^{\circ}\text{C}$	30.2 $^{\circ}\text{C}$	35.2 $^{\circ}\text{C}$
10	(6.2 ± 0.1)	(9.2 ± 0.4)	(12.5 ± 0.3)	(17.0 ± 0.2)
15	(10.0 ± 0.2)	(14.6 ± 0.3)	(19.5 ± 0.5)	(27.1 ± 0.5)
20	(14.3 ± 0.3)	(21.5 ± 0.6)	(27.4 ± 0.5)	(36.6 ± 0.6)
25	(16.1 ± 0.5)	(25.2 ± 0.8)	(36.0 ± 0.7)	(45.0 ± 0.9)

According to the investigations shown above the following mathematical equations were considered to determine the second-order rate constant k :

$$-\frac{d[\text{Ni}(\text{bipy})(\text{COD})]}{dt} = k \cdot [\text{Ni}(\text{bipy})(\text{COD})] \cdot [(\text{dmбу})]$$

$$-\frac{d[\text{Ni}(\text{bipy})(\text{COD})]}{dt} = k_{\text{obs}} \cdot [\text{Ni}(\text{bipy})(\text{COD})]$$

$$k_{\text{obs}} = k \cdot [(\text{dmбу})]$$

The observed linear dependence of the rate constants k_{obs} on the concentration of dmбу at different temperatures is shown in Figure 2.17. The higher the reaction temperature, the bigger is the slope of the regression straight line. Furthermore, all four lines show no intercept so that an irreversible reaction can be assumed.

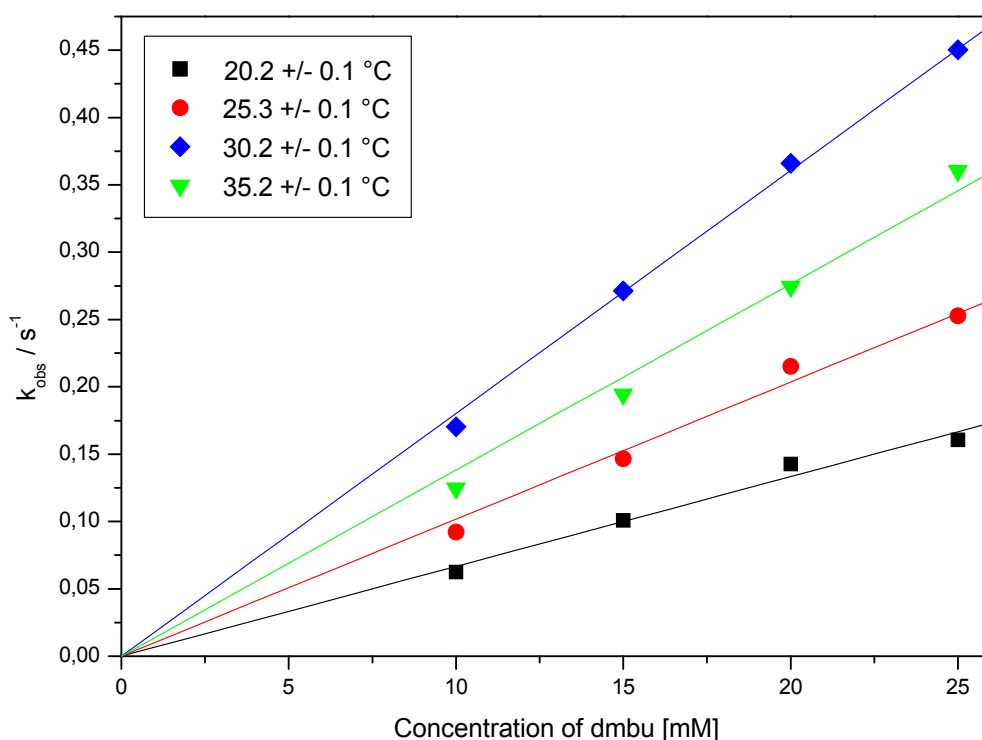


Figure 2.17: k_{obs} vs. dmбу-concentration at four different temperatures; $[\text{Ni}(\text{bipy})(\text{COD})] = 0.25 \text{ mM}$.

The second-order rate constants k were determined from the slopes of the regression straights (see Table 2.4).

2.2 Nickel (0) Complexes with bcp, dcpa and dmbu

Table 2.4: Second-order reaction rate constants of the reaction of [Ni(bipy)(COD)] with dmbu in THF.

T [°C]	k [s ⁻¹ · M ⁻¹]
20.2 ± 0.1	(17 ± 2) · 10 ⁻⁴
25.3 ± 0.1	(28 ± 2) · 10 ⁻⁴
30.2 ± 0.1	(39 ± 1) · 10 ⁻⁴
35.2 ± 0.1	(47 ± 1) · 10 ⁻⁴

An Eyring plot of the reaction allowed the determination of the activation parameters ΔH^\ddagger and ΔS^\ddagger from the temperature dependence of the rate constant (see Figure 2.18).

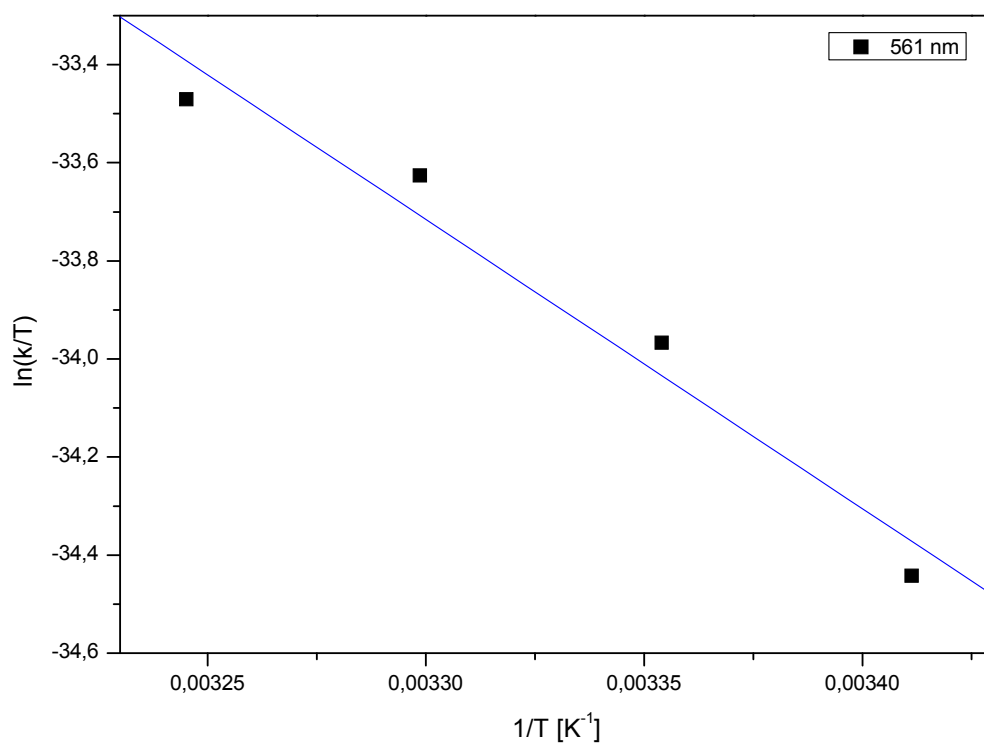


Figure 2.18: Eyring plot for the reaction of [Ni(bipy)(COD)] with 1,4-dimethoxy-2-butyne in THF determined from Table 2.4.

For the activation enthalpy ΔH^\ddagger we obtained $(49 \pm 7) \text{ kJ} \cdot \text{mol}^{-1}$ and for the activation entropy ΔS^\ddagger $(-118 \pm 24) \text{ J} \cdot \text{K}^{-1} \cdot \text{mol}^{-1}$ (see Table 2.5).

Table 2.5: Activation parameters for the reaction of [Ni(bipy)(COD)] with dmbu.

$\Delta H^\#$	$49 \pm 7 \text{ kJ/mol}$
$\Delta S^\#$	$-118 \pm 24 \text{ J/K} \cdot \text{mol}$

The negative activation entropy calculated for the reaction is in accordance with the findings for the formation of [Ni(bipy)(bcp)], where a similar negative value for $\Delta S^\#$ was obtained (see Table 2.6).

Table 2.6: Activation parameters and reaction rate constants for the formation of [Ni(bipy)(bcp)][142] and [Ni(bipy)(dmbu)].

	[Ni(bipy)(bcp)]	[Ni(bipy)(dmbu)]
$\Delta H^\# \text{ [kJ/mol]}$	47 ± 3	49 ± 7
$\Delta S^\# \text{ [J/K} \cdot \text{mol]}$	-68 ± 9	-118 ± 24
$k \text{ (-5.2 } ^\circ\text{C)} \text{ [s}^{-1} \cdot \text{M}^{-1}]$	$1.29 \pm 0,02$	—
$k \text{ (20.2 } ^\circ\text{C)} \text{ [s}^{-1} \cdot \text{M}^{-1}]$	—	$(17 \pm 2) \cdot 10^{-4}$

These results also support an associative mechanism for the reaction of [Ni(bipy)(COD)] with 1,4-dimethoxy-2-butyne. Following the same arguments as discussed above (see 2.2.2.1), we think that an associative mechanism is rather unlikely as well.

From our kinetic findings, we therefore propose the same mechanism for the formation of [Ni(bipy)(dmbu)] as for the bcp complex, with a highly ordered transition state in the course of the reaction (see Figure 2.19).

In a fast pre-equilibrium step one of the bonds between the nickel(0) center and COD is cleaved transforming the four-coordinated [Ni(bipy)(COD)] complex into a reactive three-coordinated species. In a following step, 1-4-dimethoxy-2-butyne binds to the free coordination site before the product complex [Ni(bipy)(COD)] is formed and the remaining bond to COD is broken.

2.2 Nickel (0) Complexes with bcp, dcpa and dmbu

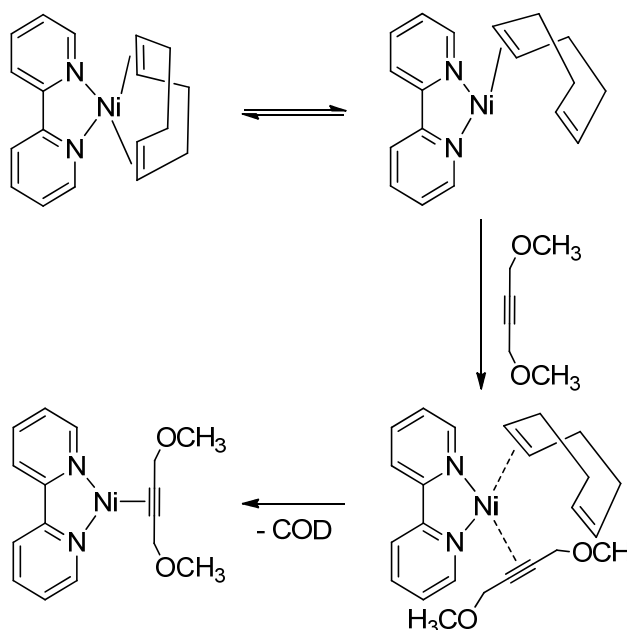


Figure 2.19: Proposed mechanism for the reaction of $[\text{Ni}(\text{bipy})(\text{dmbu})]$ with 1,4-dimethoxy-2-butyne.

However, this proposed reaction scheme is a simplified mechanistic view of the reaction because THF solvent molecules can also undergo addition and the COD ligand can coordinate other complex units to form clusters. In that regard, it would have been interesting to obtain activation volumes for additional kinetic information. However, these measurements were not possible in our case due to the extreme sensitivity of the nickel(0) complexes toward traces of dioxygen and the occurring decomposition.

The rate constants of the reaction of $[\text{Ni}(\text{bipy})(\text{COD})]$ with bcp and dmbu are very different; the reaction of the nickel complex with dmbu proved to be slower than the reaction with bcp. At 20.2 °C dmbu reacts with $[\text{Ni}(\text{bipy})(\text{COD})]$ by a factor of 1000 slower than bcp at 5.2 °C (see Table 2.6). Thus, we conclude that the coordination of dmbu is inhibited kinetically as well. Nevertheless, the reaction rate of dmbu is faster compared to the related reaction of $[\text{Ni}(\text{bipy})(\text{COD})]$ with dcpa. A reason for this might be electronic effects of the two methoxy groups on the triple bond of dmbu.

2.3 Copper(I) Complexes with bcp and dcpa

Prior to the investigations on nickel(0) complexes with the ligands bcp, dcpa and dmbu described herein, isoelectronic bcp and dcpa Cu(I) complexes were successfully synthesized and characterized in the Schindler research group.[143]

2.3.1 Molecular Structures

2.3.1.1 [Cu(bipy)(bcp)]PF₆[143]

By mixing copper(I) salt, bipyridine and an excess amount of the olefin bcp in acetone, the pale yellow complex [Cu(bipy)(bcp)]PF₆ could be synthesized and crystals suitable for X-ray analysis were obtained. The molecular structure of the cation is shown in Figure 2.20.

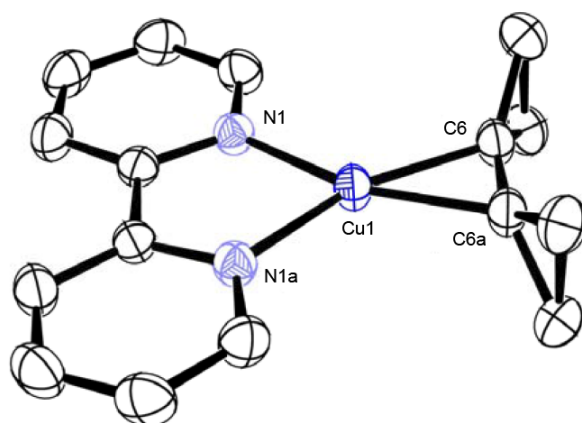


Figure 2.20: ORTEP plot of the cation [Cu(bipy)(bcp)]⁺, hydrogen atoms are omitted for clarity. Ellipsoids are drawn at 50 % probability level.[143]

The geometry of [Cu(bipy)(bcp)]PF₆ can be described as square planar where the copper(I) center is coordinated by two pyridyl nitrogen atoms and by the double bond of bcp. Due to the space group *C*2/*c* there is a plane of symmetry in the molecule. The values for the Cu–N (1.98(2) Å) and Cu–C distances (1.96(2) Å) are comparable to related ternary copper(I) olefin complexes.[162–167] Due to the different hybridization of the coordinated carbon atoms in the complex (sp³), an expansion of the coordinated double bond compared to the uncoordinated ligand is observed. Compared to the distance of the coordinated

2.3 Copper(I) Complexes with bcp and dcpa

C–C bond of the nickel complex (1.42(2) Å) (see 2.2.1.1), the double bond in the copper(I) complex is shorter (1.36(3) Å), which confirms that the Cu(I) ion is the poorer π -back-bonding transition metal cation as nickel. In this concept, electrons are partially transferred from d-orbitals of the metal center to anti-bonding molecular orbitals of the alkene bcp which strengthens the metal–ligand bond, but weakens the double bond within the ligand (C–C bond is enlarged).

2.3.1.2 [Cu(bipy)(dcpa)]PF₆[143]

The analogue alkyne complex with dicyclopropylacetylene (dcpa) as ligand was synthesized in the same way as [Cu(bipy)bcp]PF₆. It was possible to obtain yellow crystals suitable for X-ray structure analysis after diffusion of diethyl ether into the solution. The molecular structure of the cation of [Cu(bipy)dcpa]PF₆ is shown in Figure 2.21. The coordination environment of the copper(I) ion is almost trigonal planar with two pyridine nitrogen atoms and the side-on coordinated ligand dicyclopropylacetylene.

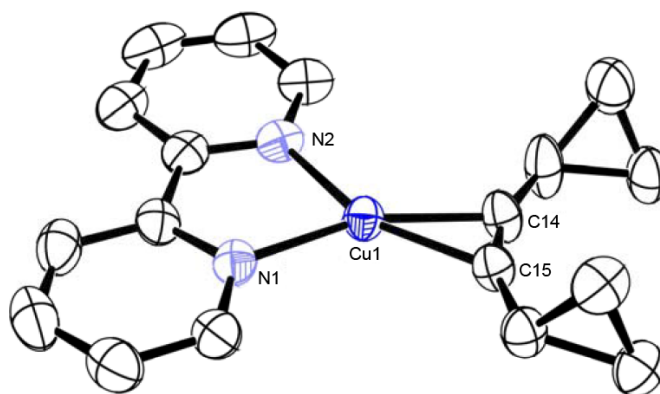


Figure 2.21: ORTEP plot of the cation [Cu(bipy)(dcpa)]⁺, hydrogen atoms are omitted for clarity. Ellipsoids are drawn at 50 % probability level.[143]

As expected the observed Cu–N bond angles and distances are comparable to those determined for [Cu(bipy)bcp]PF₆ and the C–C bond length of the coordinated dcpa ligand (1.23(4) Å) is only slightly larger than in the free molecule (1.19(3) Å).[168] Due to the different hybridization of the coordinated carbon atoms in the complex (sp²), the two cyclopropyl rings of dcpa are bended out of plane as shown in the figure.

Compared with the related nickel(0) complex $[\text{Ni}(\text{bipy})(\text{dcpa})]$ the distance of the C–C alkyne bond found in the Ni(0) complex is larger (1.28(3) Å). As described above, this goes with the fact that copper(I) is supposed to be the poorer back-bonding metal center as nickel(0).

2.3.2 Reactivity Towards Dioxygen

Due to the difficulty to isolate and characterize reactive copper-dioxygen intermediates it was an idea to use alkenes or alkynes as ligands to stabilize the copper(I) unit and additionally to provide a ligand that can be easily substituted by dioxygen during the oxidation process. Thus, in an experiment acetone solutions of $[\text{Cu}(\text{bipy})\text{bcp}]\text{PF}_6$ and $[\text{Cu}(\text{bipy})\text{dcpa}]\text{PF}_6$ were cooled to $-80\text{ }^\circ\text{C}$ and reacted with dry dioxygen. However, the direct reaction did not result in an O_2 -adduct complex with intensive color.

The experiment demonstrated that a simple copper complex with only bipyridine as ligand cannot stabilize a dioxygen adduct complex under these conditions. Nevertheless, an interesting oxidation reaction occurred.

According to the following equation shown in Figure 2.22 the oxidation of $[\text{Cu}(\text{bipy})\text{dcpa}]\text{PF}_6$ with atmospheric dioxygen led to a bis(μ -hydroxo)dicopper(II) complex as product.

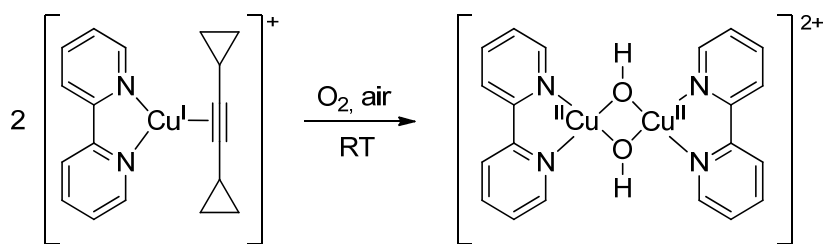


Figure 2.22: Reaction of $[\text{Cu}(\text{bipy})(\text{dcpa})]^+$ with atmospheric dioxygen affording the bis(μ -hydroxo)dicopper(II) complex $[\text{Cu}_2(\text{bipy})_2(\text{OH})_2]^{2+}$. [143]

As shown in the scheme, the dcpa molecule is no longer coordinated to the copper center and an oxidation of dcpa was not observed. A binuclear copper(II) complex was formed in which both copper ions are bridged by a hydroxo group of the inserted dioxygen. Due to the oxidation with atmospheric O_2 and not dry dioxygen, it was assumed that the hydroxo group is formed from a bis- μ -oxo precursor and traces of water. The molecular structure of the binuclear copper(II) complex is shown in Figure 2.23. [143]

2.4 Experimental

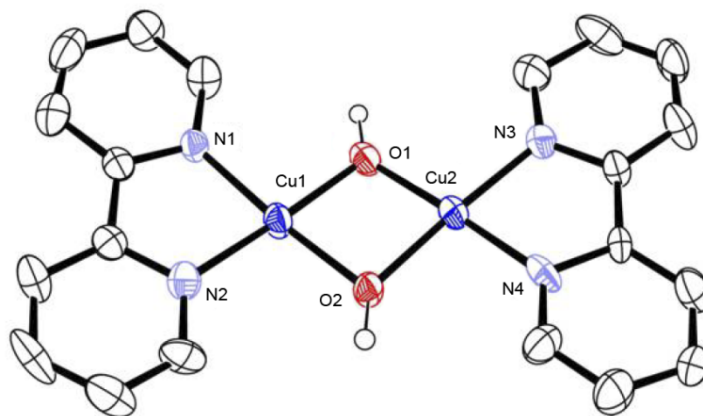


Figure 2.23: ORTEP plot of the cation $[\text{Cu}_2(\text{bipy})_2(\text{OH})_2]^{2+}$, hydrogen atoms are omitted for clarity. Ellipsoids are drawn at 50 % probability level.[143]

2.4 Experimental

2.4.1 Material and Reagents

If not otherwise stated commercially available chemicals were used. Tetrahydrofuran needed to be purified for kinetic measurements. This was achieved by predrying over KOH pellets. Afterwards it was refluxed over potassium and benzophenone under argon for several days.

All handling as well as the storage of the oxygen sensitive Ni(0) compounds and materials used in the kinetic studies was carried out in a glove box (M. Braun, Garching, Germany; $\text{O}_2 < 0.1$ ppm, $\text{H}_2\text{O} < 0.1$ ppm) within argon atmosphere.

2.4.2 Kinetic Measurements

Variable temperature stopped-flow measurements allowed the collection of time resolved UV-Vis spectra for reaction of $[\text{Ni}(\text{bipy})(\text{COD})]$ with the ligands in THF. The solutions of the complex and ligand were prepared in a glove box under argon and transferred using syringes to the low-temperature stopped-flow instrument.

The reaction was studied under pseudo-first-order conditions ($c([\text{Ni}(\text{bipy})(\text{COD})]) \ll c([\text{ligand}])$). The nickel(0) precursor complex was diluted in a 10 ml volumetric flask to obtain an exact concentration of

$1 \cdot 10^{-3}$ mol/L. The final concentration after mixing in the stopped-flow unit was $5 \cdot 10^{-4}$ mol/L. The concentration of the ligand solutions were 0.04 mol/L up to 0.1 mol/L (concentration is determined after mixing in the stopped-flow unit during measurement). Time-resolved UV-Vis spectra of these reactions were recorded with a TgK Scientific model SF-61SX2 low-temperature stopped-flow spectrophotometer equipped with a diode array detector (Salisbury, U.K.). Spectral changes in the range of 300-700 nm were observed using a quartz cell with a path length of 1 cm. Data fitting was performed using the integrated software Kinetic Studio (TgK Scientific, UK) and Origin (OriginLab Corporation, Northhampton, MA, USA). Details on such studies have been described previously.[169]

2.4.3 Synthesis of the Complexes

The ligand 1,4-dimethoxy-2-butyne (dmbu) was obtained commercially (Sigma-Aldrich). Bicyclopropylidene (bcp) and dicyclopropylacetylene (dcpa) have been provided by Prof. A. de Meijere.

2.4.3.1 [Ni(COD)₂]

The starting nickel(0) complex [Ni(COD)₂] was prepared according to a procedure described in literature.[170]

2.4.3.2 [Ni(bipy)(COD)]

The precursor complex [Ni(bipy)(COD)] was prepared by the reaction of [Ni(COD)₂] and 2,2'-bipyridine according to literature.[171]

2.4.3.3 [Ni(bipy)(dmbu)]

To a stirred purple suspension of 25.8 mg (0.08 mmol) [Ni(bipy)(COD)] in 2 ml THF 116 mg (1.02 mmol) dmbu in 2 ml THF was added. The resulting dark red solution was stirred furthermore for 1 hour. Diffusion of n-pentane into the solution at -20 °C did not result in crystals suitable for X-ray structure determination. The molecular structure of [Ni(bipy)(COD)] was optimized using Avogadro's structure optimization set to Universal Force Field (UFF) with steepest descent (iterative optimization algorithm; convergence at $10e^{-7}$).[159]

3 Ni(0) and Cu(I) Complexes with the Adamantane Ligand tctd

3.1 Introduction

Copper complexes containing unsaturated compounds and their possible application in organic synthesis as catalysts were investigated in our research group previously. Therefore, bidentate chelate ligands with nitrogen donor atoms suitable for complexation of copper(I) ions, such as bipyridine and phenanthroline, were used to synthesize numerous complexes.[143] Several of these complexes are able to coordinate unsaturated hydrocarbons, e.g. olefins or alkynes.

Within a collaboration with the research group of Prof. P. R. Schreiner (JLU Gießen, Institute for Organic Chemistry), who is interested in the functionalization of diamondoids (examples shown in Figure 3.1[172, 173]), it was the goal to synthesize and characterize organic copper and nickel polymers with adamantane derivatives which should have interesting properties.

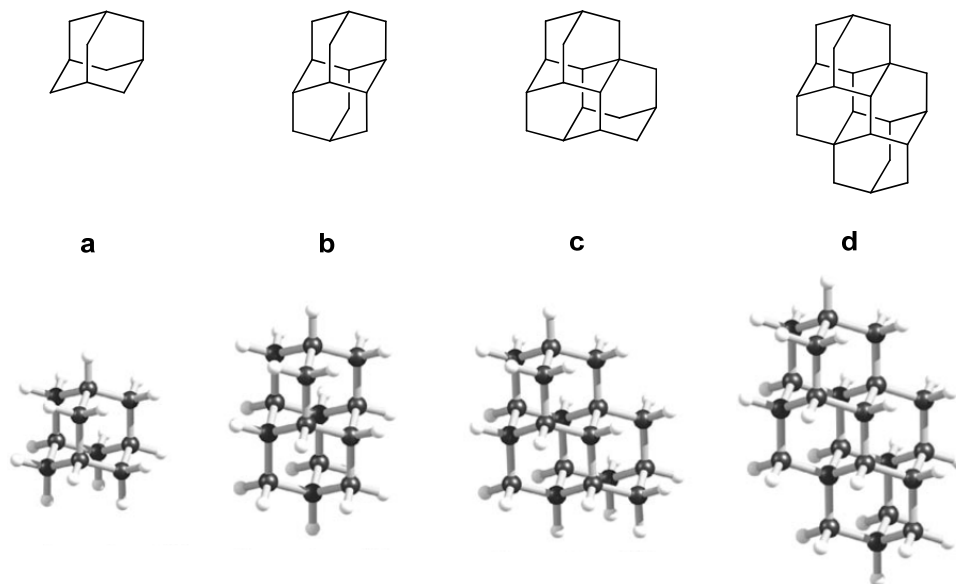


Figure 3.1: Small selection of diamondoids: Adamantane (a), diamantane (b), triamantane (c) and (*anti*)-tetramantane (d).[172]

Adamantane (tricyclo[3.3.1.1^{3,7}]decane) is the simplest diamondoid and a colorless cycloalkane with a campher-like odor. It consists of four cyclohexane

molecules attached in chair conformation, which is the most stable conformation of all isomers with the formula $C_{10}H_6$. It has unique properties because it is both rigid and stress-free. Adamantane was first discovered in petroleum by the Czech chemists S. Landa and V. Machacek in 1933.[174] Due to the carbon atom arrangement, which is the same in the adamantane molecule and the diamond crystal, its name derived from Greek *adamantinos* (meaning of diamond). As an unfunctionalized hydrocarbon, adamantane is not very useful and has only few applications. However, there are many derivatives that are applied in pharmaceutical products, polymers, coating materials and molecular electronics. In collaboration with the research group of Prof. Schreiner it was decided to use the unsaturated adamantane derivative tetracyclo[7.3.1.1^{4,12}.0^{2,7}]tetradeca-6,11-diene (tctd) (Figure 3.2) for the complexation of copper(I) as well as nickel(0).

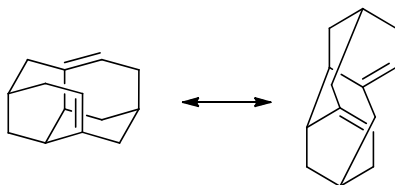


Figure 3.2: Structure of tetracyclo[7.3.1.1^{4,12}.0^{2,7}]tetradeca-6,11-diene (tctd).

The diene tctd is an intermediate in the synthesis of protodiamantane **3.2** (pentacyclo[7.3.1.1^{4,12}.0^{1,7}.0^{6,11}]tetradecane), which is the most likely isomer in the rearrangement sequence leading from tetrahydro-binor-S **3.1**[175] to adamantane **3.3**[176] shown in Figure 3.3.

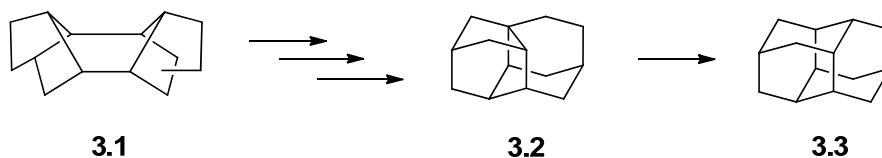


Figure 3.3: Rearrangement sequence from tetrahydro-binor-S (**3.1**) affording adamantane (**3.3**) involving the intermediate protodiamantane (**3.2**).[177]

The synthesis of protodiamantane is achieved by a cleavage-recombination sequence of 1,6-dibromodiamantane **3.4**. Therefore, **3.4** is reductively cleaved by activated zinc powder in dimethylformamide affording the fixed chair diene tetracyclo[7.3.1.1^{4,12}.0^{2,7}] tetradeca-6,11-diene **3.5**. The best conditions for the prep-

3.2 Copper(I) Complexes with tctd

ation of **3.2** from **3.5** involves the reaction with aqueous HBr (48 %) in hexane at 0 °C which gives a mixture of 6-bromodiamantane **3.6** (45 %) and 6-bromoprotodiamantane **3.7** (55 %). After refluxing with tri-*n*-butyl tin hydride in benzene the resulting product protodiamantane (55 %) can be separated by preparative gas chromatography.[177]

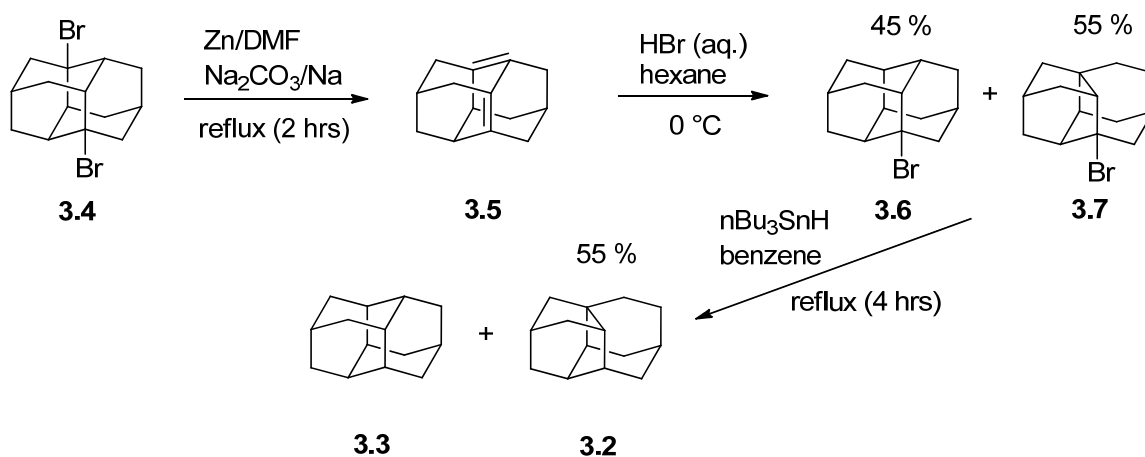


Figure 3.4: Synthesis of protodiamantane (**3.2**) from 1,6-dibromodiamantane involving the diene tctd.[177]

The diene tctd not only has potential as an intermediate for the synthesis of disubstituted diamantanes and protodiamantanes, but also provides a diagnostic tool for the investigation of mechanistic details regarding olefin additions. Furthermore, this derivative could have some potential for the formation of coordination polymers in complex chemistry due to its unsaturated character.

3.2 Copper(I) Complexes with tctd

3.2.1 Molecular Structure of [Cu₂(bipy)₂(tctd)](PF₆)₂

The preparation of a copper(I) complex with the ligand tctd affording [Cu₂(bipy)₂(tctd)](PF₆)₂[143] was successful applying the same experimental conditions as for the related complex [Cu(bipy)(COD)]PF₆. [178] The molecular structure of the cation of the complex is shown in Figure 3.5. The unit cell contains the complex and solvent molecule (acetone) as well as two PF₆⁻ anions.

Both copper centers are coordinated by the two nitrogen atoms of bipy and one double bond of the ligand tctd. Each center has an almost square planar coordination geometry, which is common for ternary copper olefin complexes.[157–159, 161]

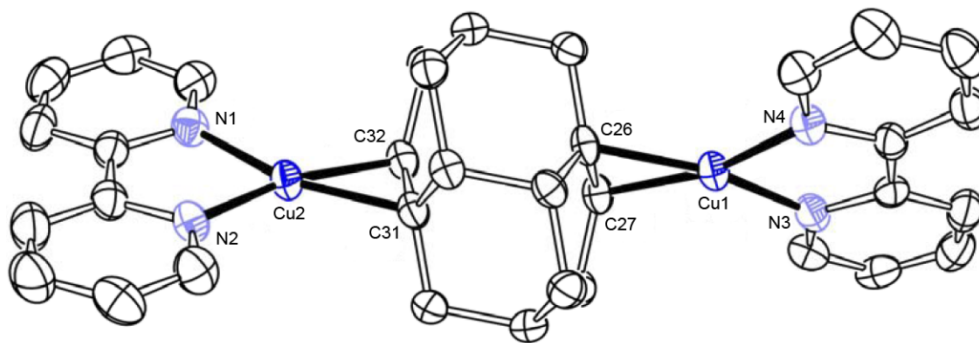


Figure 3.5: ORTEP plot of the cation $[\text{Cu}_2(\text{bipy})_2(\text{tctd})]^{2+}$, hydrogen atoms and solvent molecules are omitted for clarity. Ellipsoids are drawn at 50 % probability level.[143]

Thus, the Cu–N bond lengths have typical values of about 1.99(3) Å and are in good agreement with those found in similar ternary complexes, as well as the values for the Cu–C_{olefin} distances.[157–159, 161] Due to the coordination of copper the double bonds lengths C26–C27 and C31–C32, with values of 1.40(5) Å and 1.38 (6) Å, clearly show a widening compared to the average value of 1.33 Å for uncoordinated double bonds.

3.2.2 Molecular Structure of $[\text{Cu}_2\text{Cl}_2(\text{CH}_3\text{CN})(\text{tctd})]$

The molecular structure of the uncoordinated diene tctd has not been characterized yet due its reactivity and therefore short lifetime. It is only stable by mixing it with copper(I) chloride forming the corresponding complex. It was now possible to determine the molecular structure of the resulting product $[\text{Cu}_2\text{Cl}_2(\text{CH}_3\text{CN})(\text{tctd})]$ (see Figure 3.6). Crystallographic data, bond lengths and angles are presented in Table 3.1 and Table 3.2. The unit cell contains two copper(I) centers, of which Cu2 is coordinated by one double bond of the diene tctd and a chloride anion Cl4. The second copper ion Cu1 is coordinated to the nitrogen of the solvent molecule acetonitrile and another tctd ligand. Both copper centers are bridged by a chloride anion (Cl3) and form a chain consisting of the

3.2 Copper(I) Complexes with tctd

copper(I) complex molecules. A fragment of this chain $[\text{Cu}_2\text{Cl}_2(\text{CH}_3\text{CN})(\text{tctd})]_n$ is shown in Figure 3.7. The coordination sphere of each copper center is almost square planar, which is in line with the copper(I) tctd complex reported by Henß and other similar complexes reported in literature.[143, 157–159, 161] Furthermore, the bond lengths of the coordinated double bonds C1-C12 and C7-C16 of tctd, with values of 1.376(4) Å and 1.389(4) Å, are shorter than in the complex $[\text{Cu}_2(\text{bipy})_2(\text{tctd})](\text{PF}_6)_2$, but still show a widening compared to an average unsubstituted double bond (1.33 Å).

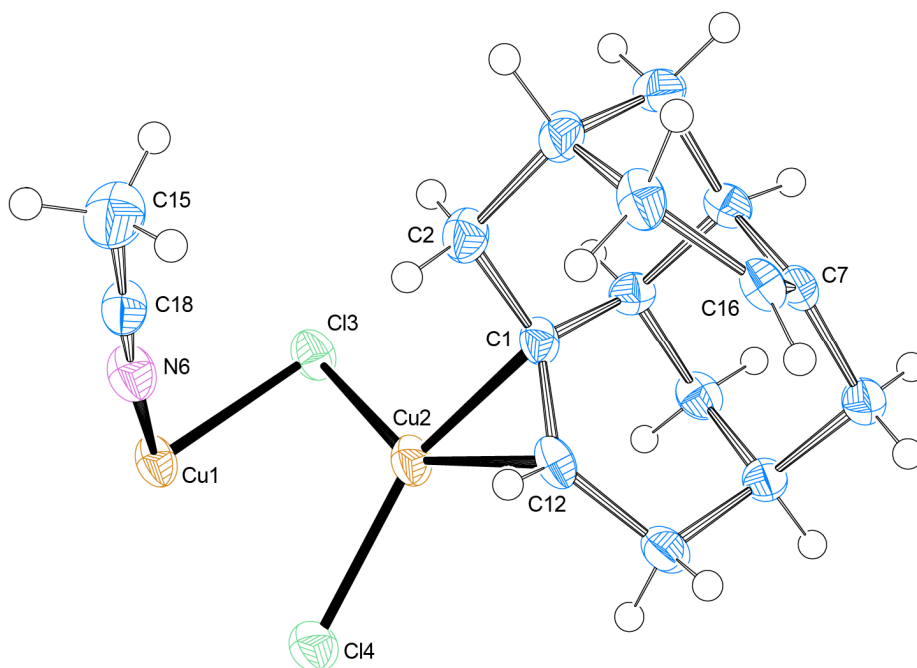


Figure 3.6: ORTEP plot of the full complex molecule $[\text{Cu}_2\text{Cl}_2(\text{CH}_3\text{CN})(\text{tctd})]$. Ellipsoids are drawn at 50 % probability level.

Table 3.1: Crystal data and structure refinement for $[\text{Cu}_2\text{Cl}_2(\text{CH}_3\text{CN})(\text{tctd})]$.

Internal identification code	schindler12048
Empirical formula	$\text{C}_{16} \text{H}_{21} \text{Cl}_2 \text{Cu}_2 \text{N}$
Formula weight	425.32
Temperature	190 (2) K
Wavelength	0.71073 Å
Crystal system, space group	Triclinic, $P\bar{1}$
Unit cell dimensions	$a = 8.4200(17) \text{ Å}$ $\alpha = 85.68(3)^\circ$ $b = 9.3220(19) \text{ Å}$ $\beta = 78.77(3)^\circ$

	$c = 10.383(2) \text{ \AA}$	$\gamma = 84.49(3)^\circ$
Volume	$794.3(3) \text{ \AA}^3$	
Z, calculated density	2, 1.778 Mg/m ³	
Absorption coefficient	3.004 mm^{-1}	
F(000)	432	
Crystal size	0.3 x 0.09 x 0.08 mm	
Theta range for data collection	2.00 to 27.41 $^\circ$	
Limiting indices	$-10 \leq h \leq 10, -12 \leq k \leq 12, -13 \leq l \leq 13$	
Reflections collected / unique	13762 / 3602 [R(int) = 0.0617]	
Completeness to theta = 27.41	99.5 %	
Absorption correction	Empirical	
Refinement method	Full-matrix least-squares on F ²	
Data / restraints / parameters	3602 / 0 / 274	
Goodness-of-fit on F ²	1.016	
Final R indices [I > 2sigma(I)]	R1 = 0.0331, wR2 = 0.0747	
R indices (all data)	R1 = 0.0500, wR2 = 0.0812	
Largest diff. peak and hole	0.436 and -0.569 e. \AA^{-3}	

Table 3.2: Selected bond lengths [\AA] and angles [$^\circ$] for $[\text{Cu}_2\text{Cl}_2(\text{CH}_3\text{CN})(\text{tctd})]$.

C(1)-C(12)	1.376(4)	C(12)-Cu(2)	2.063(3)	Cl(4)-Cu(1)	2.7296(12)
C(1)-C(2)	1.512(4)	Cl(3)-Cu(2)	2.2943(11)	Cu(1)-N(6)	2.006(2)
C(7)-C(16)	1.389(4)	Cl(3)-Cu(1)	2.2949(11)	C(18)-N(6)	1.137(4)
C(1)-Cu(2)	2.062(2)	Cl(4)-Cu(2)	2.2469(10)		
C(12)-C(1)-Cu(2)	70.54(15)	Cl(3)-Cu(1)-Cl(4)	90.88(3)		
C(1)-C(12)-Cu(2)	70.51(15)	C(1)-Cu(2)-C(12)	38.96(11)		
C(16)-C(7)-C(8)	122.4(3)	C(1)-Cu(2)-Cl(4)	146.29(8)		
N(6)-C(18)-C(15)	179.3(4)	C(12)-Cu(2)-Cl(4)	108.18(8)		
Cu(2)-Cl(3)-Cu(1)	77.36(3)	C(1)-Cu(2)-Cl(3)	108.36(8)		
Cu(2)-Cl(4)-Cu(1)	69.61(3)	C(12)-Cu(2)-Cl(3)	147.19(8)		
N(6)-Cu(1)-Cl(3)	100.39(7)	Cl(4)-Cu(2)-Cl(3)	104.59(3)		
N(6)-Cu(1)-Cl(4)	98.07(8)	C(18)-N(6)-Cu(1)	172.1(3)		

3.3 Synthesis of Ni(0) Polymers with tctd

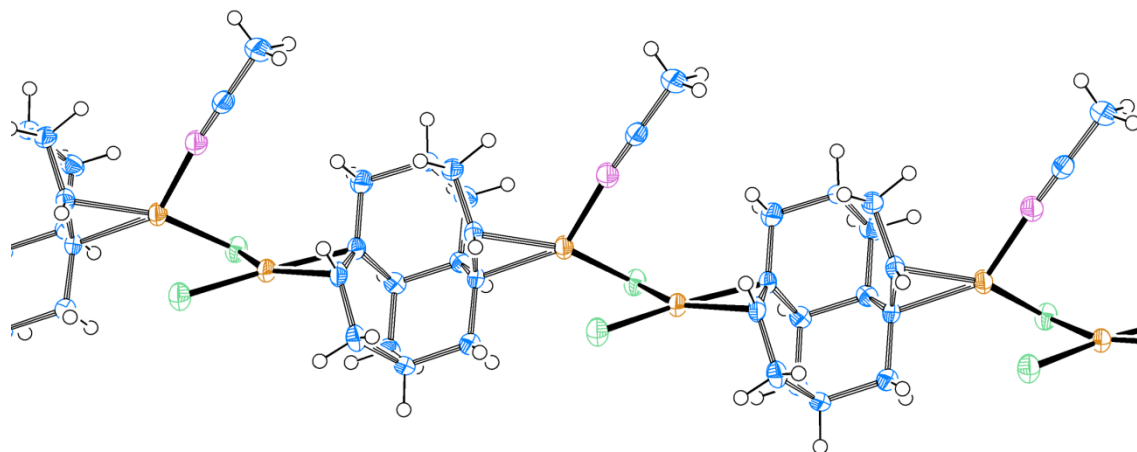


Figure 3.7: ORTEP plot of a fragment of the copper(I) chain $[\text{Cu}_2\text{Cl}_2(\text{CH}_3\text{CN})(\text{tctd})]_n$. Ellipsoids are drawn at 50% probability level.

3.3 Synthesis of Ni(0) Polymers with tctd

There was also great interest in the synthesis of uncharged Ni(0) polymers with the ligand tctd. Therefore, $\text{Ni}(\text{COD})_2$ was used as Ni(0) precursor. By mixing the complex with the ligand tctd, both COD ligands should be replaced to give an uncharged polymeric Ni(0) chain (see Figure 3.8).

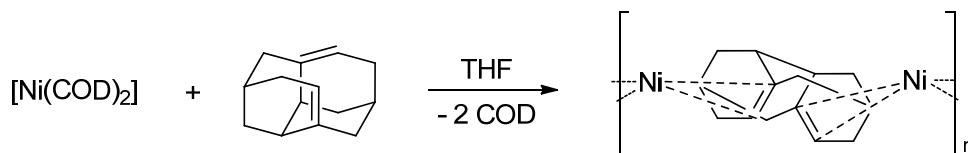


Figure 3.8: Reaction scheme for the synthesis of $[\text{Ni}(\text{tctd})]_n$ in THF.

The optimized molecular structure of $[\text{Ni}_x(\text{tctd})_y]_n$ (Universal force field (UFF)[159]) is shown in Figure 3.9. Mixing the slightly yellow solution of $[\text{Ni}(\text{COD})_2]$ in THF with tctd affords a slightly brown solution after several hours of stirring. Unfortunately, crystals suitable for X-ray diffraction could not be obtained due to its high sensitivity towards traces of dioxygen and autocatalytic reactions.

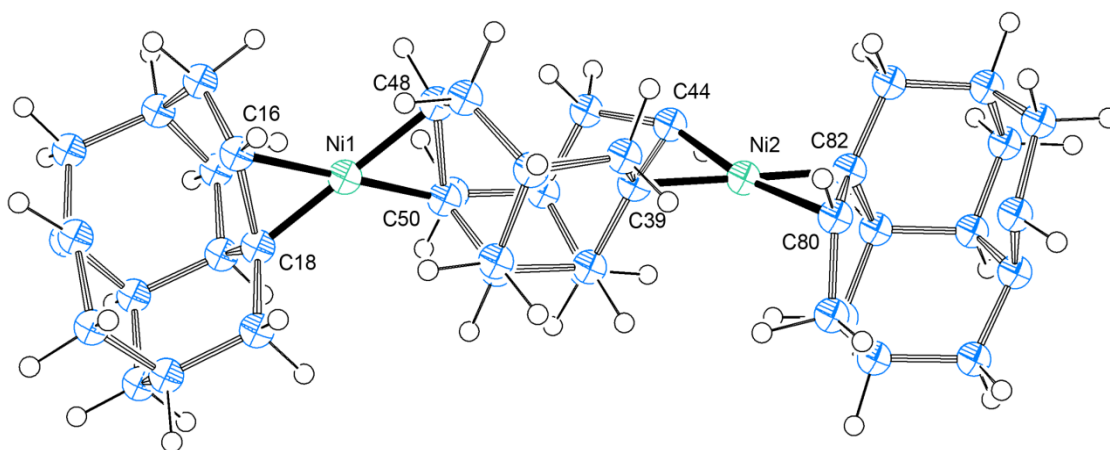


Figure 3.9: Proposed molecular structure for a fragment of the nickel(0) chain $[\text{Ni}_x(\text{tctd})_y]_n$ (UFF optimized).

3.4 Experimental

3.4.1 Materials and Reagents

Commercial reagents were used as obtained without further purification. Solvents were dried according to standard procedures. All handling and storage of oxygen sensitive compounds and materials used was carried out in a glove box (M. Braun, Garching, Germany; $\text{O}_2 < 0.1$ ppm, $\text{H}_2\text{O} < 0.1$ ppm) within an argon atmosphere.

3.4.2 Crystallography

Single crystals suitable for X-ray diffraction were mounted on the tip of a glass rod using inert perfluoropolyether oil. The X-ray crystallographic data were collected on a BRUKER NONIUS FR591 Kappa CCD diffractometer equipped with low temperature systems. Mo- K_α radiation ($\lambda = 0.71073$ Å) and a graphite monochromator was used. The structures were solved by direct methods in SHELXS97 and SHELXL 2013 and refined by using full-matrix least squares in SHELXL97.[179]

3.4 Experimental

3.4.3 Synthesis of tctd

Synthesis of the ligand tetracyclo[7.3.1.1^{4,12}.0^{2,7}] tetradeca-6,11-diene was performed in the research group of Prof. Schreiner (JLU Gießen, Institute for Organic Chemistry) by Boryslav A. Tkachenko.[177]

3.4.4 Synthesis of $[\text{Cu}_2\text{Cl}_2(\text{CH}_3\text{CN})(\text{tctd})]$

$[\text{Cu}_2\text{Cl}_2(\text{CH}_3\text{CN})(\text{tctd})]$ was synthesized by mixing copper(I)chloride with the ligand tctd in order to stabilize the diene by B. A. Tkachenko.[177] Crystals suitable for X-ray diffraction studies were obtained by recrystallization from acetonitrile.

3.4.5 Synthesis of $[\text{Ni}_x(\text{tctd})_y]_n$

Preparation of the ligand tctd was done by stirring 275 mg (0.716 mmol) of $[\text{Cu}_2\text{Cl}_2(\text{tctd})]$ in ammonia solution for several hours. After extraction with diethyl ether the organic layer was separated and dried over anhydrous MgSO_4 . Evaporation of the solvent afforded 124 mg (0.666 mmol, 93 %) of tctd. The free ligand is stable for approx. 2-3 hours. To synthesize the Ni(0) complex the ligand was transferred into the glove box.

To a stirred slightly yellow solution of 70 mg (0.25 mmol) of $[\text{Ni}(\text{COD})_2]$ in THF 124 mg of tctd (0.666 mmol) was added. The resulting light brown solution was stirred furthermore for several hours. Diffusion of n-pentane into the solution at -20 °C did not result in crystals suitable for X-ray structure determination. The molecular structure of $[\text{Ni}_x(\text{tctd})_y]_n$ was optimized using Avogadro's structure optimization set to Universal Force Field (UFF) with steepest descent (iterative optimization algorithm; convergence at 10e^{-7}).[159]

4 Ni(0) and Cu(I) Complexes with the Ligand O-BPy and Derivatives

4.1 Introduction

It is well known that various Ni(0) complexes induce catalytic reactions, such as oligomerization of alkenes, dienes and alkynes as well as C-C coupling reactions (see 1.4). In this regard, studies on ligand exchange reactions of the Ni(0) complex bis(cyclooctadiene)nickel(0) were performed in our research group previously.[19, 140, 139] $[\text{Ni}(\text{COD})_2]$ undergoes various ligand exchange reactions due to its labile ligand COD, which can be easily displaced by other ligands and is therefore widely used as Ni(0) precursor complex.

As previously reported in literature $[\text{Ni}(\text{COD})_2]$ reacts with 2,2'-bipyridine (bipy) in a 1:1 ratio in THF to afford the complex $[\text{Ni}(\text{bipy})(\text{COD})]$ (see Figure 4.1).[180] In this reaction one COD molecule is replaced by the ligand bipy.

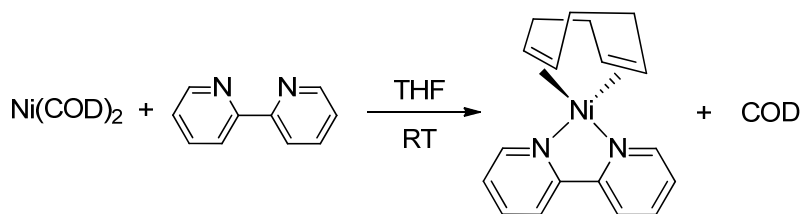


Figure 4.1: Reaction scheme for the synthesis of $[\text{Ni}(\text{bipy})(\text{COD})]$. [180]

Efforts to synthesize a binuclear nickel(0) complex using an open-ended tetradentate ligand and to investigate the formation kinetically were performed in our group by M. Leibold.[141] Therefore, 1,2-bis(2,2'-bipyridine-6-yl)ethane (O-BPy) (Figure 4.2), which consists of two bipyridyl units bridged by ethane, was synthesized from 2,2'-bipyridine[181] and reacted with $[\text{Ni}(\text{COD})_2]$.

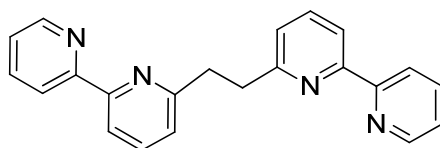


Figure 4.2: Structure of 1,2-bis(2,2'-bipyridine-6-yl)ethane (O-BPy). [181]

Mixing $[\text{Ni}(\text{COD})_2]$ with O-BPy in THF resulted in a dark green complex solution. Diffusion of pentane into the solution led to the formation of dark green crystals suitable for X-ray diffraction.[141] Analogue to the reaction with bipy, a binuclear complex with two nickel centers, the ligand O-BPy and two coordinated COD molecules, was expected (see Figure 4.3).

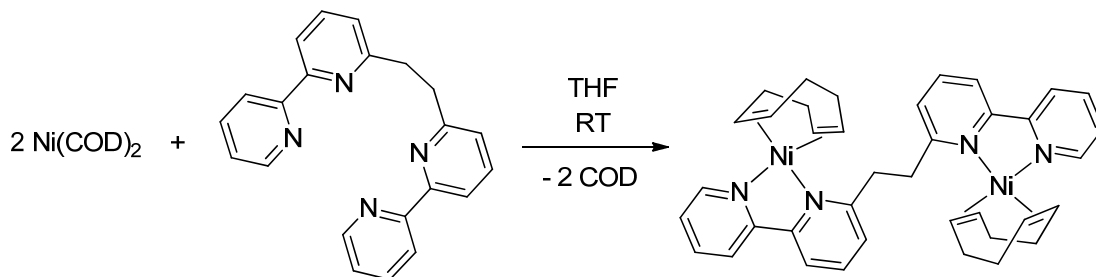


Figure 4.3: Reaction scheme for the synthesis of $[\text{Ni}_2(\text{O-BPy})(\text{COD})_2]$.

Surprisingly, the X-ray diffraction studies showed a binuclear complex with coordinated 1,3-butadiene. Instead of COD, one molecule of butadiene was coordinated to each nickel center (see Figure 4.4). The molecular structure of the complex is shown in Figure 4.5.[141]

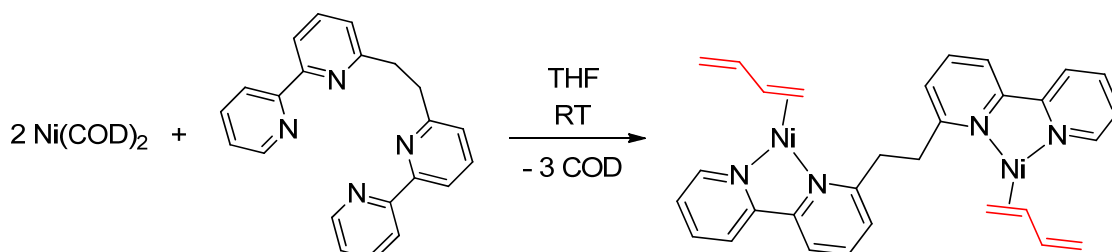


Figure 4.4: Reaction scheme for the synthesis of $[\text{Ni}_2(\text{O-BPy})(\eta^2\text{-C}_4\text{H}_6)_2]$.

Both nickel centers, which are identical due to an inversion center between C11 and C11a, are bridged by the ligand O-BPy and coordinated to one double bond, C12-C13 / C12a-C13a, of a butadiene molecule. Therefore, the geometry of the nickel(0) complex $[\text{Ni}_2(\text{O-BPy})(\eta^2\text{-C}_4\text{H}_6)_2]$ can be best described as trigonal planar. The two nickel atoms are separated by 8.092 Å.

4.1 Introduction

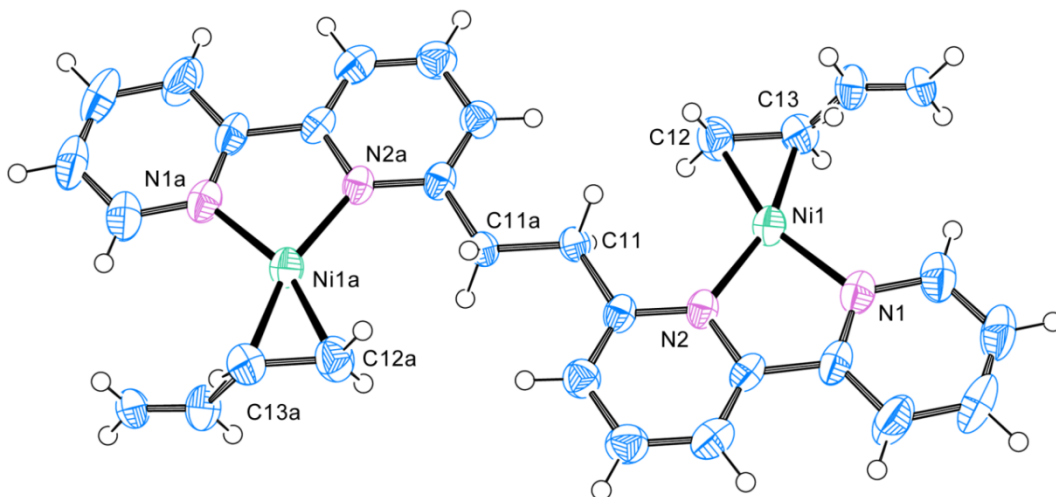


Figure 4.5: ORTEP plot of the binuclear complex $[\text{Ni}_2(\text{O-BPy})(\eta^2\text{-C}_4\text{H}_6)_2]$. Ellipsoids are drawn at 50% probability level.[141]

The only comparable and reported binuclear nickel complex with coordinated butadiene is the structurally characterized complex $[\mu\text{-C}_4\text{H}_6\text{-}\{\text{Ni}_2(\eta^2\text{-C}_4\text{H}_6)_2(\text{bipy})_2\}]$. [182] However, since no butadiene was used as an educt in this reaction a cleavage of COD was supposed (see Figure 4.4). As described above, Ni(0) catalyzes the cyclooligomerization of 1,3-butadiene to COD amongst other isomers (see 1.4.1.2). Within a collaboration with the research group of Prof. M. C. Holthausen (Goethe University Frankfurt am Main, Institute for Inorganic and Analytical Chemistry) a mechanism for the cleavage of COD was proposed (see Figure 4.6).[141]

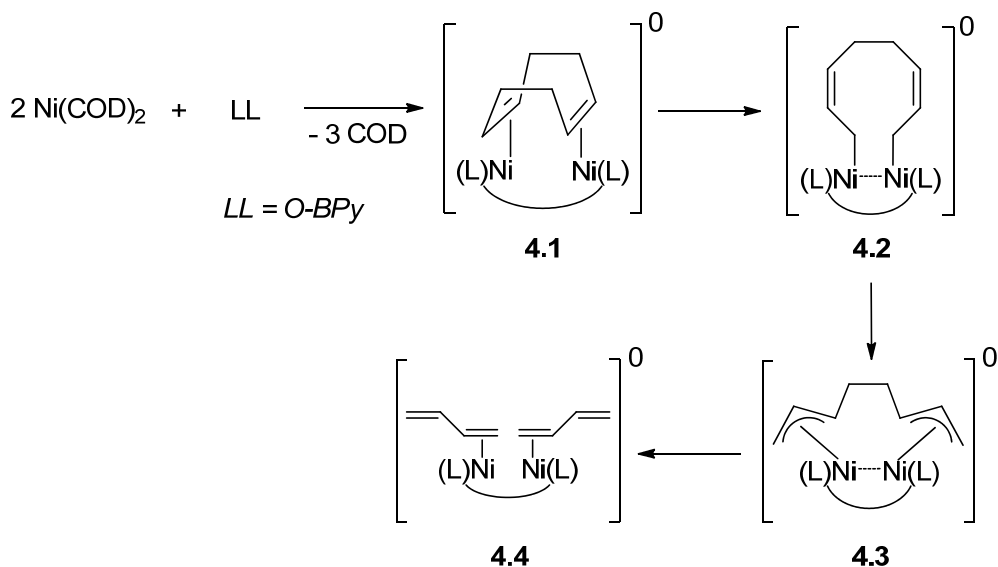


Figure 4.6: Proposed mechanism for the cleavage of 1,5-cyclooctadiene.[141]

This mechanism involves the formation of a $\mu-(\eta^2, \eta^2\text{-COD})\text{-Ni}_2\text{-(O-BPy)}$ intermediate **4.1**, which reacts to a $\mu-(\eta^1, \eta^1\text{-})$ -allylic complex **4.2** and a $\mu-(\eta^3, \eta^3\text{-})$ -allylic complex **4.3**. In the final step, the complex $[\text{Ni}_2(\text{O-BPy})(\eta^2\text{-C}_4\text{H}_6)_2]$ **4.4** is formed by a cleavage reaction and coordination of butadiene. The allylic complexes also occur as intermediates in the catalytic cycle of the technical synthesis of COD shown in Figure 4.7.[8] The mechanism for the formation of $[\text{Ni}_2(\text{O-BPy})(\eta^2\text{-C}_4\text{H}_6)_2]$ therefore can be described as a back reaction of the cyclodimerization of butadiene.

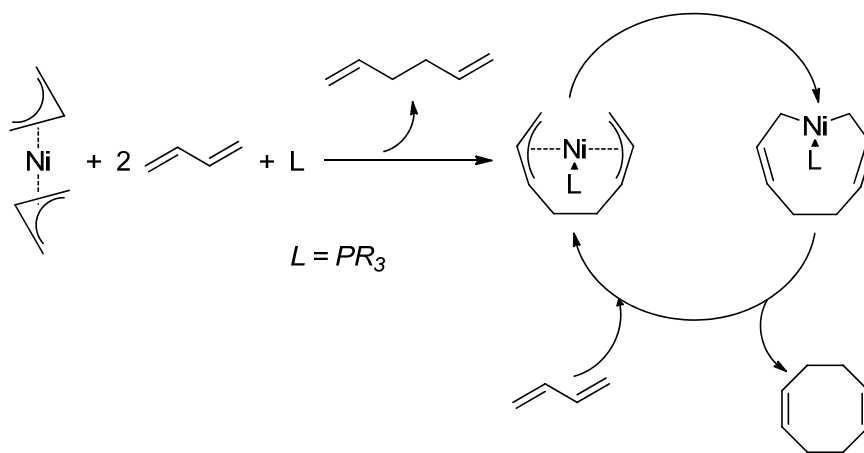


Figure 4.7: Catalytic cyclodimerization of 1,3-butadiene to 1,5-cyclooctadiene.

Furthermore, the Gibbs energy for the reaction of COD to two molecules of butadiene was calculated by Puneet Gupta in the research group of Prof. Holthausen (see Figure 4.8).

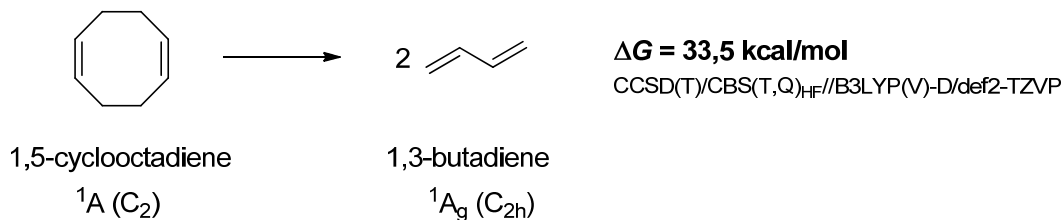


Figure 4.8: Calculated Gibbs energy for the reaction of one molecule of 1,5-cyclooctadiene to two molecules of 1,3-butdiene.[183]

Due to the fact that one molecule of 1,5-cyclooctadiene is more stable than two molecules of butadiene, the driving force of the formation of the complex has to be the coordination of butadiene and the presence of two nickel centers. Further

4.1 Introduction

DFT calculations for the formation of a binuclear as well as a mononuclear nickel complex with O-BPy and Gibbs energies are shown in Figure 4.9. These calculations showed that the formation of $[\text{Ni}(\text{O-BPy})]$ should be even more spontaneous than the formation of $[\text{Ni}_2(\text{O-BPy})(\text{COD})_2]$. Therefore, the obtained complex $[\text{Ni}_2(\text{O-BPy})(\eta^2\text{-C}_4\text{H}_6)_2]$ was a remarkable result.

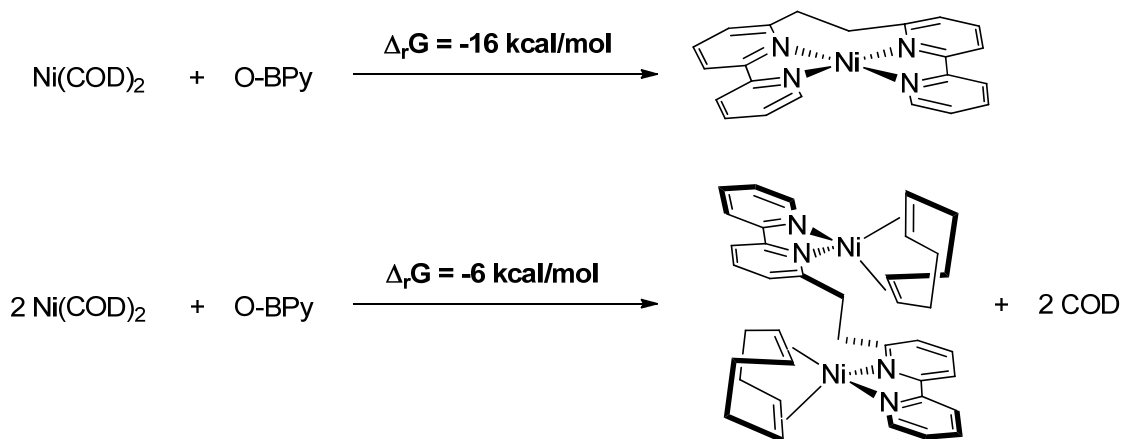


Figure 4.9: Calculated Gibbs energies for the formation of $[\text{Ni}(\text{O-BPy})]$ and $[\text{Ni}_2(\text{O-BPy})(\eta^2\text{-C}_4\text{H}_6)_2]$. [183]

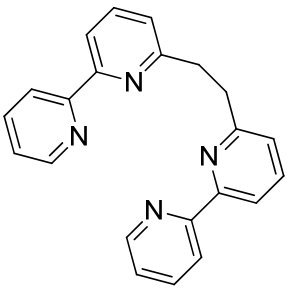
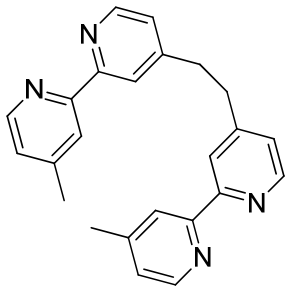
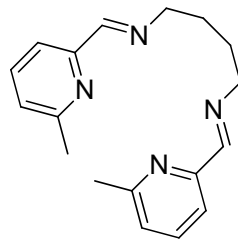
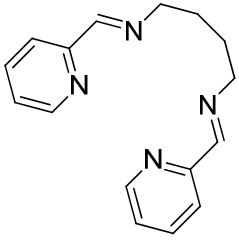
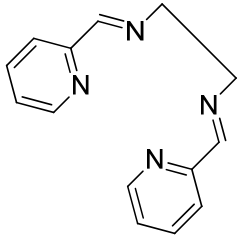
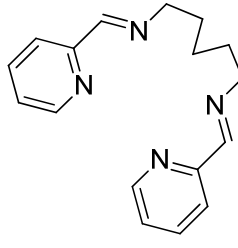
Because of different theoretical findings by Holthausen and co-workers, investigations on this reaction and its mechanism were performed in more detail.

4.2 Results

Experiments on the formation of the nickel(0) complex $[\text{Ni}_2(\text{O-BPy})(\eta^2\text{-C}_4\text{H}_6)_2]$ were repeated. Additionally, several derivatives of the ligand system O-BPy were used to investigate their influence on the formation of the respective nickel complexes (see Table 4.1).

Furthermore, Cu(I) salts were reacted with O-BPy to afford a dinuclear isoelectronic copper(I) complex which should be compared to the obtained nickel(0) complex.

Table 4.1: Ligands used in the synthesis of Ni(0) complexes.

1,2-bis(2,2'-bipyridine-6-yl)ethane (O-BPy)	1,2-bis(4'-methyl-2,2'-bipyridine-4-yl)ethane (Me-BPy)	<i>N,N'</i> -bis((6-methylpyridine-2-yl)methylene)butane-1,4-diamine (mpmbd)
		
<i>N,N'</i> -bis(pyridine-2-ylmethylene)butane-1,4-diamine (pmbd)	<i>N,N'</i> -bis(pyridine-2-ylmethylene)ethane-1,2-diamine (pmed)	<i>N,N'</i> -bis(pyridine-2-ylmethylene)pentane-1,5-diamine (pmpd)
		

4.2.1 Ligands

4.2.1.1 O-BPy

1,2-Bis(2,2'-bipyridine-6-yl)ethane (O-BPy) was synthesized in a two-step reaction according to a procedure described in literature.[181] The intermediate 6-methyl-2,2'-bipyridine **4.7** was obtained by methylation of 2,2'-bipyridine **4.5** in the 6-position with methyllithium and a subsequent oxidation of the reduced intermediate **4.6** with KMnO_4 (see Figure 4.10).

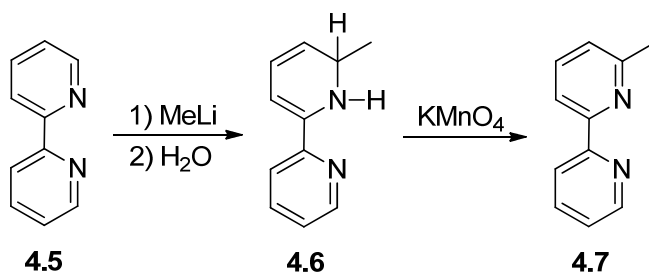


Figure 4.10: Synthesis of 6-methyl-2,2'-bipyridine.

Metalation of **4.7** with lithium diisopropylamide and coupling of the intermediate **4.8** with 1,2-dibromoethane afforded the tetradendate ligand O-BPy **4.9** (see Figure 4.11).

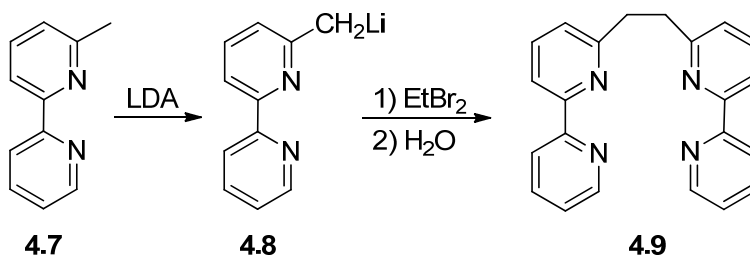


Figure 4.11: Synthesis of 1,2-bis(2,2'-bipyridine-6-yl)ethane.

Recrystallization from methanol gave pale yellow crystals suitable for X-ray diffraction. The determined molecular structure of O-BPy, which is in accordance with the reported protonated ligand structure $\text{O-BPy} \cdot 2 \text{ HBF}_4$ by Seddon et al.[184], is shown in Figure 4.12. Crystallographic data as well as selected bond lengths and angles are given in Table 4.2 and Table 4.3.

The sp^2 -hybridization and aromatic character of the two pyridine units can be shown by obtained bond lengths ranging between 1.3402 (15) Å and 1.3957(16) Å and bond angles of about 120°. The bond lengths of C5-C6 and C5a-C6a between the two pyridyl rings are much larger with 1.4907(16) Å due to their non-aromatic character. Furthermore, both bipyridine units are at an angle of 111.98(12)° to each other for the smallest possible steric effect.

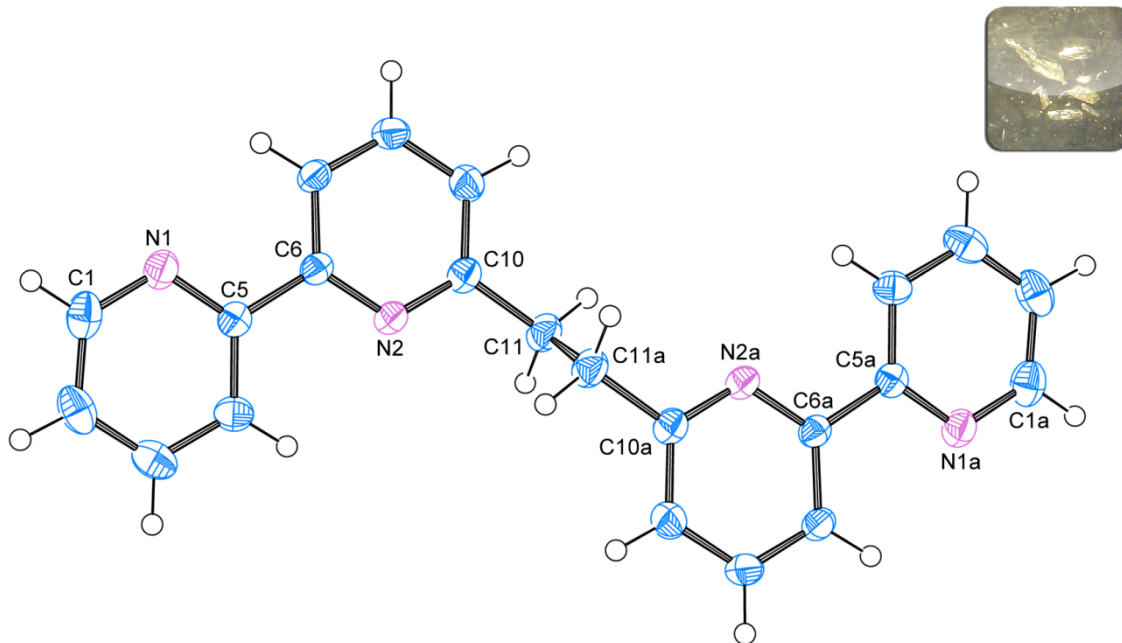


Figure 4.12: ORTEP plot of the ligand O-BPy. Ellipsoids are drawn at 50% probability level.

Table 4.2: Crystal data and structure refinement for O-BPy.

Internal identification code	schindler14036
Empirical formula	C ₂₂ H ₁₈ N ₄
Formula weight	338.40
Temperature	150 (2) K
Wavelength	0.71073 Å
Crystal system, space group	Monoclinic, $P2_1/n$
Unit cell dimensions	$a = 6.5720(13)$ Å $\alpha = 90^\circ$ $b = 11.946(2)$ Å $\beta = 90.00(3)^\circ$ $c = 11.040(2)$ Å $\gamma = 90^\circ$
Volume	866.7(3) Å ³
Z, calculated density	2, 1.297 Mg/m ³

4.2 Results

Absorption coefficient	0.079 mm ⁻¹
F(000)	356
Crystal size	0.500 x 0.330 x 0.300 mm
Theta range for data collection	2.512 to 27.494 °
Limiting indices	-8≤h≤8, -15≤k≤15, -14≤l≤13
Reflections collected / unique	10053 / 1959 [R(int) = 0.0541]
Completeness to theta = 25.242	99.0 %
Absorption correction	Empirical
Refinement method	Full-matrix least-squares on F ²
Data / restraints / parameters	1959 / 0 / 118
Goodness-of-fit on F ²	1.044
Final R indices [I>2sigma(I)]	R1 = 0.0447, wR2 = 0.1186
R indices (all data)	R1 = 0.0545, wR2 = 0.1268
Extinction coefficient	n/a
Largest diff. peak and hole	0.200 and -0.208 e. Å ⁻³

Table 4.3: Selected bond lengths [Å] and angles [°] for **O-BPy**.

N(1)-C(1)	1.3402(15)	N(2)-C(10)	1.3428(14)	C(11)-C(11a)	1.529(2)
N(1)-C(5)	1.3477(14)	C(5)-C(6)	1.4907(16)		
N(2)-C(6)	1.3448(14)	C(10)-C(11)	1.5096(15)		
<hr/>					
C(1)-N(1)-C(5)	116.94(10)	N(2)-C(6)-C(5)	116.27(9)		
C(6)-N(2)-C(10)	118.15(9)	N(2)-C(10)-C(11)	115.92(10)		
N(1)-C(5)-C(6)	116.57(9)	C(10)-C(11)-C(11a)	111.98(12)		

4.2.1.2 Mpmbd

The tetradentate Schiff base ligand *N,N*-Bis((6-methylpyridine-2-yl)methylene)butane-1,4-diamine (mpmbd) was synthesized as previously reported in literature.[185] In a condensation reaction 6-methylpyridine-2-carboxaldehyde was reacted with 1,4-diaminobutane in dehydrated ethanol and refluxed for several hours (Figure 4.13).

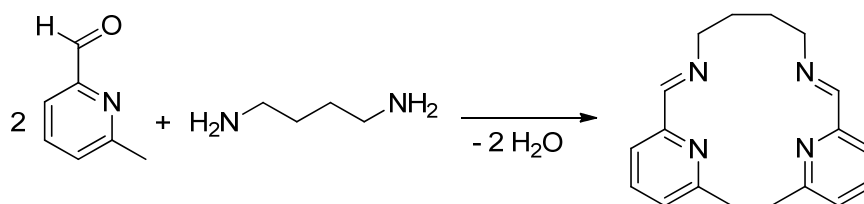


Figure 4.13: Synthesis of *N,N'*-Bis((6-methylpyridine-2-yl)methylene)butane-1,4-diamine.

The ligand was recrystallized from EtOH/H₂O (5:1 volume ratio) and crystals suitable for X-ray diffraction could be obtained. The molecular structure of mpmbd is shown in Figure 4.14. Crystallographic data, bond lengths and bond angles are presented in Table 4.4 and Table 4.5. Mpmbd has an inversion center between C8 and C8a and both symmetrical units are separated by 1.521(2) Å which is almost the same as for the ligand O-BPy. The bond angle between C8a-C8-C7 is also 113.48(13)° to obtain the smallest steric hindrance.

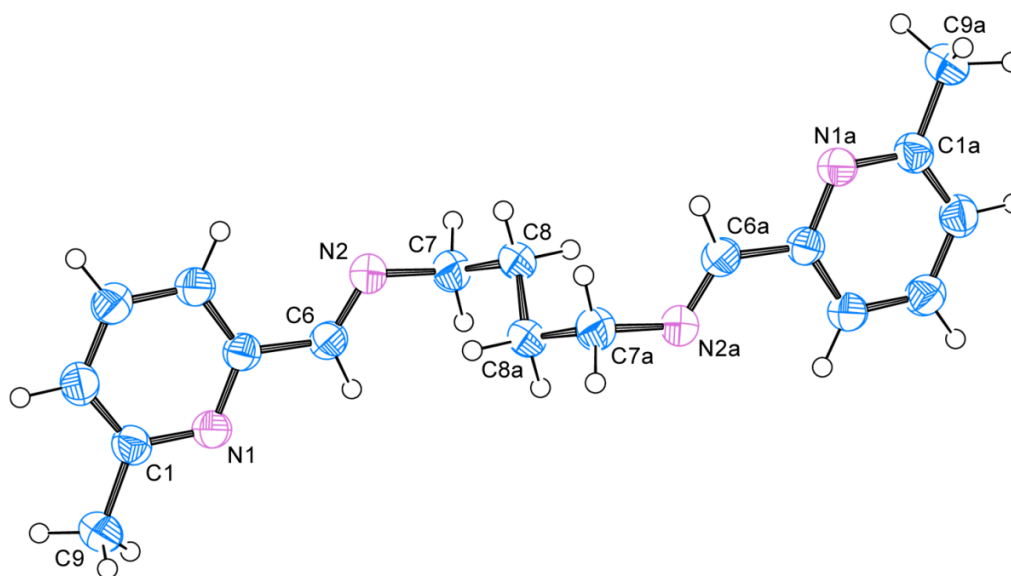


Figure 4.14: ORTEP plot of the ligand mpmbd. Ellipsoids are drawn at 50 % probability level.

Table 4.4: Crystal data and structure refinement for mpmbd.

Internal identification code	schindler13008
Empirical formula	C ₉ H ₁₁ N ₂
Formula weight	147.20

4.2 Results

Temperature	190 (2) K
Wavelength	0.71073 Å
Crystal system, space group	Monoclinic, $P2_1/c$
Unit cell dimensions	$a = 4.8920(10)$ Å $\alpha = 90^\circ$ $b = 21.201(4)$ Å $\beta = 102.06(3)^\circ$ $c = 8.0630(16)$ Å $\gamma = 90^\circ$
Volume	817.8(3) Å ³
Z, calculated density	4, 1.196 Mg/m ³
Absorption coefficient	0.073 mm ⁻¹
F(000)	316
Crystal size	0.500 x 0.300 x 0.100 mm
Limiting indices	$-6 \leq h \leq 6$, $-27 \leq k \leq 23$, $-9 \leq l \leq 10$
Reflections collected / unique	8132 / 1880 [R(int) = 0.0419]
Completeness to $\theta = 25.242$	99.7 %
Absorption correction	Empirical
Max. and min. transmission	0.69044 and 0.57072
Refinement method	Full-matrix least-squares on F ²
Data / restraints / parameters	1880 / 0 / 157
Goodness-of-fit on F ²	1.022
Final R indices [I > 2sigma(I)]	R1 = 0.0402, wR2 = 0.0937
R indices (all data)	R1 = 0.0613, wR2 = 0.1038
Extinction coefficient	n/a
Largest diff. peak and hole	0.116 and -0.158 e. Å ⁻³

Table 4.5: Selected bond lengths [Å] and angles [°] for mpmbd.

C(1)-N(1)	1.3452(16)	N(2)-C(6)	1.2637(15)	C(7)-C(8)	1.5212(19)
C(1)-C(9)	1.5012(18)	N(2)-C(7)	1.4592(16)	C(8)-C(8a)	1.521(2)
N(1)-C(1)-C(9)	116.11(12)	N(2)-C(7)-C(8)	110.80(11)		
C(6)-N(2)-C(7)	117.47(10)	C(8a)-C(8)-C(7)	113.48(13)		

4.2.1.3 Pmed, pmbd, pmpd

The ligands *N,N'*-bis(pyridine-2-ylmethylene)ethane-1,2-diamine (pmed) **4.10**, *N,N'*-bis(pyridine-2-ylmethylene)butane-1,4-diamine (pmbd) **4.11** and *N,N'*-bis(pyridine-2-ylmethylene)pentane-1,5-diamine (pmpd) **4.12** were synthesized analogue to a procedure described in literature.[185] In a condensation reaction pyridine-2-carboxaldehyde was reacted with 1,2-diaminoethane, 1,4-diaminobutane and 1,5-diaminopentane in dehydrated ethanol and refluxed for several hours to give the corresponding Schiff bases (Figure 4.15).

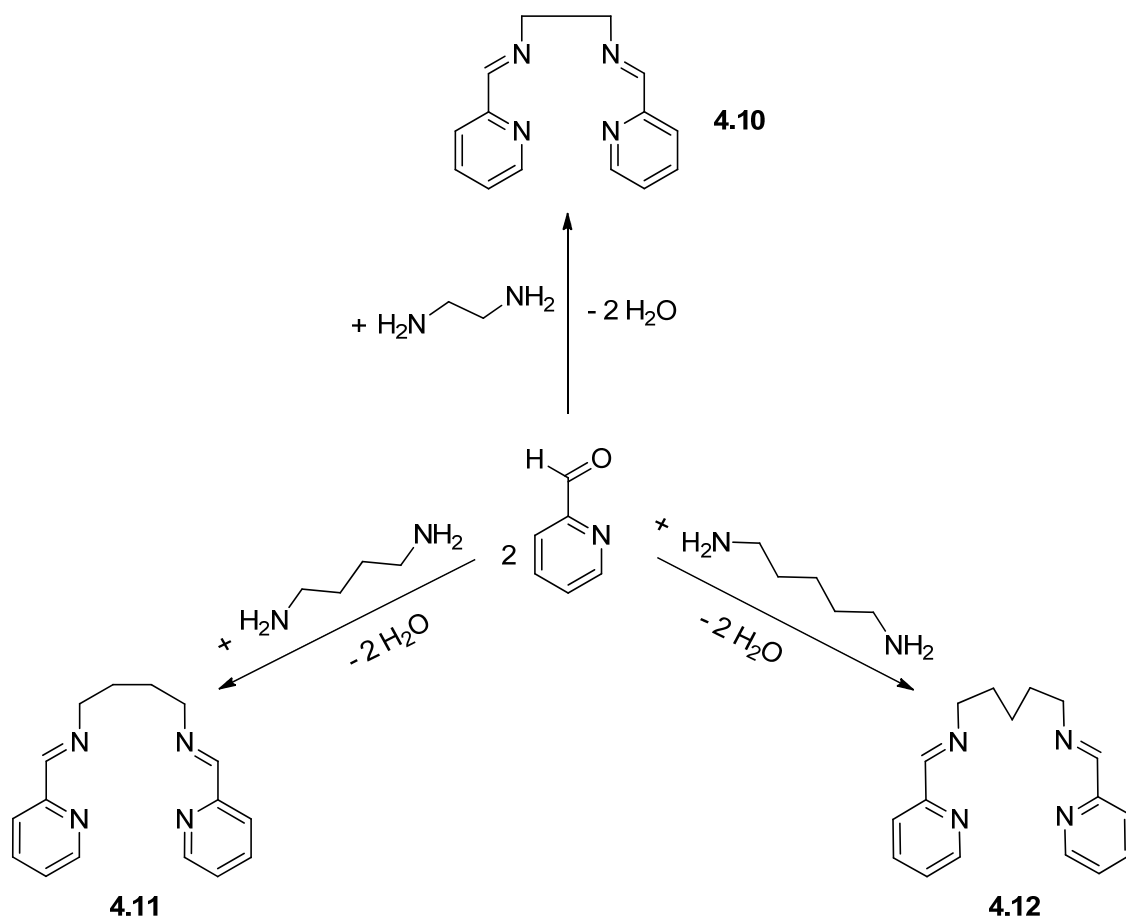


Figure 4.15: Synthesis of *N,N'*-bis(pyridine-2-ylmethylene)ethane-1,2-diamine (**4.10**), *N,N'*-bis(pyridine-2-ylmethylene)butane-1,4-diamine (**4.11**), and *N,N'*-bis(pyridine-2-ylmethylene)pentane-1,5-diamine (**4.12**).

Cooling of a saturated solution of pmbd in methanol to -20 °C afforded crystals suitable for X-ray diffraction after several days. The molecular structure of pmbd is shown in Figure 4.16. Crystallographic data, bond lengths and bond angles are given in Table 4.6 and Table 4.7. Pmbd has an inversion center be-

4.2 Results

tween C8 and C8a and both symmetrical units are separated by 1.523(3) Å which is almost the same as for the ligand O-BPy and mpmbd. Likewise, the ligand has an elongated structure to obtain the smallest steric hindrance.

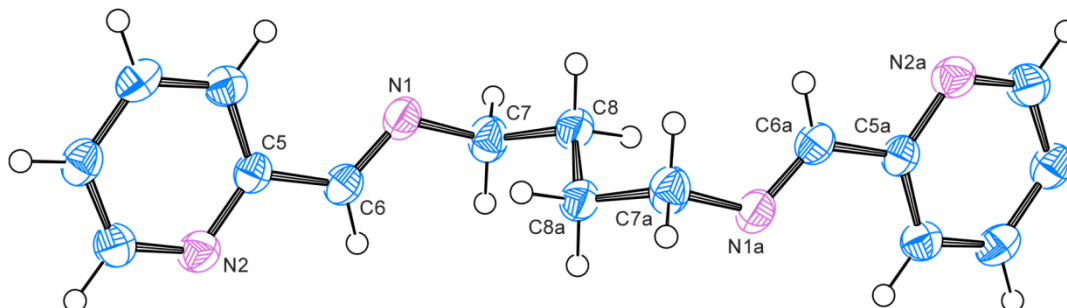


Figure 4.16: ORTEP plot of the ligand pmbd. Ellipsoids are drawn at 50 % probability level.

Table 4.6: Crystal data and structure refinement for pmbd.

Internal identification code	schindler14040
Empirical formula	C ₁₆ H ₁₈ N ₄
Formula weight	266.34
Temperature	150 (2) K
Wavelength	0.71073 Å
Crystal system, space group	Monoclinic, $P2_1/c$
Unit cell dimensions	$a = 9.2010(18) \text{ Å}$ $\alpha = 90^\circ$ $b = 8.8580(18) \text{ Å}$ $\beta = 107.28(3)^\circ$ $c = 9.3030(19) \text{ Å}$ $\gamma = 90^\circ$
Volume	724.0(3) Å ³
Z, calculated density	2, 1.222 Mg/m ³
Absorption coefficient	0.076 mm ⁻¹
F(000)	284
Crystal size	0.860 x 0.300 x 0.100 mm
Theta range for data collection	2.318 to 27.496 °
Limiting indices	-11 ≤ h ≤ 11, -11 ≤ k ≤ 11, -12 ≤ l ≤ 12
Reflections collected / unique	11105 / 1654 [R(int) = 0.1632]
Completeness to theta = 25.242	99.9 %
Absorption correction	Empirical

Max. and min. transmission	0.69044 and 0.57072
Refinement method	Full-matrix least-squares on F ²
Data / restraints / parameters	1654 / 0 / 91
Goodness-of-fit on F ²	1.024
Final R indices [I>2sigma(I)]	R1 = 0.0494, wR2 = 0.1219
R indices (all data)	R1 = 0.0700, wR2 = 0.1320
Extinction coefficient	n/a
Largest diff. peak and hole	0.184 and -0.216 e. Å ⁻³

Table 4.7: Selected bond lengths [Å] and angles [°] for pmbd.

C(6)-N(1)	1.2661(17)	N(1)-C(7)	1.2637(15)	C(7)-C(8)	1.5179(19)
C(5)-N(2)	1.3450(18)	C(5)-C(6)	1.4799(17)	C(8)-C(8a)	1.523(3)
N(2)-C(5)-C(6)	115.20(11)	C(6)-N(1)-C(7)	117.21(12)		
C(5)-C(6)-N(1)	122.02(13)	C(7)-C(8)-C(8a)	113.70(14)		

Crystals of the ligands pmed and pmpd suitable for X-ray diffraction could not be obtained during this work.

4.2.1.4 Me-BPy

The ligand 1,2-bis(4'-methyl-2,2'-bipyridine-4-yl)ethane was purchased commercially from Tokyo Chemical Industry Co., TCI (Japan).

4.2.2 Ni(0) Complexes

The nickel(0) complexes were synthesized by reacting the ligands with the precursor complex $[\text{Ni}(\text{COD})_2]$ in different ratios. Derivatives of the ligand O-BPy were used to change the properties of the system and to investigate their influence on the formation of the complexes.

4.2.2.1 $[\text{Ni}(\text{O-BPy})]$

$[\text{Ni}(\text{COD})_2]$ was mixed in a 2:1 as well as in a 1:1 ratio with the ligand O-BPy in THF at room temperature for several hours (see Figure 4.17). The color of the solution turned immediately from yellow to dark blue. Crystals suitable for X-ray diffraction could be obtained by slow diffusion of n-pentane into a THF solution at $-20\text{ }^\circ\text{C}$. The molecular structure shown in Figure 4.18 shows the mononuclear complex $[\text{Ni}(\text{O-BPy})]$. Crystallographic data, selected bond lengths and bond angles are given in Table 4.8 and Table 4.9. Contrary to previous results, the formation of the binuclear complex $[\text{Ni}_2(\text{O-BPy})(\eta^2\text{-C}_4\text{H}_6)_2]$ could not be observed during this work.

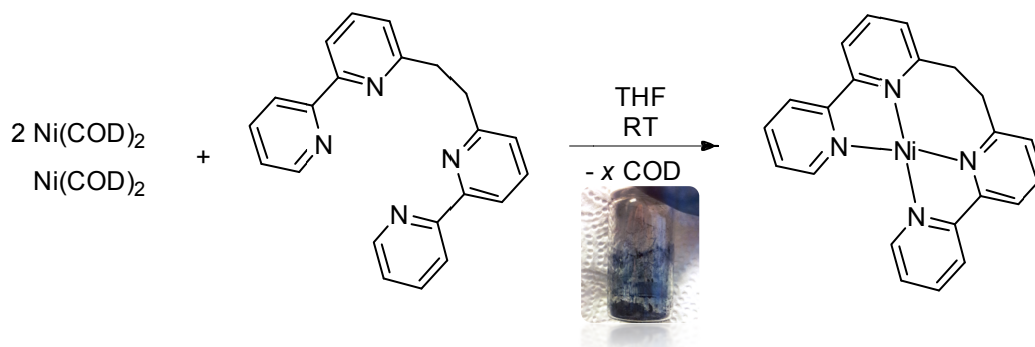


Figure 4.17: Reaction scheme for the synthesis of $[\text{Ni}(\text{O-BPy})]$ using Ni/ligand ratios of 2:1 and 1:1.

The determined structure of $[\text{Ni}(\text{O-BPy})]$ shows a distorted tetrahedral coordination of the nickel center by the four nitrogen atoms of the ligand. The Ni–N bond lengths with distances of 1.920(6) and 1.964(2) Å are similar to those in the binuclear complex obtained by M. Leibold[141] and comparable to other nickel(0) complexes with 2,2'-bipyridine reported in literature.[46, 142,143]. The C–C bond length between C11–C12 of the coordinated O-BPy ligand (1.559(10) Å) is only slightly larger than in the free molecule (1.529(2) Å).

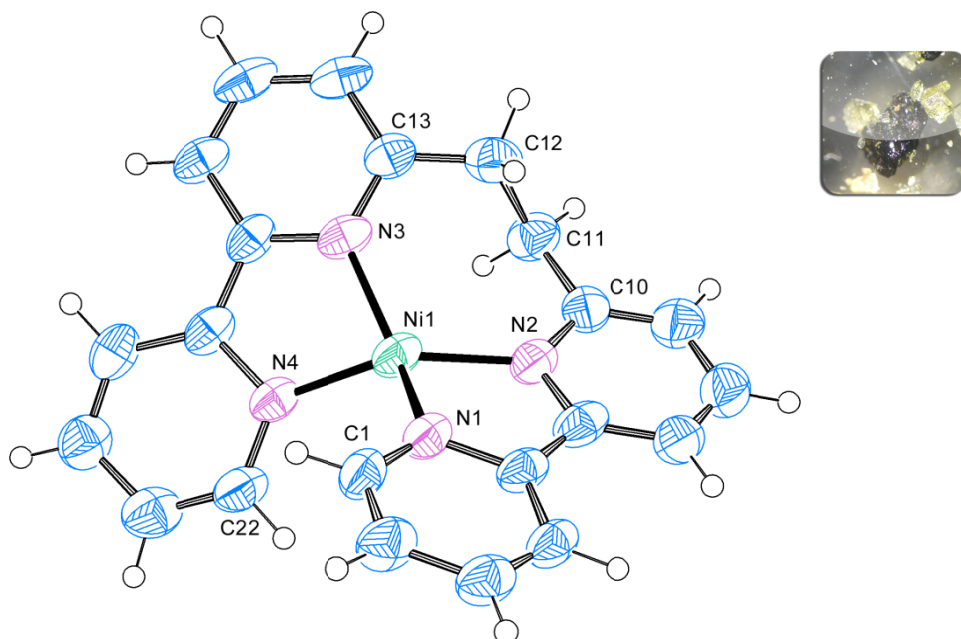


Figure 4.18: ORTEP plot of the full complex molecule [Ni(O-BPy)]. Ellipsoids are drawn at 50 % probability level. Solvent molecules are omitted for clarity.

Table 4.8: Crystal data and structure refinement for [Ni(O-BPy)].

Internal identification code	schindler12076
Empirical formula	C ₄₇ H ₃₆ N ₈ Ni ₂ O
Formula weight	846.26
Temperature	190 (2) K
Wavelength	0.71073 Å
Crystal system, space group	Monoclinic, <i>C2/c</i>
Unit cell dimensions	$a = 27.345(6) \text{ Å}$ $\alpha = 90^\circ$ $b = 9.6750(19) \text{ Å}$ $\beta = 104.61(3)^\circ$ $c = 29.131(6) \text{ Å}$ $\gamma = 90^\circ$
Volume	7458(3) Å ³
Z, calculated density	8, 1.507 Mg/m ³
Absorption coefficient	1.061 mm ⁻¹
F(000)	3504
Crystal size	0.25 x 0.20 x 0.15 mm
Theta range for data collection	1.54 to 24.45 °
Limiting indices	-31 ≤ h ≤ 31, -9 ≤ k ≤ 11, -33 ≤ l ≤ 33
Reflections collected / unique	25492 / 6062 [R(int) = 0.0808]

4.2 Results

Completeness to theta = 24.45	98.3 %
Absorption correction	Empirical
Max. and min. transmission	0.69044 and 0.57072
Refinement method	Full-matrix least-squares on F ²
Data / restraints / parameters	6062 / 0 / 523
Goodness-of-fit on F ²	1.161
Final R indices [I>2sigma(I)]	R1 = 0.0724, wR2 = 0.1568
R indices (all data)	R1 = 0.1091, wR2 = 0.1693
Largest diff. peak and hole	0.464 and -0.477 e. Å ⁻³

Table 4.9: Selected bond lengths [Å] and angles [°] for [Ni(O-BPy)].

Ni(1)-N(1)	1.920(6)	Ni(1)-N(4)	1.926(5)	C(12)-C(13)	1.497(9)
Ni(1)-N(2)	1.964(5)	C(10)-C(11)	1.482(10)		
Ni(1)-N(3)	1.962(6)	C(11)-C(12)	1.559(10)		
N(1)-Ni(1)-N(4)	100.6(2)	C(1)-N(1)-Ni(1)	128.0(4)		
N(1)-Ni(1)-N(3)	149.8(2)	C(22)-N(4)-Ni(1)	126.4(4)		
N(4)-Ni(1)-N(3)	81.8(2)	C(18)-N(4)-Ni(1)	115.8(5)		
N(1)-Ni(1)-N(2)	82.0(2)	N(2)-C(10)-C(11)	115.8(5)		
N(4)-Ni(1)-N(2)	147.6(2)	C(10)-C(11)-C(12)	112.8(6)		
N(3)-Ni(1)-N(2)	112.0(2)	C(13)-C(12)-C(11)	112.0(6)		
C(10)-N(2)-Ni(1)	128.4(5)	N(3)-C(13)-C(12)	114.8(6)		
C(13)-N(3)-Ni(1)	128.1(4)	N(2)-C(10)-C(11)	115.8(6)		

4.2.2.2 $[\text{Ni}_2(\text{O-BPy})(\eta^2\text{-C}_4\text{H}_6)_2]$

To obtain the dinuclear nickel complex with butadiene, $[\text{Ni}(\text{COD})_2]$ was reacted with O-BPy in a 2:1 ratio and an excess of gaseous 1,3-butadiene (Figure 4.19).

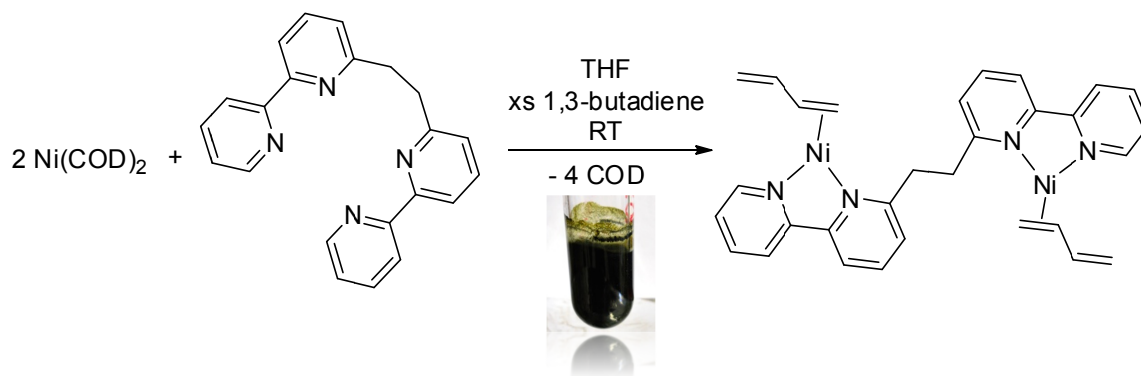


Figure 4.19: Reaction scheme for the synthesis of $[\text{Ni}_2(\text{O-BPy})(\eta^2\text{-C}_4\text{H}_6)_2]$ using a Ni/ligand ratio of 2:1 and an excess amount of 1,3-butadiene.

The complex solution turned immediately green and a dark green solid precipitated. Due to the use of an excess of butadiene, it is proposed that COD is replaced as a ligand from the binuclear nickel complex, which is in equilibrium with the monomer $[\text{Ni}(\text{O-BPy})]$. The precipitation of the green solid can be attributed to catalytic oligomerization reactions due to the excess of butadiene. Filtering of the suspension and diffusion of pentane at $-20\text{ }^\circ\text{C}$ into the THF solution did not result in crystals suitable for X-ray diffraction. The complex decomposed within several days and the color of the solution turned brown. Further characterization was done by performing UV-Vis experiments (4.2.4.1).

4.2.2.3 $[\text{Ni}(\text{pmbd})]$

For the synthesis of $[\text{Ni}(\text{pmbd})]$ the Schiff base ligand pmbd was mixed with $[\text{Ni}(\text{COD})_2]$ in a 1:1 and 1:2 ratio in THF at room temperature for several hours (see Figure 4.20). The color of the solution turned immediately to dark brown. After diffusion of n-pentane into a THF solution at $-20\text{ }^\circ\text{C}$ crystals suitable for X-ray diffraction could be obtained. The molecular structure in Figure 4.21 shows the mononuclear complex. Crystallographic data, selected bond lengths and bond angles are presented in Table 4.10 and Table 4.11. The formation of a binuclear complex with this ligand could not be observed during this work.

4.2 Results

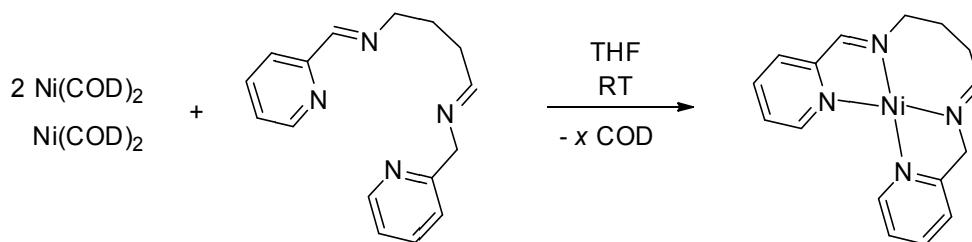


Figure 4.20: Reaction scheme for the synthesis of [Ni(pmbd)] using Ni/ligand ratios of 2:1 and 1:1.

The nickel center of [Ni(pmbd)] has a distorted tetrahedral environment and is ligated by the four nitrogen atoms of pmbd. Furthermore, the complex has a vertical mirror plane and the obtained Ni–N bond lengths with distances of 1.912(2) Å and 1.9385(18) Å are slightly shorter than in the analogue complex [Ni(O-BPy)] and the binuclear complex $[\text{Ni}_2(\text{O-BPy})(\eta^2\text{-C}_4\text{H}_6)_2]$ obtained by M. Leibold.[141] The C–C bond length between C8–C8a of the coordinated pmbd ligand is slightly enlarged compared to the free molecule.

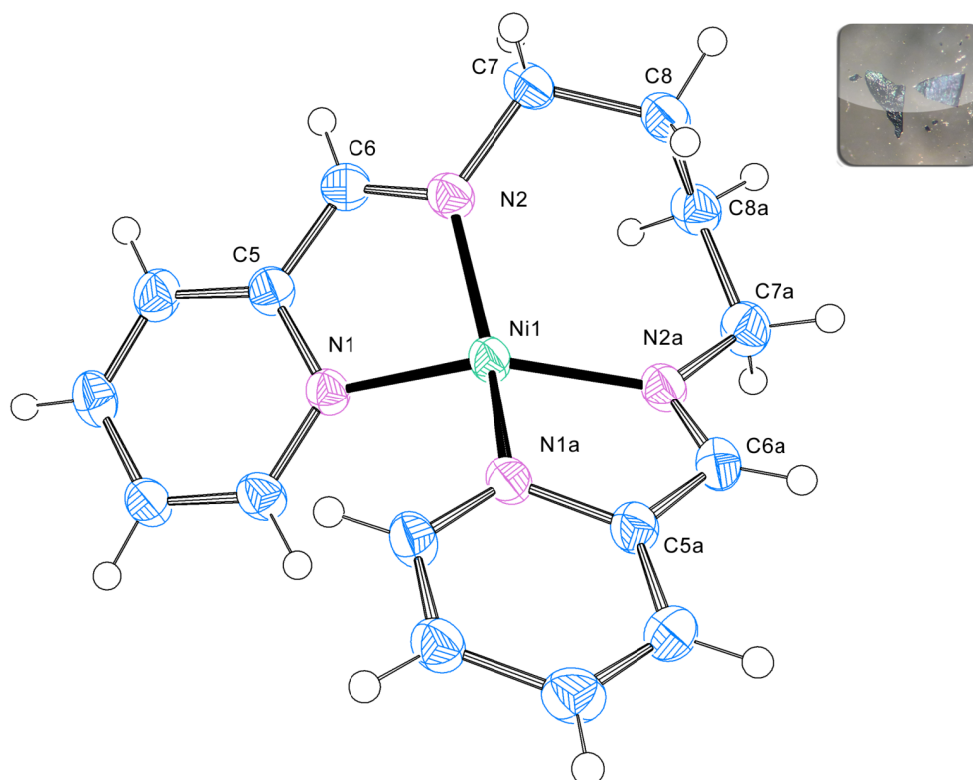


Figure 4.21: ORTEP plot of the full complex molecule [Ni(pmbd)]. Ellipsoids are drawn at 50 % probability level. Solvent molecules are omitted for clarity.

Table 4.10: Crystal data and structure refinement for [Ni(pmbd)].

Internal identification code	schindler12075
Empirical formula	C ₂₀ H ₂₆ N ₄ Ni O
Formula weight	397.16
Temperature	193 (2) K
Wavelength	0.71073 Å
Crystal system, space group	Orthorhombic, <i>P</i> 2 ₁ 2 ₁ 2
Unit cell dimensions	a = 13.014(3) Å α = 90 ° b = 7.9580(16) Å β = 90 ° c = 9.0770(18) Å γ = 90 °
Volume	940.1(11) Å ³
Z, calculated density	2, 1.403 Mg/m ³
Absorption coefficient	1.048 mm ⁻¹
F(000)	420
Crystal size	0.560 x 0.20 x 0.18 mm
Theta range for data collection	2.24 to 27.51 °
Limiting indices	-16 ≤ h ≤ 11, -10 ≤ k ≤ 9, -10 ≤ l ≤ 11
Reflections collected / unique	5714 / 2124 [R(int) = 0.0376]
Completeness to theta = 27.51	99.7 %
Absorption correction	Empirical
Max. and min. transmission	0.8337 and 0.5914
Refinement method	Full-matrix least-squares on F ²
Data / restraints / parameters	2124 / 0 / 171
Goodness-of-fit on F ²	1.025
Final R indices [I > 2σ(I)]	R1 = 0.0333, wR2 = 0.0758
R indices (all data)	R1 = 0.0454, wR2 = 0.0804
Absolute structure parameter	-0.06(3)
Largest diff. peak and hole	0.289 and -0.459 e. Å ⁻³

Table 4.11: Selected bond lengths [Å] and angles [°] for [Ni(pmbd)].

Ni(1)-N(1)	1.9385(18)	Ni(1)-N(2a)	1.912(2)	C(7)-N(2)	1.473(3)
Ni(1)-N(2)	1.912(2)	C(6)-N(2)	1.312(3)	C(7)-C(8)	1.520(4)

4.2 Results

Ni(1)-N(1a)	1.9385(18)	C(5)-N(1)	1.379(3)	C(8)-C(8a)	1.532(5)
N(2a)-Ni(1)-N(2)	110.12(12)	C(5)-N(1)-Ni(1)	113.32(15)		
N(2a)-Ni(1)-N(1)	82.55(9)	N(1)-C(5)-C(6)	112.6(2)		
N(2)-Ni(1)-N(1)	146.70(9)	N(2)-C(6)-C(5)	116.4(3)		
N(2a)-Ni(1)-N(1a)	146.70(9)	N(2)-C(7)-C(8)	112.1(2)		
N(2)-Ni(1)-N(1a)	82.55(9)	C(7)-C(8)-C(8a)	113.2(3)		
N(1)-Ni(1)-N(1a)	103.88(10)				

4.2.2.4 [Ni(mpmbd)]

Two hydrogen atoms of the pyridyl groups of the ligand mpmbd were substituted by methyl groups to add more steric hindrance and to prevent the formation of a mononuclear nickel complex. Therefore, the Schiff base ligand mpmbd was mixed with $[\text{Ni}(\text{COD})_2]$ in a 1:1 and 1:2 ratio in THF at room temperature for several hours (see Figure 4.22).

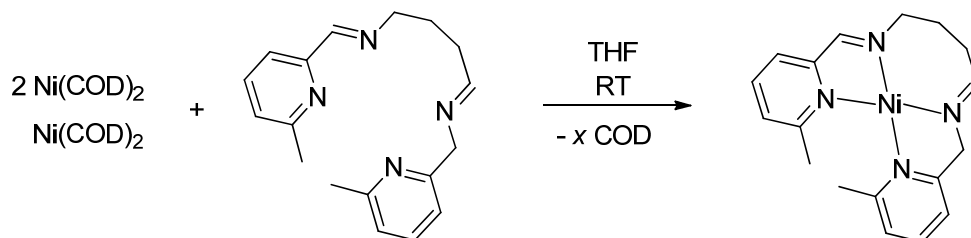


Figure 4.22: Reaction scheme for the synthesis of $[\text{Ni}(\text{mpmbd})]$ using Ni/ligand ratios of 2:1 and 1:1.

The color of the solution turned immediately dark violet. After diffusion of n-pentane into a THF solution at -20°C crystals suitable for X-ray diffraction could be obtained. However, the formation of a binuclear complex with mpmbd could not be observed. The molecular structure depicted in Figure 4.23 shows the mononuclear complex $[\text{Ni}(\text{mpmbd})]$. Crystallographic data, selected bond lengths and bond angles are given in Table 4.12 and Table 4.13.

The nickel center of $[\text{Ni}(\text{mpmbd})]$ has a distorted tetrahedral environment and is coordinated by the four nitrogen atoms of mpmbd. The obtained Ni–N bond lengths between Ni1–N1 with $1.9493(19)$ Å and Ni1–N3 with $1.9424(19)$ Å are

slightly larger than in the complex [Ni(pmbd)] whereas the distances between Ni1-N2 with 1.889(2) Å and Ni1-N4 with 1.885(2) Å are slightly shorter. This results from the two inserted methyl groups and the therefore necessary twist of the complex molecule. Nevertheless, they could not prevent the formation of a mononuclear complex.

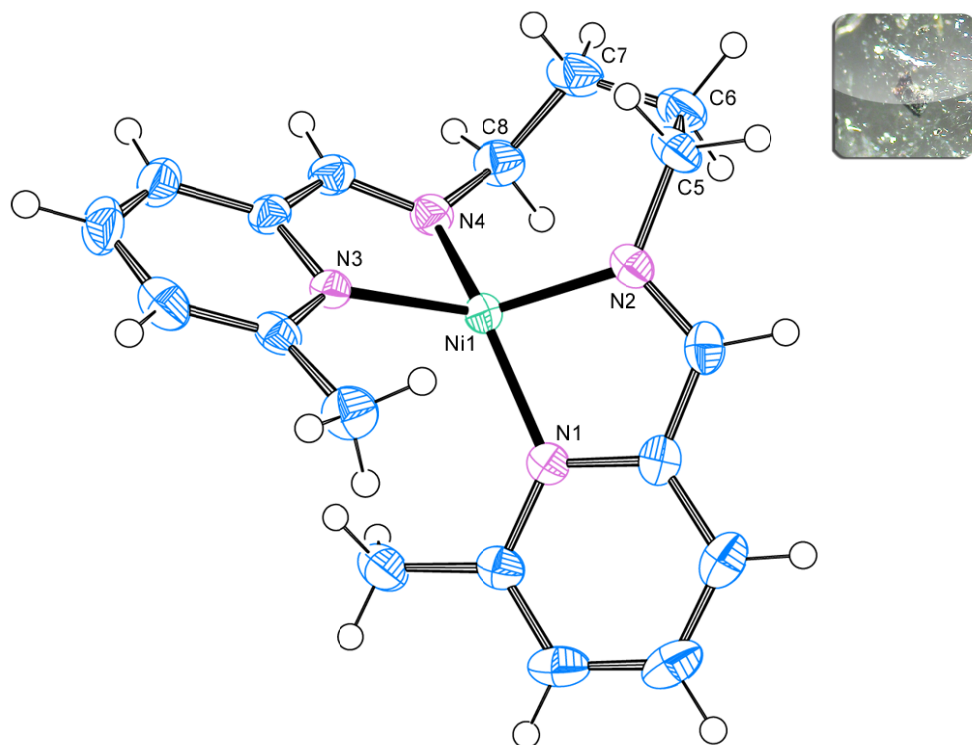


Figure 4.23: ORTEP plot of the full complex molecule [Ni(mpmbd)]. Ellipsoids are drawn at 50 % probability level.

Table 4.12: Crystal data and structure refinement for [Ni(mpmbd)].

Internal identification code	schindler13085
Empirical formula	C ₁₈ H ₂₁ N ₄ Ni
Formula weight	352.10
Temperature	190 (2) K
Wavelength	0.71073 Å
Crystal system, space group	Orthorhombic, <i>P</i> <i>b</i> <i>c</i> <i>a</i>
Unit cell dimensions	$a = 11.276(2) \text{ Å}$ $\alpha = 90^\circ$ $b = 8.5280(17) \text{ Å}$ $\beta = 90^\circ$ $c = 34.229(7) \text{ Å}$ $\gamma = 90^\circ$
Volume	3291.5(11) Å ³

4.2 Results

Z, calculated density	8, 1.421 Mg/m ³
Absorption coefficient	1.183 mm ⁻¹
F(000)	1480
Crystal size	0.250 x 0.200 x 0.150 mm
Theta range for data collection	2.163 to 27.473 °
Limiting indices	-14≤h≤14, -7≤k≤11, -43≤l≤44
Reflections collected / unique	15932 / 3761 [R(int) = 0.0694]
Completeness to theta = 25.242	99.6 %
Absorption correction	Empirical
Refinement method	Full-matrix least-squares on F ²
Data / restraints / parameters	3761 / 0 / 296
Goodness-of-fit on F ²	0.919
Final R indices [I>2sigma(I)]	R1 = 0.0377, wR2 = 0.0832
R indices (all data)	R1 = 0.0710, wR2 = 0.0937
Extinction coefficient	n/a
Largest diff. peak and hole	0.464 and -0.427 e. Å ⁻³

Table 4.13: Selected bond lengths [Å] and angles [°] for [Ni(mpmbd)].

Ni(1)-N(1)	1.9493(19)	Ni(1)-N(4)	1.885(2)	C(5)-C(6)	1.524(4)
Ni(1)-N(2)	1.889(2)	N(2)-C(5)	1.460(3)	C(6)-C(7)	1.525(4)
Ni(1)-N(3)	1.9424(19)	N(4)-C(8)	1.467(3)	C(7)-C(8)	1.523(4)
N(1)-Ni(1)-N(2)	83.07(8)	C(5)-N(2)-Ni(1)	125.67(16)		
N(1)-Ni(1)-N(3)	116.29(8)	C(8)-N(4)-Ni(1)	126.72(17)		
N(1)-Ni(1)-N(4)	135.36(8)	C(5)-C(6)-C(7)	118.2(2)		
N(2)-Ni(1)-N(3)	142.41(9)	C(8)-C(7)-C(6)	117.6(3)		
N(2)-Ni(1)-N(4)	106.42(9)	N(2)-C(5)-C(6)	113.2(2)		
N(3)-Ni(1)-N(4)	82.77(8)	N(4)-C(8)-C(7)	113.3(2)		

4.2.2.5 [Ni(pmed)] and [Ni(pmpd)]

[Ni(COD)₂] was mixed in a 2:1 and 1:1 ratio with the ligands pmed and pmpd in THF at room temperature for several hours. By changing the length of the bridge between the four donor atoms of the ligands the formation of a monomeric complex should be prevented. The color of the solution of [Ni(pmed)] turned immediately red-brown, the solution of [Ni(pmpd)] turned red-violet. Unfortunately, crystals suitable for X-ray diffraction could not be obtained during this work. UV-Vis spectra of these compounds are presented in 0.

4.2.2.6 [Ni(Me-BPy)]

A further approach to synthesize a binuclear nickel complex with a bipyridine ligand system was to use the ligand Me-BPy. This tetradentate ligand is similar to O-BPy but both 2,2'-bipyridine units are linked at the 4-position instead of the 6-position. This should prevent the formation of a monomeric complex. Furthermore, there are methyl groups introduced at the 4-position of the outer pyridine rings. For the synthesis of [Ni(Me-BPy)], [Ni(COD)₂] was mixed with Me-BPy in a 2:1 and 1:1 ratio in THF at room temperature for several hours to afford a dark purple solution. After a few weeks purple crystals could be obtained by diffusion of n-pentane into the THF solution. Unfortunately, they were too small for X-ray diffraction studies. UV-Vis spectra of this complex are given in 0.

4.2.3 Cu(I) Complexes with O-BPy and Derivatives

Analogue to the obtained nickel(0) complex [Ni₂(O-BPy)(η^2 -C₄H₆)₂] by M. Leibold[141] an isoelectronic binuclear copper(I) complex with O-BPy should be synthesized. Furthermore, it was the goal to figure out if copper(I) is also able to split COD into two molecules of butadiene.

In literature only a few mononuclear transition metal complexes with the ligand O-BPy have been reported. These include the complexes [CrCl₂(O-BPy)]Cl,[186] [Ru(O-BPy)(CH₃CN)₂](PF₆)₂[187], [Ni(O-BPy)(DMF)₂](ClO₄)₂[141] and [Cu(O-BPy)](ClO₄)₂[181]. The latter complex was reduced to the copper(I) analogue with ascorbic acid but not structurally characterized. However, mononuclear as

4.2 Results

well as binuclear complexes with the ligands 1,2-bis(6'-methyl-2,2'-bipyridine-6-yl)ethane (Me-O-BPy) and 1,2-bis(9-methyl-1,10-phenanthroline-2-yl)ethane (Me-O-BPh) (see Figure 4.24) are known.[188, 189, 190]

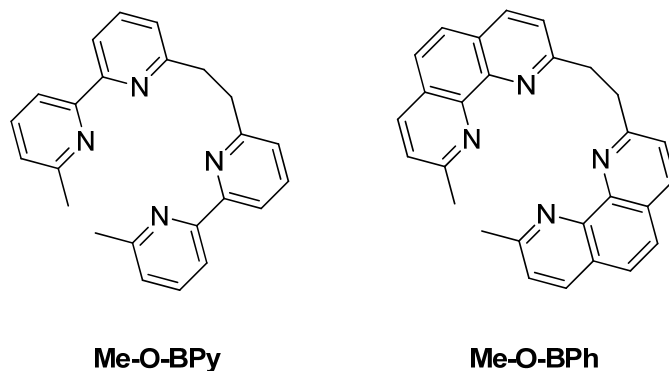


Figure 4.24: Structures of the ligands 1,2-bis(6'-methyl-2,2'-bipyridine-6-yl)ethane (Me-O-BPy) and 1,2-bis(9-methyl-1,10-phenanthroline-2-yl)ethane (Me-O-BPh).

The reaction of copper(I) with the methylated bis-bipyridine ligand Me-O-BPy and the methylated bis-phenanthroline ligand Me-O-BPh afforded the dinuclear complexes $[\text{Cu}_2(\text{Me-O-BPy})_2](\text{ClO}_4)_2$ and $[\text{Cu}_2(\text{Me-O-BPh})_2](\text{ClO}_4)_2$ (see Figure 4.25 and Figure 4.26).

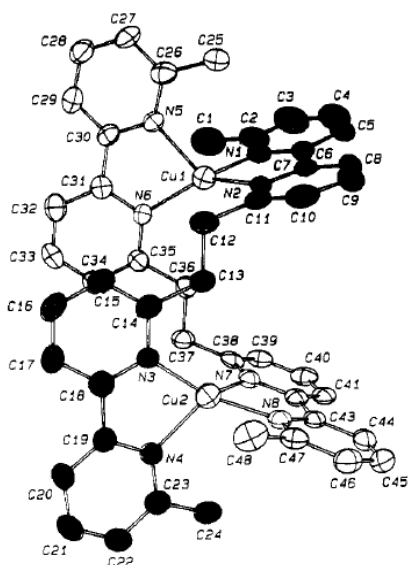


Figure 4.25: ORTEP plot of the cation $[\text{Cu}_2(\text{Me-O-BPy})_2]^{2+}$. Thermal ellipsoids are drawn at 50 % probability level.[188]

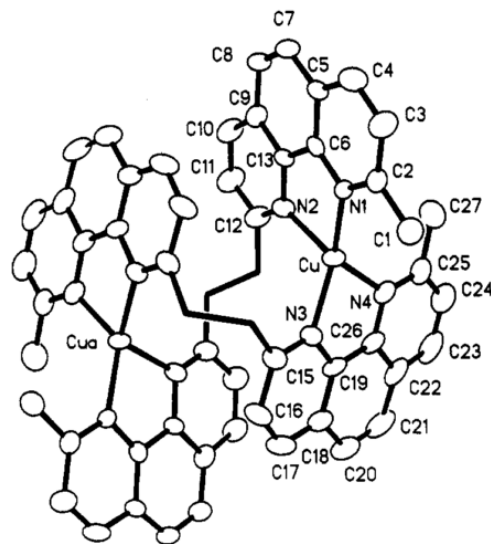


Figure 4.26: ORTEP plot of the cation $[\text{Cu}_2(\text{Me-O-BPh})_2]^{2+}$. [189]

However, the reaction of cobalt(II) with Me-O-BPh exhibits the mononuclear complex $[\text{Co}(\text{Me-O-BPh})](\text{SO}_3\text{CF}_3)_2$. Analogously, the reaction with copper(II) gives $[\text{Cu}(\text{Me-O-BPh})](\text{ClO}_4)_2$ (see Figure 4.27 and Figure 4.28).

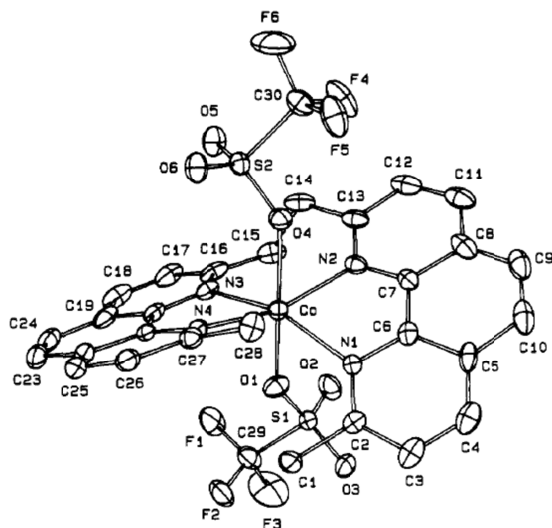


Figure 4.27: ORTEP plot of $[\text{Co}(\text{Me-O-BPh})_2](\text{SO}_3\text{CF}_3)_2$. Thermal ellipsoids are drawn at 50 % probability level.[188]

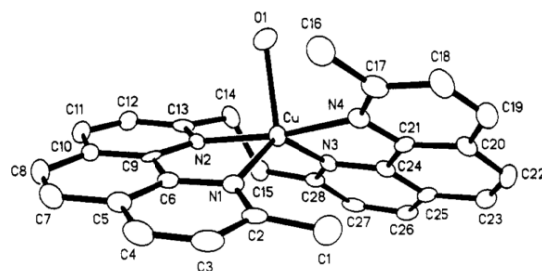


Figure 4.28: ORTEP plot of the cation $[\text{Cu}(\text{Me-O-BPh})(\text{H}_2\text{O})]^{2+}$. [189]

The first attempt to obtain the dinuclear copper(I) complex $[\text{Cu}_2(\text{O-BPy})(\text{COD})_2]^{2+}$ was a synthesis analogous to the ligand exchange reaction of $[\text{Ni}(\text{COD})_2]$ and 2,2'-bipyridine which gives $[\text{Ni}(\text{bipy})(\text{COD})]$. [180] Therefore, $[\text{Cu}(\text{COD})_2]X$ ($X = \text{ClO}_4^-$, BF_4^-) was prepared according to a procedure described in literature.[178]

4.2.3.1 $[\text{Cu}(\text{COD})_2]^+$

Colorless crystals suitable for X-ray diffraction could be obtained. The determined molecular structure (Figure 4.29) is in line with the already published structure by Munakata et al.[178] Crystallographic data, selected bond lengths and bond angles are presented in Table 4.14 and Table 4.15. The copper(I) center is coordinated to the four olefinic bonds of the two COD molecules in a quasi-tetrahedral environment. The structure of the complex and the geometry of the COD groups is analogous to those found in the isoelectronic metal compounds $[\text{Ni}(\text{COD})_2]$, $[\text{Ag}(\text{COD})_2]\text{BF}_4$ and $[\text{Pt}(\text{COD})_2]$. [172, 182–184]

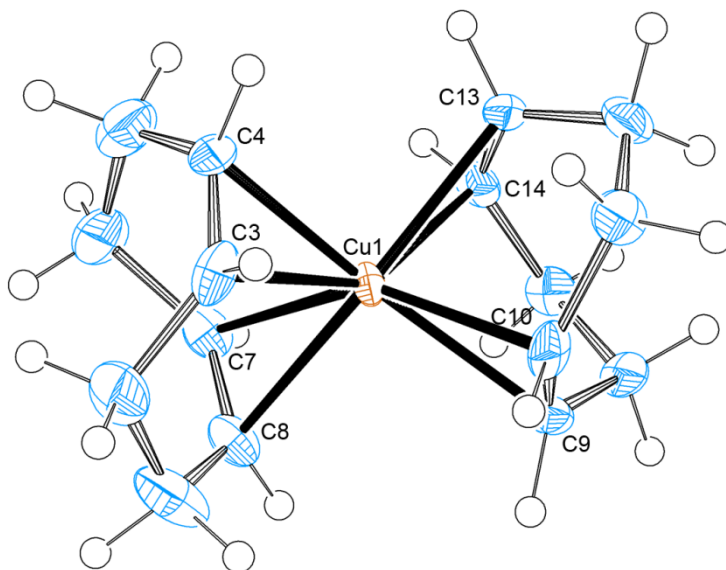


Figure 4.29: ORTEP plot of the cation $[\text{Cu}(\text{COD})_2]^+$. Ellipsoids are drawn at 50 % probability level.[178]

Table 4.14: Crystal data and structure refinement for $[\text{Cu}(\text{COD})_2]\text{ClO}_4$.

Internal identification code	schindler13014
Empirical formula	$\text{C}_{16} \text{H}_{24} \text{Cl Cu O}_4$
Formula weight	379.34
Temperature	190 (2) K
Wavelength	0.71073 Å
Crystal system, space group	Monoclinic, $P2_1/c$
Unit cell dimensions	$a = 19.437(2) \text{ Å}$ $\alpha = 90^\circ$ $b = 10.562(2) \text{ Å}$ $\beta = 116.218(6)^\circ$ $c = 17.174(3) \text{ Å}$ $\gamma = 90^\circ$
Volume	$3163.0(10) \text{ Å}^3$
Z, calculated density	8, 1.593 Mg/m ³
Absorption coefficient	1.565 mm^{-1}
F(000)	1584
Crystal size	0.550 x 0.200 x 0.200 mm
Theta range for data collection	1.168 to 27.875°
Limiting indices	$-25 \leq h \leq 25$, $-13 \leq k \leq 13$, $-22 \leq l \leq 22$
Reflections collected / unique	7200 / 7200 [R(int) = 0.0784]
Completeness to theta = 25.242	99.8 %

Absorption correction	Empirical
Refinement method	Full-matrix least-squares on F ²
Data / restraints / parameters	7200 / 0 / 398
Goodness-of-fit on F ²	1.034
Final R indices [I>2sigma(I)]	R1 = 0.0523, wR2 = 0.1150
R indices (all data)	R1 = 0.0937, wR2 = 0.1327
Extinction coefficient	n/a
Largest diff. peak and hole	0.758 and -0.745 e. Å ⁻³

Table 4.15: Selected bond lengths [Å] and angles [°] for [Cu(COD)₂](ClO₄).

Cu(1)-C(3)	2.293(7)	Cu(1)-C(8)	2.266(6)	Cu(1)-C(13)	2.314(6)
Cu(1)-C(4)	2.247(7)	Cu(1)-C(9)	2.263(7)	Cu(1)-C(14)	2.255(7)
Cu(1)-C(7)	1.298(7)	Cu(1)-C(10)	2.239(6)		
C(3)-Cu(1)-C(4)	35.3(3)	C(9)-Cu(1)-C(10)	34.5(3)		
C(7)-Cu(1)-C(8)	34.5(3)	C(13)-Cu(1)-C(14)	34.2(3)		
C(10)-Cu(1)-C(13)	81.9(3)	C(8)-Cu(1)-C(9)	95.1(3)		
C(9)-Cu(1)-C(14)	34.5(3)	C(7)-Cu(1)-C(14)	92.2(3)		
C(3)-Cu(1)-C(8)	83.2(3)	C(3)-Cu(1)-C(10)	96.3(3)		
C(7)-Cu(1)-C(4)	84.6(3)	C(4)-Cu(1)-C(13)	148.9(3)		

4.2.3.2 [Cu₂(O-BPy)₂]²⁺

Analogue to the synthesis of the nickel complexes (see 4.2.2) [Cu(COD)₂](X) (X = ClO₄⁻, BF₄⁻) was reacted with O-BPy in a 2:1 ratio. Mixing of the copper(I) complex and the ligand in acetone led to a deep red solution which turned orange after a few minutes (see

Figure 4.30). After filtration crystals suitable for X-ray diffraction could be obtained by diffusion of n-pentane into the solution. The molecular structure of the obtained binuclear complex [Cu₂(O-BPy)₂](BF₄)₂[181] is shown in Figure

4.2 Results

4.32. Crystallographic data, selected bond lengths and angles are given in Table 4.16 and Table 4.17.

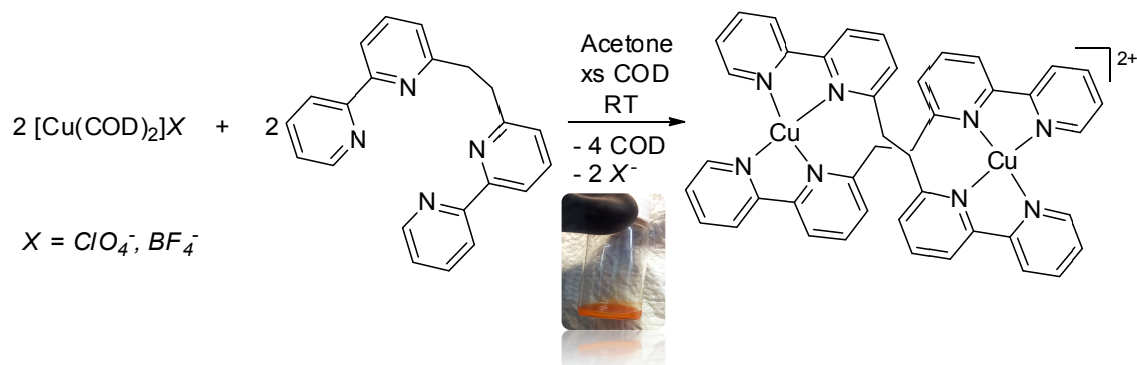


Figure 4.30: Scheme for the reaction of $[\text{Cu}(\text{COD})_2]\text{X}$ ($\text{X} = \text{ClO}_4^-, \text{BF}_4^-$) and O-BPy using a ratio of 2:1.

The same complex was obtained by mixing the tetrakis(acetonitrile)copper(I)-salts $[\text{Cu}(\text{CH}_3\text{CN})_4]\text{X}$ ($\text{X} = \text{ClO}_4^-, \text{BF}_4^-, \text{SbF}_6^-, \text{PF}_6^-$) in a 2:1 ratio with O-BPy and an excess amount of COD in acetone. All solutions turned red and after a few minutes to orange to afford the binuclear copper(I) complex with two coordinated molecules of O-BPy (see Figure 4.31).

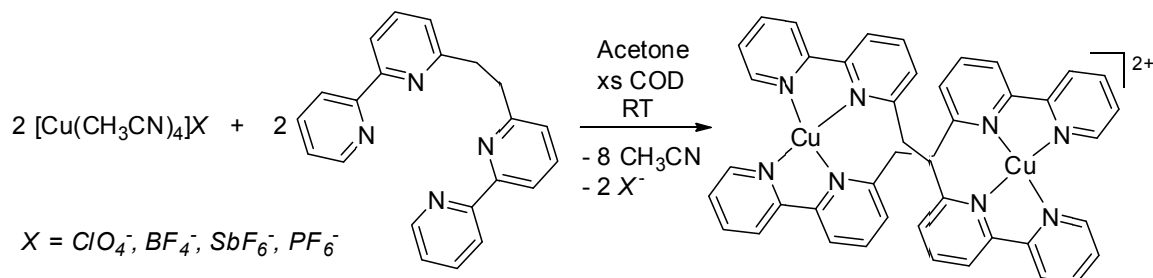


Figure 4.31: Scheme for the reaction of $[\text{Cu}(\text{CH}_3\text{CN})_4]\text{X}$ ($\text{X} = \text{ClO}_4^-, \text{BF}_4^-, \text{SbF}_6^-, \text{PF}_6^-$) and O-BPy using a ratio of 2:1 and an excess of COD.

In this dinuclear complex each copper(I) center is coordinated by four nitrogen atoms in a distorted tetrahedral geometry. However, O-BPy acts as a bridging ligand and only two nitrogen atoms of one bipyridyl unit of each O-BPy molecule bind to one copper center. The obtained bond lengths of Cu–N with distances between 1.961(14) Å and 2.093(17) Å correspond with those of the complex $[\text{Cu}_2(\text{Me-O-BPy})_2]^{2+}$ (see 4.2.3) reported by J.-M. Lehn and co-

workers.[188] However, the two Cu(I) ions are separated by only 5.693(7) Å which is slightly shorter than in the Cu(I) complex with Me-O-BPy.

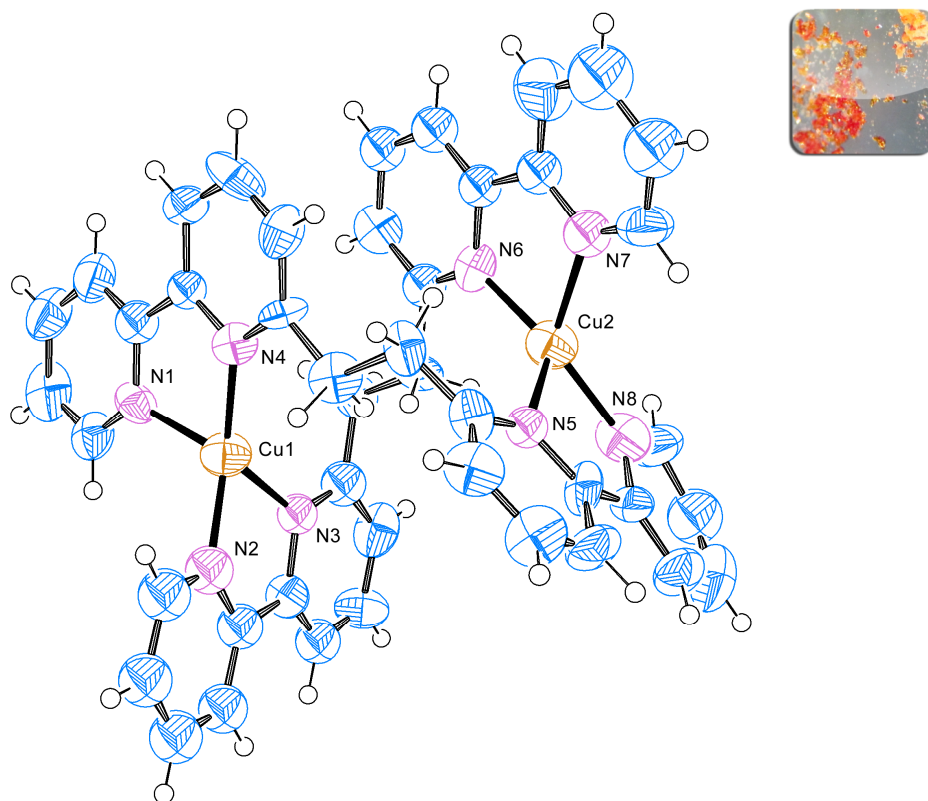


Figure 4.32: ORTEP plot of the cation $[\text{Cu}_2(\text{O-BPy})_2]^{2+}$. Ellipsoids are drawn at 50 % probability level. Solvent molecules are omitted for clarity.

Table 4.16: Crystal data and structure refinement for $[\text{Cu}_2(\text{O-BPy})_2](\text{BF}_4)_2$.

Internal identification code	schindler12017
Empirical formula	$\text{C}_{47} \text{H}_{30} \text{B}_2 \text{Cu}_2 \text{F}_8 \text{N}_4 \text{O}$
Formula weight	1023.49
Temperature	190 (2) K
Wavelength	0.71073 Å
Crystal system, space group	Triclinic, $P\bar{1}$
Unit cell dimensions	$a = 11.225(6) \text{ Å}$ $\alpha = 75.43(3)^\circ$ $b = 12.764(6) \text{ Å}$ $\beta = 75.86(2)^\circ$ $c = 17.991(9) \text{ Å}$ $\gamma = 68.13(4)^\circ$
Volume	$2282(2) \text{ Å}^3$
Z, calculated density	2, 1.489 Mg/m ³

4.2 Results

Absorption coefficient	1.011 mm ⁻¹
F(000)	1032
Crystal size	0.250 x 0.130 x 0.070 mm
Theta range for data collection	1.983 to 16.697 °
Limiting indices	-8≤h≤8, -10≤k≤10, -14≤l≤14
Reflections collected / unique	3776 / 2274 [R(int) = 0.0604]
Completeness to theta = 25.242	27.5 %
Absorption correction	Empirical
Refinement method	Full-matrix least-squares on F ²
Data / restraints / parameters	2274 / 0 / 480
Goodness-of-fit on F ²	1.197
Final R indices [I>2sigma(I)]	R1 = 0.0772, wR2 = 0.1697
R indices (all data)	R1 = 0.1023, wR2 = 0.1905
Extinction coefficient	n/a
Largest diff. peak and hole	0.447 and -0.310 e. Å ⁻³

Table 4.17: Selected bond lengths [Å] and angles [°] for [Cu₂(O-BPy)₂](BF₄)₂.

Cu(1)-N(1)	2.043(14)	Cu(1)-N(4)	1.961(14)	Cu(2)-N(7)	2.061(14)
Cu(1)-N(2)	1.985(16)	Cu(2)-N(5)	2.093(17)	Cu(2)-N(8)	1.97(2)
Cu(1)-N(3)	2.076(19)	Cu(2)-N(6)	2.005(14)		
N(4)-Cu(1)-N(2)	138.4(6)	N(8)-Cu(2)-N(6)	138.1(8)		
N(4)-Cu(1)-N(1)	82.5(6)	N(8)-Cu(2)-N(7)	127.4(5)		
N(2)-Cu(1)-N(1)	117.9(5)	N(6)-Cu(2)-N(7)	80.7(6)		
N(4)-Cu(1)-N(3)	130.9(5)	N(8)-Cu(2)-N(5)	79.3(10)		
N(2)-Cu(1)-N(3)	80.7(6)	N(6)-Cu(2)-N(5)	128.5(6)		
N(1)-Cu(1)-N(3)	106.4(5)	N(7)-Cu(2)-N(5)	104.0(6)		

4.2.3.3 [Cu(O-BPy)]²⁺

Several days after exposure to air, the binuclear copper(I) complex [Cu₂(O-BPy)₂](BF₄)₂ was oxidized to the green mononuclear copper(II) complex [Cu(O-BPy)](BF₄)₂. [181] The determined molecular structure of the cation

$[\text{Cu}(\text{O-BPy})]^{2+}$ (Figure 4.33) is in line with the already reported structure by Garber et al.[181] Crystallographic data, selected bond lengths and angles are presented in Table 4.18 and Table 4.19. The Cu(II) center is coordinated by the four nitrogen atoms of the ligand O-BPy and both bipyridine rings are related to each other by a C_2 symmetry. Consequently, the bond lengths for Cu-N1 and Cu-N1a with 1.9827(15) Å are the same as well as for Cu-N2 and Cu-N2a with 2.0102(14) Å. The longer bond distances of the copper center to the nitrogen atoms N2/N2a can be attributed to the ethyl bridge between C10-C10a.

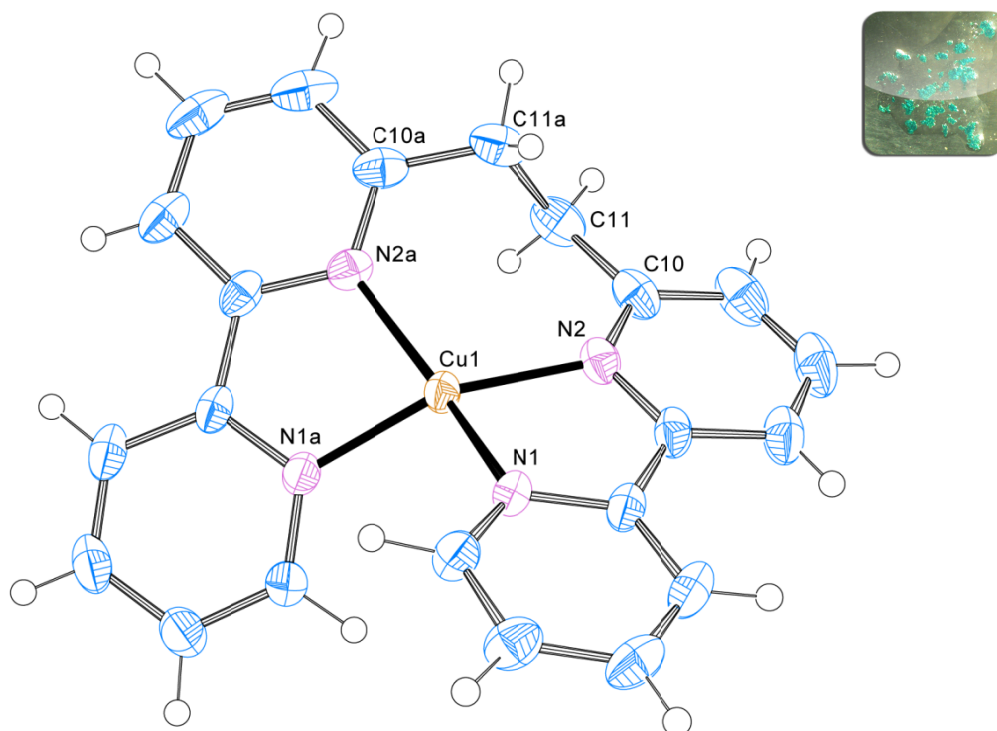


Figure 4.33: ORTEP plot of the cation $[\text{Cu}(\text{O-BPy})]^{2+}$. Ellipsoids are drawn at 50 % probability level.

Table 4.18: Crystal data and structure refinement for $[\text{Cu}(\text{O-BPy})](\text{BF}_4)_2$.

Internal identification code	schindler13022
Empirical formula	$\text{C}_{22} \text{H}_{18} \text{B}_2 \text{Cu F}_8 \text{N}_4$
Formula weight	575.56
Temperature	190 (2) K
Wavelength	0.71073 Å
Crystal system, space group	Monoclinic, $C2/c$
Unit cell dimensions	$a = 17.594(4) \text{ Å} \quad \alpha = 90^\circ$

4.2 Results

	b = 10.502(2) Å	β = 123.28(3) °
	c = 14.480(3) Å	γ = 90 °
Volume	2236.8(8) Å ³	
Z, calculated density	4, 1.709 Mg/m ³	
Absorption coefficient	1.064 mm ⁻¹	
F(000)	1156	
Crystal size	0.40 x 0.25 x 0.10 mm	
Theta range for data collection	3.33 to 27.47 °	
Limiting indices	-22≤h≤20, -11≤k≤13, -18≤l≤18	
Reflections collected / unique	10124 / 2558 [R(int) = 0.0336]	
Completeness to theta = 27.47	99.5 %	
Absorption correction	Empirical	
Refinement method	Full-matrix least-squares on F ²	
Data / restraints / parameters	2558 / 0 / 204	
Goodness-of-fit on F ²	1.048	
Final R indices [I>2sigma(I)]	R1 = 0.0301, wR2 = 0.0802	
R indices (all data)	R1 = 0.0341, wR2 = 0.0833	
Largest diff. peak and hole	0.525 and -0.383 e. Å ⁻³	

Table 4.19: Selected bond lengths [Å] and angles [°] for [Cu(O-BPy)](BF₄)₂.

Cu(1)-N(1)	1.9827(15)	Cu(1)-N(2a)	2.0102(14)	C(11)-C(11a)	1.551(4)
Cu(1)-N(1a)	1.9827(15)	N(2)-C(10)	1.350(2)		
Cu(1)-N(2)	2.0102(14)	C(10)-C(11)	1.490(3)		
N(1)-Cu(1)-N(1a)	96.26(9)	N(1a)-Cu(1)-N(2)	155.50(6)		
N(1)-Cu(1)-N(2a)	155.50(6)	N(2a)-Cu(1)-N(2)	109.76(9)		
N(1a)-Cu(1)-N(2a)	81.84(6)	C(10)-N(2)-Cu(1)	127.58(13)		
N(1)-Cu(1)-N(2)	81.84(6)	C(10)-C(11)-C(11a)	113.84(18)		

4.2.3.4 [Cu₂(O-BPy)(COD)₂](SO₃CF₃)₂

To obtain the analogue binuclear copper(I) complex with two molecules of coordinated 1,5-cyclooctadiene (see 4.1), finding the right anion was necessary. By

using the copper(I) precursor $[\text{Cu}(\text{CH}_3\text{CN})_4]\text{SO}_3\text{CF}_3$ the synthesis was finally successful. Therefore, the triflate salt and an excess of COD was solved in acetone and added dropwise to a solution of O-BPy in acetone (see Figure 4.34). The solution turned immediately red and a color change to orange was not observed. Crystals suitable for X-ray diffraction of the binuclear complex $[\text{Cu}_2(\text{O-BPy})(\text{COD})_2](\text{SO}_3\text{CF}_3)_2$ could be obtained.

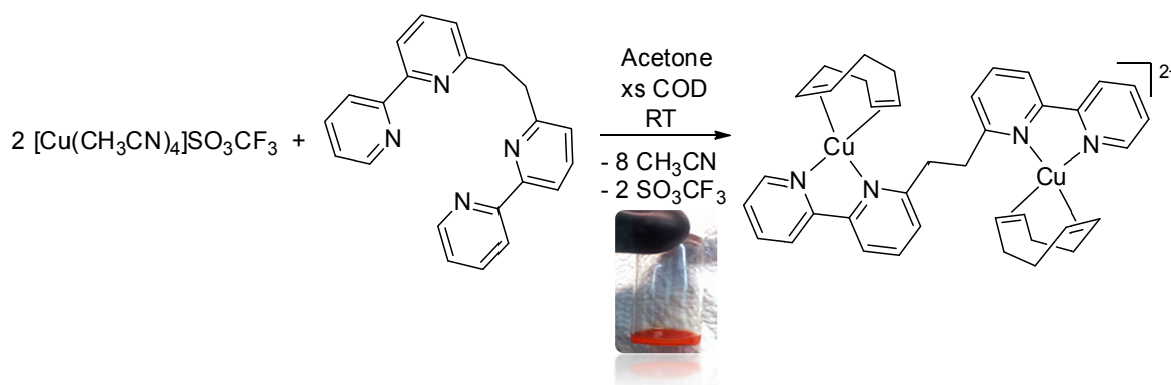


Figure 4.34: Scheme for the reaction of $[\text{Cu}(\text{CH}_3\text{CN})_4]\text{SO}_3\text{CF}_3$ and O-BPy using a ratio of 2:1 and an excess of COD affording $[\text{Cu}_2(\text{O-BPy})(\text{COD})_2](\text{SO}_3\text{CF}_3)_2$.

The cation of the complex $[\text{Cu}_2(\text{O-BPy})(\text{COD})_2]^{2+}$ is shown in Figure 4.35. Crystallographic data, selected bond lengths and angles are presented in Table 4.20 and Table 4.21. Each copper(I) center is coordinated by two nitrogen atoms of O-BPy and both double bonds of a COD ligand. The Cu–N bond lengths with an average of 2,037(3) Å are equal to other Cu–N bonds of related copper(I) complexes with phen, bipy and derivatives.[143, 167, 194–196] In contrast, the coordination of COD is weak due to very long Cu–olefin bonds compared with $[\text{Cu}(\text{bipy})(\text{COD})]^+$ [178] and other related copper(I) olefin complexes[143, 162–165]. The Cu–C distances for the equatorial olefin bonds with an average of 2.086(4) Å and the average distance of 2.608(5) Å for the axial olefin moieties indicate these very weak Cu–C bonds. The two Cu(I)–Cu(I) centers are separated by 7.272 Å which is significantly larger than in the $[\text{Cu}_2(\text{O-BPy})_2]^{2+}$ complex. It is supposed that the formation of this complex was possible because of the triflate anion which might have stronger coordination properties than other anions used before (see 4.2.3.2) and due to its size could be able to block the coordination of a second O-BPy ligand. Therefore, the coordination of two COD molecules is possible and $[\text{Cu}_2(\text{O-BPy})(\text{COD})_2](\text{SO}_3\text{CF}_3)_2$

4.2 Results

can be obtained. However, the splitting of COD into butadiene was not observed. Thus, the copper(I) complex is not able to undergo this reaction.

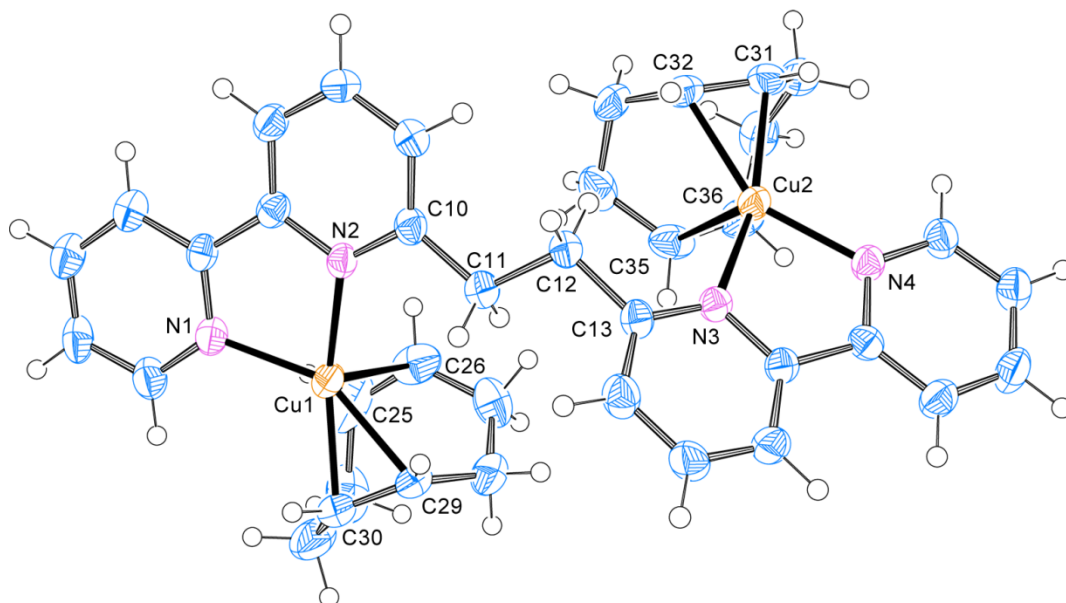


Figure 4.35: ORTEP plot of the cation $[\text{Cu}_2(\text{O-BPy})(\text{COD})_2]^{2+}$. Ellipsoids are drawn at 50 % probability level.

Table 4.20: Crystal data and structure refinement for $[\text{Cu}_2(\text{O-BPy})(\text{COD})_2](\text{SO}_3\text{CF}_3)_2$.

Internal identification code	schindler13063-a
Empirical formula	$\text{C}_{40} \text{H}_{42} \text{Cu}_2 \text{F}_6 \text{N}_4 \text{O}_6 \text{S}_2$
Formula weight	979.98
Temperature	190 (2) K
Wavelength	0.71073 Å
Crystal system, space group	Monoclinic, $I2/c$
Unit cell dimensions	$a = 19.805(4) \text{ Å}$ $\alpha = 90^\circ$ $b = 10.603(2) \text{ Å}$ $\beta = 94.94(3)^\circ$ $c = 56.866(11) \text{ Å}$ $\gamma = 90^\circ$
Volume	$11897(4) \text{ Å}^3$
Z, calculated density	12, 1.641 Mg/m ³
Absorption coefficient	1.260 mm^{-1}
F(000)	6024
Crystal size	0.20 x 0.15 x 0.14 mm
Theta range for data collection	1.44 to 27.48°

Limiting indices	-25≤h≤25, -13≤k≤11, -72≤l≤73
Reflections collected / unique	41111 / 13534 [R(int) = 0.0648]
Completeness to theta = 27.48	99.1 %
Absorption correction	Empirical
Max. and min. transmission	0.8433 and 0.7867
Refinement method	Full-matrix least-squares on F ²
Data / restraints / parameters	13534 / 0 / 811
Goodness-of-fit on F ²	0.971
Final R indices [I>2sigma(I)]	R1 = 0.0495, wR2 = 0.1248
R indices (all data)	R1 = 0.0933, wR2 = 0.1469
Largest diff. peak and hole	0.828 and -0.699 e. Å ⁻³

Table 4.21: Selected bond lengths [Å] and angles [°] for [Cu₂(O-BPy)(COD)₂](SO₃CF₃)₂.

Cu(1)-N(1)	1.995(3)	Cu(1)-C(25)	2.681(2)	Cu(2)-C(31)	2.068(4)
Cu(1)-N(2)	2.095(2)	Cu(1)-C(26)	2.582(4)	Cu(2)-C(32)	2.101(2)
Cu(2)-N(3)	2.044(3)	Cu(1)-C(29)	2.087(4)	Cu(2)-C(35)	2.543(4)
Cu(2)-N(4)	2.015(3)	Cu(1)-C(30)	2.074(3)	Cu(2)-C(36)	2.628(5)
N(1)-Cu(1)-N(2)	82.06(10)	N(3)-Cu(2)-N(4)	81.50(11)		
C(10)-N(2)-Cu(1)	130.3(2)	C(13)-N(3)-Cu(2)	128.8(2)		
N(1)-Cu(1)-C(25)	94.82(5)	N(3)-Cu(2)-C(35)	99.99(5)		
N(2)-Cu(1)-C(26)	99.79(6)	N(4)-Cu(2)-C(36)	90.70(4)		
N(2)-Cu(1)-C(29)	124.29(6)	N(4)-Cu(2)-C(31)	113.34(4)		
N(1)-Cu(1)-C(30)	111.98(7)	N(3)-Cu(2)-C(32)	124.75(5)		

4.2.3.5 [Cu₂(O-BPy)(C₄H₆)₂](SO₃CF₃)₂

The red solution of [Cu₂(O-BPy)(COD)₂](SO₃CF₃)₂ was reacted with gaseous 1,3-butadiene at -20 °C in acetone, methanol and acetonitrile to obtain the analogue butadiene complex. The acetone and methanolic solution turned yellow-orange and a yellow solid precipitated. The latter complex solution in acetonitrile did not show any reaction with butadiene. Unfortunately, it was not possi-

4.2 Results

ble to obtain crystals suitable for X-ray diffraction either from the solution or the precipitate. Infrared spectra of the complexes $[\text{Cu}_2(\text{O-BPy})(\text{COD})_2](\text{SO}_3\text{CF}_3)_2$ and $[\text{Cu}_2(\text{O-BPy})(\text{C}_4\text{H}_6)_2](\text{SO}_3\text{CF}_3)_2$ were obtained from solid samples using KBr pellets and are presented in Figure 4.36.[197] Due to the comparable chemical structures of COD and 1,3-butadiene as well as the absorbance of the ligand O-BPy, the corresponding copper(I) complexes show very similar IR spectra. However, $[\text{Cu}_2(\text{O-BPy})(\text{C}_4\text{H}_6)_2](\text{SO}_3\text{CF}_3)_2$ exhibits less bands in the C–H stretching region at 2800-3000 cm^{-1} as $[\text{Cu}_2(\text{O-BPy})(\text{COD})_2](\text{SO}_3\text{CF}_3)_2$ which can be attributed to the missing COD ligand.[198] Furthermore, the spectrum of the butadiene complex shows two additional bands in the fingerprint area at 920 and 980 cm^{-1} which can be attributed to $\delta(\text{CH}_2)_{\text{wag}}$ and $\delta(\text{CH})_{\text{bend}}$ stretching of the butadiene ligand.[198] Additional IR data is given in Table 4.22.

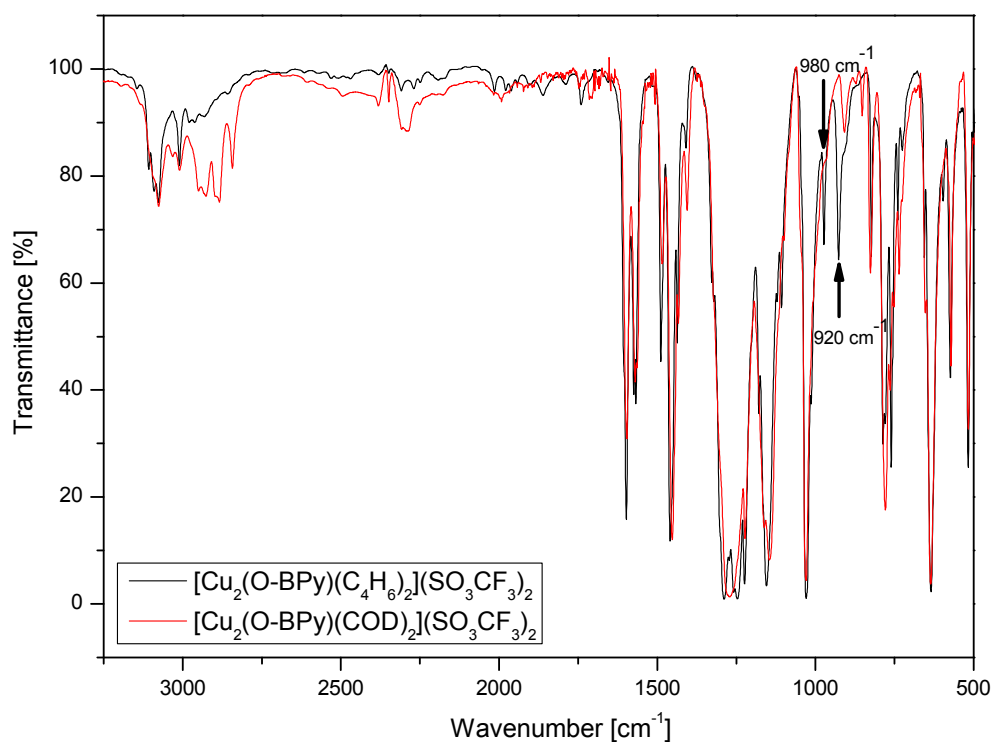


Figure 4.36: IR spectra of the copper(I) complexes $[\text{Cu}_2(\text{O-BPy})(\text{COD})_2](\text{SO}_3\text{CF}_3)_2$ and $[\text{Cu}_2(\text{O-BPy})(\text{C}_4\text{H}_6)_2](\text{SO}_3\text{CF}_3)_2$ (KBr pellets).[197]

However, due to similar IR spectra of the ligand O-BPy, COD and butadiene and problems of overlapping in many frequencies, a further detailed analysis was not possible. Hence, Cu–N stretching vibrations in the fingerprint area could not be assigned as well.

Table 4.22: IR data for $[\text{Cu}_2(\text{O-BPy})(\text{C}_4\text{H}_6)_2](\text{SO}_3\text{CF}_3)_2$ and $[\text{Cu}_2(\text{O-BPy})(\text{COD})_2](\text{SO}_3\text{CF}_3)_2$

2800-3200 cm^{-1}	$\nu(\text{CH})$	1230 cm^{-1}	$\nu(\text{C-F})$
1600 cm^{-1}	$\nu(\text{C}=\text{C})_{\text{ar}}$	1145 cm^{-1}	$\nu(\text{S-O})$
1580 cm^{-1}		980 cm^{-1}	$\delta(\text{CH})_{\text{bend}}$
1430		920 cm^{-1}	$\delta(\text{CH}_2)_{\text{wag}}$
1250 cm^{-1}	$\nu(\text{S=O})$		

4.2.4 UV-Vis Spectroscopy

UV-Vis experiments on the nickel(0) complexes have been performed.

4.2.4.1 $[\text{Ni}(\text{O-BPy})]$ vs. $[\text{Ni}_2(\text{O-BPy})(\eta^2\text{-C}_4\text{H}_6)_2]$

UV-Vis spectra of the dark blue solution of $[\text{Ni}(\text{O-BPy})]$ and the dark green solution of $[\text{Ni}_2(\text{O-BPy})(\eta^2\text{-C}_4\text{H}_6)_2]$ are shown in Figure 4.37. Both spectra show three absorption bands in THF. $[\text{Ni}(\text{O-BPy})]$ exhibits a band at 423 nm, a weak band at 557 nm and a broad band at 610 nm. For the dinuclear butadiene complex the three bands show a small shift to 421, 556 and 605 nm. Square-planar nickel(II) complexes show d-d transitions in the area of 400-555 nm and a strong absorption band in the area of 330-435 nm which can be assigned to charge-transfer transition.[199] UV-Vis spectroscopic investigations on nickel(0) complexes are not available in literature. Therefore, the obtained data could not be evaluated completely. However, the absorption bands at 421 and 423 nm are assigned to a charge-transfer transition from the metal center to the ligand, the bands at 556, 557, 605 and 610 nm are most likely d-d transitions.[199] Furthermore, there are differences in the intensities of the absorption bands of both spectra. The band at 421 nm of the dinuclear nickel butadiene complex is much stronger compared to the bands at 556 nm and 605 nm whereas the monomeric nickel species exhibits three bands of the same intensity.

Obtained UV-Vis spectra of both complexes in DMF are shown in Figure 4.38.

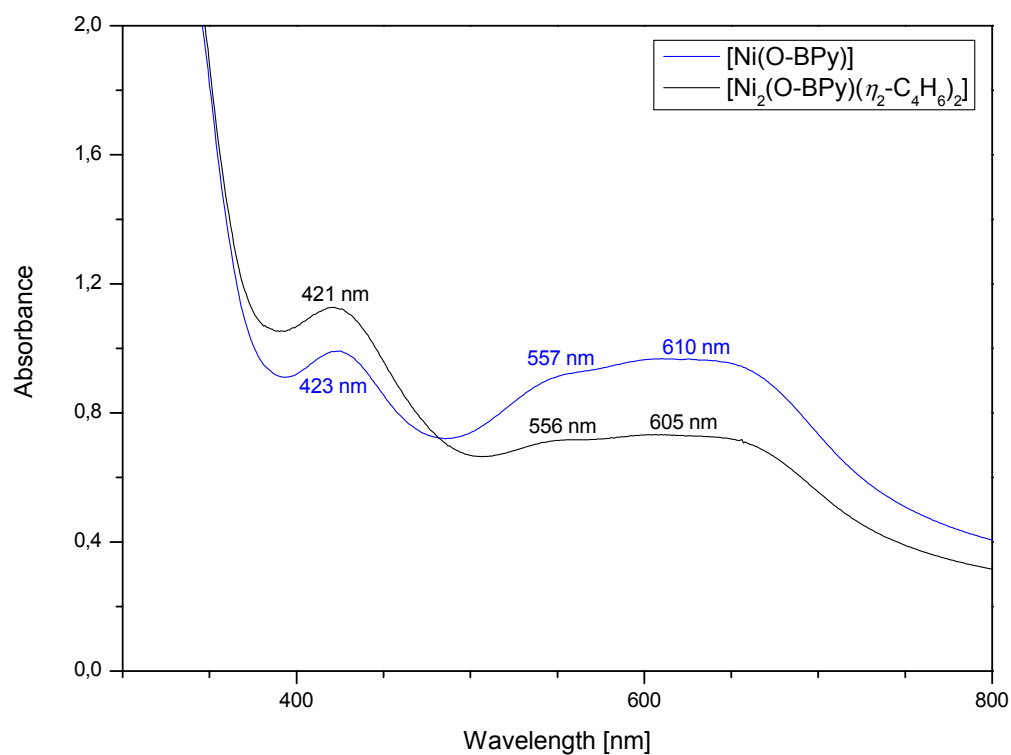


Figure 4.37: UV-Vis spectra of the complexes [Ni(O-BPy)] (blue) and [Ni₂(O-BPy)(η^2 -C₄H₆)₂] (black) in THF.

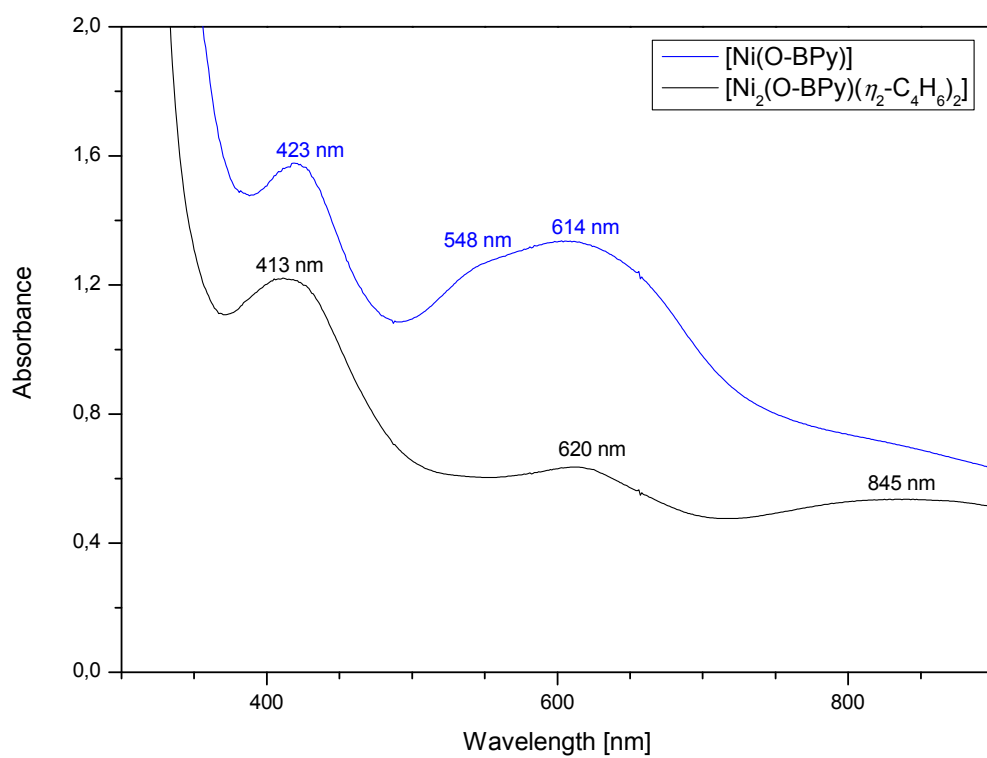


Figure 4.38: UV-Vis spectra of the complexes [Ni(O-BPy)] (blue) and [Ni₂(O-BPy)(η^2 -C₄H₆)₂] (black) in DMF.

The spectra show a small shift which can be attributed to the different influence of the solvent. [Ni(O-BPy)] has three absorption bands at 423, 548 and 614 nm whereas the butadiene complex $[\text{Ni}_2(\text{O-BPy})(\eta^2\text{-C}_4\text{H}_6)_2]$ exhibits three bands at 413, 620 and 845 nm. Thereby, the charge-transfer bands at 423 and 413 nm are stronger compared to the d-d bands at 548/614 nm and 620/845 nm.

4.2.4.2 [Ni(pmbd)]

The UV-Vis spectra of the brown complex [Ni(pmbd)] in THF with ratios of $[\text{Ni}(\text{COD})_2]$ to the ligand pmbd of 2:1 (black curve) and 1:1 (blue curve) are shown in Figure 4.39. Both complex solutions exhibit the same spectra with two intense bands at 485 and 840 nm and a weak broad band at 643 nm. Additionally, [Ni(pmbd)] obtained by using a 1:1 ratio (blue curve) exhibits a weak shoulder at 382 nm of the strong charge-transfer band at 325 nm. Both spectra show an absorbance at 485 nm which can be assigned to charge-transfer transitions, the bands at 643 nm to d-d transitions. Due to the strong absorbance at 840 nm a charge-transfer transition is most likely.[199]

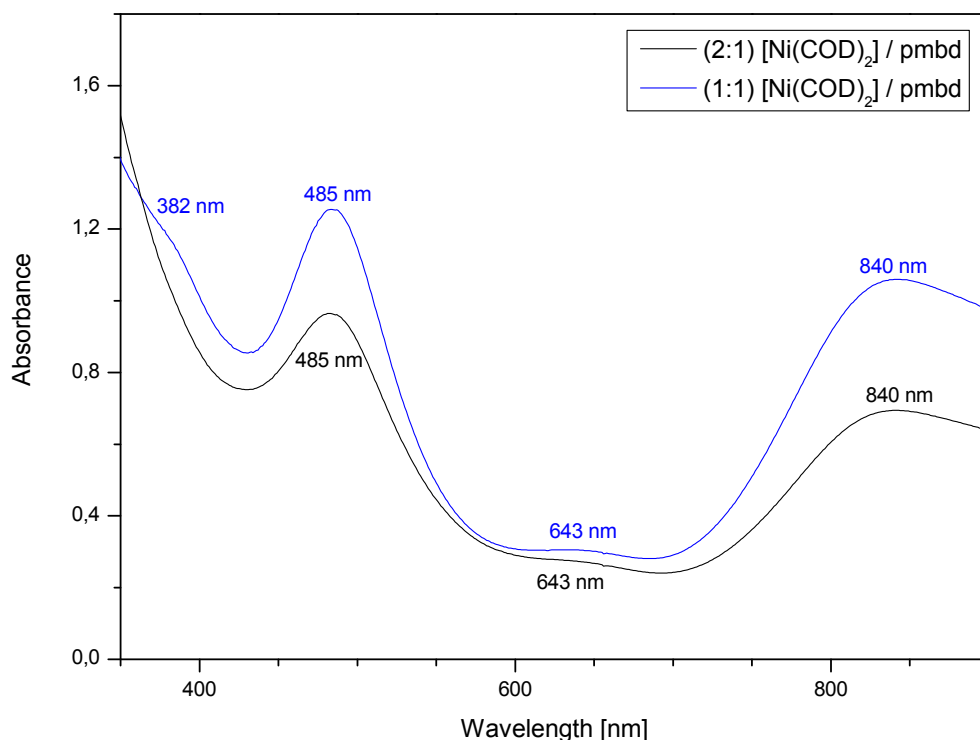


Figure 4.39: UV-Vis spectra of the complex [Ni(pmbd)] in THF.

4.2.4.3 [Ni(mpmbd)]

Figure 4.40 shows the UV-Vis spectra of [Ni(mpmbd)] obtained by the reaction of [Ni(COD)₂] and mpmbd in a 2:1 (black curve) and 1:1 ratio (blue curve) in THF. In contrast to the complex [Ni(pmbd)], [Ni(mpmbd)] has a dark purple color and both spectra obtained exhibit four absorption bands. The band at 375 nm is a weak shoulder of the very strong band at 325 nm which can be attributed to charge-transfer transitions. Bands assigned to metal d-d transitions can be observed at 537 (539) nm with a weak shoulder at 655 nm and a small broad band at 818 (819) nm.[199]

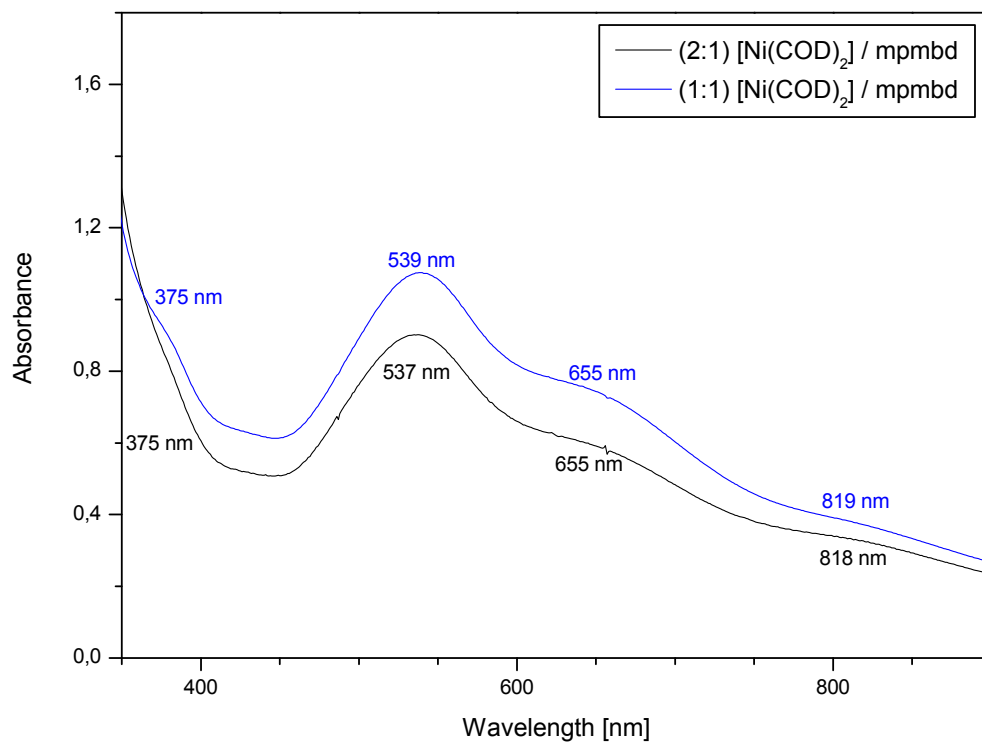


Figure 4.40: UV-Vis spectra of the complex [Ni(mpmbd)] in THF.

4.2.4.4 [Ni(pmed)]

The UV-Vis spectra of the complex [Ni(pmed)] in THF with ratios of [Ni(COD)₂] to the ligand pmed of 2:1 (black curve) and 1:1 (blue curve) are shown in Figure 4.41. Contrary to the measured complexes above, two different spectra were obtained. The complex solution with a 2:1 ratio has a brown color with three absorption maxima whereas the solution with a 1:1 ratio has a red-brown color and exhibits five absorption bands. The first sharp and strong band at 387 nm of the blue curve (1:1 ratio) can be assigned to charge-transfer transitions between the nickel(0) center and the ligand. The three bands at 455, 520, and 655 nm can be attributed to d-d transitions whereas for the strong band at 849 nm a charge-transfer transition is most likely. In contrast, the black curve (1:1 ratio) exhibits only three weak and broad bands at 490, 645 and 852 nm which can be attributed to metal d-d transitions.[199] Due the difference in the obtained spectra it is supposed that using a 2:1 ratio of [Ni(COD)₂] to pmpd possibly forms a dinuclear nickel complex with different coordination geometry.

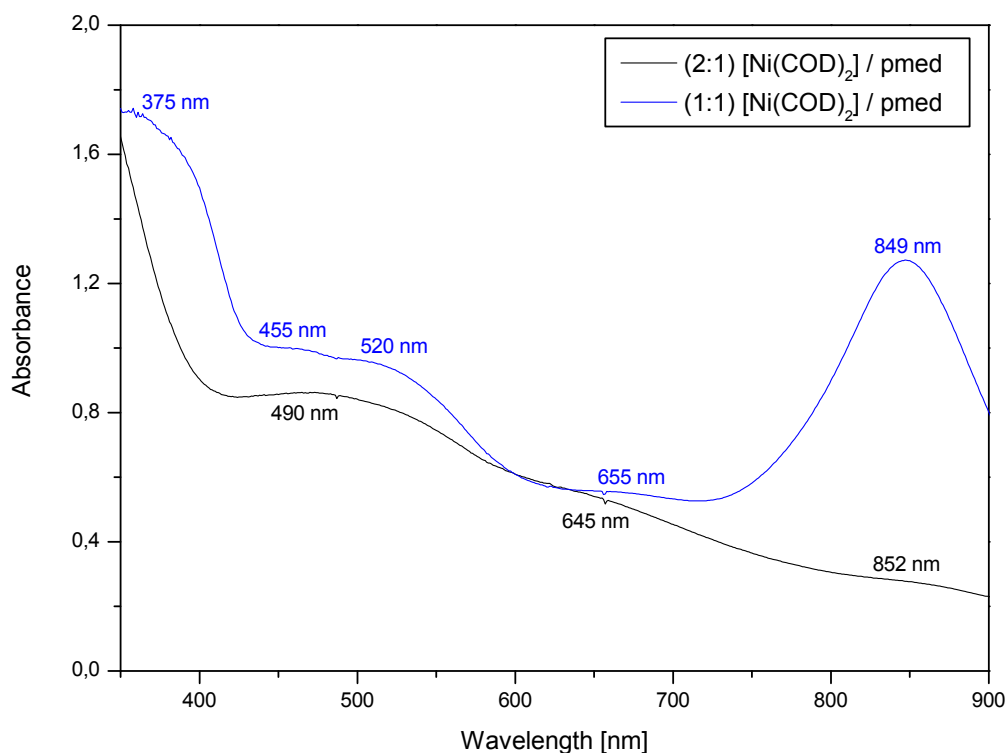


Figure 4.41: UV-Vis spectra of the complex [Ni(pmed)] in THF.

4.2.4.5 [Ni(pmpd)]

Figure 4.42 shows the UV-Vis spectra of [Ni(pmpd)] obtained by the reaction of [Ni(COD)₂] and pmpd with a ratio of 2:1 (black curve) and 1:1 (blue curve) in THF. Both complex solutions have a dark red-violet color and exhibit two absorption bands. Both spectra show a strong band at 531 (525) nm and an additional smaller broad band. Using a 2:1 ratio leads to the formation of a band at 642 nm whereas a 1:1 ratio forms a small broad band at 840 nm. All observed bands can be assigned to metal d-d transitions. The sharp strong charge-transfer band is shifted to lower wavelengths (308 nm (2:1) and 325 nm (1:1)).[199]

Due the difference in the obtained spectra it is supposed that using a 2:1 ratio of [Ni(COD)₂] to pmpd could possibly form a dinuclear nickel complex.

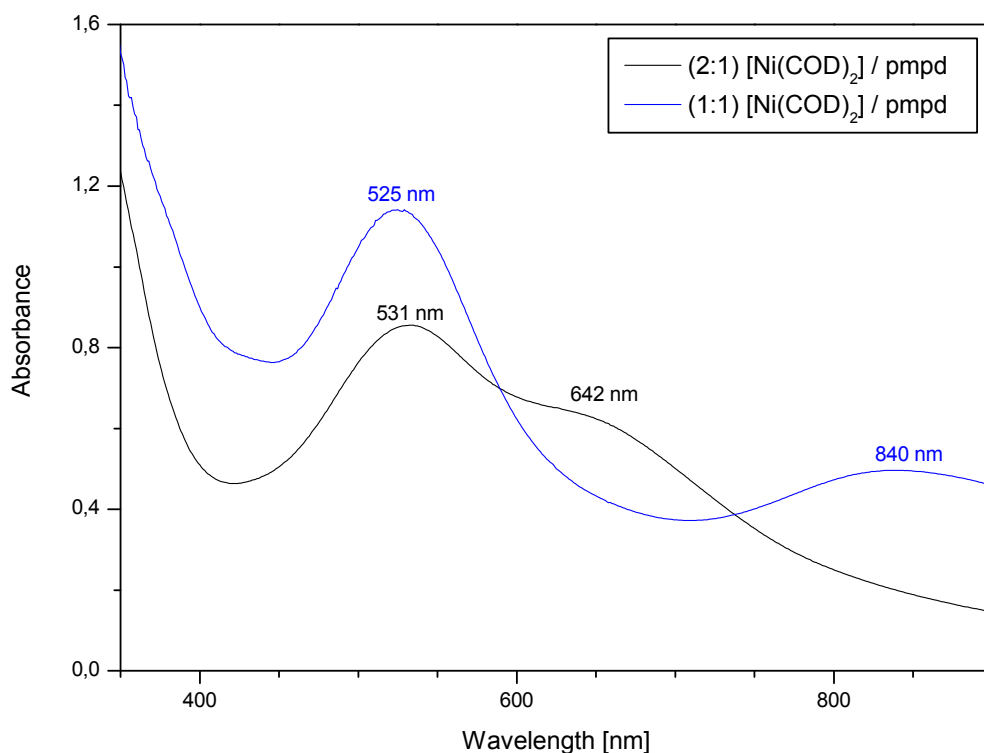


Figure 4.42: UV-Vis spectra of the complex [Ni(pmpd)] in THF.

4.2.4.6 [Ni(Me-BPy)]

The UV-Vis spectra of the complex [Ni(Me-BPy)] in THF with ratios of [Ni(COD)₂] to the ligand Me-BPy of 2:1 (black curve) and 1:1 (blue curve) are shown in Figure 4.43. The complex solutions have a dark purple color similar to [Ni(mpmbd)] and [Ni(bipy)(COD)] and both exhibit three absorption bands. A small shoulder of the strong charge-transfer band at 310 nm can be observed at 370 nm. Furthermore, the sharp intense band at 574 nm can also be assigned to a charge-transfer transition whereas the weak broad band at 870 nm can be attributed to a d-d transition.[199]

Due to the similarity of the obtained spectra to [Ni(bipy)(COD)][141] which also shows a strong absorption band at 568 nm and a weak broad band at 850 nm a binuclear complex with coordinated COD is most likely formed. O-BPy and bipy have similar electronic properties and in case of [Ni(bipy)(COD)] the olefin COD is also coordinated. The obtained small shift of the bands could be attributed to different coordination geometries of both complexes.

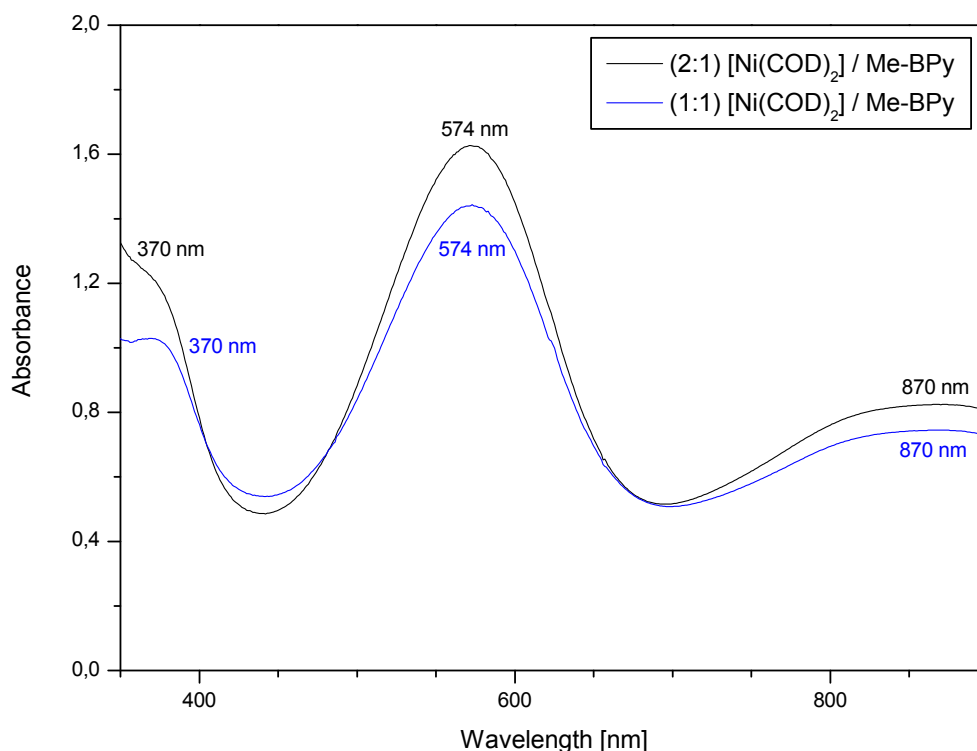


Figure 4.43: UV-Vis spectra of the complex [Ni(Me-BPy)] in THF.

4.3 Experimental

4.3.1 Materials and Reagents

Commercial reagents were used as obtained without further purification except for amines and aldehydes which have been further purified by distillation. Solvents were dried according to standard procedures. Tetrakis(acetonitrile)copper(I)-salts were either obtained commercially from Aldrich or synthesized from copper(I) oxide according to a method described in the literature.[200] All handling and storage of oxygen sensitive compounds and materials used was carried out in a glove box (M. Braun, Garching, Germany; $O_2 < 0.1$ ppm, $H_2O < 0.1$ ppm) within an argon atmosphere.

4.3.2 Crystallography

Single crystals suitable for X-ray diffraction were mounted on the tip of a glass rod using inert perfluoropolyether oil. The X-ray crystallographic data were collected on a STOE IPDS- or a BRUKER NONIUS FR591 KappaCCD diffractometer equipped with low temperature systems. Mo- K_α radiation ($\lambda = 0.71073$ Å) and a graphite monochromator (STOE IPDS) was used. The structures were solved by direct methods in SHELXS97 and SHELXL 2013 and refined by using full-matrix least squares in SHELXL97.[179]

4.3.3 NMR Spectroscopy

1H -NMR and ^{13}C -NMR spectra were recorded on a Bruker-Aspect 2000/3000 400-MHz spectrometer by Dr. H. Hausmann (JLU Gießen, Institute for Organic Chemistry).

4.3.4 UV-Vis Spectroscopy

UV-Vis absorbance spectra were measured at room temperature using an Agilent 8453 spectrophotometer and quartz cuvettes ($d = 10$ mm).

4.3.5 IR Spectroscopy

IR measurements were performed on a Jasco FT/IR 4100 spectrometer. All samples were measured as KBr-pellet at room temperature.

4.3.6 Synthesis of the Ligands

4.3.6.1 O-BPy

The ligand 1,2-Bis(2,2'-bipyridin-6-yl)ethane was synthesized and purified as previously described in literature.[181]

$^1\text{H-NMR}$ (CDCl_3/TMS) δ 8.67 (d, 2H, *bipy-H*), 8.46 (d, 2H, *bipy-H*), 8.20 (d, 2H, *bipy-H*), 7.80 (dt, 2H, *bipy-H*), 7.69 (t, 2H, *bipy-H*), 7.29 (m, 2H, *bipy-H*), 7.17 (d, 2H, *bipy-H*), 3.43 (s, 4H, $-\text{CH}_2$);

$^{13}\text{C-NMR}$ (CDCl_3/TMS) δ 160.7 (sp^2 , *bipy-C*), 156.6 (sp^2 , *bipy-C*), 155.5 (sp^2 , *bipy-C*), 149.1 (sp^2 , *bipy-C*), 137.1 (sp^2 , *bipy-C*), 136.8 (sp^2 , *bipy-C*), 123.5 (sp^2 , *bipy-C*), 123.0 (sp^2 , *bipy-C*), 121.3 (sp^2 , *bipy-C*), 118.4 (sp^2 , *bipy-C*), 37.7 (sp^3 , $\text{CH}_2\text{-C}$).

4.3.6.2 Me-BPy

The ligand 1,2-bis(4'-methyl-2,2'-bipyridine-4-yl)ethane was purchased commercially from Tokyo Chemical Industry Co., TCI (Japan).

4.3.6.3 Mpmbd, pmbd, pmed, pmpd

The ligands *N,N'*-Bis((6-methylpyridine-2-yl)methylene)butane-1,4-diamine (mpmbd), *N,N'*-bis(pyridine-2-ylmethylene)butane-1,4-diamine (pmbd), *N,N'*-bis(pyridine-2-yl-methylene)-ethane-1,2-diamine (pmed) and *N,N'*-bis(pyridine-2-ylmethylene)pentane-1,5-diamine (pmpd) were synthesized and purified according to a procedure described in literature.[185]

Mpmbd: $^1\text{H-NMR}$ (CDCl_3/TMS) δ 8.36 (s, 2H, *imine-H*), 7.79 (d, 2H, *pyridine-H*), 7.62 (t, 2H, *pyridine-H*), 7.17 (d, 2H, *pyridine-H*), 3.71 (m, 4H, $-\text{CH}_2$), 2.59 (s, 6H, $-\text{CH}_3$), 1.81 (m, 4H, $-\text{CH}_2$);

4.3 Experimental

^{13}C -NMR (CDCl_3/TMS) δ 162.3 (sp^2 , *pyridine*-C), 158.1 (sp^2 , *imine*-C), 154.0 (sp^2 , *pyridine*-C), 136.8 (sp^2 , *pyridine*-C), 124.3 (sp^2 , *pyridine*-C), 118.3 (sp^2 , *pyridine*-C), 61.3 (sp^3 , CH_2 -C), 28.5 (sp^3 , CH_2 -C), 24.4 (sp^3 , CH_3 -C).

Pmbd: ^1H -NMR (CDCl_3/TMS) δ 8.64 (d, 2H, *pyridine*-H), 8.39 (s, 2H, *imine*-H), 7.98 (d, 2H, *pyridine*-H), 7.74 (t, 2H, *pyridine*-H), 7.30 (m, 2H, *pyridine*-H), 3.74 (m, 4H, $-\text{CH}_2$), 1.84 (m, 4H, $-\text{CH}_2$);

^{13}C -NMR (CDCl_3/TMS) δ 161.9 (sp^2 , *pyridine*-C), 154.5 (sp^2 , *imine*-C), 149.5 (sp^2 , *pyridine*-C), 136.5 (sp^2 , *pyridine*-C), 124.7 (sp^2 , *pyridine*-C), 121.3 (sp^2 , *pyridine*-C), 61.2 (sp^3 , CH_2 -C), 28.5 (sp^3 , CH_2 -C).

Pmed: ^1H -NMR (CDCl_3/TMS) δ 8.63 (d, 2H, *pyridine*-H), 8.42 (s, 2H, *imine*-H), 7.98 (d, 2H, *pyridine*-H), 7.73 (t, 2H, *pyridine*-H), 7.30 (t, 2H, *pyridine*-H), 4.05 (s, 4H, $-\text{CH}_2$);

^{13}C -NMR (CDCl_3/TMS) δ 163.4 (sp^2 , *pyridine*-C), 154.4 (sp^2 , *imine*-C), 149.4 (sp^2 , *pyridine*-C), 136.6 (sp^2 , *pyridine*-C), 124.8 (sp^2 , *pyridine*-C), 121.4 (sp^2 , *pyridine*-C), 61.3 (sp^3 , CH_2 -C).

Pmpd: ^1H -NMR (CDCl_3/TMS) δ 8.64 (d, 2H, *pyridine*-H), 8.38 (s, 2H, *imine*-H), 7.97 (d, 2H, *pyridine*-H), 7.73 (t, 2H, *pyridine*-H), 7.30 (t, 2H, *pyridine*-CH₂), 3.69 (m, 4H, $-\text{CH}_2$), 1.80 (m, 4H, $-\text{CH}_2$), 1.49 (m, 2H, $-\text{CH}_2$);

^{13}C -NMR (CDCl_3/TMS) δ 161.8 (sp^2 , *pyridine*-C), 154.6 (sp^2 , *imine*-C), 149.4 (sp^2 , *pyridine*-C), 136.5 (sp^2 , *pyridine*-C), 124.6 (sp^2 , *pyridine*-C), 121.2 (sp^2 , *pyridine*-C), 61.4 (sp^3 , CH_2 -C), 30.5 (sp^3 , CH_2 -C), 25.1 (sp^3 , CH_3 -C).

4.3.7 Synthesis of the Ni(0) Complexes

4.3.7.1 $[\text{Ni}(\text{COD})_2]$

Bis(1,5-cyclooctadiene)nickel(0) was synthesized as previously described in literature.[170]

All following complexes were prepared under inert conditions in a glove box.

4.3.7.2 $[\text{Ni}(\text{O-BPy})]$

Mixing 50 mg (0.18 mmol) of $[\text{Ni}(\text{COD})_2]$ with 31 mg (0.092 mmol) of the ligand O-BPy in THF, respectively 50 mg (0.18 mmol) $[\text{Ni}(\text{COD})_2]$ and

62 mg (0.18 mmol) O-BPy, gave a dark blue solution. After stirring for 3 hours and diffusion of n-pentane into the solution, crystals suitable for X-ray structure determination were obtained.

4.3.7.3 [Ni₂(O-BPy)(η^2 -C₄H₆)₂]

A solution of 50 mg (0.18 mmol) [Ni(COD)₂] and 31 mg (0.092 mmol) O-BPy in THF was reacted with gaseous 1,3-butadiene at -20 °C. The solution turned immediately green and a dark green solid precipitated. Filtering and diffusion of pentane into the THF solution did not result in crystals suitable for X-ray diffraction during this work.

4.3.7.4 [Ni(pmbd)]

By mixing 50 mg (0.18 mmol) of [Ni(COD)₂] and 24 mg (0.091 mmol) of the ligand pmbd in THF, respectively 30 mg (0.11 mmol) [Ni(COD)₂] and 29 mg (0.11 mmol) pmpd, the solution turned brown. After stirring for 2-3 hours and diffusion of n-pentane into the solution crystals suitable for X-ray diffraction could be obtained.

4.3.7.5 [Ni(mpmbd)]

To a solution of 50 mg (0.18 mmol) of [Ni(COD)₂] in THF 26 mg (0.089 mmol) of the ligand mpmbd, respectively 52 mg (0.18 mmol), was added. After stirring for a few hours and diffusion of n-pentane into the dark violet solution crystals suitable for X-ray diffraction could be obtained.

4.3.7.6 [Ni(pmed)]

To 50 mg (0.18 mmol) of [Ni(COD)₂] in THF 23 mg (0.10 mmol) of pmed, respectively 44 mg (0.19 mmol), was added. The resulting dark red-brown solution was stirred for 2 hours. Diffusion on n-pentane into the THF solution did not result in crystals suitable for X-ray structure determination.

4.3 Experimental

4.3.7.7 [Ni(pmpd)]

Mixing 50 mg (0.18 mmol) of [Ni(COD)₂] with 25 mg (0.089 mmol) of the ligand pmpd in THF, respectively 50 mg (0.18 mmol) of [Ni(COD)₂] and 50 mg (0.18 mmol) pmpd, gave a dark red-violet solution. Crystals suitable for X-ray structure determination could not be obtained.

4.3.7.8 [Ni(Me-BPy)]

To 50 mg (0.18 mmol) of [Ni(COD)₂] in THF 33 mg (0.091 mmol) of the ligand Me-BPy, respectively 66 mg (0.18 mmol), was added. The solution turned dark purple and was stirred for 2 hours. Diffusion of n-pentane into the solution did not afford crystals suitable for X-ray diffraction during this work.

4.3.8 Synthesis of the Cu(I) Complexes

All following complexes were prepared under inert conditions in a glove box.

4.3.9 [Cu(COD)₂]⁺

Bis(1,5-cyclooctadiene)copper(I)-perchlorate and -tetrafluoroborate were prepared according to a procedure described in literature.[178]

4.3.9.1 [Cu₂(O-BPy)₂](BF₄)₂

To a solution of 35 mg (0.10 mmol) of O-BPy and 108 mg (1.00 mmol) of COD in acetone 75 mg (0.21 mmol) of [Cu(COD)₂]₂BF₄ was added. The resulting orange suspension was stirred furthermore for 1 hour. After filtration and diffusion of diethyl ether into the solution at -20 °C, crystals suitable for X-ray structure determination could be obtained.

Mixing 50 mg (0.16 mmol) of [Cu(CH₃CN)₄]₂BF₄ in acetone with 27 mg (0.079 mmol) of the ligand O-BPy and 150 mg (1.39 mmol) of COD gave a deep

red solution which turned orange with an orange precipitate after a few minutes of stirring. After filtration and diffusion of diethyl ether into the solution crystals suitable for X-ray diffraction could be obtained.

4.3.9.2 [Cu(O-BPy)](BF₄)₂

[Cu₂(O-BPy)₂](BF₄)₂ is quite stable towards dioxygen but stirring an solution of 50 mg (0.051 mmol) of the copper(I) complex under air for several days resulted in a change of color from orange to green. It was allowed to stand until crystallization occurred and crystals suitable for X-ray structure determination were obtained.

4.3.9.3 [Cu₂(O-BPy)(COD)₂](SO₃CF₃)₂

A solution of 50 mg (0.13 mmol) [Cu(CH₃CN)₄]SO₃CF₃ dissolved in a small amount of acetone was added to a solution of 23 mg (0.068 mmol) O-BPy and 130 mg (1.20 mmol) COD in acetone under vigorous stirring. After diffusion of diethyl ether into the dark red solution crystals suitable for X-ray diffraction could be obtained.

4.3.9.4 [Cu₂(O-BPy)(C₄H₆)₂](SO₃CF₃)₂

A solution of 50 mg (0.049 mmol) of [Cu₂(O-BPy)(COD)₂](SO₃CF₃)₂ in acetone as well as in methanol was reacted with gaseous 1,3-butadiene at -20 °C. The color changed from red to yellow-orange and a small amount of a yellow solid precipitated. Filtration and diffusion of diethyl ether into the solution did not result in crystals suitable for X-ray determination.

5 Reactivity of Nickel Complexes with Macrocyclic Ligands

5.1 Introduction

Activation of small molecules by transition metal sites is of great importance for a wide variety of organic transformations which can be both, natural and industrial. In that regard, low valent redox-active metal centers with low coordination numbers are well suited systems. Therefore, the better understanding of the formation and reactivity of these compounds is of high interest.

Ligand selection and design is of significant importance, whereas macrocyclic ligands proved to be quite useful. Recently, Nam and co-workers published a review article on mononuclear metal–O₂ complexes bearing the macrocyclic tetramethylated cyclam ligand 14-tmc and the tetramethylated cyclen ligand 12-tmc (see Figure 5.1) or derivatives for various metal ions, such as chromium, manganese, iron, cobalt and nickel.[144]

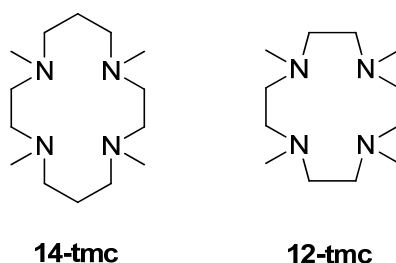


Figure 5.1: Structures of the macrocyclic ligands 1,4,8,11-tetramethyl-1,4,8,11-tetraazacyclotetradecane (14-tmc) and 1,4,7,10-tetramethyl-1,4,7,10-tetraazacyclodecane (12-tmc).

Thereby, the formation and spectroscopic characterization of a nickel(II)-superoxo complex $[\text{Ni}(\text{14-tmc})\text{O}_2]^+$, obtained by the reaction of $[\text{Ni}(\text{14-tmc})(\text{CH}_3\text{CN})]^{2+}$ with H_2O_2 in presence of a base or the low valent complex $[\text{Ni}(\text{14-tmc})]^+$ and dioxygen, was reported.[137]

Furthermore, a nickel(III)-peroxo complex could be structurally characterized by using the macrocyclic ligand 12-tmc. The reaction of $[\text{Ni}(\text{12-tmc})(\text{CH}_3\text{CN})]^{2+}$ with H_2O_2 in the presence of a base afforded the green peroxo complex

$[\text{Ni}(\text{12-tmc})\text{O}_2]^+$ (see 1.5.3.3).[136] However, not only macrocyclic ligands but also chelating monoanionic β -diketiminato ligands have been successfully utilized for stabilizing reactive low oxidation states of transition metals in the past.[201] In that regard, investigations on the reactivity of isolable β -diketiminato-nickel(I) complexes with sterically demanding aryl substituents showed remarkable reactivities due to their capability of even binding dinitrogen to give Ni–N₂ complexes or activating dihydrogen to afford hydridonickel(II) complexes in absence of donor solvents.[202–206] Driess and co-workers used β -diketiminato-nickel(I) precursors as strong reducing agents to activate nitrous oxide, dioxygen, the heavier chalcogenes sulfur, selenium, tellurium as well as white phosphorous.[124] By reacting the dinuclear Ni(I) complex $[(\text{L}^{\text{iPr}}\text{Ni})_2(\mu\text{-}\eta^3\text{-C}_6\text{H}_5\text{Me})]$ **5.1** ($\text{L}^{\text{iPr}} = \text{HC}(\text{CMeNC}_6\text{H}_3\text{iPr}_2)_2$) with dry dioxygen they were able to isolate and structurally characterize the first room temperature stable nickel(II)-superoxo complex **5.2** (see Figure 5.2).

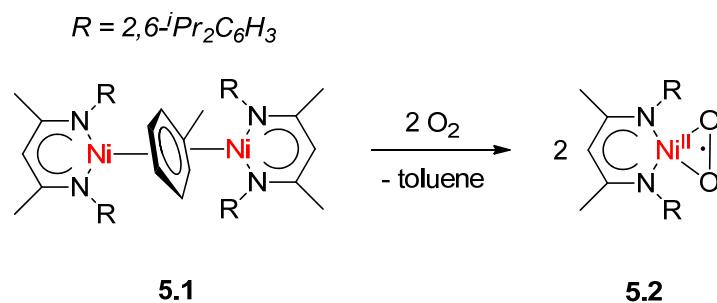


Figure 5.2: Formation of the superoxo-nickel(II) complex (**4.2**) from the dinuclear β -diketiminato-toluene-nickel complex (**5.1**).[126]

With the aim of isolating a “nickel-oxo” species $\text{L}^{\text{iPr}}\text{Ni}=\text{O}$, complex **5.1** was furthermore reacted with nitrous oxide to induce an oxygen atom transfer from N₂O to the nickel center. Studies on this type of reaction with nickel carbene complexes have been reported previously.[207] Figure 5.3 shows the reaction of the dinuclear nickel(I) complex **5.1** with dry nitrous oxide in toluene at -20 °C which afforded the dinuclear β -diketiminato-hydroxonickel(II) complex **5.4**. [126]

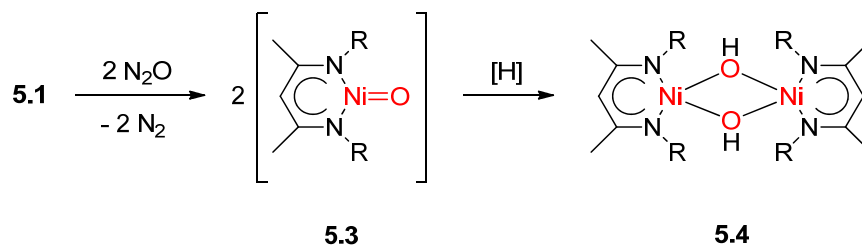


Figure 5.3: Activation of nitrous oxide with the dinuclear β -diketiminato-toluene-nickel(I) complex (**5.1**) affording di- β -diketiminato-bis(μ -hydroxo)-nickel(II) (**5.4**).[124]

It is supposed that the “nickel-oxo” species **5.3** is formed by monooxygenation of **5.1** by N_2O and the release of dinitrogen. Subsequently, protonation and dimerization leads to the dinuclear hydroxo-nickel complex **5.4**. The molecular structure of **5.4** is shown in Figure 5.4.[124]

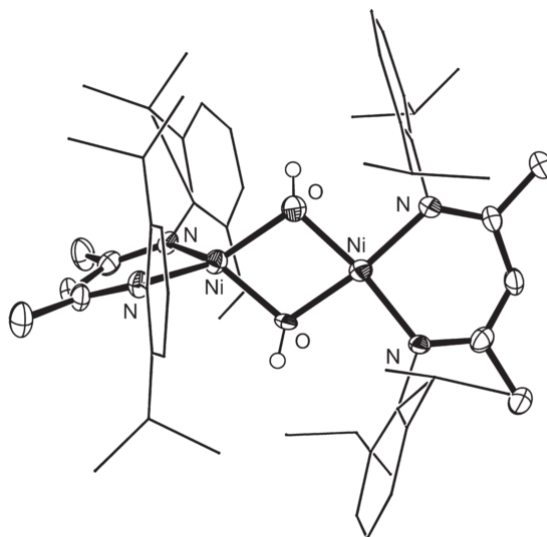


Figure 5.4: Molecular structure of di- β -diketiminato-bis(μ -hydroxo)-nickel(II) (**5.4**).[124]

Activation of N_2O is not only of interest to the removal as a green-house gas but also to the use in organic chemistry as a selective oxidizing agent.

So far, a nickel complex with coordinated N_2O or a “nickel-oxo” species could not be isolated and characterized. In this regard, efforts were made to synthesize a macrocyclic nickel(I) complex and to form a “Ni- N_2O ” species by the reaction with nitrous oxide in this work. Furthermore, macrocyclic nickel(II) complexes were reacted with hydrogen peroxide, sodium peroxide as well as potassium superoxide to obtain the respective nickel-oxygen adduct species.

5.2 Results

Nickel complexes with the macrocyclic ligands 1,4,8,11-tetramethyl-1,4,8,11-tetraazacyclotetradecane (14-tmc) and the isomer *rac*-5,7,7,12,14,14-hexamethyl-1,4,8,11-tetraazacyclotetradecane (tetB) were synthesized. Results of reactions regarding nickel-oxygen adducts will be presented in the following.

5.2.1 Synthesis and Reactions of Nickel Complexes bearing 14-tmc

5.2.1.1 Ligand 14-tmc

The ligand 1,4,8,11-tetramethyl-1,4,8,11-tetraazacyclotetradecane (14-tmc) is a tetraaza macrocyclic ligand affording complexes with a planar array of donor atoms and minimal steric hindrance which is highly desirable for metal-oxygen adducts. 14-tmc is prepared by methylation of the ligand 1,4,8,11-tetraazacyclotetradecane (cyclam). In literature a simple and fast synthesis of cyclam via a template reaction is described by E. Barefield (see Figure 5.5).[208]

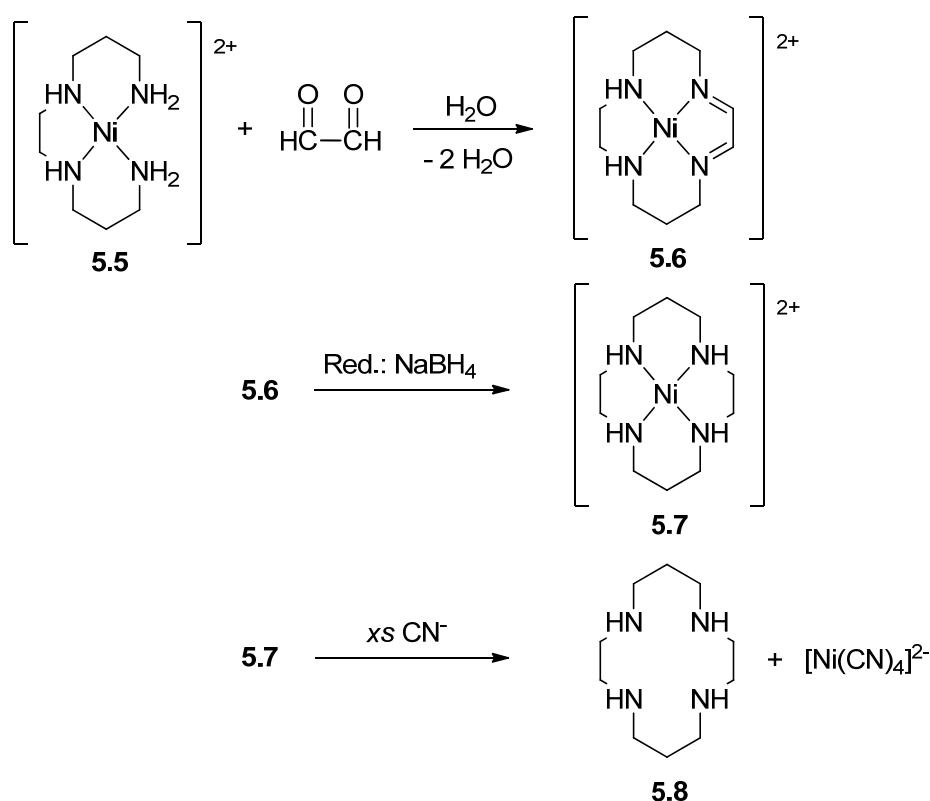


Figure 5.5: Reaction scheme for the synthesis of cyclam (5.8).[208]

5.2 Results

To obtain the blue starting nickel complex **5.5**, the amine 1,5,8,12-tetraazadodecane is dissolved with $\text{Ni}(\text{ClO}_4)_2 \cdot 6 \text{H}_2\text{O}$ in water. Adding glyoxal affords the nickel diimine complex **5.6** which is reduced using sodium tetraborohydride to give $[\text{Ni}(\text{cyclam})]^{2+}$ **5.7**. An excess amount of cyanide is added to the solution to obtain the free ligand cyclam **5.8**.

The ligand 14-tmc **5.9** is synthesized by Eschweiler-Clarke methylation of cyclam using formic acid and formaldehyde (see Figure 5.6).[209]

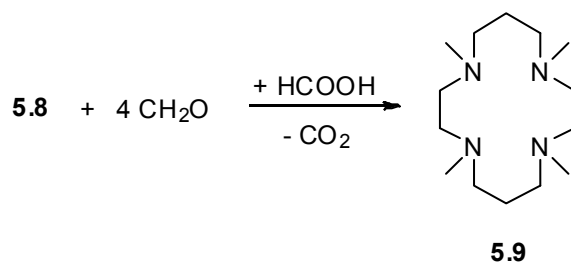


Figure 5.6: Reaction scheme for the synthesis of 14-tmc (**5.9**).[209]

5.2.1.2 Synthesis of $[\text{Ni}(\text{14-tmc})]^{2+}$

It is well known that different stereoisomers of $[\text{Ni}(\text{14-tmc})]^{2+}$ are formed depending on the synthesis route applied (see Figure 5.7).[210] Direct combination of a nickel(II) salt and 14-tmc gives the *R,S,R,S* isomer **5.10** whereas methylation of a $[\text{Ni}(\text{cyclam})]^{2+}$ complex results in the formation of the *R,S,S,R* species **5.11**. The *R,S,R,S* isomer tends to form four coordinate or five coordinate mono-solvento species whilst the *R,S,S,R* isomer affords octahedral complexes with solvent molecules in axial positions. However, interconversion of the two isomers can occur in which the *R,S,R,R* isomer **5.12** is a likely intermediate in the rearrangement process.[211]

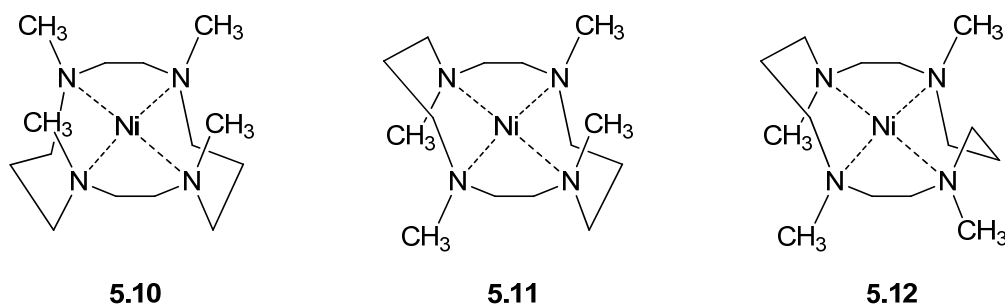


Figure 5.7: Stereoisomers of $[\text{Ni}(\text{14-tmc})]^{2+}$: (**5.10**) *R,S,R,S* (**5.11**) *R,S,S,R* (**5.12**) *R,S,R,R*. [210]

If conditions favoring the four coordinate complex are applied, only the *R,S,R,S* and *R,S,R,R* isomers are expected, if ligands or coordinating solvents are available the *R,S,S,R* isomer is prevalent. Molecular structures of the *R,S,R,S* and *R,S,S,R* isomers are presented in the following.

5.2.1.2.1 [Ni(14-tmc)](ClO₄)₂

The complex [Ni(14-tmc)](ClO₄)₂ was synthesized according to a procedure described in literature by Barefield.[209] Crystals suitable for X-ray diffraction were obtained after recrystallization from acetone. Figure 5.8 shows the determined molecular structure of the dark pink *R,S,R,S* isomer which is in line with the already reported structure by Crick et al.[210] Crystallographic data, selected bond lengths and angles are given in Table 5.1 and Table 5.2. The nickel center is coordinated by the four nitrogen atoms of 14-tmc and shows almost square planar coordination with some tetrahedral distortion by the N4-Ni1-N3 and N1-Ni1-N2 bond angles of 168-171°. All four methyl groups of 14-tmc are on the same side of the Ni-N plane.

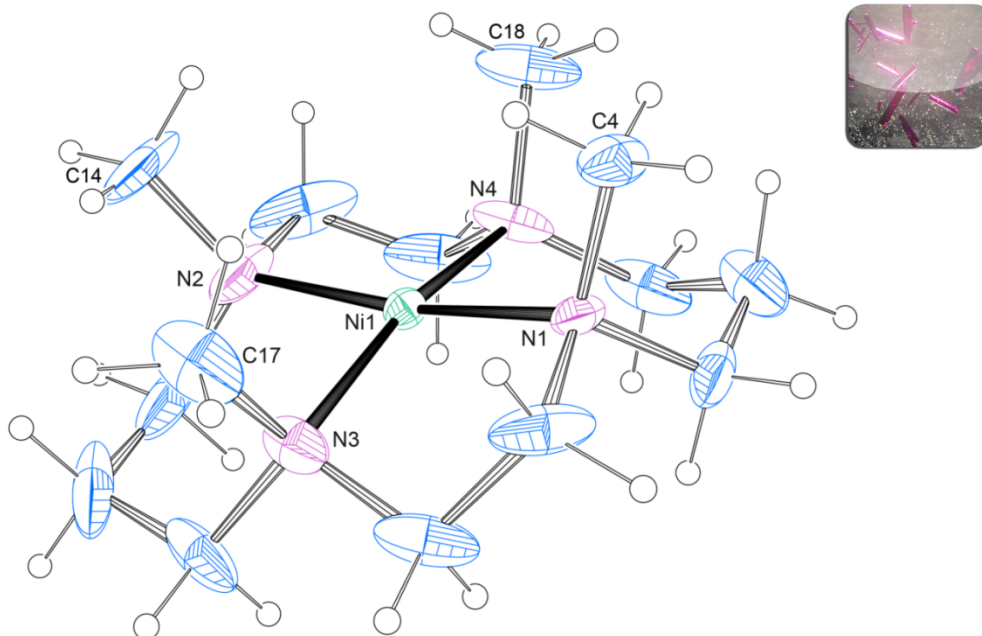


Figure 5.8: ORTEP plot of the cation [Ni(14-tmc)]²⁺ (*R,S,R,S* isomer). Ellipsoids are drawn at 25 % probability level. Solvent molecules are omitted for clarity.

Table 5.1: Crystal data and structure refinement for [Ni(14-tmc)](ClO₄)₂.

Internal identification code	schindler14041
Empirical formula	C ₁₇ H ₃₈ Cl ₂ N ₄ Ni O ₉
Formula weight	572.12
Temperature	150 (2) K
Wavelength	0.71073 Å
Crystal system, space group	Orthorhombic, <i>P</i> 2 ₁ 2 ₁ 2 ₁
Unit cell dimensions	a = 8.3661(17) Å α = 90 ° b = 11.336(2) Å β = 90 ° c = 22.388(5) Å γ = 90 °
Volume	2502.6(9) Å ³
Z, calculated density	4, 1.518 Mg/m ³
Absorption coefficient	1.036 mm ⁻¹
F(000)	1208
Crystal size	0.200 x 0.100 x 0.100 mm
Theta range for data collection	1.543 to 27.502 °
Limiting indices	-10 ≤ h ≤ 10, -14 ≤ k ≤ 13, -31 ≤ l ≤ 34
Reflections collected / unique	33745 / 5685 [R(int) = 0.1625]
Completeness to theta = 25.242	100.0 %
Absorption correction	Empirical
Refinement method	Full-matrix least-squares on F ²
Data / restraints / parameters	5685 / 0 / 304
Goodness-of-fit on F ²	0.980
Final R indices [I > 2σ(I)]	R1 = 0.0512, wR2 = 0.1065
R indices (all data)	R1 = 0.0927, wR2 = 0.1235
Extinction coefficient	n/a
Largest diff. peak and hole	0.423 and -0.428 e. Å ⁻³

Table 5.2: Selected bond lengths [Å] and angles [°] for [Ni(14-tmc)](ClO₄)₂.

Ni(1)-N(1)	1.969(5)	Ni(1)-N(4)	1.965(7)	N(3)-C(17)	1.486(11)
Ni(1)-N(2)	1.974(7)	N(1)-C(4)	1.473(9)	N(4)-C(18)	1.510 (10)
Ni(1)-N(3)	1.968 (6)	N(2)-C(14)	1.480(11)		

N(4)-Ni(1)-N(3)	168.4(3)	N(1)-Ni(1)-N(2)	171.0(3)
N(4)-Ni(1)-N(1)	93.6(3)	Ni(1)-N(1)-C(4)	112.3(4)
N(3)-Ni(1)-N(1)	87.0(3)	Ni(1)-N(2)-C(14)	111.6(6)
N(4)-Ni(1)-N(2)	86.6(4)	Ni(1)-N(3)-C(17)	112.9(6)
N(3)-Ni(1)-N(2)	94.7(4)	Ni(1)-N(4)-C(18)	113.5(6)

5.2.1.2.2 [Ni(14-tmc)(MeCN)₂](ClO₄)₂

[Ni(14-tmc)(MeCN)₂](ClO₄)₂ was prepared according to the synthetic route reported by Barefield.[209] Crystals suitable for X-ray diffraction were obtained after recrystallization from acetonitrile. The molecular structure of the pale purple *R,S,S,R* isomer is shown in Figure 5.9. Crystallographic data, selected bond lengths and angles are given in Table 5.3 and Table 5.4. Two methyl groups (C4/C7 and C4a/C7a) of 14-tmc are on each side of the nickel-nitrogen plane. The nickel(II) center shows an octahedral geometry being coordinated by the four nitrogen atoms of 14-tmc and the two nitrogen atoms of the solvent molecules acetonitrile in axial position.

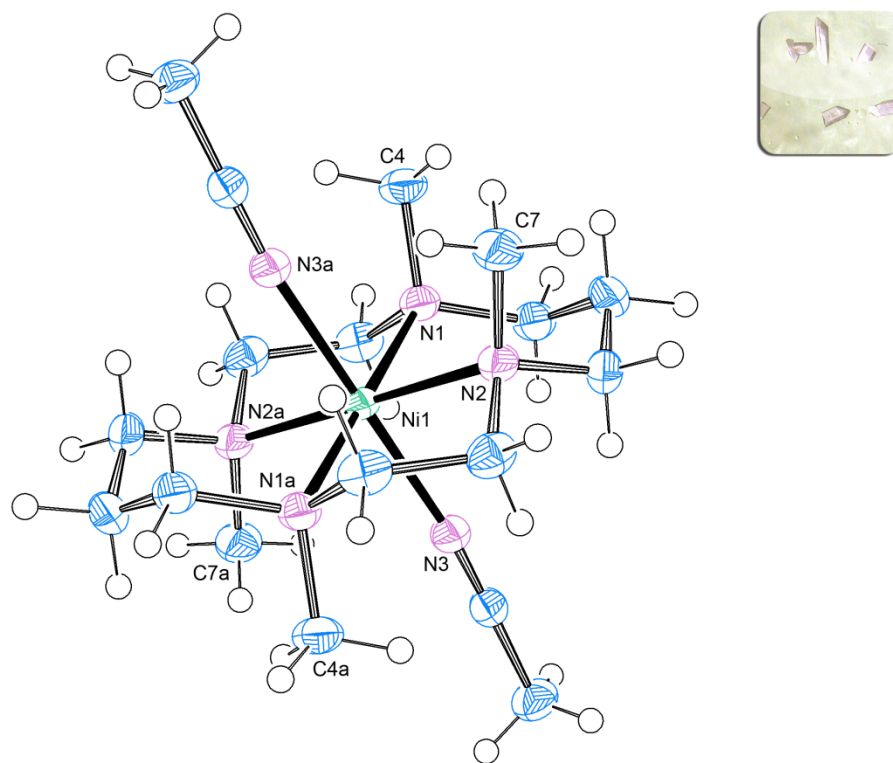


Figure 5.9: ORTEP plot of the cation [Ni(14-tmc)(MeCN)₂]²⁺ (*R,S,S,R* isomer). Ellipsoids are drawn at 50 % probability level. Free solvent molecules are omitted for clarity.

Table 5.3: Crystal data and structure refinement for [Ni(14-tmc)(MeCN)₂](ClO₄)₂.

Internal identification code	schindler13096
Empirical formula	C ₂₂ H ₄₄ Cl ₂ N ₈ Ni O ₈
Formula weight	678.26
Temperature	190 (2) K
Wavelength	0.71073 Å
Crystal system, space group	Monoclinic, <i>P</i> 2 ₁ / <i>c</i>
Unit cell dimensions	$a = 10.271(2) \text{ Å}$ $\alpha = 90^\circ$ $b = 14.691(3) \text{ Å}$ $\beta = 107.73(3)^\circ$ $c = 10.718(2) \text{ Å}$ $\gamma = 90^\circ$
Volume	1540.4(6) Å ³
Z, calculated density	2, 1.462 Mg/m ³
Absorption coefficient	0.860 mm ⁻¹
F(000)	716
Crystal size	0.600 x 0.380 x 0.360 mm
Theta range for data collection	2.429 to 27.475 °
Limiting indices	-13 ≤ h ≤ 12, -19 ≤ k ≤ 18, -13 ≤ l ≤ 13
Reflections collected / unique	14411 / 3514 [R(int) = 0.0974]
Completeness to theta = 25.242	100.0 %
Absorption correction	Empirical
Refinement method	Full-matrix least-squares on F ²
Data / restraints / parameters	3514 / 0 / 276
Goodness-of-fit on F ²	1.035
Final R indices [I > 2σ(I)]	R1 = 0.0334, wR2 = 0.0821
R indices (all data)	R1 = 0.0424, wR2 = 0.0866
Largest diff. peak and hole	0.319 and -0.438 e. Å ⁻³

Table 5.4: Selected bond lengths [Å] and angles [°] for [Ni(14-tmc)(MeCN)₂](ClO₄)₂.

Ni(1)-N(1)	2.1333(14)	Ni(1)-N(2a)	2.1513(14)	N(1)-C(4)	1.488(2)
Ni(1)-N(1a)	2.1333(14)	Ni(1)-N(3)	2.1129(14)	N(2)-C(7)	1.488(2)
Ni(1)-N(2)	2.1513(14)	Ni(1)-N(3a)	2.1128(14)		

N(3)-Ni(1)-N(3a)	180.0(0)	N(1)-Ni(1)-N(2a)	93.55(6)
N(1)-Ni(1)-N(3a)	90.55(5)	N(1a)-Ni(1)-N(2a)	86.45(6)
N(1)-Ni(1)-N(3)	89.45(5)	N(3a)-Ni(1)-N(2)	89.34(6)
N(3a)-Ni(1)-N(2a)	90.66(6)	N(1)-Ni(1)-N(2)	86.45(6)
N(3)-Ni(1)-N(2a)	89.34(6)	N(1)-Ni(1)-N(1a)	180.00(9)

5.2.1.3 Synthesis of $[\text{Ni}(\text{14-tmc})]\text{ClO}_4$

$[\text{Ni}(\text{14-tmc})](\text{ClO}_4)_2$ was dissolved in a small amount of acetonitrile and reduced with beads of the alloy sodium amalgam (5 % Na) to afford the respective nickel(I) complex (see Figure 5.10). The course of the reaction was traceable by a change of color from blue to green (see Figure 5.11).

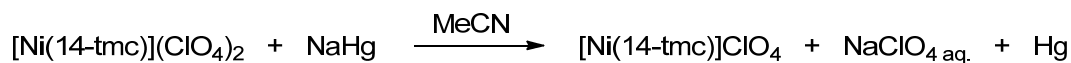


Figure 5.10: Reduction of $[\text{Ni}(\text{14-tmc})](\text{ClO}_4)_2$ with NaHg in acetonitrile.

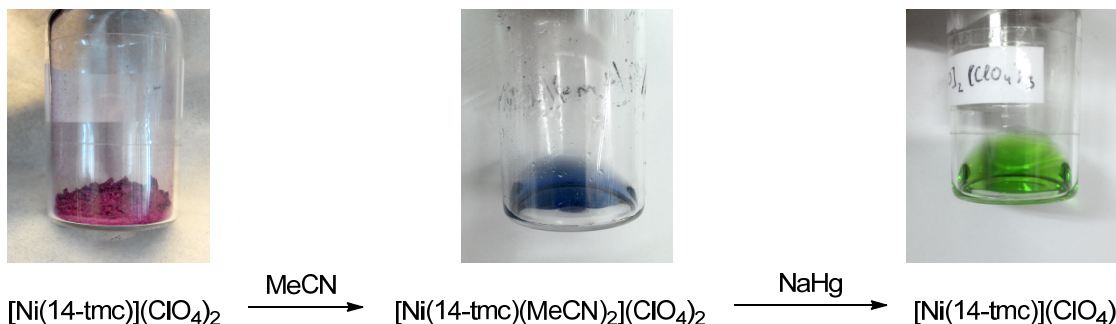


Figure 5.11: Color change in course of the reaction of $[\text{Ni}(\text{14-tmc})](\text{ClO}_4)_2$ with NaHg (5 % Na) in acetonitrile.

5.2.1.4 Reaction of $[\text{Ni}(\text{14-tmc})]\text{ClO}_4$ with Nitrous Oxide

$[\text{Ni}(\text{14-tmc})]\text{ClO}_4$ and nitrous oxide were reacted with the intention of obtaining a “nickel-oxo” species by monooxygenation of the complex by N_2O and a release of dinitrogen (see Figure 5.12).

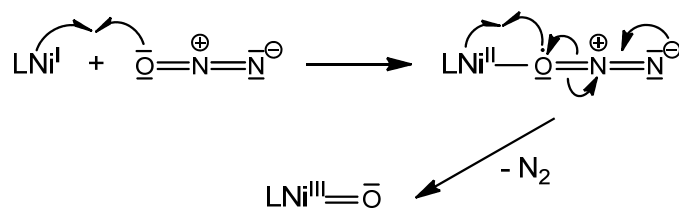


Figure 5.12: Scheme for the proposed reaction of a Ni(I) complex with N₂O.

Therefore, the reactivity of [Ni(14-tmc)]ClO₄ has been examined by reacting the complex with dry N₂O gas at -40 °C in acetonitrile. The course of the reaction was traceable by a change of color from green to brown. After a few minutes the color of the solution turned yellow-green (see Figure 5.13).

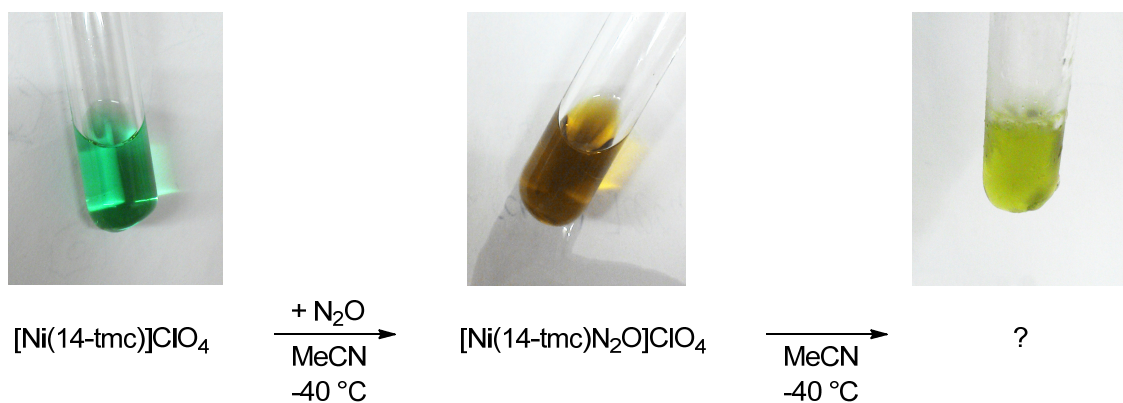


Figure 5.13: Color change in course of the reaction of [Ni(14-tmc)]ClO₄ and nitrous oxide in acetonitrile at -40 °C.

From the yellow-green complex solution colorless and green crystals suitable for X-ray diffraction could be obtained.

5.2.1.5 [Na(14-tmc)]ClO₄

Surprisingly, X-ray diffraction studies of the colorless crystals revealed the structure of the sodium complex [Na(14-tmc)]ClO₄. In literature not many macrocyclic sodium complexes are known. However, a sodium complex bearing 14-tmc as a ligand could be synthesized in methanol using NaSCN by Herlinger et al.[212] They were able to characterize the corresponding complex [Na(14-tmc)]SCN using elemental analysis, IR- and NMR spectroscopy.

Figure 5.14 shows the molecular structure of $[\text{Na}(\text{14-tmc})]\text{ClO}_4$. Crystallographic data, selected bond lengths and angles are presented in Table 5.5 and Table 5.6. All four methyl groups of 14-tmc are on one side of the Na–N plane (*R,S,R,S*) in which sodium is being coordinated by all four nitrogen atoms of the ligand and the ClO_4^- counter ion in a most likely square-pyramidal geometry.

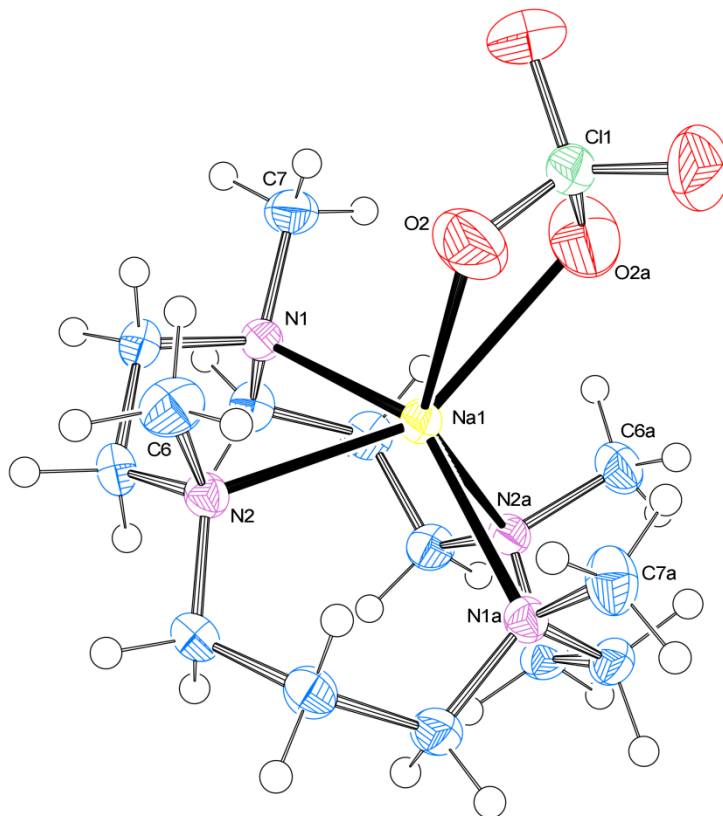


Figure 5.14: ORTEP plot of $[\text{Na}(\text{14-tmc})]\text{ClO}_4$. Ellipsoids are drawn at 50 % probability level.

Table 5.5: Crystal data and structure refinement for $[\text{Na}(\text{14-tmc})](\text{ClO}_4)$.

Internal identification code	schindler13103
Empirical formula	$\text{C}_{14} \text{H}_{32} \text{Cl} \text{N}_4 \text{Na} \text{O}_4$
Formula weight	378.87
Temperature	190 (2) K
Wavelength	0.71073 Å
Crystal system, space group	Monoclinic, $C2/c$
Unit cell dimensions	$a = 13.692(3) \text{ Å}$ $\alpha = 90^\circ$ $b = 9.2320(18) \text{ Å}$ $\beta = 91.43(3)^\circ$

5.2 Results

	$c = 14.850(3) \text{ \AA}$	$\gamma = 90^\circ$
Volume	1876.5(6) \AA^3	
Z, calculated density	4, 1.341 Mg/m^3	
Absorption coefficient	0.252 mm^{-1}	
F(000)	816	
Crystal size	0.350 x 0.100 x 0.050 mm	
Theta range for data collection	2.661 to 27.462 $^\circ$	
Limiting indices	$-14 \leq h \leq 17$, $-11 \leq k \leq 11$, $-16 \leq l \leq 19$	
Reflections collected / unique	6865 / 2132 [R(int) = 0.0779]	
Completeness to theta = 25.242	99.5 %	
Absorption correction	Empirical	
Refinement method	Full-matrix least-squares on F^2	
Data / restraints / parameters	2132 / 0 / 112	
Goodness-of-fit on F^2	1.041	
Final R indices [I > 2sigma(I)]	R1 = 0.0463, wR2 = 0.1185	
R indices (all data)	R1 = 0.0564, wR2 = 0.1237	
Extinction coefficient	n/a	
Largest diff. peak and hole	0.364 and -0.325 e. \AA^{-3}	

Table 5.6: Selected bond lengths [\AA] and angles [$^\circ$] for $[\text{Na}(\text{14-tmc})](\text{ClO}_4)$.

Na(1)-N(1)	2.4828(16)	Na(1)-N(2a)	2.4760(15)	N(1)-C(7)	1.464(2)
Na(1)-N(2)	2.4760(15)	Na(1)-O(2)	2.562(2)	N(2)-C(6)	1.467(2)
Na(1)-N(1a)	2.4828 (16)	Na(1)-O(2a)	2.562(2)	Cl(1)-O(2)	1.4309(17)
N(2)-Na(1)-N(1)	75.85(5)	N(2)-Na(1)-O(2)	94.84(5)		
N(1)- Na(1)-N(2a)	87.86(5)	N(1a)-Na(1)-O(2)	99.55(6)		
N(2a)-Na(1)-N(1a)	75.85(5)	N(2a)-Na(1)-O(2)	144.55(5)		
N(1a)-Na(1)-N(2)	87.85(5)	Cl(1)-O(2)-Na(1)	52.95(8)		
N(1)-Na(1)-O(2)	109.68(6)	O(2)-Cl(1)-O(2a)	105.90(16)		

To form this macrocyclic sodium complex, nickel has to be replaced as the metal center which only occurs in presence of a stronger ligand. A patent for the preparation of diacetonitrile reveals the nature of this ligand.[213] Next to the reduction of the nickel(II) center, the sodium metal also reacts with the solvent acetonitrile to form diacetonitrile in two steps. Thereby, a reductive condensation affords sodium-beta-iminobutyronitrile **5.13**, sodium cyanide and methane (see Figure 5.15).

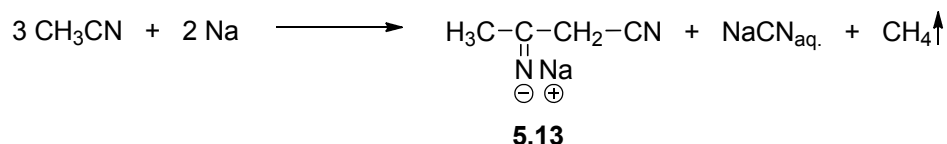


Figure 5.15: Side reaction occurring by reduction with Na in acetonitrile.[213]

Cyanide and nickel(II) give the complex $[\text{Ni}(\text{CN})_4]^{2-}$ which allows sodium to act as metal center of the macrocyclic 14-tmc complex.

To suppress this side reaction the solvent was changed from acetonitrile to propionitrile in the following.

5.2.1.6 $[\text{Ni}(14\text{-tmc})(\text{OH})]\text{ClO}_4$

Green crystals obtained by the reaction of $[\text{Ni}(14\text{-tmc})]\text{ClO}_4$ and N_2O in acetonitrile as well as in propionitrile were suitable for X-ray diffraction studies. Figure 5.16 shows the molecular structure of the obtained hydroxo complex $[\text{Ni}(14\text{-tmc})\text{OH}]\text{ClO}_4$. Crystallographic data, selected bond lengths and angles are given in Table 5.7 and Table 5.8. Due to the change of color of the “ N_2O -adduct” complex solution from brown to yellow-green (see Figure 5.13) it is supposed that a transient “nickel-oxo” species is formed which acts as a hydrogen scavenger to yield the hydroxo complex (see 5.1).

A macrocyclic nickel-hydroxo complex with 14-tmc has already been synthesized by Kieber-Emmons et al. in 2004.[214] Addition of dry O_2 gas at room temperature in THF to $[\text{Ni}(14\text{-tmc})]\text{SO}_3\text{CF}_3$ led to a color change from pale blue to green and the formation of $[\text{Ni}(14\text{-tmc})\text{OH}]\text{SO}_3\text{CF}_3$. Using FT-IR spectroscopy a band at 3628 cm^{-1} could be assigned to the $\tilde{\nu}(\text{O-H})$ mode of the terminal hydroxo group. Contrary to the structure found in this work the methyl groups of the 14-tmc ligand were allocated on both sides of the nickel nitrogen plane

5.2 Results

(*R,S,S,R* isomer). The complex depicted in Figure 5.16 shows the *R,S,R,S* isomer with all four methyl groups on one side. Nevertheless, the geometry is also likewise square-pyramidal with nickel being coordinated by the four nitrogen atoms of 14-tmc in the basal area and the hydroxo group in axial position. The Ni–OH bond length with a distance of 1.928(2) Å is slightly shorter than in the complex reported in literature (1.955 Å).[214]

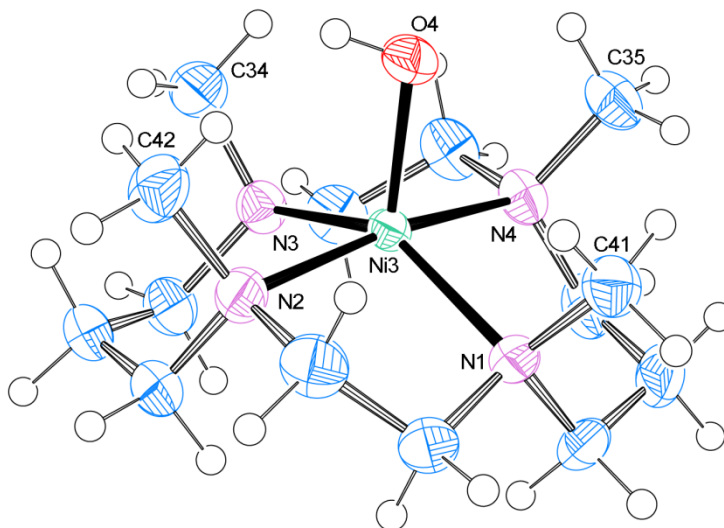


Figure 5.16: ORTEP plot of the cation $[\text{Ni}(\text{14-tmc})\text{OH}]^+$. Ellipsoids are drawn at 50 % probability level.

Table 5.7: Crystal data and structure refinement for $\text{Na}[\text{Ni}_2(\text{14-tmc})_2(\text{OH})_2](\text{ClO}_4)_3$.

Internal identification code	schindler14024-b	
Empirical formula	$\text{C}_{30} \text{H}_{69} \text{Cl}_3 \text{N}_9 \text{Ni}_2 \text{O}_{14} \text{Na}$	
Formula weight	1026.67	
Temperature	150 (2) K	
Wavelength	0.71073 Å	
Crystal system, space group	Triclinic, $P\bar{1}$	
Unit cell dimensions	$a = 11.885(2) \text{ Å}$	$\alpha = 75.20(3)^\circ$
	$b = 12.252(3) \text{ Å}$	$\beta = 73.46(3)^\circ$
	$c = 17.313(3) \text{ Å}$	$\gamma = 77.50(3)^\circ$
Volume	$2308.3(9) \text{ Å}^3$	
Z, calculated density	2, 1.4770 Mg/m ³	
Absorption coefficient	1.066 mm ⁻¹	
F(000)	1086.8	

Crystal size	0.53 x 0.15 x 0.07 mm
Theta range for data collection	3.84 to 54.96 °
Limiting indices	-15≤h≤15, -15≤k≤15, -22≤l≤22
Reflections collected / unique	38391 / 10533 [R(int) = 0.0559]
Completeness to theta = 25.242	99.5 %
Absorption correction	Empirical
Refinement method	Full-matrix least-squares on F ²
Data / restraints / parameters	10533 / 42 / 577
Goodness-of-fit on F ²	1.005
Final R indices [I>2sigma(I)]	R1 = 0.0437, wR2 = 0.1168
R indices (all data)	R1 = 0.0609, wR2 = 0.1261
Extinction coefficient	n/a
Largest diff. peak and hole	0.80 and -0.60 e. Å ⁻³

Table 5.8: Selected bond lengths [Å] and angles [°] for Na[Ni₂(14-tmc)₂(OH)₂](ClO₄)₃.

Ni(3)-N(1)	2.126(2)	Ni(3)-N(4)	2.154(2)	N(2)-C(42)	1.480(4)
Ni(3)-N(2)	2.135(2)	Ni(3)-O(4)	1.928(2)	N(3)-C(34)	1.474(4)
Ni(3)-N(3)	2.148(2)	N(1)-C(41)	1.486(4)	N(4)-C(35)	1.482(4)
N(1)-Ni(3)-N(2)	84.63(9)	N(1)-Ni(3)-O(4)	107.66(9)		
N(1)-Ni(3)-N(3)	147.25(9)	N(2)-Ni(3)-O(4)	96.09(9)		
N(2)-Ni(3)-N(3)	93.15(9)	N(3)-Ni(3)-O(4)	105.07(9)		
N(2)-Ni(3)-N(4)	170.98(9)	N(4)-Ni(3)-O(4)	92.94(9)		
N(3)-Ni(3)-N(4)	84.45(9)				

Two molecules of the [Ni(14-tmc)OH]ClO₄ complex are bridged by a coordinated sodium cation to form the binuclear nickel(II) complex molecule Na[Ni₂(14-tmc)₂(OH)₂](ClO₄)₃. The molecular structure is shown in Figure 5.17. Sodium in the center is also coordinated by two perchlorate counter ions in axial position.

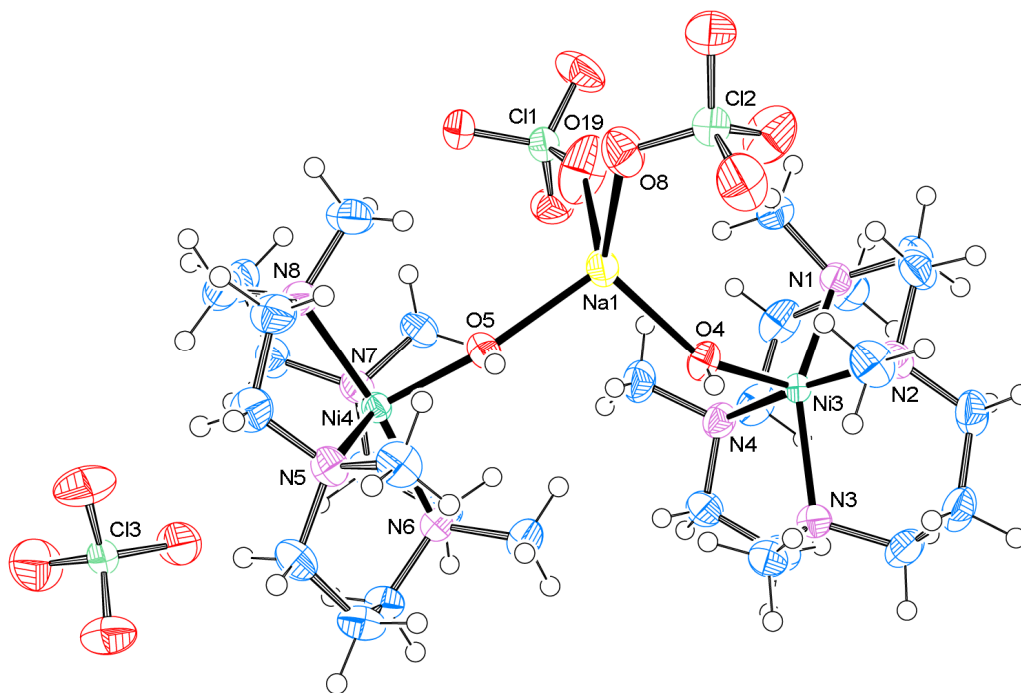


Figure 5.17: ORTEP plot of the full complex molecule of $\text{Na}[\text{Ni}_2(14\text{-tmc})_2(\text{OH})_2](\text{ClO}_4)_3$. Solvent molecules are omitted for clarity.

The proton of the hydroxo group of $[\text{Ni}(14\text{-tmc})\text{OH}]\text{ClO}_4$ was also observed using IR spectroscopy. The obtained spectrum shown in Figure 5.18 exhibits an absorption band at 3635 cm^{-1} which could be assigned to the $\tilde{\nu}(\text{O-H})$ mode of the terminal O-H group according to literature.[214] A sharp signal can be observed due to the absence of intermolecular hydrogen bonding of the free hydroxyl group. Therefore, using $[\text{Ni}(14\text{-tmc})]\text{ClO}_4$ as nickel(I) precursor is a considerable disadvantage because due to the presence of crystal water the hydroxo complex is formed. It was not possible to obtain the anhydrous nickel(II) complex with perchlorate as the counter ion (see Figure 5.19). Recrystallization in absolute ethanol and drying the compound in vacuo at $80\text{ }^\circ\text{C}$ for several times was only partially successful. The obtained IR spectrum still showed a broad band (due to hydrogen bonding) at 3475 cm^{-1} which can be assigned to crystal water $\tilde{\nu}(\text{O-H})$.

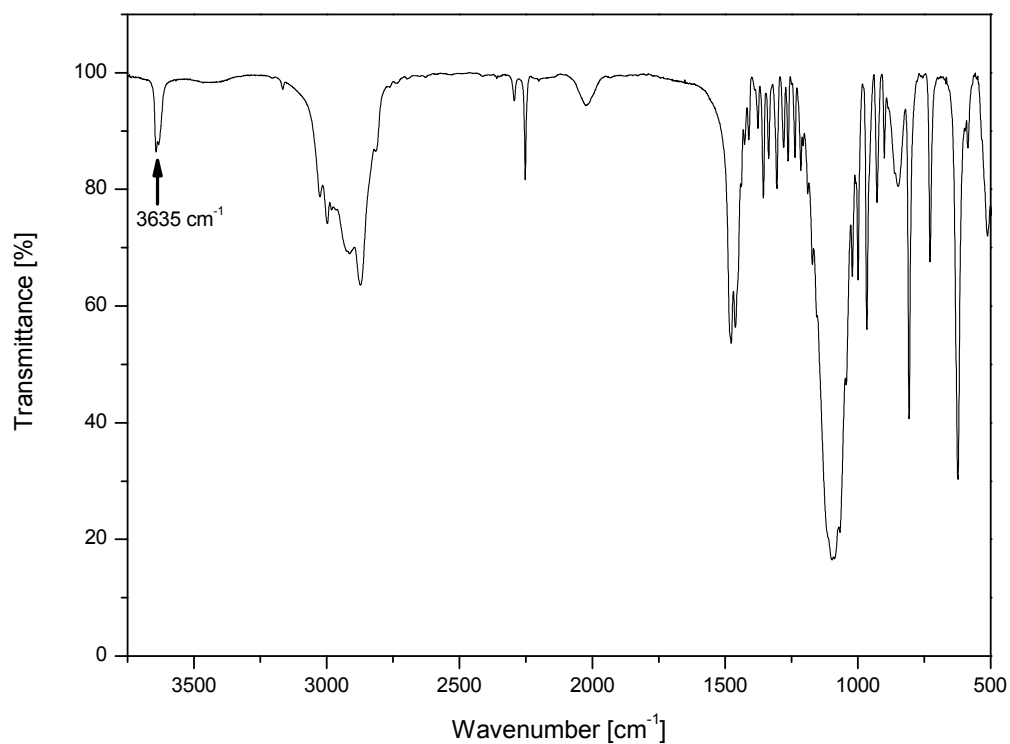


Figure 5.18: IR spectrum of the nickel(II)-hydroxo complex $[\text{Ni}(14\text{-tmc})\text{OH}]\text{ClO}_4$.

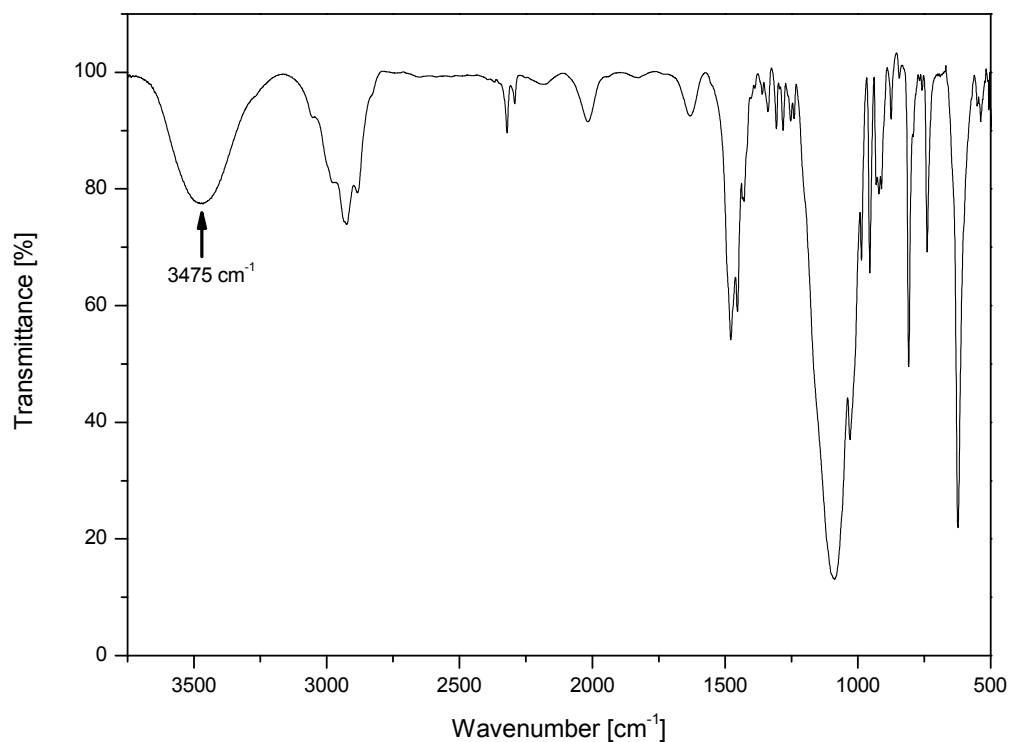


Figure 5.19: IR spectrum of the complex $[\text{Ni}(14\text{-tmc})](\text{ClO}_4)_2$ after recrystallization in absolute ethanol and drying in vacuo at 80°C .

5.2.1.7 Reaction of $[\text{Ni}(14\text{-tmc})]\text{SO}_3\text{CF}_3$ and Nitrous Oxide

Due to problems with crystal water in the nickel 14-tmc perchlorate complex the counter ion was exchanged to triflate. The synthesis was done according to a procedure described in literature.[209] Reaction of anhydrous $\text{Ni}(\text{SO}_3\text{CF}_3)_2$ and 14-tmc in absolute ethanol gave a pink powder of $[\text{Ni}(14\text{-tmc})](\text{SO}_3\text{CF}_3)_2$ (see Figure 5.20).

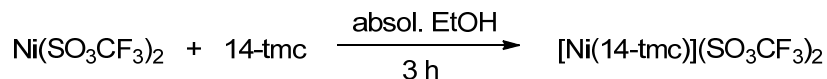


Figure 5.20: Scheme for the reaction of $\text{Ni}(\text{SO}_3\text{CF}_3)_2$ and 14-tmc.

The obtained IR spectrum of the complex depicted in Figure 5.21 shows only a very weak broad band at 3471 cm^{-1} which can be assigned to $\tilde{\nu}(\text{O-H})$ to small amounts of residual crystal water.

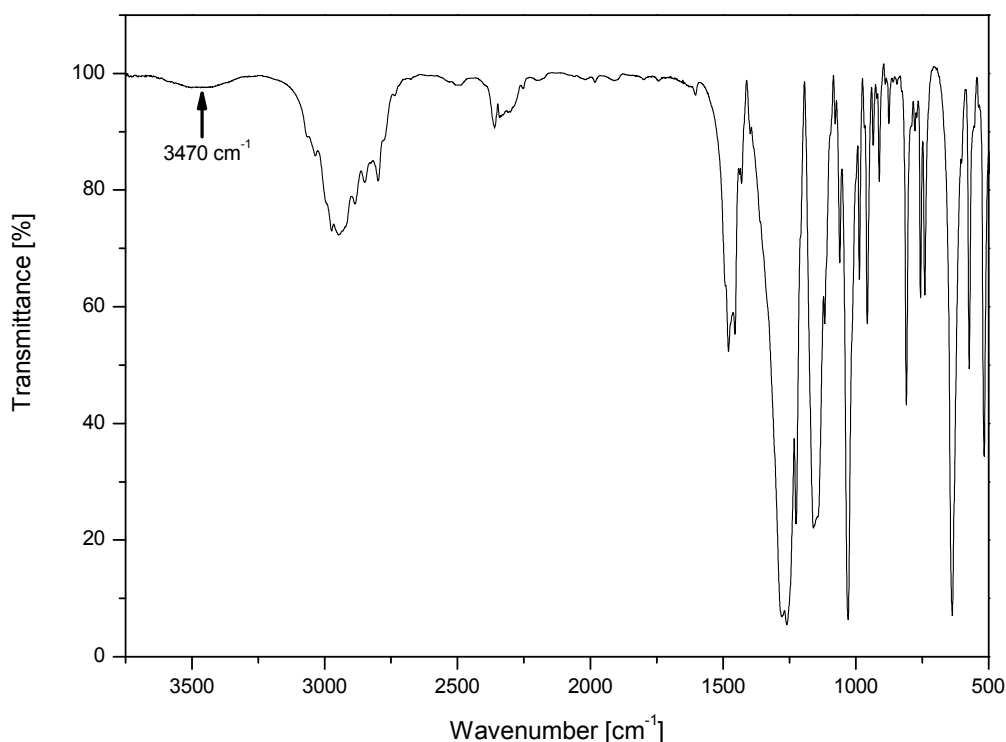


Figure 5.21: IR spectrum of the complex $[\text{Ni}(14\text{-tmc})](\text{SO}_3\text{CF}_3)_2$.

Reduction of $[\text{Ni}(\text{14-tmc})](\text{SO}_3\text{CF}_3)_2$ in propionitrile with sodium amalgam (5 % Na) afforded a green complex solution of $[\text{Ni}(\text{14-tmc})]\text{SO}_3\text{CF}_3$ (see Figure 5.22).

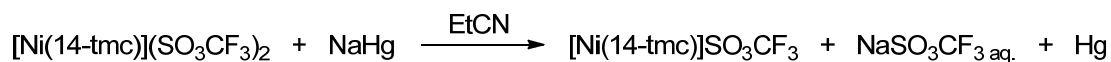


Figure 5.22: Reduction of $[\text{Ni}(\text{14-tmc})](\text{SO}_3\text{CF}_3)_2$ with NaHg in propionitrile.

UV-Vis experiments were performed in EtCN and showed a strong absorption band at 350 nm which is in accordance with literature.[215] It was also possible to obtain blue-green crystals of the nickel(I) complex. Unfortunately, difficulties in handling of the crystals (due to their extreme sensitivity) did not allow the determination of the structure by X-Ray analysis during this work to confirm this result. Ram et al. already published a crystal structure of the complex after reducing $[\text{Ni}(\text{14-tmc})](\text{SO}_3\text{CF}_3)_2$ in THF/ CH_3CN (10:1) yielding the *R,S,S,R* isomer cocrystallized with sodium triflate.[216]

Furthermore, $[\text{Ni}(\text{14-tmc})]\text{SO}_3\text{CF}_3$ was reacted with dry N_2O gas at $-80\text{ }^\circ\text{C}$ in propionitrile to afford a brown complex solution of $[\text{Ni}(\text{14-tmc})(\text{N}_2\text{O})]\text{SO}_3\text{CF}_3$ (see Figure 5.23).

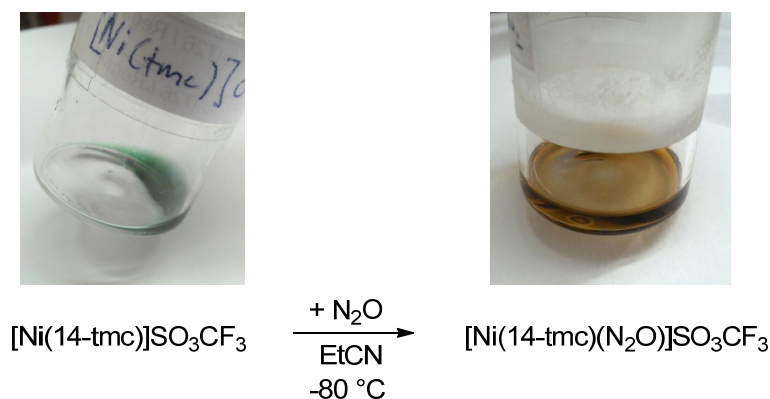


Figure 5.23: Color change in course of the reaction of $[\text{Ni}(\text{14-tmc})]\text{SO}_3\text{CF}_3$ and nitrous oxide in propionitrile at $-80\text{ }^\circ\text{C}$.

Contrary to the reaction with the nickel(I) precursor and perchlorate as counter ion the brown solution of $[\text{Ni}(\text{14-tmc})(\text{N}_2\text{O})]\text{SO}_3\text{CF}_3$ was stable at $-80\text{ }^\circ\text{C}$ for several weeks. UV-Vis spectra of both complexes in EtCN at $-80\text{ }^\circ\text{C}$ were obtained. The spectra depicted in Figure 5.24 show the absorbance of the green complex solution of $[\text{Ni}(\text{14-tmc})]\text{SO}_3\text{CF}_3$ (green curve) with one band at 678 nm

5.2 Results

and the brown solution of $[\text{Ni}(\text{14-tmc})(\text{N}_2\text{O})]\text{SO}_3\text{CF}_3$ (brown curve) exhibiting a band at 460 nm.

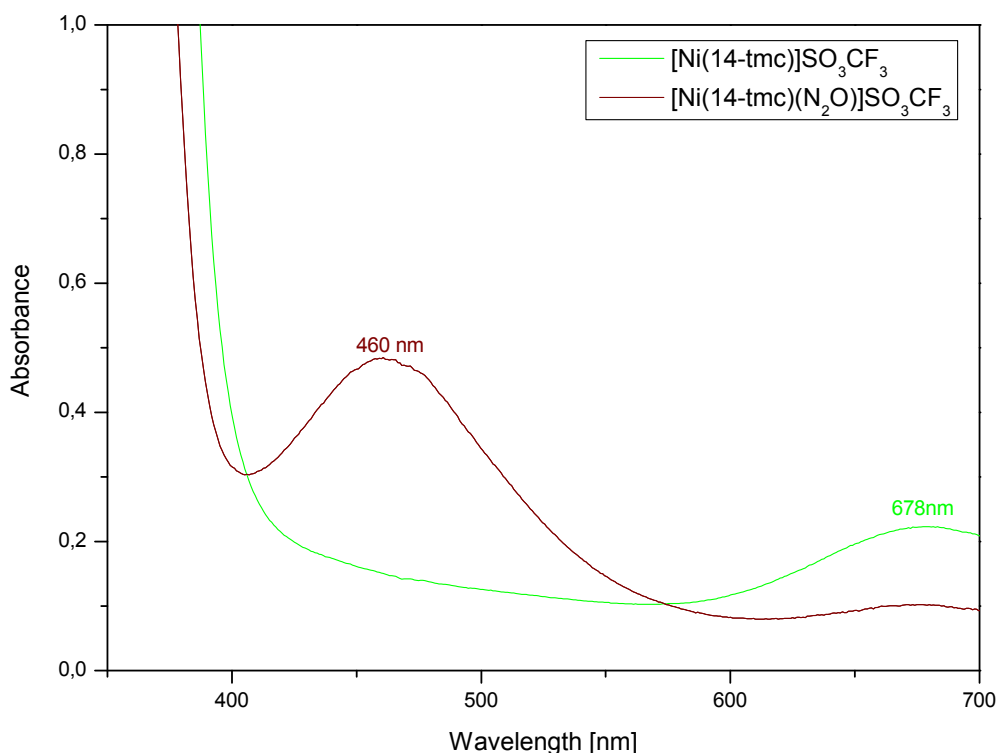


Figure 5.24: UV-Vis spectra of $[\text{Ni}(\text{14-tmc})]\text{SO}_3\text{CF}_3$ (green) and $[\text{Ni}(\text{14-tmc})(\text{N}_2\text{O})]\text{SO}_3\text{CF}_3$ (brown) in propionitrile at $-80\text{ }^\circ\text{C}$.

Furthermore, brown crystals of $[\text{Ni}(\text{14-tmc})(\text{N}_2\text{O})]\text{SO}_3\text{CF}_3$ could be obtained after a few days at $-80\text{ }^\circ\text{C}$. Unfortunately, they were not suitable for X-ray diffraction studies.

5.2.1.8 Reaction of $[\text{Ni}(\text{14-tmc})]^{2+}$ with Peroxides and Superoxides

In literature the nickel(III) side-on peroxo complex $[\text{Ni}(\text{12-tmc})\text{O}_2]\text{SO}_3\text{CF}_3$ could be synthesized by reacting the nickel(II) precursor in acetonitrile at $0\text{ }^\circ\text{C}$ with five equivalents of hydrogen peroxide and two equivalents of triethylamine (Et_3N).^[136] The complex obtained was persistent at $25\text{ }^\circ\text{C}$ for several days which allowed to isolate crystals and structurally characterize the nickel-dioxygen adduct complex.

Analogue to this reaction the nickel complex $[\text{Ni}(\text{14-tmc})](\text{SO}_3\text{CF}_3)_2$ was also reacted with ten eq. of H_2O_2 in presence of ten eq. of Et_3N in acetonitrile and

methanol at 25 °C yielding the end-on superoxo adduct $[\text{Ni}(\text{14-tmc})\text{O}_2]\text{SO}_3\text{CF}_3$ (see Figure 5.25).[137]

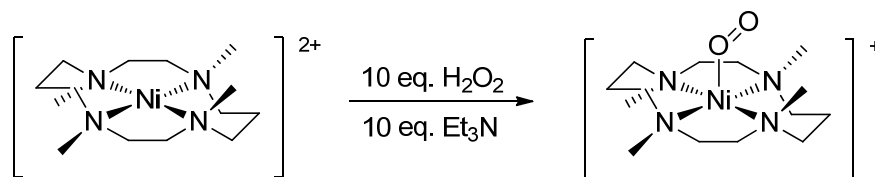


Figure 5.25: Scheme for the reaction of $[\text{Ni}(\text{14-tmc})]^{2+}$ and hydrogen peroxide in presence of triethylamine.[137]

Contrary to the side-on peroxo complex this nickel-dioxygen adduct species could only be characterized spectroscopically and by DFT calculations.

Efforts were made in this work to isolate and structurally characterize an end-on superoxo-nickel species which are presented in the following.

5.2.1.8.1 Reaction of $[\text{Ni}(\text{14-tmc})]^{2+}$ and H_2O_2

$[\text{Ni}(\text{14-tmc})](\text{ClO}_4)_2$ was reacted with ten eq. of H_2O_2 in presence of the base Et_3N in acetonitrile as well as in methanol at room temperature. Due to a fast color change of the solution from blue to green, which turned to a yellow and a red solution, the reaction was repeated at -60 °C. The obtained UV-Vis spectra in acetonitrile are shown in Figure 5.26.[197]

The blue complex solution of $[\text{Ni}(\text{14-tmc})(\text{MeCN})_2](\text{ClO}_4)_2$ (blue curve) shows an absorption band at 382 nm and a weak broad band at 608 nm. After the reaction with $\text{H}_2\text{O}_2/\text{Et}_3\text{N}$ at room temperature the solution turned to green followed by two color changes to yellow and red. Therefore, the recorded spectrum of the reaction of the nickel(II) complex with $\text{H}_2\text{O}_2/\text{Et}_3\text{N}$ at room temperature (olive curve) shows only a mixture of several species with bands at 342, 425, 485 and a weak broad band at 689 nm. The green complex solution obtained was only stable at -60 °C and shows four absorption bands (green curve) with a strong band at 340 nm, a small shoulder at 412 nm, a very weak band at 505 nm and a broad weak band at 689 nm. All four bands are characteristic for the end-on nickel-superoxo complex and agree with findings in literature.[137] The green complex solution was stored at -30 °C with the aim of isolating crystals. Unfor-

5.2 Results

Unfortunately, it was not possible to obtain crystals suitable for X-ray diffraction studies.

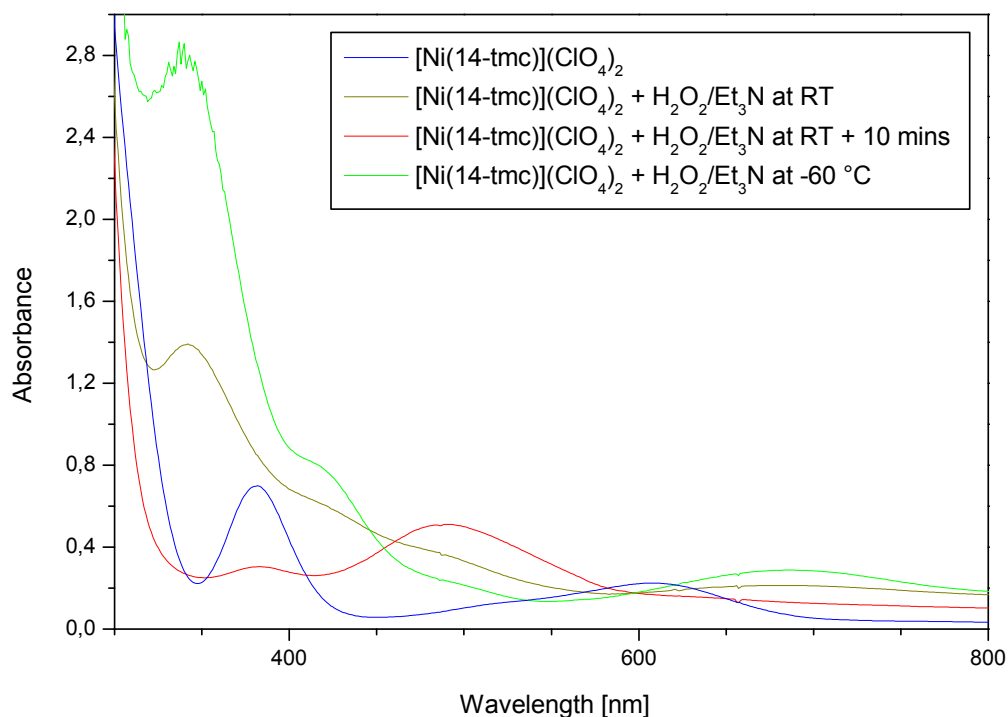


Figure 5.26: UV-Vis spectra of the reaction of $[\text{Ni}(\text{14-tmc})](\text{ClO}_4)_2$ and $\text{H}_2\text{O}_2/\text{Et}_3\text{N}$ in acetonitrile at different temperatures.[197]

The spectrum of the red complex solution was obtained ten minutes after the reaction of $[\text{Ni}(\text{14-tmc})(\text{MeCN})_2](\text{ClO}_4)_2$ with $\text{H}_2\text{O}_2/\text{Et}_3\text{N}$ (red curve). It shows two bands at 382 and 490 nm. Diffraction studies of red crystals obtained from the solution showed the structure of the nickel(II) complex $[\text{Ni}(\text{14-tmc})]^{2+}$ indicating the decomposition of the green nickel-superoxo complex.

The obtained UV-Vis spectra of the reaction of $[\text{Ni}(\text{14-tmc})](\text{ClO}_4)_2$ and $\text{H}_2\text{O}_2/\text{Et}_3\text{N}$ in methanol at room temperature are depicted in Figure 5.27. The red curve shows the spectrum of the red complex solution of $[\text{Ni}(\text{14-tmc})]^{2+}$ in methanol with two bands at 397 and 517 nm. After the reaction with hydrogen peroxide the color changed to green forming the nickel-superoxo species with its characteristic absorption bands at 411, 502 and 694 nm. The resulting solution was stable for several hours. With the purpose of isolating crystals the complex solution was stored at $-30\text{ }^\circ\text{C}$. Nevertheless, it was not possible to obtain crystals suitable for X-ray diffraction during this work.

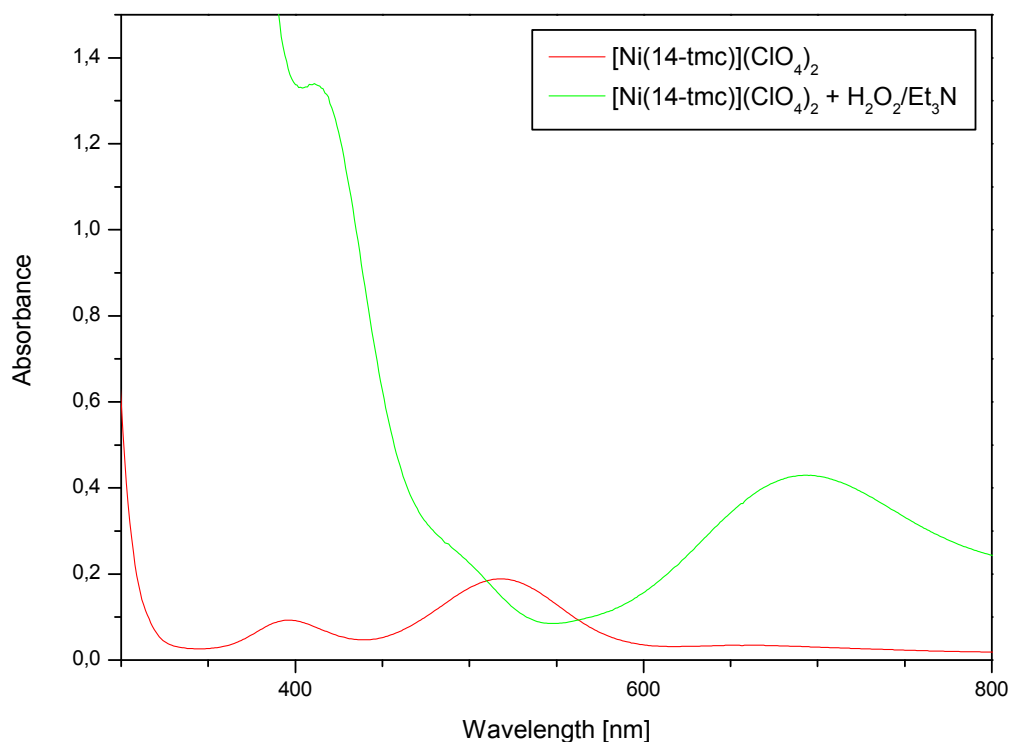


Figure 5.27: UV-Vis spectra of the reaction of $[\text{Ni}(\text{14-tmc})](\text{ClO}_4)_2$ and $\text{H}_2\text{O}_2/\text{Et}_3\text{N}$ in methanol at room temperature.[197]

5.2.1.8.2 Reaction of $[\text{Ni}(\text{14-tmc})]^{2+}$ and Na_2O_2

Analogous to the reaction with hydrogen peroxide the nickel(II) complex $[\text{Ni}(\text{14-tmc})](\text{ClO}_4)_2$ was reacted with sodium peroxide in presence of the crown ether [15]-crown-5. The blue solution turned green within 15 minutes. UV-Vis spectra obtained are depicted in Figure 5.28 showing the absorbance spectra of the blue complex solution of $[\text{Ni}(\text{14-tmc})(\text{MeCN})_2](\text{ClO}_4)_2$ (blue curve) and the green solution after the reaction with Na_2O_2 (green curve).

The latter shows three absorption bands at 340, 418 and a weak broad band at 696 nm. All bands exhibit only a small shift compared to the reaction with hydrogen peroxide with different absorbance ratios. Therefore, it is supposed that a nickel-superoxo complex is most likely formed.

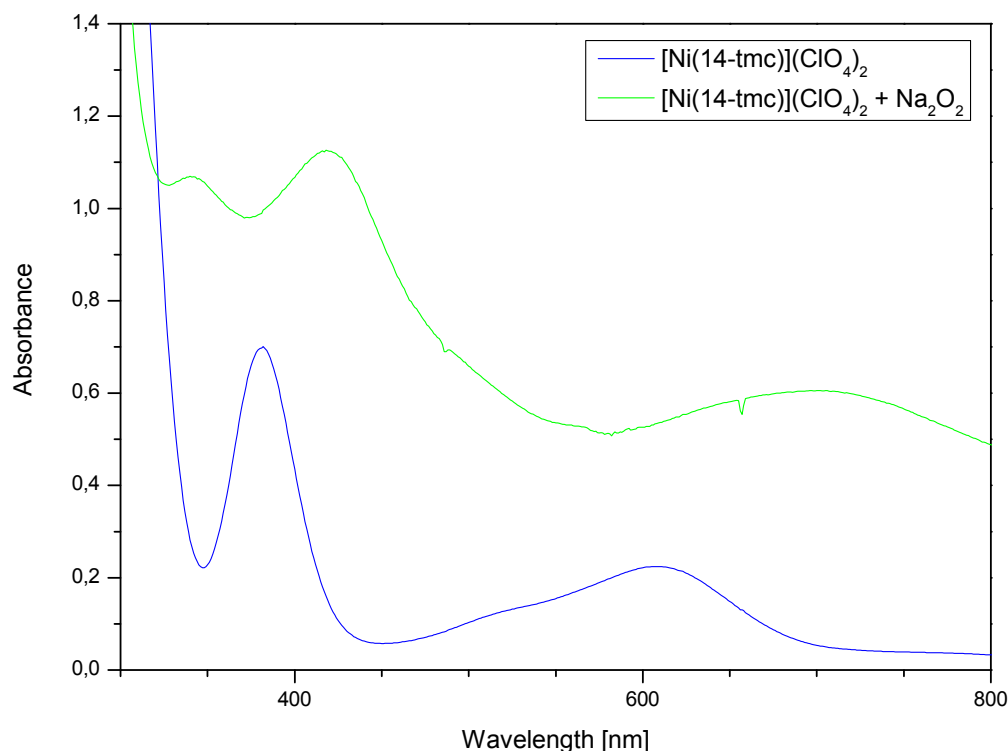


Figure 5.28: UV-Vis spectra of the reaction of $[\text{Ni}(\text{14-tmc})](\text{ClO}_4)_2$ and Na_2O_2 in acetonitrile at room temperature.[197]

5.2.2 Synthesis and Reactions of Nickel Complexes bearing tetB

5.2.2.1 Ligand tetB

A further derivative of the ligand cyclam is the macrocyclic ligand 5,5,7,12,12,14-hexamethyl-1,4,8,11-tetraazacyclotetradecane (tet) which also proved to be a useful system for stabilizing metal-oxygen species. Recently, an end-on peroxo-copper complex bearing this ligand could be structurally characterized by Hoppe et al.[217] Efforts were made in this work to obtain a nickel-oxygen adduct using tet.

There are two diastereomers of the ligand tet, the *meso* form (tetA – *R,S*) and the *racemic* form (tetB – *SS, RR*) (Figure 5.33). The ligand tetB was synthesized according to a publication of Curtis and co-workers.[218]

The ligand is synthesized in several steps. At first, 1,2-diaminoethane is reacted with hydrobromic acid (49 %) under cooling to yield the organic salt 1,2-diaminoethane dihydrobromide **5.13** (see Figure 5.29).

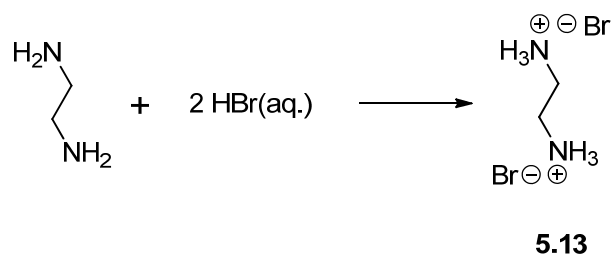


Figure 5.29: Reaction scheme for the synthesis of 1,2-diaminoethane dihydrobromide (5.13).

In a further reaction step, acetone and 1,2-diaminoethane is added to **5.13** and heated to 45 °C.

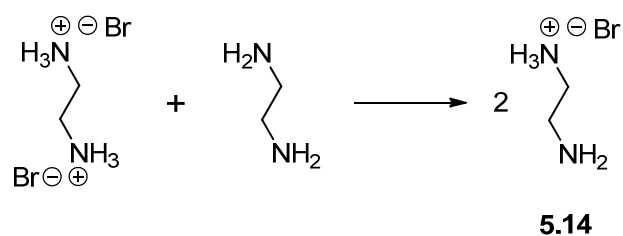


Figure 5.30: Reaction scheme for the synthesis of 1,2-diaminoethane monohydrobromide (5.14).

Therefore, **5.13** reacts with 1,2-diaminoethane which affords 1,2-diaminoethane monohydrobromide **5.14** (see Figure 5.30) and two molecules of acetone undergo a base-catalyzed aldol condensation to yield mesityl oxide **5.15** (see Figure 5.31).

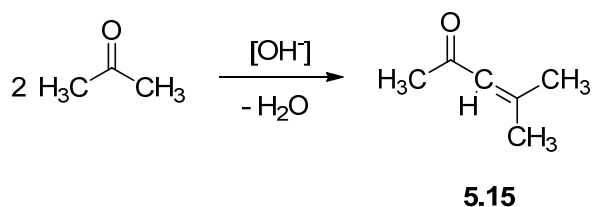


Figure 5.31: Reaction scheme for the aldol condensation of acetone yielding 4-methylpent-3-en-2-one (5.15).

5.2 Results

In a Michael addition the diamine **5.14** reacts with the α,β -unsaturated mesityl oxide to give a substituted β -aminoketone which then cyclises in pairs to trans-[14]-diene dihydrobromide dihydrate **5.16** (see Figure 5.32).

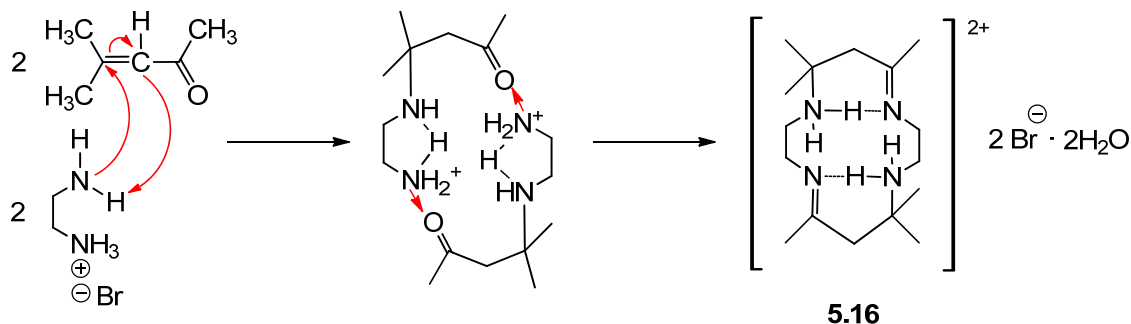


Figure 5.32: Michael addition of (5.14) and (5.15) to form trans-[14]-diene dihydrobromide dihydrate (5.16).

Finally, **5.16** is reduced with sodium borohydride in methanol and 2M potassium hydroxide solution is added to give tetA and tetB. The two isomers can be separated by fractional crystallization due to the insolubility of tetA in cold water (see Figure 5.33).

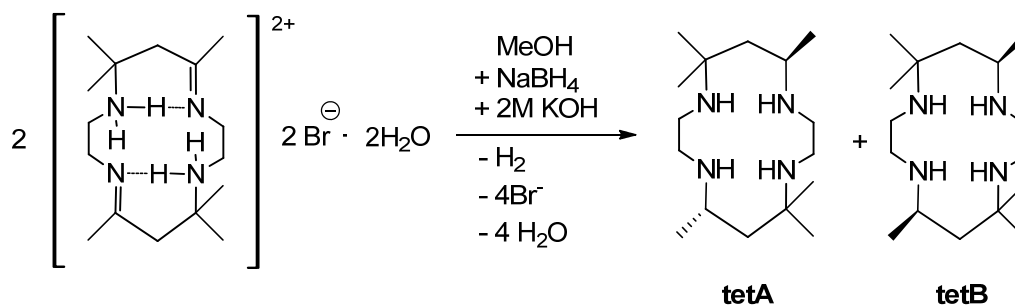


Figure 5.33: Reaction scheme for the reduction of **5.16** to tetA and tetB with sodium borohydride in methanol.

5.2.2.2 $[\text{Ni}(\text{tetB})](\text{ClO}_4)_2$

The macrocyclic complex $[\text{Ni}(\text{tetB})](\text{ClO}_4)_2$ was synthesized according to a procedure described in literature (see Figure 5.34).^[219]

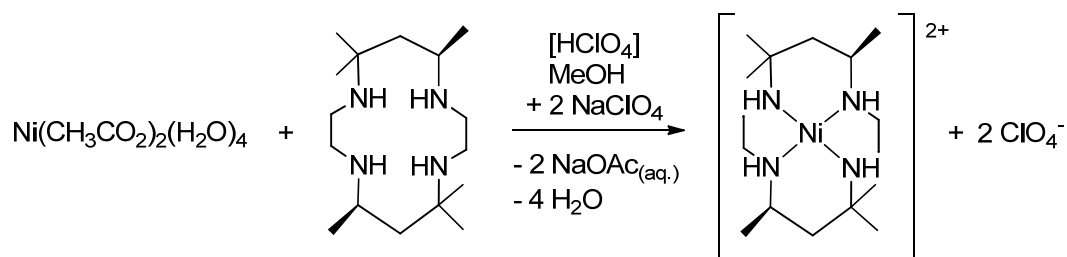


Figure 5.34: Reaction scheme for the synthesis of $[\text{Ni}(\text{tetB})](\text{ClO}_4)_2$.

Yellow-orange crystals could be isolated from an orange solution which were suitable for X-ray diffraction studies. Figure 5.35 shows the determined molecular structure of the cation $[\text{Ni}(\text{tetB})]^{2+}$ which is in line with the previously reported structure by Curtis et al.[220] Crystallographic data, selected bond lengths and angles are presented in Table 5.9 and Table 5.10. The nickel(II) center is coordinated by the four nitrogen atoms of the macrocyclic ligand in a square-planar geometry. The two methyl groups C11 and C14 of tetB are on the same side of the nickel–nitrogen plane indicating the *S,S* isomer. The Ni–N bond lengths are only slightly shorter than in the macrocyclic complex $[\text{Ni}(\text{14-tmc})]^{2+}$ with distances between 1.936(4) and 1.956(4) Å.

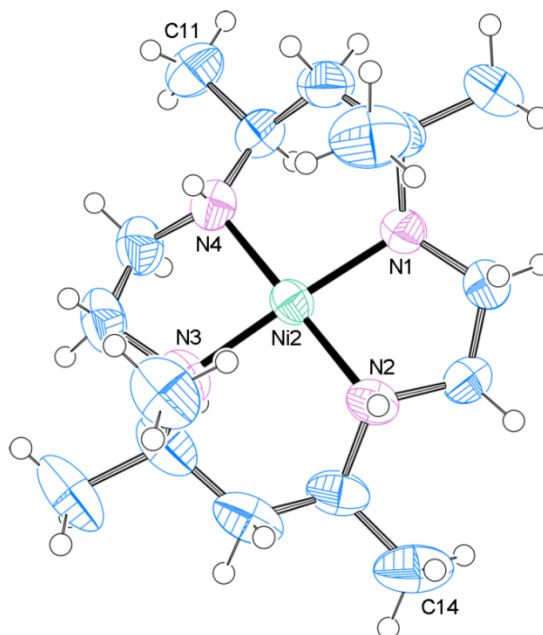


Figure 5.35: ORTEP plot of the cation $[\text{Ni}(\text{tetB})]^{2+}$. Ellipsoids are drawn at 50 % probability level.

Table 5.9: Crystal data and structure refinement for [Ni(tetB)](ClO₄)₂.

Internal identification code	schindler13045
Empirical formula	C ₁₆ H ₃₆ Cl ₂ N ₄ Ni O ₈
Formula weight	542.10
Temperature	293 (2) K
Wavelength	0.71073 Å
Crystal system, space group	Monoclinic, <i>P</i> 2 ₁ / <i>c</i>
Unit cell dimensions	$a = 14.251(3) \text{ Å}$ $\alpha = 90^\circ$ $b = 19.177(4) \text{ Å}$ $\beta = 93.46(3)^\circ$ $c = 17.463(4) \text{ Å}$ $\gamma = 90^\circ$
Volume	4763.8(17) Å ³
Z, calculated density	8, 1.512 Mg/m ³
Absorption coefficient	1.087 mm ⁻¹
F(000)	2288
Theta range for data collection	3.16 to 25.69 °
Limiting indices	-17≤h≤14, -21≤k≤23, -20≤l≤19
Reflections collected / unique	28225 / 8332 [R(int) = 0.0566]
Completeness to theta = 25.69	92.0 %
Absorption correction	Empirical
Refinement method	Full-matrix least-squares on F ²
Data / restraints / parameters	8332 / 0 / 712
Goodness-of-fit on F ²	1.043
Final R indices [I>2sigma(I)]	R1 = 0.0504, wR2 = 0.1258
R indices (all data)	R1 = 0.0839, wR2 = 0.1598
Largest diff. peak and hole	0.510 and -0.874 e. Å ⁻³

Table 5.10: Selected bond lengths [Å] and angles [°] for [Ni(tetB)](ClO₄)₂.

Ni(2)-N(1)	1.946(4)	Ni(2)-N(2)	1.956(4)	Ni(2)-N(3)	1.936(4)
Ni(2)-N(4)	1.952(4)				
N(1)-Ni(2)-N(2)	84.50(16)	N(2)-Ni(2)-N(4)	179.43(17)		
N(1)-Ni(2)-N(3)	173.66(18)	N(1)-Ni(2)-N(4)	95.70(17)		
N(2)-Ni(2)-N(3)	94.95(18)	N(3)-Ni(2)-N(4)	84.91(19)		

5.2.2.2.1 Reaction of $[\text{Ni}(\text{tetB})](\text{ClO}_4)_2$ and H_2O_2

$[\text{Ni}(\text{tetB})](\text{ClO}_4)_2$ was reacted with ten eq. of H_2O_2 in presence of the base Et_3N in methanol at different temperatures. The UV-Vis spectra obtained are shown in Figure 5.36. Dissolving the complex in methanol resulted in a yellow solution with one absorption band at 455 nm (black curve). Adding hydrogen peroxide to the solution at room temperature led to a color change from yellow to orange (orange curve). Analogous to the reaction of $[\text{Ni}(\text{14-tmc})]^{2+}$ it was possible to obtain a green solution after the reaction with H_2O_2 at $-60\text{ }^\circ\text{C}$ which was only stable at temperatures $\leq -60\text{ }^\circ\text{C}$. The afforded nickel-oxygen adduct complex exhibits three bands at 390, 435 and 595 nm (green curve). Warming up the solution resulted in a color change back to yellow. With the aim of isolating crystals the obtained green solution was stored at $-80\text{ }^\circ\text{C}$ for several weeks. Unfortunately, it was not possible to obtain crystals suitable for X-ray diffraction. Thus, it remained unclear which species formed within the reaction with H_2O_2 since there are no reports about nickel-oxygen adducts with the ligand tet in literature.

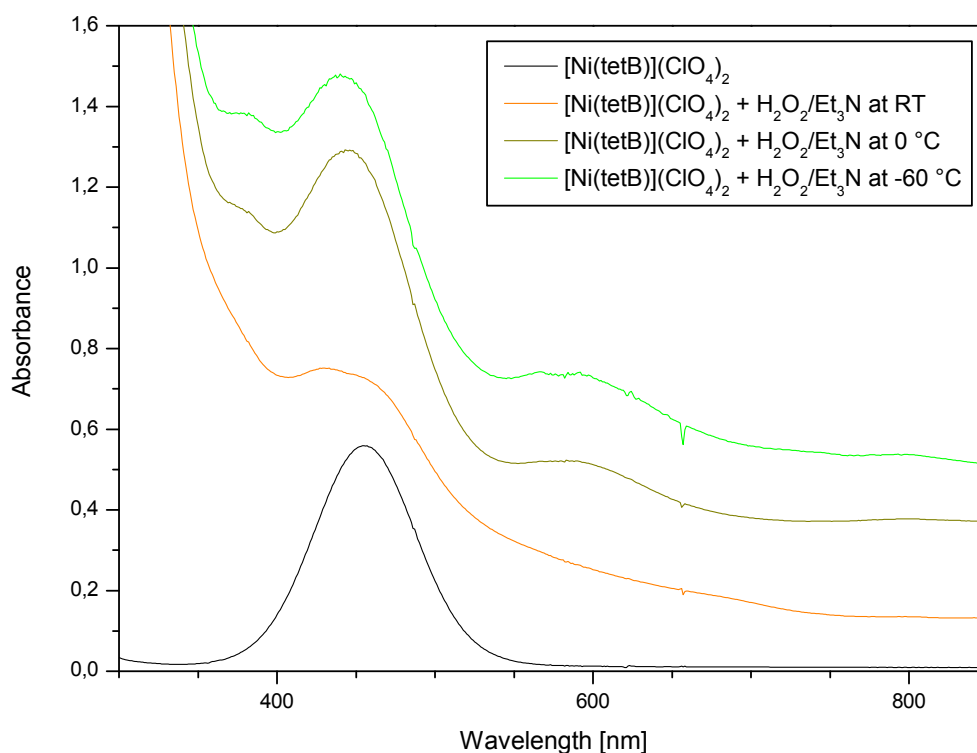


Figure 5.36: UV-Vis spectra of the reaction of $[\text{Ni}(\text{tetB})](\text{ClO}_4)_2$ and $\text{H}_2\text{O}_2/\text{Et}_3\text{N}$ in methanol at different temperatures.

5.2.2.2.2 Reaction of $[\text{Ni}(\text{tetB})](\text{ClO}_4)_2$ and KO_2

Furthermore, $[\text{Ni}(\text{tetB})](\text{ClO}_4)_2$ was reacted with KO_2 in a 1:1 ratio in acetonitrile. The color of the solution changed from yellow-orange to brown after a few hours. The UV-Vis spectra obtained are shown in Figure 5.37. $[\text{Ni}(\text{tetB})](\text{ClO}_4)_2$ in acetonitrile exhibits three narrow bands at 358, 467 and 552 nm and a broad band at 927 nm. After the reaction with potassium superoxide only a weak band at 360 nm exhibits with a small shoulder at 425 nm. With regard to the color and the obtained spectrum of the solution it is rather unlikely that a nickel-oxygen adduct complex was formed. It was not possible to obtain crystals suitable for X-ray diffraction.

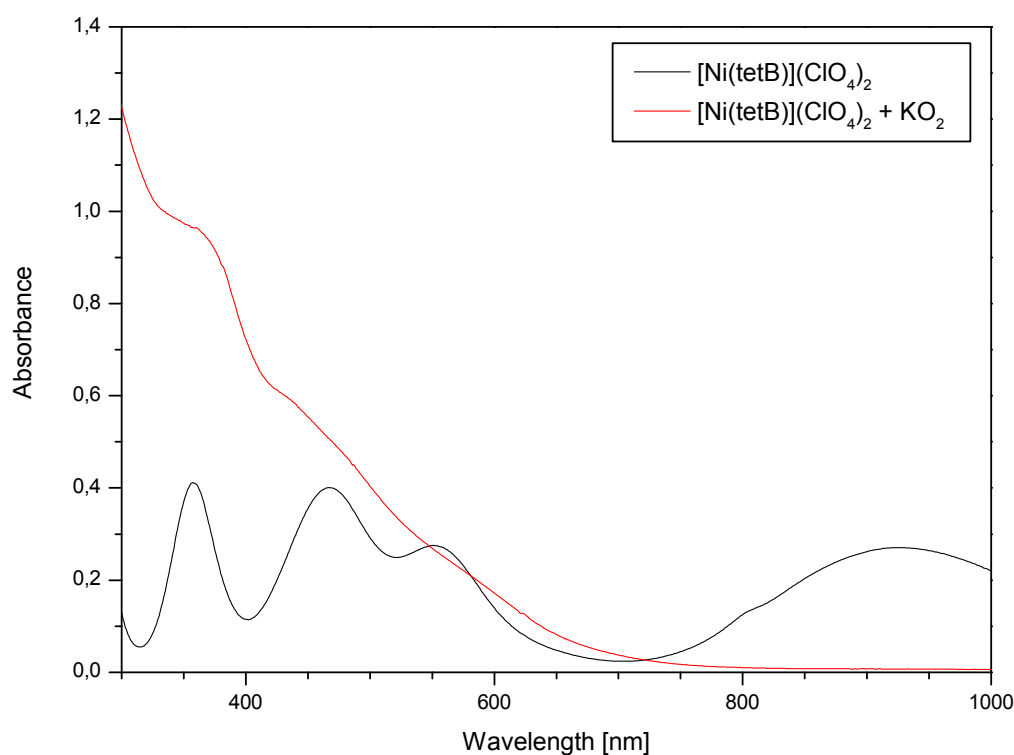


Figure 5.37: UV-Vis spectra of the reaction of $[\text{Ni}(\text{tetB})](\text{ClO}_4)_2$ and KO_2 in acetonitrile at room temperature.

5.2.2.2.3 Reaction of $[\text{Ni}(\text{tetB})](\text{ClO}_4)_2$ and Na_2O_2

$[\text{Ni}(\text{tetB})](\text{ClO}_4)_2$ was also reacted with Na_2O_2 in presence of [15]-crown-5 in acetonitrile. Analogue to the reaction with potassium superoxide the color of the solution turned from yellow-orange to brown within a few minutes. UV-Vis experiments were not performed during this work.

5.3 Experimental

5.3.1 Materials and Reagents

Commercial reagents were used as obtained without further purification. Solvents were dried according to standard procedures. All handling and storage of oxygen sensitive compounds and materials used was carried out in a glove box (M. Braun, Garching, Germany; $\text{O}_2 < 0.1$ ppm, $\text{H}_2\text{O} < 0.1$ ppm) within an argon atmosphere.

5.3.2 Crystallography

Single crystals suitable for X-ray diffraction were mounted on the tip of a glass rod using inert perfluoropolyether oil. The X-ray crystallographic data were collected on a STOE IPDS- or a BRUKER NONIUS FR591 KappaCCD diffractometer equipped with low temperature systems. Mo-K_α radiation ($\lambda = 0.71073$ Å) and a graphite monochromator (STOE IPDS) was used. The structures were solved by direct methods in SHELXS97 and SHELXL 2013 and refined by using full-matrix least squares in SHELXL97.[179]

5.3.3 NMR Spectroscopy

^1H -NMR and ^{13}C -NMR spectra were recorded on a Bruker-Aspect 2000/3000 400-MHz spectrometer by Dr. H. Hausmann (JLU Gießen, Institute for Organic Chemistry).

5.3 Experimental

5.3.4 UV-Vis Spectroscopy

If not mentioned otherwise UV-Vis absorbance spectra were measured at room temperature using an Agilent 8453 spectrophotometer and quartz cuvettes ($d = 10$ mm). The UV-Vis spectrum of the reaction of $[\text{Ni}(14\text{-tmc})]\text{SO}_3\text{CF}_3$ and nitrous oxide in propionitrile at -80.0 °C was recorded with a TgK Scientific model SF-61SX2 low-temperature stopped-flow spectrophotometer equipped with a diode array detector (Salisbury, U.K.). Spectral changes in the range of 300-700 nm were observed using an immersion probe with a path length of 2 mm.

5.3.5 IR Spectroscopy

IR measurements were performed on a Jasco FT/IR 4100 spectrometer. All samples were measured as KBr-pellet at room temperature.

5.3.6 Synthesis of the Ligands

5.3.6.1 14-tmc

The ligand 1,4,8,11-tetramethyl-1,4,8,11-tetraazacyclotetradecane was obtained commercially by Sigma Aldrich.

5.3.6.1.1.1 TetB

The macrocyclic ligand *rac*-5,5,7,12,12,14-hexamethyl-1,4,8,11-tetraazacyclotetradecane (tetB) was synthesized according to a procedure described in literature.[218]

$^1\text{H-NMR}$ (CDCl_3/TMS) δ 3.22 (s (wide), 4H, $-\text{NH}$), 2.90-2.86 (m, 2H, $-\text{CHCH}_3$), 2.79-2.76 (m, 2H, $-\text{CHCH}_3\text{-NH-CH}_2\text{-CH}_2\text{-NH-C(CH}_3)_2$), 2.76-2.72 (m, 4H, $-\text{CHCH}_3\text{-NH-CH}_2\text{-CH}_2\text{-NH-C(CH}_3)_2$), 2.34-2.28 (m, 2H, $-\text{CHCH}_3\text{-NH-CH}_2\text{-CH}_2\text{-NH-C(CH}_3)_2$), 1.78-1.71 (m, 2H, $-\text{C(CH}_3)_2\text{-CH}_2\text{-CHCH}_3$), 1.09 (s, 12H, $-\text{C(CH}_3)_2$), 1.06-1.01 (m, 2H, $-\text{C(CH}_3)_2\text{-CH}_2\text{-CHCH}_3$), 0.99 (d, 6H, $-\text{CH-CH}_3$); $^{13}\text{C-NMR}$ (CDCl_3/TMS) δ 52.7 (sp^3 , $-\text{C(CH}_3)_2$), 51.5 (sp^3 , $-\text{CHCH}_3$), 48.1 (sp^3 , $-\text{CHCH}_3\text{-NH-CH}_2\text{-CH}_2\text{-NH-C(CH}_3)_2$), 43.9 (sp^3 , $-\text{C(CH}_3)_2\text{-CH}_2\text{-CHCH}_3$), 41.2

(sp³, -CHCH₃-NH-CH₂-CH₂-NH-C(CH₃)₂), 29.4 (sp³, -C(CH₃)₂), 28.3 (sp³, -C(CH₃)₂), 21.3 (sp³, -CH-CH₃).

5.3.7 Synthesis of the Nickel Complexes

5.3.7.1 [Ni(14-tmc)]²⁺

500 mg of Ni(SO₃CF₃)₂ (1.40 mmol) and 395 mg (1.54 mmol) of 14-tmc were refluxed in absolute ethanol for 3 hours. The resulting purple solution was filtered and the solvent was evaporated. Drying in vacuo at 80 °C yielded 720 mg (84 %) of [Ni(14-tmc)](SO₃CF₃)₂. Cooling of a saturated solution in acetone and acetonitrile gave crystals suitable for X-ray diffraction.

5.3.7.2 [Ni(tetB)](ClO₄)₂

The nickel(II) complex [Ni(tetB)](ClO₄)₂ was prepared according to a procedure described in literature.[219] Cooling of a saturated methanolic solution yielded crystals suitable for X-ray diffraction.

5.3.7.3 [Ni(14-tmc)]⁺

25 mg (0.042 mmol) of [Ni(14-tmc)]²⁺ was reduced with 182 mg (0.819 mmol) of 5 % - NaHg in a small amount of propionitrile. Stirring for 30 minutes afforded a green solution of [Ni(14-tmc)]⁺. Blue-green crystals were obtained by cooling the saturated solution to -80 °C which were only stable at very low temperatures under exclusion of air.

5.3.7.4 Reaction of [Ni(14-tmc)]⁺ and Nitrous Oxide

A solution of 25 mg (0.042 mmol) of [Ni(14-tmc)]⁺ in propionitrile was reacted with dry gaseous nitrous oxide at -80 °C.

5.3 Experimental

5.3.7.5 Reaction of $[\text{Ni}(\text{14-tmc})](\text{ClO}_4)_2$ and H_2O_2

40 mg (0.082 mmol) of $[\text{Ni}(\text{14-tmc})](\text{ClO}_4)_2$ was dissolved in a small amount of acetonitrile as well as in methanol. To both solutions 0.1 ml of Et_3N and 0.2 mL H_2O_2 (12 %) was added at different temperatures. UV-Vis spectra of the resulting green solutions were recorded.

5.3.7.6 Reaction of $[\text{Ni}(\text{tetB})](\text{ClO}_4)_2$ and $\text{H}_2\text{O}_2/\text{Et}_3\text{N}$

20 mg (0.042 mmol) of $[\text{Ni}(\text{tetB})](\text{ClO}_4)_2$ was dissolved in a small amount of methanol to give a yellow solution. 0.1 ml of Et_3N and 0.2 mL H_2O_2 (12 %) was added at $-60\text{ }^\circ\text{C}$ and the color changed to green. UV-Vis experiments on this reaction were performed.

5.3.7.7 Reaction of $[\text{Ni}(\text{14-tmc})](\text{ClO}_4)_2/[\text{Ni}(\text{tetB})](\text{ClO}_4)_2$ and Na_2O_2

20 mg (0.039 mmol) of $[\text{Ni}(\text{14-tmc})](\text{ClO}_4)_2$ and 20 mg (0.039 mmol) of $[\text{Ni}(\text{tetB})](\text{ClO}_4)_2$ were dissolved in a small amount of acetonitrile. To both solutions 3.0 mg (0.039 mmol) of Na_2O_2 and [15]-crown-5 was added. UV-Vis spectra of the resulting solutions were recorded.

5.3.7.8 Reaction of $[\text{Ni}(\text{tetB})](\text{ClO}_4)_2$ and KO_2

20 mg (0.037 mmol) of $[\text{Ni}(\text{tetB})](\text{ClO}_4)_2$ and 2.6 mg (0.037 mmol) of KO_2 were dissolved in a small amount of acetonitrile. The color of the solution turned to brown. UV-Vis spectra of the solutions were recorded.

6 Summary/Zusammenfassung

6.1 Summary

Today, almost all industrial chemicals have involved a catalytic reaction step during their manufacturing process with palladium and platinum compounds being used as the most common catalysts. However, nickel also forms a wide variety of organometallic compounds and the big advantage of using them as catalysts is the much lower cost (ten to fifty times cheaper than Pd and Pt). A large number of Ni(0) complexes is used as homogenous catalyst in cyclooligomerization reactions of alkenes, cycloalkenes, dienes, alkynes and carboxylation reactions of dienes. The aim of this work therefore was to gain a better understanding of the reactivity of Ni(0) complexes and thus finding novel ways to replace expensive noble metal catalysts based on Pd and Pt.

Bicyclopropylidene (bcp), dicyclopropylacetylene (dcpa) and 1,4-dimethoxy-2-butyne (dmbu), which have been synthesized previously in the research group of Prof. A. de Meijere (University of Göttingen, Institute for Organic Chemistry), are interesting molecular building blocks in various transition metal-catalyzed cyclization reactions. Ni(0) complexes with these ligands were synthesized according to the following equation shown in Figure 6.1:

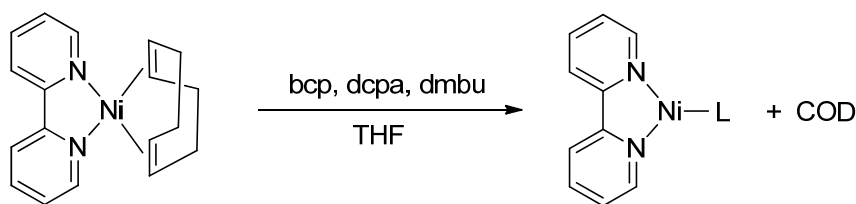


Figure 6.1: Scheme for the reaction of [Ni(bipy)(COD)] with the unsaturated ligands bcp, dcpa and dmbu.

This substitution reaction has been investigated kinetically by UV-Vis spectroscopy using “stopped-flow” techniques. Details on these studies are presented in chapter 2 of this work. From the results of the kinetic investigations a mechanism with a highly ordered transition state in course of the reaction of [Ni(bipy)(COD)] with bcp and dmbu is proposed. Investigations on the reaction

with dcpa could not be evaluated due to a reversible substitution reaction. However, the reaction rate was significantly slower compared to the reaction with bcp and dmbu. The rate constants of the reaction of $[\text{Ni}(\text{bipy})(\text{COD})]$ with bcp and dmbu were very different though; at 20.2 °C dmbu reacted by a factor of 1000 slower than bcp at 5.2 °C. Nevertheless, the obtained results are promising for possible future applications of these compounds in synthetic organic chemistry. Furthermore, molecular structures of the product complexes could be obtained. As an example the molecular structure of $[\text{Ni}(\text{bipy})(\text{dcpa})]$ is shown in Figure 6.2.

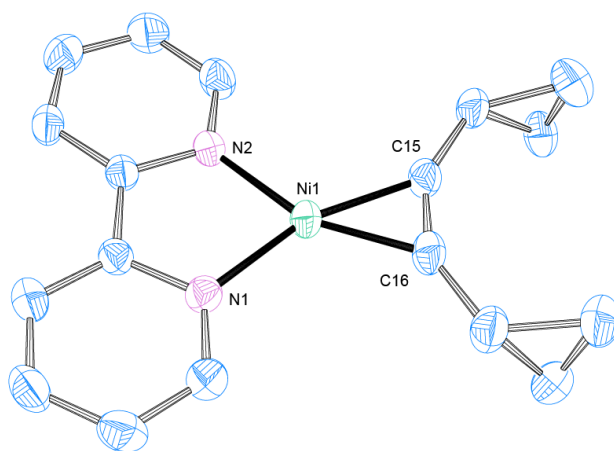


Figure 6.2: ORTEP plot of $[\text{Ni}(\text{bipy})(\text{dcpa})]$, hydrogen atoms are omitted for clarity. Ellipsoids are drawn at 50 % probability level.[143]

Additionally, the molecular structures of the isoelectronic copper(I) complexes $[\text{Cu}(\text{bipy})(\text{bcp})]^+$ and $[\text{Cu}(\text{bipy})(\text{dcpa})]^+$ were obtained. X-ray analysis showed that they are isostructural to the corresponding Ni(0) complexes. So far only titanium, cobalt and platinum complexes with the ligand bcp have been reported.

The reaction of a more complex olefin is described in chapter 3. In collaboration with the research group of Prof. P. R. Schreiner (JLU Gießen, Institute for Organic Chemistry) efforts were made to obtain copper(I) and nickel(0) coordination polymers with the adamantane derivative tetracyclo[7.3.1.1^{4,12}.0^{2,7}]tetradeca-6.11-diene (tctd). Unfortunately, the uncharged coordination polymer $[\text{Ni}_x(\text{tctd})_y]_n$ could not be isolated. In contrast, it was possible to obtain the copper(I) polymer $[\text{Cu}_2\text{Cl}_2](\text{CH}_3\text{CN})(\text{tctd})_n$ for the first time. The molecular structure of the complex is shown in Figure 6.3.

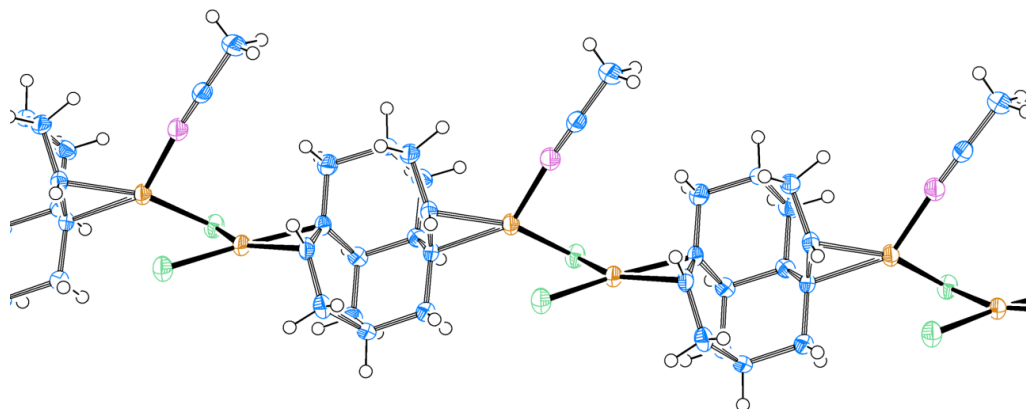


Figure 6.3: ORTEP plot of a fragment of the copper(I) chain $[\text{Cu}_2\text{Cl}_2](\text{CH}_3\text{CN})(\text{tctd})_n$. Ellipsoids are drawn at 50% probability level.

Furthermore, studies on ligand exchange reactions of the nickel(0) complex bis(cyclooctadiene)nickel(0) ($[\text{Ni}(\text{COD})_2]$) and N-Donor ligands have been performed which are presented in chapter 4. Efforts synthesizing a binuclear nickel(0) complex using the tetradentate ligand 1,2-bis(2,2'-bipyridine-6-yl)ethane (O-BPy) afforded the complex $[\text{Ni}_2(\text{O-BPy})(\eta^2\text{-C}_4\text{H}_6)_2]$ with coordinated butadiene instead of COD. The molecular structure determined by X-ray diffraction studies is shown in Figure 6.4.

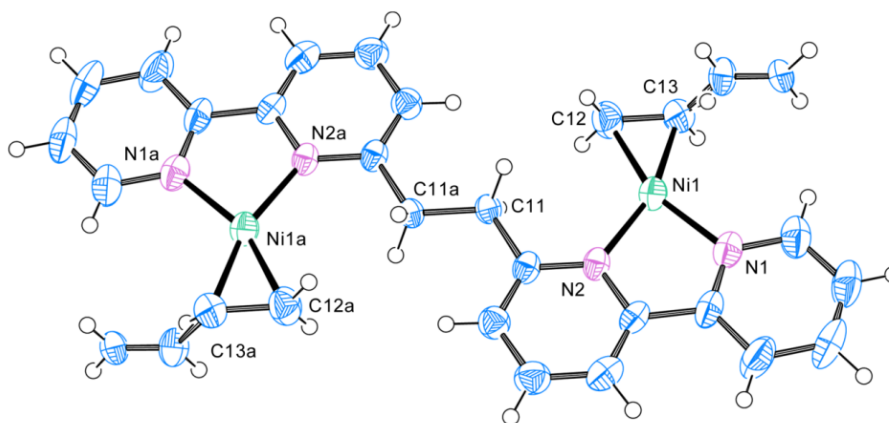


Figure 6.4: ORTEP plot of the binuclear complex $[\text{Ni}_2(\text{O-BPy})(\eta^2\text{-C}_4\text{H}_6)_2]$. Ellipsoids are drawn at 50% probability level.[141]

Since no butadiene was used as an educt in this reaction a cleavage of COD catalyzed by the nickel(0) complex was supposed. This was a remarkable result

due to the fact that one molecule COD is lower of energy than two molecules 1,3-butadiene. Within a collaboration with the research group of Prof. M. C. Holthausen (Goethe University Frankfurt am Main, Institute for Inorganic and Analytical Chemistry) DFT calculations for the formation of the binuclear as well as a mononuclear nickel complex with O-BPy were performed. Calculated Gibbs energies showed that the formation of $[\text{Ni}(\text{O-BPy})]$ should be more spontaneous than the formation of $[\text{Ni}_2(\text{O-BPy})(\text{COD})_2]$. Therefore, efforts were made to investigate this reaction in more detail using the ligand O-BPy and derivatives. Unfortunately, the binuclear nickel(0) complex with coordinated butadiene could not be isolated during this work. However, it was possible to structurally characterize several mononuclear complexes with the applied ligands (see Figure 6.5): $[\text{Ni}(\text{O-BPy})]$, $[\text{Ni}(\text{pmbd})]$ and $[\text{Ni}(\text{mpmbd})]$.

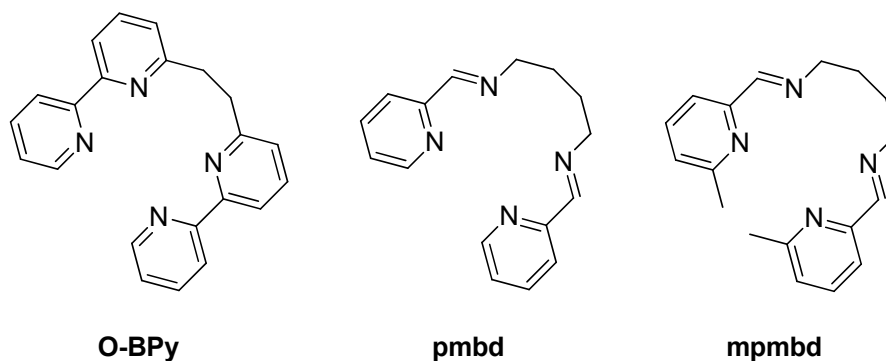


Figure 6.5: Structures of the ligands 1,2-bis(2,2'-bipyridine-6-yl)ethane (O-BPy), *N,N'*-bis((6-methylpyridine-2-yl)methylene)butane-1,4-diamine (mpmbd) and *N,N'*-bis(pyridine-2-ylmethylene)butane-1,4-diamine (pmbd).

As an example, the molecular structure of the mononuclear Ni(0) complex $[\text{Ni}(\text{O-BPy})]$ is shown in Figure 6.6.

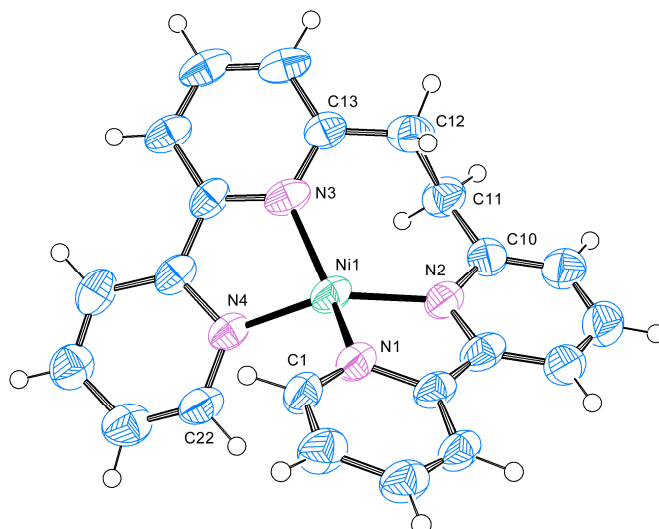


Figure 6.6: ORTEP plot of the complex $[\text{Ni}(\text{O-BPy})]$. Ellipsoids are drawn at 50 % probability level. Solvent molecules are omitted for clarity.

Due to difficulties isolating and characterizing the sensitive nickel(0) complexes isoelectronic copper(I) complexes with O-BPy were also prepared. It was possible to synthesize the copper(I) complex $[\text{Cu}_2(\text{O-BPy})(\text{COD})_2]$ which was expected by the reaction of $[\text{Ni}(\text{COD})_2]$ and O-BPy in the first place. The molecular structure of this complex is presented in Figure 6.7.

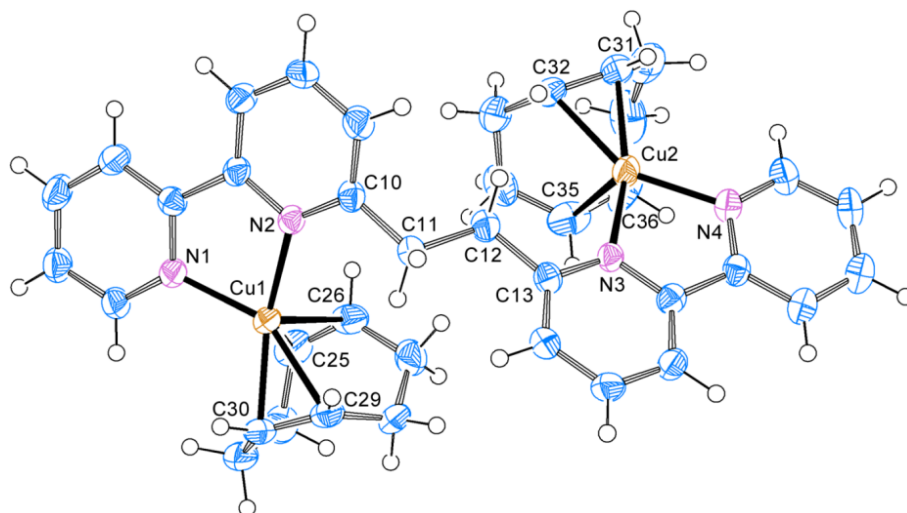


Figure 6.7: ORTEP plot of the cation $[\text{Cu}_2(\text{O-BPy})(\text{COD})_2]^{2+}$. Ellipsoids are drawn at 50 % probability level.

The obtained results showed that the cleavage of COD is highly depending on the reaction conditions applied which emphasizes the sensitivity of nickel(0) complexes. DFT calculations showed generally higher stability of the mononuclear complexes. The experimental results presented herein confirmed these calculations. Instead of nickel, the dinuclear copper(I) complex with coordinated COD could be obtained. However, a cleavage of COD into butadiene was not observed.

Developing transition metal complexes, which are able to selectively and catalytically oxidize organic substrates under mild conditions, is a fascinating and challenging task in today's chemistry. Therefore, studies on the activation of small molecules (e.g. O₂, NO, N₂O) and the formation and reactivity of short-lived model metal-oxygen intermediates are of great interest.

The number of reported nickel-oxygen intermediates has been comparatively low in this field. So far, recent results published by Nam and co-workers triggered our interests in nickel-dioxygen adduct complexes and their reactivity (chapter 5). In that regard, macrocyclic ligands proved to be quite useful for the synthesis of mononuclear metal-O₂ complexes. Efforts were made in this work to synthesize nickel-dioxygen adducts with the macrocyclic ligands 1,4,8,11-tetramethyl-1,4,8,11-tetraazacyclotetradecane (14-tmc) and *rac*-5,5,7,12,12,14-hexamethyl-1,4,8,11-tetraazacyclotetradecane (tetB). Therefore, the respective nickel(II) complexes were reacted with hydrogen peroxide, sodium peroxide as well as potassium superoxide with the aim of isolating a nickel end-on superoxo species. Performed UV-Vis experiments showed the formation of a nickel end-on superoxo complex. However, it was not possible to isolate and structurally characterize the nickel-dioxygen adduct yet. By reducing [Ni(14-tmc)](ClO₄)₂ with sodium amalgam to the nickel(I) complex and reacting it with gaseous nitrous oxide, it was the aim to obtain the "nickel-oxo" complex. This species was most likely formed as an intermediate. However, it was only possible to isolate and characterize the nickel-hydroxo complex Na[Ni₂(14-tmc)₂(OH)₂](ClO₄)₃ (Figure 6.8).

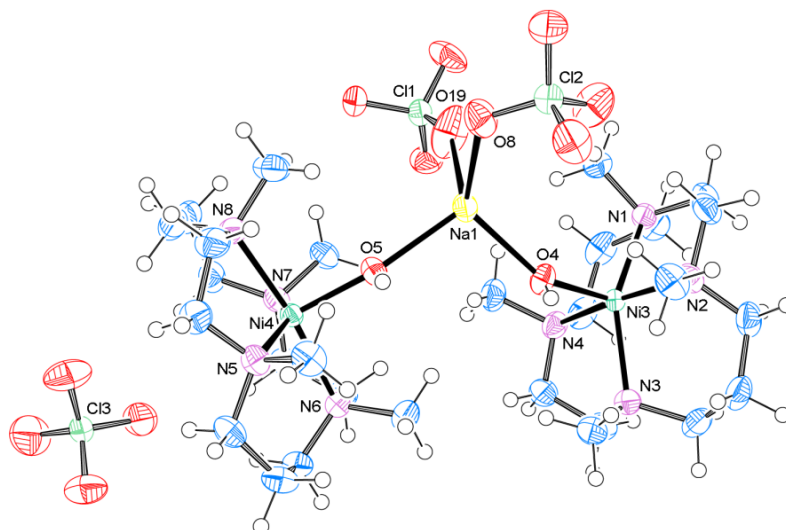


Figure 6.8: ORTEP plot of the full complex molecule of $\text{Na}[\text{Ni}_2(14\text{-tmc})_2(\text{OH})_2](\text{ClO}_4)_3$. Solvent molecules are omitted for clarity. Ellipsoids are drawn at 50 % probability level.

The analogue complex with triflate as counter ion was able to activate N_2O and a brown solution stable at $-80\text{ }^\circ\text{C}$ could be obtained. Low temperature UV-Vis experiments on this reaction have been performed and are presented herein. Unfortunately, the nickel nitrous oxide adduct complex could not be isolated and structurally characterized yet. However, the stability of this adduct complex is promising for future experiments and might provide access to a “nickel-oxo” species.

6.2 Zusammenfassung

In der heutigen Zeit wird angenommen, dass fast alle chemischen Erzeugnisse eine katalytische Stufe in ihrem Produktionsprozess durchlaufen. Hierbei sind Organokatalysatoren auf Basis von Palladium und Platin sehr weit verbreitet und werden am häufigsten genutzt. Dennoch bietet es sich an Nickel zu verwenden, welches ebenfalls eine Vielzahl an organometallischen Verbindungen bildet, dabei aber um ein Vielfaches günstiger ist (zehn bis fünfzig Mal billiger als Pd und Pt). Nickel(0)-Komplexe stellen eine große Anzahl an homogenen Nickel-Katalysatoren dar und sind weit verbreitet bei Cyclooligomerisierungsreaktionen

von Alkenen, Cycloalkenen, Dienen und Alkinen sowie bei Carboxylierungsreaktionen von Dienen.

Ziel dieser Arbeit war es, das Reaktionsverhalten von Ni(0)-Komplexen besser zu verstehen, um neue Wege zu finden teure Edelmetallkatalysatoren auf Pd- und Pt-Basis zu ersetzen.

Bicyclopropyliden (bcp), Dicyclopropylacetylen (dcpa) und 1,4-Dimethoxy-2-butan (dmbu) sind interessante Verbindungen, welche als „molekulare Bausteine“ in zahlreichen Übergangsmetall-katalysierten Reaktionen verwendet werden. Diese Verbindungen wurden zuvor in der Arbeitsgruppe von Prof. A. de Meijere (Universität Göttingen, Institut für Organische Chemie) dargestellt und als Liganden genutzt, um die entsprechenden Ni(0)-Komplexe nach folgender Reaktionsgleichung darzustellen:

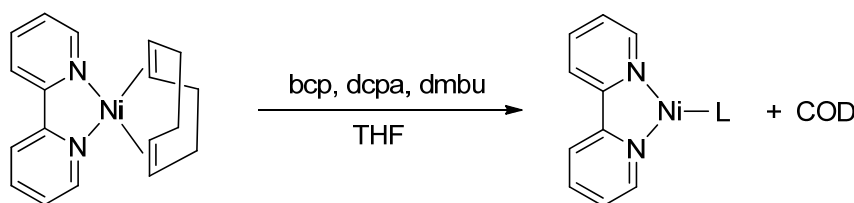


Abbildung 6.9: Schema der Reaktion von [Ni(bipy)(COD)] mit den ungesättigten Liganden bcp, dcpa und dmbu.

Kinetische Untersuchungen zu dieser Ligandenaustauschreaktion wurden mit Hilfe von „Stopped-Flow“-Messungen durchgeführt (Kapitel 2). Ergebnisse dieser Untersuchungen lassen bei der Reaktion von [Ni(bipy)(COD)] mit bcp und dmbu auf einen Mechanismus mit einem hochgeordneten Übergangszustand schließen. Die Reaktion des Ni(0) Komplexes mit dem Liganden dcpa konnten aufgrund einer reversiblen Reaktion nicht ausgewertet werden. Dennoch ist zu erkennen, dass die Austauschreaktion deutlich langsamer verläuft als mit den Liganden bcp und dmbu. Die Geschwindigkeitskonstanten der Reaktion zwischen [Ni(bipy)(COD)] und bcp sowie dmbu unterschieden sich jedoch stark. Bei 20,2 °C verlief die Reaktion mit dmbu um den Faktor 1000 langsamer als mit bcp bei 5,2 °C. Insgesamt sind die durch die Untersuchungen erhaltenen Ergebnisse vielversprechend für zukünftige mögliche Anwendungen im synthetischen Bereich. Des Weiteren konnten die Molekülstrukturen der Produktkom-

plexe erhalten werden. Beispielhaft ist dabei die Struktur des Komplexes $[\text{Ni}(\text{bipy})(\text{dcpa})]$ in Abbildung 6.10 gezeigt.

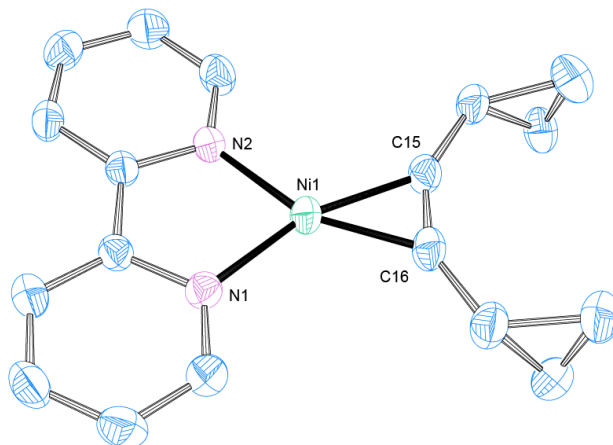


Abbildung 6.10: Molekülstruktur des Komplexes $[\text{Ni}(\text{bipy})(\text{dcpa})]$. Ellipsoide mit 50 % Aufenthaltswahrscheinlichkeit.

Zusätzlich konnten die isoelektronischen Kupfer(I)-Komplexe $[\text{Cu}(\text{bipy})(\text{bcp})]^+$ und $[\text{Cu}(\text{bipy})(\text{dcpa})]^+$ kristallographisch charakterisiert werden. Diese zeigten isostrukturelle Eigenschaften zu den Nickel(0)-Komplexen. Bisher konnten nur Metallkomplexe mit Titan, Kobalt sowie Platin mit dem Liganden bcp charakterisiert werden.

Die Reaktion mit einem etwas ungewöhnlicheren und komplexen Olefin ist in Kapitel 3 dieser Arbeit beschrieben. In Kooperation mit der Arbeitsgruppe von Prof. P. R. Schreiner (JLU Gießen, Institut für Organische Chemie) wurde versucht organische Kupfer(I)- sowie Nickel(0)-Koordinationspolymere mit dem Adamantan-Derivat tetracyclo[7.3.1.1^{4,12}.0^{2,7}]tetradeca-6,11-dien (tctd) darzustellen. Leider konnte das ungeladene Nickel-Koordinationspolymer des Typs $[\text{Ni}_x(\text{tctd})_y]_n$ nicht isoliert und charakterisiert werden. Im Gegensatz dazu war es möglich das Kupfer-Koordinationspolymer $[\text{Cu}_2\text{Cl}_2](\text{CH}_3\text{CN})(\text{tctd})_n$ erstmals darzustellen und kristallographisch zu charakterisieren. Die Molekülstruktur des Komplexes ist in Abbildung 6.11 dargestellt.

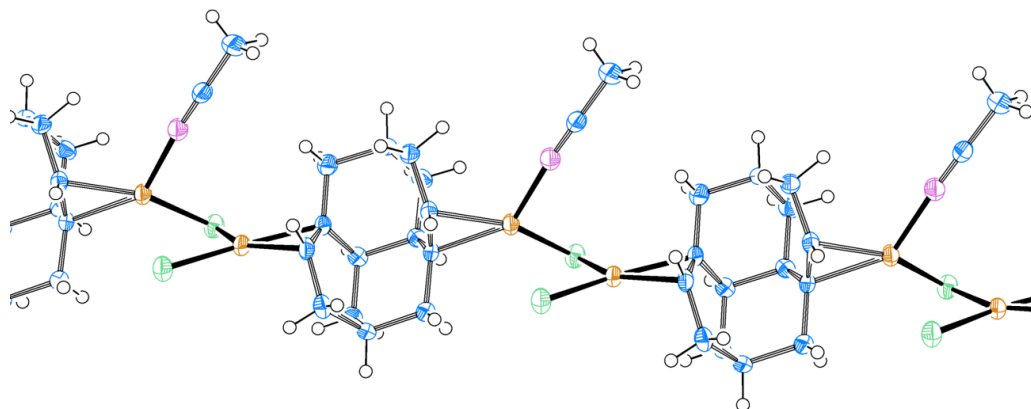


Abbildung 6.11: Molekülstruktur eines Fragments des Kupfer(I)-Koordinationspolymers $[\text{Cu}_2\text{Cl}_2](\text{CH}_3\text{CN})(\text{tctd})_n$. Ellipsoide mit 50 % Aufenthaltswahrscheinlichkeit.

Des Weiteren wurden Untersuchungen zu Ligandenaustauschreaktionen des Komplexes Bis(cyclooctadien)nickel(0) ($[\text{Ni}(\text{COD})_2]$) mit N-Donor Liganden durchgeführt (Kapitel 4). Bei dem Versuch einen zweikernigen Nickel(0)-Komplex mit dem Liganden 1,2-Bis(2,2'-bipyridin-6-yl)ethan (O-BPy) darzustellen wurde stattdessen der Komplex $[\text{Ni}_2(\text{O-BPy})(\eta^2\text{-C}_4\text{H}_6)_2]$ mit koordiniertem 1,3-Butadien erhalten. Die Molekülstruktur des Komplexes ist in Abbildung 6.12 gezeigt.

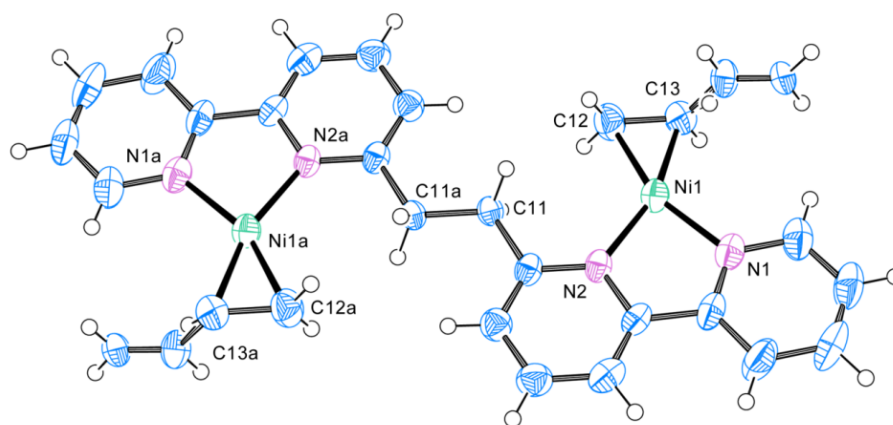


Abbildung 6.12: Molekülstruktur des dimeren Komplexes $[\text{Ni}_2(\text{O-BPy})(\eta^2\text{-C}_4\text{H}_6)_2]$. Ellipsoide mit 50 % Aufenthaltswahrscheinlichkeit.[141]

Da bei der Reaktion kein Butadien als Edukt eingesetzt wurde, wird eine Spaltung des COD Liganden, katalysiert durch den Nickel(0)-Komplex, vermutet. Dies ist ein überraschendes Ergebnis, da ein Molekül COD energieärmer ist als zwei Moleküle Butadien. In Zusammenarbeit mit der Arbeitsgruppe von Prof. M. C. Holthausen wurden DFT-Berechnungen (Goethe Universität Frankfurt am Main, Institut für Anorganische und Analytische Chemie) für die Bildung des zweikernigen sowie eines einkernigen Nickel-Komplexes mit O-BPy durchgeführt. Berechnete Gibbs-Energien zeigten dabei, dass die Bildung des Komplexes $[\text{Ni}(\text{O-BPy})]$ der Bildung des Komplexes $[\text{Ni}_2(\text{O-BPy})(\text{COD})_2]$ bevorzugt sein müsste. Daraufhin wurde diese Reaktion sowohl unter Verwendung des Liganden O-BPy als auch verschiedener Derivate weiter untersucht. Leider konnte dabei der zweikernige Nickel-Komplex mit koordiniertem Butadien nicht erhalten werden. Jedoch war es möglich mehrere einkernige Komplexe mit den verwendeten Liganden (vgl. Abbildung 6.13) darzustellen und kristallographisch zu charakterisieren: $[\text{Ni}(\text{O-BPy})]$, $[\text{Ni}(\text{pmbd})]$ und $[\text{Ni}(\text{mpmbd})]$.

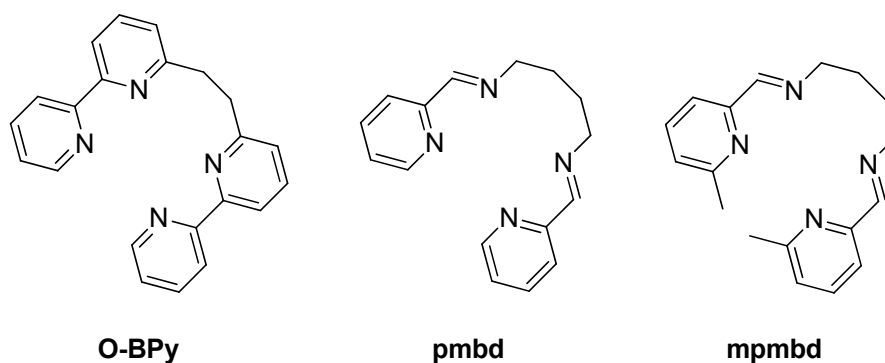


Abbildung 6.13: Strukturen der Liganden 1,2-Bis(2,2'-bipyridin-6-yl)ethan (O-BPy), *N,N'*-Bis((6-methylpyridin-2-yl)methylen)butan-1,4-diamin (mpmbd) und *N,N'*-Bis(pyridin-2-ylmethylen)butan-1,4-diamin (pmbd).

Beispielhaft ist dabei die Molekülstruktur des Komplexes $[\text{Ni}(\text{O-BPy})]$ in Abbildung 6.14 gezeigt.

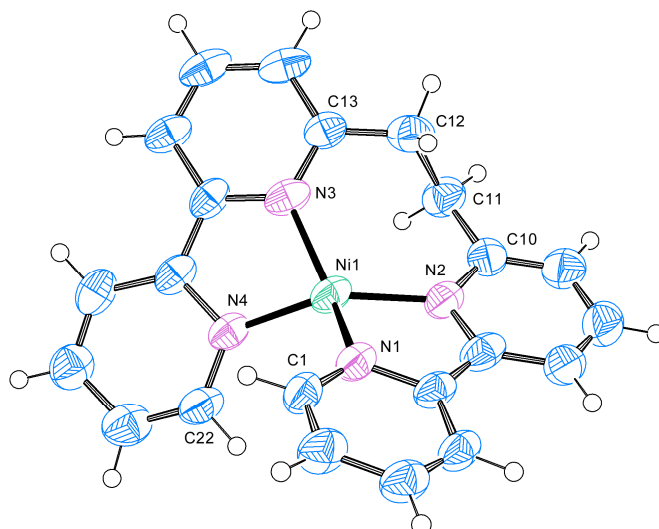


Abbildung 6.14: Molekülstruktur des einkernigen Komplexes $[\text{Ni}(\text{O-BPy})]$. Ellipsoide mit 50 % Aufenthaltswahrscheinlichkeit.

Aufgrund der sehr empfindlichen Nickel(0)-Komplexe und der dadurch erschwerten Darstellung und Charakterisierung, wurden auch isoelektronische Kupfer(I)-Komplexe mit O-BPy synthetisiert. Dabei war es möglich den zweikernigen Cu(I)-Komplex $[\text{Cu}_2(\text{O-BPy})(\text{COD})_2]$ kristallographisch zu charakterisieren, welcher zunächst in der Reaktion von Nickel mit O-BPy erwartet wurde. Die Molekülstruktur des Komplexes ist in Abbildung 6.15 gezeigt.

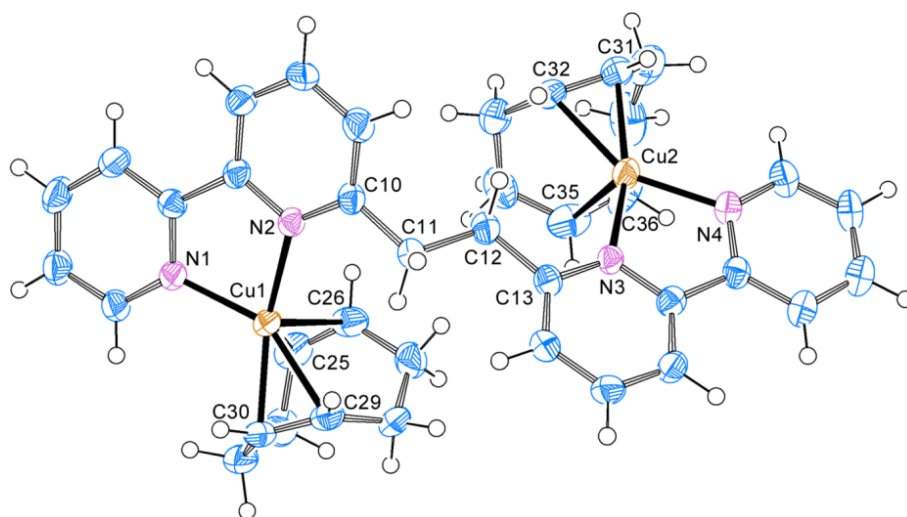


Abbildung 6.15: Molekülstruktur des Kations $[\text{Cu}_2(\text{O-BPy})(\text{COD})_2]^{2+}$. Ellipsoide mit 50 % Aufenthaltswahrscheinlichkeit.

Die Ergebnisse zeigten, dass die Spaltung von COD sehr stark von den gewählten Reaktionsbedingungen abhängt, welches die Empfindlichkeit der Nickel(0) Systeme noch einmal verdeutlicht. DFT Berechnungen zeigten, dass generell eine höhere Stabilität der einkernigen Komplexe vorliegt. Die in dieser Arbeit ermittelten Ergebnisse bestätigen diese Theorie. Anstatt eines zweikernigen Nickel-Komplexes mit koordiniertem COD konnte der entsprechende Kupfer(I)-Komplex dargestellt werden. Jedoch war eine Spaltung von COD zu Butadien nicht zu beobachten.

Die Entwicklung von Übergangsmetallkomplexen, welche katalytisch und selektiv in der Lage sind organische Verbindungen unter milden Reaktionsbedingungen zu oxidieren, ist eine herausfordernde und vorherrschende Fragestellung in der heutigen Chemie. Dabei sind Untersuchungen zur Aktivierung kleiner Moleküle (z.B. O₂, NO, N₂O) und die Bildung sowie das Reaktionsverhalten von kurzlebigen Metall-Sauerstoff-Intermediaten von großem Interesse.

Die Anzahl an publizierten Nickel-Sauerstoff-Komplexen ist dabei sehr gering. Kürzlich veröffentlichte Ergebnisse von Nam et al. weckten jedoch unser Interesse an Nickel-Sauerstoff-Addukten und deren Untersuchung. Im Hinblick darauf erwiesen sich makrozyklische Liganden bei der Stabilisierung solcher Spezies als besonders nützlich. Mit Hilfe der makrozyklischen Liganden 1,4,8,11-tetramethyl-1,4,8,11-tetraazacyclotetradecan (14-tmc) und *rac*-5,5,7,12,12,14-hexymethyl-1,4,8,11-tetraazacyclotetradecan (tetB) sollten Nickel-Sauerstoff-Addukt Komplexe dargestellt werden. Dabei wurden die jeweiligen Nickel(II)-Komplexe mit Wasserstoffperoxid, Natriumperoxid und Kaliumsuperoxid umgesetzt, mit dem Ziel einen end-on Superoxo-Komplex zu erhalten. UV-Vis spektroskopische Untersuchungen bestätigten die Bildung dieser Spezies, jedoch konnten bisher keine geeigneten Kristalle für eine Einkristallmessung isoliert werden. Durch Reduktion von [Ni(14-tmc)](ClO₄)₂ mit Natriumamalgam konnte der entsprechende Nickel(I)-Komplex dargestellt werden. Dieser wurde mit Distickstoffmonoxid umgesetzt, um einen „Nickel-Oxo-Komplex“ darzustellen.

Es war jedoch nur möglich, den Nickel-Hydroxo-Komplex Na[Ni₂(14-tmc)₂(OH)₂](ClO₄)₃ darzustellen und kristallographisch zu charakterisieren (vgl. Abbildung 6.16), wobei ein „Nickel-Oxo-Komplex“ wahrscheinlich intermediär vorlag.

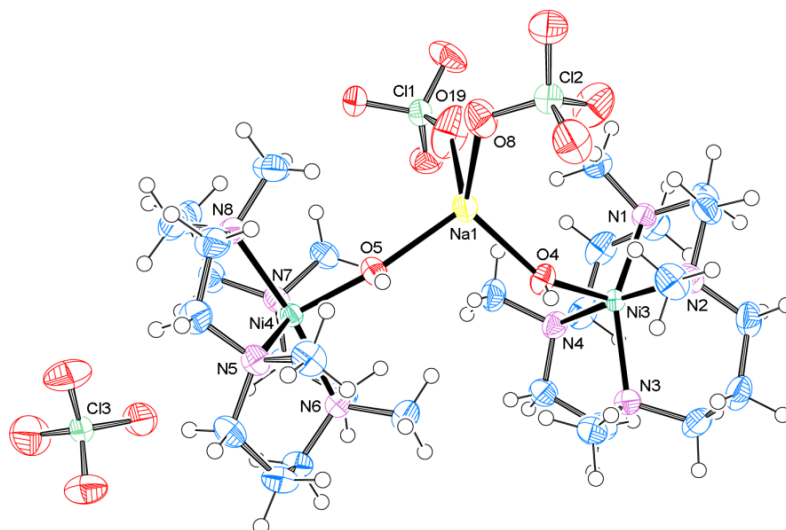


Abbildung 6.16: Molekülstruktur des Komplexes $\text{Na}[\text{Ni}_2(14\text{-tmc})_2(\text{OH})_2](\text{ClO}_4)_3$. Ellipsoide mit 50 % Aufenthaltswahrscheinlichkeit. Lösungsmittelmoleküle wurden zur besseren Übersicht weggelassen.

Der analoge Komplex mit Triflat als Gegenion war in der Lage N_2O zu aktivieren. Dabei konnte bei der Umsetzung eine braune Lösung erhalten werden, welche bei Temperaturen unterhalb von $-80\text{ }^\circ\text{C}$ stabil blieb. UV-Vis spektroskopische Untersuchungen wurden hierzu bei tiefen Temperaturen durchgeführt. Leider konnten bisher keine messbaren Kristalle des „Ni– N_2O -Adduktkomplexes“ erhalten werden. Jedoch ist die Stabilität des Komplexes sehr vielversprechend und könnte zukünftig die Darstellung eines „Nickel-Oxo-Komplexes“ ermöglichen.

7 List of Figures

1.1: Overview of the most common nickel ores.....	1
1.2: Equation for the Mond process.....	2
1.3: Cyclodimerization and cyclotrimerization products of cyclopropene.....	4
1.4: Catalytic cycle for the nickel-catalyzed cyclooligomerization of cyclopropenes.....	5
1.5: Molecular structures of analogue Ni(0) complexes of reactive intermediates proposed in Figure 1.4 determined by X-ray analysis.....	6
1.6: Products of the nickel-catalyzed cyclooligomerization of 1,3-butadiene.....	6
1.7: Reaction pathway of the nickel-catalyzed cyclooligomerization of 1,3-butadiene.....	7
1.8: Reaction mechanism of the cyclotetramerization of acetylene; Reppe et al.	9
1.9: Reaction scheme for the cyclooligomerization of acetylene; Eisch et al.....	10
1.10: Molecular structure of 2,2-bipyridyl(η^2 -diphenylacetylene)nickel.....	10
1.11: Possible coordination modes of carbon dioxide to nickel.....	11
1.12: Reaction of bis(1,5-cyclooctadiene)nickel(0) with tricyclohexylphosphine and carbon dioxide.....	11
1.13: Reaction of 2,3-Dimethyl-1,3-butadiene and CO ₂ using a nickel(0) complex.....	12
1.14: Reaction of 1,3-butadiene and CO ₂ using [Ni(COD) ₂]/TMEDA.....	13
1.15: Catalytic reaction of 1,3-butadiene and CO ₂ using [Ni(COD) ₂]/P(O ⁱ Pr) ₃ .	14
1.16: Proposed reaction course for the catalytic formation of 2-methylene-3-vinylcyclopentanecarboxylic acid.....	14
1.17: Overall equation for the reaction of CO ₂ with H ₂ affording methane.....	16
1.18: Formation of methane by the methyl-coenzyme M reductase.....	16
1.19: Structure of the coenzyme F430.....	17
1.20: Proposed mechanism of methyl-coenzyme M reductase.....	18
1.21: Equations for the dismutase reaction catalyzed by SODs.....	18
1.22: Ni-SOD: A hexameric assembly of 4-helix bundles. Ni ions displayed in dark gray.....	19
1.23: Structure of the active site of Ni-SOD (oxidized state, Ni ^{III}).....	19
1.24: Proposed catalytic mechanism for Ni-SOD.....	20

1.25: Ni–O _x structure types obtained from Ni(II) complexes and H ₂ O ₂	21
1.26: Side-on Ni(II)-peroxo complex obtained from the reaction of Ni(t-BuNC) ₄ and dioxygen.	22
1.27: Reaction scheme for the oxygenation of [(PhTt ^{Ad})Ni(CO)] at -78 °C affording [(PhTt ^{Ad})Ni(O ₂)].	23
1.28: Formation of a side-on superoxo-nickel(II) complex from β-diketiminato- (toluene)nickel(I).....	23
1.29: Molecular structure of a β-diketiminato-supported Ni–O ₂ complex.	23
1.30: Molecular structure of [Ni(12-tmc)O ₂] ⁺	24
1.31: DFT optimized structure of [Ni(14-tmc)O ₂] ⁺	24
1.32: Structures of bicyclopopylidene (bcp), dicyclopopylacetylene (dcpa) and dimethoxybutyne (dmbu).....	25
1.33: Scheme for the reaction of [Ni(bipy)(COD)] with the unsaturated ligands bcp, dcpa and dmbu.....	26
1.34: Structure of tetracyclo[7.3.1.1 ^{4,12} .0 ^{2,7}] tetradeca-6,11-diene (tctd).	26
1.35: Reaction scheme for the synthesis of [Ni ₂ (O-BPy)(η ² -C ₄ H ₆) ₂].	27
1.36: Structures of the ligands 1,4,8,11-tetramethyl-1,4,8,11- tetraazacyclotetradecane (14-tmc) <i>rac</i> -5,5,7,12,12,14-hexymethyl-1,4,8,11- tetraazacyclotetradecane (tetB).	28
1.37: Proposed scheme for the reaction of [Ni(14-tmc)] ⁺ with nitrous oxide.	28
2.1: Structures of bicyclopopylidene (bcp), 1,4-dicyclopopylacetylene (dcpa) and 1,4-dimethoxy-2-butyne (dmbu).	29
2.2: Synthesis of the first Ti complex of bcp.....	30
2.3: Synthesis of the first Co complex of bcp.....	30
2.4: Synthesis of the first Pt complex of bcp.	30
2.5: Reaction scheme for the synthesis of the Ni(0) complexes [Ni(bipy)bcp], [Ni(bipy)dcpa] and [Ni(bipy)dmbu].	31
2.6: ORTEP plot of [Ni(bipy)(bcp)], hydrogen atoms are omitted for clarity. Ellipsoids are drawn at 50 % probability level.....	32
2.7: ORTEP plot of [Ni(bipy)(dcpa)], hydrogen atoms are omitted for clarity. Ellipsoids are drawn at 50 % probability level.....	33
2.8: Proposed molecular structure for [Ni(bipy)(dmbu)] (UFF optimized), hydrogen atoms are omitted for clarity.	34

2.9: Time-resolved UV-Vis spectra of the reaction of $[\text{Ni}(\text{bipy})(\text{COD})]$ with bicyclopropylidene in THF; $[\text{Ni}(\text{bipy})(\text{COD})] = 0.25 \text{ mM}$, $[\text{bcp}] = 30 \text{ mM}$, xs COD; $T = -20.2 \text{ }^{\circ}\text{C}$, $t = 299.5 \text{ s}$, $\Delta t = 1 \text{ s}$	35
2.10: k_{obs} vs. bcp-concentration at four different temperatures at 561 nm; $[\text{Ni}(\text{bipy})(\text{COD})] = 0.25 \text{ mM}$	36
2.11: Postulated reaction mechanism for the reaction of $[\text{Ni}(\text{bipy})(\text{COD})]$ with bicyclopropylidene.....	37
2.12: Reaction of $[\text{Ni}(\text{bipy})(\text{COD})]$ and L_1 ; $\text{R} = \text{CO}_2\text{Me}$, $\text{R}_1 = \text{CH}_3$	37
2.13: Time-resolved UV-Vis spectra of the reaction of $[\text{Ni}(\text{bipy})(\text{COD})]$ with dicyclopropylacetylene in THF; $[\text{Ni}(\text{bipy})(\text{COD})] = 0.25 \text{ mM}$, $[\text{dcpa}] = 30 \text{ mM}$, xs COD; $T = 20.1 \text{ }^{\circ}\text{C}$, $t = 51.3 \text{ s}$, $\Delta t = 1 \text{ s}$	38
2.14: k_{obs} vs. dcpa-concentration at four different temperatures at 561 nm; $[\text{Ni}(\text{bipy})(\text{COD})] = 0.25 \text{ mM}$	39
2.15: Time-resolved UV-Vis spectra of the reaction of $[\text{Ni}(\text{bipy})(\text{COD})]$ with 1,4-dimethoxy-2-butyne in THF; $[\text{Ni}(\text{bipy})(\text{COD})] = 0.25 \text{ mM}$, $[\text{dmbu}] = 25 \text{ mM}$, xs COD; $T = 20.2 \text{ }^{\circ}\text{C}$, $t = 45 \text{ s}$, $\Delta t = 1 \text{ s}$	40
2.16 Absorbance vs. time for the reaction of $[\text{Ni}(\text{bipy})(\text{COD})]$ with 1,4-dimethoxy-2-butyne at 561 nm and fit to a single exponential function; $[\text{Ni}(\text{bipy})(\text{COD})] = 0.25 \text{ mM}$, $[\text{dmbu}] = 25 \text{ mM}$, xs COD; $T = 20.2 \text{ }^{\circ}\text{C}$	41
2.17: k_{obs} vs. dmbu-concentration at four different temperatures; $[\text{Ni}(\text{bipy})(\text{COD})] = 0.25 \text{ mM}$	42
2.18: Eyring plot for the reaction of $[\text{Ni}(\text{bipy})(\text{COD})]$ with 1,4-dimethoxy-2-butyne in THF determined from Table 2.4.....	43
2.19: Proposed mechanism for the reaction of $[\text{Ni}(\text{bipy})(\text{dmbu})]$ with 1,4-dimethoxy-2-butyne.	45
2.20: ORTEP plot of the cation $[\text{Cu}(\text{bipy})(\text{bcp})]^+$, hydrogen atoms are omitted for clarity. Ellipsoids are drawn at 50 % probability level.	46
2.21: ORTEP plot of the cation $[\text{Cu}(\text{bipy})(\text{dcpa})]^+$, hydrogen atoms are omitted for clarity. Ellipsoids are drawn at 50 % probability level.	47
2.22: Reaction of $[\text{Cu}(\text{bipy})(\text{dcpa})]^+$ with atmospheric dioxygen affording the bis(μ -hydroxo)dicopper(II) complex $[\text{Cu}_2(\text{bipy})_2(\text{OH})_2]^{2+}$	48
2.23: ORTEP plot of the cation $[\text{Cu}_2(\text{bipy})_2(\text{OH})_2]^{2+}$, hydrogen atoms are omitted for clarity. Ellipsoids are drawn at 50 % probability level.....	49
3.1: Small selection of diamondoids: Adamantane (a), diamantane (b), triamantane (c) and (<i>anti</i>)-tetramantane (d).	51

3.2: Structure of tetracyclo[7.3.1.1 ^{4,12} .0 ^{2,7}]tetradeca-6,11-diene (tctd).	52
3.3: Rearrangement sequence from tetrahydro-binor-S (3.1) affording diamantane (3.3) involving the intermediate protodiamantane (3.2).....	52
3.4: Synthesis of protodiamantane (3.2) from 1,6-dibromodiamantane involving the diene tctd.....	53
3.5: ORTEP plot of the cation [Cu ₂ (bipy) ₂ (tctd)] ²⁺ , hydrogen atoms and solvent molecules are omitted for clarity. Ellipsoids are drawn at 50 % probability level.	54
3.6: ORTEP plot of the full complex molecule [Cu ₂ Cl ₂ (CH ₃ CN)(tctd)]. Ellipsoids are drawn at 50 % probability level.....	55
3.7: ORTEP plot of a fragment of the copper(I) chain [Cu ₂ Cl ₂ (CH ₃ CN)(tctd)] _n . Ellipsoids are drawn at 50% probability level.....	57
3.8: Reaction scheme for the synthesis of [Ni(tctd)] _n in THF.	57
3.9: Proposed molecular structure for a fragment of the nickel(0) chain [Ni _x (tctd) _y] _n (UFF optimized).	58
4.1: Reaction scheme for the synthesis of [Ni(bipy)(COD)].	61
4.2: Structure of 1,2-bis(2,2'-bipyridin-6-yl)ethane (O-BPy).	61
4.3: Reaction scheme for the synthesis of [Ni ₂ (O-BPy)(COD) ₂].	62
4.4: Reaction scheme for the synthesis of [Ni ₂ (O-BPy)(η^2 -C ₄ H ₆) ₂].	62
4.5: ORTEP plot of the binuclear complex [Ni ₂ (O-BPy)(η^2 -C ₄ H ₆) ₂]. Ellipsoids are drawn at 50% probability level.	63
4.6: Proposed mechanism for the cleavage of 1,5-cyclooctadiene.	63
4.7: Catalytic cyclodimerization of 1,3-butadiene to 1,5-cyclooctadiene.	64
4.8: Calculated Gibbs energy for the reaction of one molecule of 1,5- cyclooctadiene to two molecules of 1,3-butdiene.	64
4.9: Calculated Gibbs energies for the formation of [Ni(O-BPy)] and [Ni ₂ (O-BPy)(η^2 -C ₄ H ₆) ₂].	65
4.10: Synthesis of 6-methyl-2,2'-bipyridine.	67
4.11: Synthesis of 1,2-bis(2,2'-bipyridine-6-yl)ethane.	67
4.12: ORTEP plot of the ligand O-BPy. Ellipsoids are drawn at 50% probability level.	68
4.13: Synthesis of <i>N,N</i> -Bis((6-methylpyridine-2-yl)methylene)butane-1,4- diamine.	70
4.14: ORTEP plot of the ligand mpmbd. Ellipsoids are drawn at 50 % probability level.	70

4.15: Synthesis of <i>N,N</i> -bis(pyridine-2-ylmethylene)ethane-1,2-diamine (4.10) <i>N,N</i> -bis(pyridine-2-ylmethylene)butane-1,4-diamine (4.11), and <i>N,N</i> - bis(pyridine-2-ylmethylene)pentane-1,5-diamine (4.12).	72
4.16: ORTEP plot of the ligand pmbd. Ellipsoids are drawn at 50 % probability level.	73
4.17: Reaction scheme for the synthesis of [Ni(O-BPy)] using Ni/ligand ratios of 2:1 and 1:1.	75
4.18: ORTEP plot of the full complex molecule [Ni(O-BPy)]. Ellipsoids are drawn at 50 % probability level. Solvent molecules are omitted for clarity.	76
4.19: Reaction scheme for the synthesis of [Ni ₂ (O-BPy)(η^2 -C ₄ H ₆) ₂] using a Ni/ligand ratio of 2:1 and an excess amount of 1,3-butadiene.	78
4.20: Reaction scheme for the synthesis of [Ni(pmbd)] using Ni/ligand ratios of 2:1 and 1:1.	79
4.21: ORTEP plot of the full complex molecule [Ni(pmbd)]. Ellipsoids are drawn at 50 % probability level. Solvent molecules are omitted for clarity.	79
4.22: Reaction scheme for the synthesis of [Ni(mpmbd)] using Ni/ligand ratios of 2:1 and 1:1.	81
4.23: ORTEP plot of the full complex molecule [Ni(mpmbd)]. Ellipsoids are drawn at 50 % probability level.	82
4.24: Structures of the ligands 1,2-bis(6'-methyl-2,2'-bipyridine-6-yl)ethane (Me-O-BPy) and 1,2-bis(9-methyl-1,10-phenanthroline-2-yl)ethane (Me-O-BPh).	85
4.25: ORTEP plot of the cation [Cu ₂ (Me-O-BPy) ₂] ²⁺ . Thermal ellipsoids are drawn at 50 % probability level.	85
4.26: ORTEP plot of the scation [Cu ₂ (Me-O-BPh) ₂] ²⁺	85
4.27: ORTEP plot of [Co(Me-O-BPh) ₂](SO ₃ CF ₃) ₂ . Thermal ellipsoids are drawn at 50 % probability level.	86
4.28: ORTEP plot of the cation [Cu(Me-O-BPh)(H ₂ O)] ²⁺	86
4.29: ORTEP plot of the cation [Cu(COD) ₂] ⁺ . Ellipsoids are drawn at 50 % probability level.	87
4.30: Scheme for the reaction of [Cu(COD) ₂]X (X = ClO ₄ ⁻ , BF ₄ ⁻) and O-BPy using a ratio of 2:1.	89
4.31: Scheme for the reaction of [Cu(CH ₃ CN) ₄]X (X = ClO ₄ ⁻ , BF ₄ ⁻ , SbF ₆ ⁻ , PF ₆ ⁻) and O-BPy using a ratio of 2:1 and an excess of COD.	89

4.32: ORTEP plot of the cation $[\text{Cu}_2(\text{O-BPy})_2]^{2+}$. Ellipsoids are drawn at 50 % probability level. Solvent molecules are omitted for clarity.....	90
4.33: ORTEP plot of the cation $[\text{Cu}(\text{O-BPy})]^{2+}$. Ellipsoids are drawn at 50 % probability level.	92
4.34: Scheme for the reaction of $[\text{Cu}(\text{CH}_3\text{CN})_4]\text{SO}_3\text{CF}_3$ and O-BPy using a ratio of 2:1 and an excess of COD affording $[\text{Cu}_2(\text{O-BPy})(\text{COD})_2](\text{SO}_3\text{CF}_3)_2$..	94
4.35: ORTEP plot of the cation $[\text{Cu}_2(\text{O-BPy})(\text{COD})_2]^{2+}$. Ellipsoids are drawn at 50 % probability level.	95
4.36: IR spectra of the copper(I) complexes $[\text{Cu}_2(\text{O-BPy})(\text{COD})_2](\text{SO}_3\text{CF}_3)_2$ and $[\text{Cu}_2(\text{O-BPy})(\text{C}_4\text{H}_6)_2](\text{SO}_3\text{CF}_3)_2$ (KBr pellets).....	97
4.37: UV-Vis spectra of the complexes $[\text{Ni}(\text{O-BPy})]$ (blue) and $[\text{Ni}_2(\text{O-BPy})(\eta^2\text{-C}_4\text{H}_6)_2]$ (black) in THF.....	99
4.38: UV-Vis spectra of the complexes $[\text{Ni}(\text{O-BPy})]$ (blue) and $[\text{Ni}_2(\text{O-BPy})(\eta^2\text{-C}_4\text{H}_6)_2]$ (black) in DMF.....	99
4.39: UV-Vis spectra of the complex $[\text{Ni}(\text{pmbd})]$ in THF.	100
4.40: UV-Vis spectra of the complex $[\text{Ni}(\text{mpmbd})]$ in THF.	101
4.41: UV-Vis spectra of the complex $[\text{Ni}(\text{pmed})]$ in THF.	102
4.42: UV-Vis spectra of the complex $[\text{Ni}(\text{pmpd})]$ in THF.	103
4.43: UV-Vis spectra of the complex $[\text{Ni}(\text{Me-BPy})]$ in THF.	104
5.1: Structures of the macrocyclic ligands 1,4,8,11-tetramethyl-1,4,8,11-tetraazacyclotetradecane (14-tmc) and 1,4,7,10-tetramethyl-1,4,7,10-tetraazacyclodecane (12-tmc).....	111
5.2: Formation of the superoxo-nickel(II) complex (4.2) from the dinuclear β -diketiminato-toluene-nickel complex (5.1).	112
5.3: Activation of nitrous oxide with the dinuclear β -diketiminato-toluene-nickel(I) complex (5.1) affording di- β -diketiminato-bis(μ -hydroxo)-nickel(II) (5.4).....	113
5.4: Molecular structure of di- β -diketiminato-bis(μ -hydroxo)-nickel(II) (5.4). .	113
5.5: Reaction scheme for the synthesis of cyclam (5.8).....	114
5.6: Reaction scheme for the synthesis of 14-tmc (5.9).....	115
5.7: Stereoisomers of $[\text{Ni}(\text{14-tmc})]^{2+}$: (5.10) <i>R,S,R,S</i> (5.11) <i>R,S,S,R</i> (5.12) <i>R,S,R,R</i>	115

5.8: ORTEP plot of the cation $[\text{Ni}(\text{14-tmc})]^{2+}$ (<i>R,S,R,S</i> isomer). Ellipsoids are drawn at 25 % probability level. Solvent molecules are omitted for clarity.	116
5.9: ORTEP plot of the cation $[\text{Ni}(\text{14-tmc})(\text{MeCN})_2]^{2+}$ (<i>R,S,S,R</i> isomer). Ellipsoids are drawn at 50 % probability level. Free solvent molecules are omitted for clarity.....	118
5.10: Reduction of $[\text{Ni}(\text{14-tmc})](\text{ClO}_4)_2$ with NaHg in acetonitrile.	120
5.11: Color change in course of the reaction of $[\text{Ni}(\text{14-tmc})](\text{ClO}_4)_2$ with NaHg (5 % Na) in acetonitrile.	120
5.12: Scheme for the proposed reaction of a Ni(I) complex with N_2O	121
5.13: Color change in course of the reaction of $[\text{Ni}(\text{14-tmc})]\text{ClO}_4$ and nitrous oxide in acetonitrile at $-40\text{ }^\circ\text{C}$	121
5.14: ORTEP plot of $[\text{Na}(\text{14-tmc})]\text{ClO}_4$. Ellipsoids are drawn at 50 % probability level.	122
5.15: Side reaction occurring by reduction with Na in acetonitrile.	124
5.16: ORTEP plot of the cation $[\text{Ni}(\text{14-tmc})\text{OH}]^+$. Ellipsoids are drawn at 50 % probability level.	125
5.17: ORTEP plot of the full complex molecule of $\text{Na}[\text{Ni}_2(\text{14-tmc})_2(\text{OH})_2](\text{ClO}_4)_3$. Solvent molecules are omitted for clarity.	127
5.18: IR spectrum of the nickel(II)-hydroxo complex $[\text{Ni}(\text{14-tmc})\text{OH}]\text{ClO}_4$	128
5.19: IR spectrum of the complex $[\text{Ni}(\text{14-tmc})](\text{ClO}_4)_2$ after recrystallization in absolute ethanol and drying in vacuo at $80\text{ }^\circ\text{C}$	128
5.20: Scheme for the reaction of $\text{Ni}(\text{SO}_3\text{CF}_3)_2$ and 14-tmc.	129
5.21: IR spectrum of the complex $[\text{Ni}(\text{14-tmc})](\text{SO}_3\text{CF}_3)_2$	129
5.22: Reduction of $[\text{Ni}(\text{14-tmc})](\text{SO}_3\text{CF}_3)_2$ with NaHg in propionitrile.....	130
5.23: Color change in course of the reaction of $[\text{Ni}(\text{14-tmc})]\text{SO}_3\text{CF}_3$ and nitrous oxide in propionitrile at $-80\text{ }^\circ\text{C}$	130
5.24: UV-Vis spectra of $[\text{Ni}(\text{14-tmc})]\text{SO}_3\text{CF}_3$ (green) and $[\text{Ni}(\text{14-tmc})(\text{N}_2\text{O})]\text{SO}_3\text{CF}_3$ (brown) in propionitrile at $-80\text{ }^\circ\text{C}$	131
5.25: Scheme for the reaction of $[\text{Ni}(\text{14-tmc})]^{2+}$ and hydrogen peroxide in presence of triethylamine.	132
5.26: UV-Vis spectra of the reaction of $[\text{Ni}(\text{14-tmc})](\text{ClO}_4)_2$ and $\text{H}_2\text{O}_2/\text{Et}_3\text{N}$ in acetonitrile at different temperatures.	133
5.27: UV-Vis spectra of the reaction of $[\text{Ni}(\text{14-tmc})](\text{ClO}_4)_2$ and $\text{H}_2\text{O}_2/\text{Et}_3\text{N}$ in methanol at room temperature.....	134

5.28: UV-Vis spectra of the reaction of $[\text{Ni}(\text{14-tmc})](\text{ClO}_4)_2$ and Na_2O_2 in acetonitrile at room temperature.	135
5.29: Reaction scheme for the synthesis of 1,2-diaminoethane dihydrobromide (5.13).	136
5.30: Reaction scheme for the synthesis of 1,2-diaminoethane monohydrobromide (5.14).	136
5.31: Reaction scheme for the aldol condensation of acetone yielding 4-methylpent-3-en-2-one (5.15).	136
5.32: Michael addition of (5.14) and (5.15) to form trans-[14]-diene dihydrobromide dihydrate (5.16).	137
5.33: Reaction scheme for the reduction of 5.16 to tetA and tetB with sodium borohydride in methanol.	137
5.34: Reaction scheme for the synthesis of $[\text{Ni}(\text{tetB})](\text{ClO}_4)_2$	138
5.35: ORTEP plot of the cation $[\text{Ni}(\text{tetB})]^{2+}$. Ellipsoids are drawn at 50 % probability level.	138
5.36: UV-Vis spectra of the reaction of $[\text{Ni}(\text{tetB})](\text{ClO}_4)_2$ and $\text{H}_2\text{O}_2/\text{Et}_3\text{N}$ in methanol at different temperatures.	140
5.37: UV-Vis spectra of the reaction of $[\text{Ni}(\text{tetB})](\text{ClO}_4)_2$ and KO_2 in acetonitrile at room temperature.	141
6.1: Scheme for the reaction of $[\text{Ni}(\text{bipy})(\text{COD})]$ with the unsaturated ligands bcp, dcpa and dmbu.	147
6.2: ORTEP plot of $[\text{Ni}(\text{bipy})(\text{dcpa})]$, hydrogen atoms are omitted for clarity. Ellipsoids are drawn at 50 % probability level.	148
6.3: ORTEP plot of a fragment of the copper(I) chain $[\text{Cu}_2\text{Cl}_2](\text{CH}_3\text{CN})(\text{tctd})_n$. Ellipsoids are drawn at 50% probability level.	149
6.4: ORTEP plot of the binuclear complex $[\text{Ni}_2(\text{O-BPy})(\eta^2\text{-C}_4\text{H}_6)_2]$. Ellipsoids are drawn at 50% probability level.	149
6.5: Structures of the ligands 1,2-bis(2,2'-bipyridine-6-yl)ethane (O-BPy), <i>N,N'</i> -bis((6-methylpyridine-2-yl)methylene)butane-1,4-diamine (mpmbd) and <i>N,N'</i> -bis(pyridine-2-ylmethylene)butane-1,4-diamine (pmbd).	150
6.6: ORTEP plot of the complex $[\text{Ni}(\text{O-BPy})]$. Ellipsoids are drawn at 50 % probability level. Solvent molecules are omitted for clarity.	151
6.7: ORTEP plot of the cation $[\text{Cu}_2(\text{O-BPy})(\text{COD})_2]^{2+}$. Ellipsoids are drawn at 50 % probability level.	151

6.8: ORTEP plot of the full complex molecule of $\text{Na}[\text{Ni}_2(14\text{-tmc})_2(\text{OH})_2](\text{ClO}_4)_3$. Solvent molecules are omitted for clarity. Ellipsoids are drawn at 50 % probability level.	153
6.9: Schema der Reaktion von $[\text{Ni}(\text{bipy}(\text{COD}))]$ mit den ungesättigten Liganden bcp, dcpa und dmbu.	154
6.10: Molekülstruktur des Komplexes $[\text{Ni}(\text{bipy})(\text{dcpa})]$. Ellipsoide mit 50 % Aufenthaltswahrscheinlichkeit.	155
6.11: Molekülstruktur eines Fragments des Kupfer(I)-Koordinations-polymers $[\text{Cu}_2\text{Cl}_2](\text{CH}_3\text{CN})(\text{tctd})_n$. Ellipsoide mit 50 % Aufenthaltswahrscheinlichkeit.	156
6.12: Molekülstruktur des dimeren Komplexes $[\text{Ni}_2(\text{O-BPy})(\eta^2\text{-C}_4\text{H}_6)_2]$. Ellipsoide mit 50 % Aufenthaltswahrscheinlichkeit.	156
6.13: Strukturen der Liganden 1,2-Bis(2,2'-bipyridin-6-yl)ethan (O-BPy), <i>N,N</i> -Bis((6-methylpyridin-2-yl)methylen)butan-1,4-diamin (mpmbd) und <i>N,N'</i> -Bis(pyridin-2-ylmethylen)butan-1,4-diamin (pmbd).	157
6.14: Molekülstruktur des einkernigen Komplexes $[\text{Ni}(\text{O-BPy})]$. Ellipsoide mit 50 % Aufenthaltswahrscheinlichkeit.	158
6.15: Molekülstruktur des Kations $[\text{Cu}_2(\text{O-BPy})(\text{COD})_2]^{2+}$. Ellipsoide mit 50 % Aufenthaltswahrscheinlichkeit.	158
6.16: Molekülstruktur des Komplexes $\text{Na}[\text{Ni}_2(14\text{-tmc})_2(\text{OH})_2](\text{ClO}_4)_3$. Ellipsoide mit 50 % Aufenthaltswahrscheinlichkeit. Lösungsmittelmoleküle wurden zur besseren Übersicht weggelassen.	160

8 List of Tables

1.1: Reaction of 1,3-butadiene with nickel acetylacetonate and Al(OEt)Et ₂ ; control of oligomerization using R ₃ P ligands. Conditions: 30 °C, 5 bar.	8
1.2: Nickel-containing enzymes.	15
2.1: Activation parameters for the reaction of [Ni(bipy)(COD)] with bcp.	36
2.2: Activation parameters and reaction rate constants for the formation of [Ni(bipy)(bcp)] and [Ni(bipy)(L ₁)].	38
2.3: Measured reaction rates of the reaction of [Ni(bipy)(COD)] with dmbu in THF; [Ni(bipy)(COD)] = 0.25 mM.	41
2.4: Second-order reaction rate constants of the reaction of [Ni(bipy)(COD)] with dmbu in THF.	43
2.5: Activation parameters for the reaction of [Ni(bipy)(COD)] with dmbu.	44
2.6: Activation parameters and reaction rate constants for the formation of [Ni(bipy)(bcp)] and [Ni(bipy)(dmbu)].	44
3.1: Crystal data and structure refinement for [Cu ₂ Cl ₂ (CH ₃ CN)(tctd)].	55
3.2: Selected bond lengths [Å] and angles [°] for [Cu ₂ Cl ₂ (CH ₃ CN)(tctd)].	56
4.1: Ligands used in the synthesis of Ni(0) complexes.	66
4.2: Crystal data and structure refinement for O-BPy.	68
4.3: Selected bond lengths [Å] and angles [°] for O-BPy.	69
4.4: Crystal data and structure refinement for mpmbd.	70
4.5: Selected bond lengths [Å] and angles [°] for mpmbd.	71
4.6: Crystal data and structure refinement for pmbd.	73
4.7: Selected bond lengths [Å] and angles [°] for pmbd.	74
4.8: Crystal data and structure refinement for [Ni(O-BPy)].	76
4.9: Selected bond lengths [Å] and angles [°] for [Ni(O-BPy)].	77
4.10: Crystal data and structure refinement for [Ni(pmbd)].	80
4.11: Selected bond lengths [Å] and angles [°] for [Ni(pmbd)].	80
4.12: Crystal data and structure refinement for [Ni(mpmbd)].	82
4.13: Selected bond lengths [Å] and angles [°] for [Ni(mpmbd)].	83
4.14: Crystal data and structure refinement for [Cu(COD) ₂]ClO ₄	87
4.15: Selected bond lengths [Å] and angles [°] for [Cu(COD) ₂]ClO ₄	88
4.16: Crystal data and structure refinement for [Cu ₂ (O-BPy) ₂](BF ₄) ₂	90

4.17: Selected bond lengths [\AA] and angles [$^\circ$] for $[\text{Cu}_2(\text{O-BPy})_2](\text{BF}_4)_2$	91
4.18: Crystal data and structure refinement for $[\text{Cu}(\text{O-BPy})](\text{BF}_4)_2$	92
4.19: Selected bond lengths [\AA] and angles [$^\circ$] for $[\text{Cu}(\text{O-BPy})](\text{BF}_4)_2$	93
4.20: Crystal data and structure refinement for $[\text{Cu}_2(\text{O-BPy})(\text{COD})_2](\text{SO}_3\text{CF}_3)_2$	95
4.21: Selected bond lengths [\AA] and angles [$^\circ$] for $[\text{Cu}_2(\text{O-BPy})(\text{COD})_2](\text{SO}_3\text{CF}_3)_2$	96
4.22: IR data for $[\text{Cu}_2(\text{O-BPy})(\text{C}_4\text{H}_6)_2](\text{SO}_3\text{CF}_3)_2$ and $[\text{Cu}_2(\text{O-BPy})(\text{COD})_2](\text{SO}_3\text{CF}_3)_2$	98
5.1: Crystal data and structure refinement for $[\text{Ni}(14\text{-tmc})](\text{ClO}_4)_2$	117
5.2: Selected bond lengths [\AA] and angles [$^\circ$] for $[\text{Ni}(14\text{-tmc})](\text{ClO}_4)_2$	117
5.3: Crystal data and structure refinement for $[\text{Ni}(14\text{-tmc})(\text{MeCN})_2](\text{ClO}_4)_2$. ..	119
5.4: Selected bond lengths [\AA] and angles [$^\circ$] for $[\text{Ni}(14\text{-tmc})(\text{MeCN})_2](\text{ClO}_4)_2$. ..	119
5.5: Crystal data and structure refinement for $[\text{Na}(14\text{-tmc})](\text{ClO}_4)$	122
5.6: Selected bond lengths [\AA] and angles [$^\circ$] for $[\text{Na}(14\text{-tmc})](\text{ClO}_4)$	123
5.7: Crystal data and structure refinement for $\text{Na}[\text{Ni}_2(14\text{-tmc})_2(\text{OH})_2](\text{ClO}_4)_3$. ..	125
5.8: Selected bond lengths [\AA] and angles [$^\circ$] for $\text{Na}[\text{Ni}_2(14\text{-tmc})_2(\text{OH})_2](\text{ClO}_4)_3$	126
5.9: Crystal data and structure refinement for $[\text{Ni}(\text{tetB})](\text{ClO}_4)_2$	139
5.10: Selected bond lengths [\AA] and angles [$^\circ$] for $[\text{Ni}(\text{tetB})](\text{ClO}_4)_2$	139

9 Bibliography

- (1) Hollemann, A. F.; Wiberg, E. *Lehrbuch der Anorganischen Chemie*; 102nd ed.; Verlag de Gruyter: Berlin, 2007.
- (2) Kindler, J. M.; Gliech, M. Rutherford - Lexikon der Elemente, Internet-Edition <http://uniterra.de/>.
- (3) Diether, D.; Leonardus; Gerstenberg, A.; Lavinsky, R. <http://www.mineralienatlas.de> **2012**.
- (4) Riedel, E. *Allgemeine und Anorganische Chemie*; 10th ed.; de Gruyter: Berlin, New York, 2010.
- (5) Kuck, P. H. *US Geol. Surv.* **2012**, 108–109.
- (6) Keim, W. *Angew. Chemie* **1990**, 102, 251–260.
- (7) Cornils, B.; Hermann, W. A. *Applied Homogeneous Catalysis with Organometallic Compounds*; Vol. 1.; Wiley-VCH: Weinheim, New York, 2002.
- (8) Jolly, P.; Wilke, G. *The Organic Chemistry of Nickel*; Vol. 1 & 2.; Academic Press: New York, London, 1974.
- (9) Tamaru, Y. *Modern Organonickel Chemistry*; Wiley-VCH: Weinheim, 2005.
- (10) Yamaguchi, J.; Muto, K.; Itami, K. *European J. Org. Chem.* **2013**, 2013, 19–30.
- (11) Rosen, B. M.; Quasdorf, K. W.; Wilson, D. a; Zhang, N.; Resmerita, A.-M.; Garg, N. K.; Percec, V. *Chem. Rev.* **2011**, 111, 1346–1416.
- (12) Montgomery, J. *Angew. Chemie* **2004**, 116, 3980–3998.
- (13) Ikeda, S. *Angew. Chemie* **2003**, 115, 5276–5278.
- (14) Zhang, Y.; Riduan, S. N. *Angew. Chemie* **2011**, 123, 6334–6336.
- (15) Cokoja, M.; Bruckmeier, C.; Rieger, B.; Herrmann, W. a.; Kühn, F. E. *Angew. Chemie* **2011**, 123, 8662–8690.

- (16) Schleyer, P. v. R.; Williams, J. E.; Blanchard, K. R. *J. Am. Chem. Soc.* **1970**, *92*, 2377–2386.
- (17) Binger, P.; Schroth, G.; McMeeking, J. *Angew. Chemie* **1974**, *86*, 518–519.
- (18) Binger, P.; McMeeking, J.; Schäfer, H. *Chem. Ber.* **1984**, *117*, 1551–1560.
- (19) Weiß, H.; Hampel, F.; Donaubauer, W.; Grundl, M. A.; Bats, J. W.; Hashmi, A. S. K.; Schindler, S. *Organometallics* **2001**, *20*, 1713–1715.
- (20) Isaeva, L. S.; Peganova, T. A.; Petrovskii, P. V.; Kravtsov, D. N. *J. Organomet. Chem.* **1989**, *376*, 141–148.
- (21) Binger, P.; Doyle, M. J.; McMeeking, J.; Krüger, C. *J. Organomet. Chem.* **1977**, *135*, 405–414.
- (22) Binger, P.; Doyle, M. J. *J. Organomet. Chem.* **1978**, *162*, 195–207.
- (23) Binger, P.; Biedenbach, B. *Chem. Ber.* **1987**, *120*, 601–605.
- (24) Binger, P.; Schuchardt, U. *Chem. Ber.* **1981**, *114*, 3313–3324.
- (25) Binger, P.; Schuchardt, J.; McMeeking, J. *Chem. Ber.* **1980**, *113*, 2372–2382.
- (26) Reed, H. W. B. *J. Chem. Soc.* **1954**, 1931–1941.
- (27) Wilke, G. *Angew. Chemie* **1988**, *1*, 189–211.
- (28) Wilke, G. *Angew. Chemie* **1963**, *75*, 10–20.
- (29) Wilke, G. *J. Organomet. Chem.* **1980**, *200*, 349–364.
- (30) Wilke, G.; Jolly, P. W.; Tkatchenko, I. *Angew. Chemie* **1971**, *83*, 329.
- (31) Benn, R.; Buessemeier, B.; Holle, S.; Jolly, P. W.; Mynott, R.; Tkatchenko, I.; Wilke, G. *J. Organomet. Chem.* **1985**, *279*, 63–86.
- (32) Henc, B.; Jolly, P. W.; Salz, R.; Wilke, G.; Benn, R.; Hoffmann, E. G.; Schroth, G.; Seevogel, K.; Al., E. *J. Organomet. Chem.* **1980**, *191*, 425–448.
- (33) Tobisch, S.; Ziegler, T. *J. Am. Chem. Soc.* **2002**, *124*, 4881–4893.

- (34) Tobisch, S.; Ziegler, T. *J. Am. Chem. Soc.* **2002**, *124*, 13290–13301.
- (35) Brenner, W.; Heimbach, P.; Hey, H.; Mueller, E. W.; Wilke, G. *Liebigs Ann. Chem.* **1969**, *727*, 161–182.
- (36) <http://www.vestamid.de/product/vestamid/en/products-services/product-overview/pages/default.aspx>.
- (37) <http://c8-ings.evonik.com/sites/dc/Downloadcenter/Evonik/Product/C8-Rings/en/Buildingblocks.pdf>.
- (38) Markert, T. Monocyclic aldehydes obtained by hydroformylation of (di)-methyl-cyclooct(adi)enes used as perfumes or perfume boosters, <http://www.google.es/patents/DE19817043A1?cl=en>, 1999.
- (39) Reppe, W.; Sweckendiek, W. *J. Ann.* **1948**, 104–116.
- (40) Reppe, W.; Schichting, O.; Klager, K.; Toepel, T. *Ann.* **1948**, *560*, 1–92.
- (41) Wilke, G. *Pure Appl. Chem.* **1978**, *50*, 677–690.
- (42) Gausing, W.; Wilke, G. *Angew. Chemie* **1978**, *90*, 380.
- (43) Geibel, W.; Wilke, G.; Goddard, R.; Krüger, C.; Meynott, R. **1978**, *160*, 139–147.
- (44) Bogdanovic, B.; Kroner, M.; Wilke, G. *Ann.* **1966**, *397*, 1–23.
- (45) Wilke, G. *Angew. Chemie* **1960**, *72*, 581–582.
- (46) Eisch, J. J.; Ma, X.; Han, K. I.; Gitua, J. N.; Krüger, C. **2001**, 77–88.
- (47) Correa, A.; León, T.; Martin, R. *J. Am. Chem. Soc.* **2014**, *136*, 1062–1069.
- (48) Dedieu, A.; Ingold, F. **1989**, *28*, 1694–1695.
- (49) Jegat, C.; Fouassier, M.; Tranquille, M.; Mascetti, J.; Tommasi, I.; Aresta, M.; Ingold, F.; Dedieu, A. *Inorg. Chem.* **1993**, *32*, 1279–1289.
- (50) Aresta, M.; Nobile, C. F.; Albano, V. G.; Forni, E.; Massanero, M. **1975**, 636–637.

- (51) Behr, A. *Carbon Dioxide Activation by Metal Complexes*; VCH: Weinheim, 1988.
- (52) Halmann, M. *Chemical Fixation of Carbon Dioxide*; CRC Press: Boca Raton, 1993.
- (53) *Catalytic Activation of Carbon Dioxide*; Ayers, W., Ed.; ACS Symposium Series 363, 1988.
- (54) Walther, D. *Coord. Chem. Rev.* **1987**, *79*, 135–174.
- (55) Leitner, W. *Coord. Chem. Rev.* **1996**, *153*, 257–284.
- (56) Walther, D. *Nachr. Chem. Tech. Öab.* **1992**, *40*, 1214.
- (57) Walther, D.; Dinjus, E.; Görls, H. *J. Organomet. Chem.* **1985**, *286*, 103–114.
- (58) Hoberg, H.; Peres, Y.; Milchereit, A.; Gross, S. *J. Organomet. Chem.* **1988**, *345*, c17–19.
- (59) Takimoto, M.; Mori, M. *J. Am. Chem. Soc.* **2001**, *123*, 2895–2896.
- (60) Takimoto, M.; Mori, M. *J. Am. Chem. Soc.* **2002**, *124*, 10008–10009.
- (61) Walther, D.; Dinjus, E. *Z. Chem.* **1982**, *22*, 228.
- (62) Walther, D.; Dinjus, E. *Z. Chem.* **1984**, *24*, 63.
- (63) Hoberg, H.; Apotecher, B. *J. Organomet. Chem.* **1984**, *270*, c15–17.
- (64) Hoberg, H.; Schaefer, D.; Oster, B. W. *J. Organomet. Chem.* **1984**, *266*, 313–320.
- (65) Dzhemilev, U. M.; Kunakova, R. V.; Sidorova, V. V. *Bull Acad. Sci. USSR Div. Chem. Sci.* **1985**, *34*, 2102–2106.
- (66) Hoberg, H.; Peres, Y.; Milchereit, A. *J. Organomet. Chem.* **1986**, *307*, c41–43.
- (67) Hoberg, H.; Groß, S.; Milchereit, A. *Angew. Chemie* **1987**, *99*, 567–569.
- (68) Dixon, N. E.; Gazzola, C.; Watters, J. J.; Blakeley, R. L.; Zerner, B. *J. Am. Chem. Soc.* **1975**, *97*, 4131–4133.

- (69) Blakeley, R. L.; Zerner, B. *J. Mol. Catal.* **1984**, *23*, 263–292.
- (70) Karplus, P. A.; Pearson, M. a.; Hausinger, R. P. *Acc. Chem. Res.* **1997**, *30*, 330–337.
- (71) Albracht, S. P. *Biochim. Biophys. Acta* **1994**, *1188*, 167–204.
- (72) Huynh, B. H.; Czechowski, M. H.; Krüger, H. J.; DerVartanian, D. V; Peck, H. D.; LeGall, J. *Proc. Natl. Acad. Sci. U. S. A.* **1984**, *81*, 3728–3732.
- (73) Evans, D. J.; Pickett, C. J. *Chem. Soc. Rev.* **2003**, *32*, 268.
- (74) Volbeda, A.; Fontecilla-camps, J. C. *Dalt. Trans.* **2003**, 4030–4038.
- (75) Ermler, U.; Grabarse, W.; Shima, S.; Goubeaud, M.; Thauer, R. K. *Science* **1997**, *278*, 1457–1462.
- (76) Holliger, C.; Pierik, A. J.; Reijerse, E. J.; Hagen, W. R. *J. Am. Chem. Soc.* **1993**, *115*, 5651–5656.
- (77) Won, H.; Olson, K. D.; Michael, F.; Wolfe, R. S. *Comments Inorg. Chem.* **1993**, *15*, 1–26.
- (78) Stavropoulos, P.; Muetterties, M. C.; Carrie, M.; Holm, R. H. *J. Am. Chem. Soc.* **1991**, *113*, 8485–8492.
- (79) Shin, W.; Anderson, M. E.; Lindahl, P. A. *J. Am. Chem. Soc.* **1993**, *115*, 5522–5526.
- (80) Qiu, D.; Kumar, M.; Ragsdale, S. W.; Spiro, T. G. *Science* **1994**, *264*, 817–819.
- (81) Ito, M.; Kotera, M.; Matsumoto, T.; Tatsumi, K. *Proc. Natl. Acad. Sci. U. S. A.* **2009**, *106*, 11862–11866.
- (82) Kim, F. J.; Kim, H. P.; Hah, Y. C.; Roe, J. H. *Eur. J. Biochem.* **1996**, *241*, 178–185.
- (83) Choudhury, S. B.; Lee, J. W.; Davidson, G.; Yim, Y. I.; Bose, K.; Sharma, M. L.; Kang, S. O.; Cabelli, D. E.; Maroney, M. J. *Biochemistry* **1999**, *38*, 3744–3752.

- (84) Palenik, B.; Brahamsha, B.; Larimer, F. W.; Land, M.; Hauser, L.; Chain, P.; Lamerdin, J.; Regala, W.; Allen, E. E.; McCarren, J.; Paulsen, I.; Dufresne, A.; Partensky, F.; Webb, E. A.; Waterbury, J. *Nature* **2003**, *424*, 1037–1042.
- (85) Barondeau, D. P.; Kassmann, C. J.; Bruns, C. K.; Tainer, J. a; Getzoff, E. D. *Biochemistry* **2004**, *43*, 8038–8047.
- (86) Dai, Y.; Wensink, P. C.; Abeles, R. H. *J. Biol. Chem.* **1999**, *274*, 1193–1195.
- (87) Pochapsky, T. C.; Ju, T.; Dang, M.; Beaulieu, R.; Pagani, G. M.; OuYang, B. In *Nickel and Its Surprising Impact in Nature*; John Wiley & Sons, Ltd, 2007; pp. 473–500.
- (88) Szajna-Fuller, E.; Rudzka, K.; Arif, A. M.; Berreau, L. M. *Inorg. Chem.* **2007**, *46*, 5499–5507.
- (89) Mulrooney, S. B.; Hausinger, R. P. *FEMS Microbiol. Rev.* **2003**, *27*, 239–261.
- (90) Clugston, S. L.; Barnard, J. F.; Kinach, R.; Miedema, D.; Ruman, R.; Daub, E.; Honek, J. F. *Biochemistry* **1998**, *37*, 8754–8763.
- (91) Clugston, S. L.; Honek, J. F. *J. Mol. Evol.* **2000**, *50*, 491–495.
- (92) Berkessel, A. *Bioorg. Chem.* **1991**, *19*, 101–115.
- (93) Ellefson, W. L.; Wolfe, R. S. *J. Biol. Chem.* **1981**, *256*, 4259–4262.
- (94) Pfaltz, A.; Jaun, B.; Fassler, A.; Eschenmoser, A.; Jaenchen, R.; Gilles, H. H.; Diekert, G.; Thauer, R. K. *Helv. Chim. Acta* **1982**, *65*, 828–865.
- (95) Färber, G.; Keller, W.; Kratky, C.; Jaun, B.; Pfaltz, A.; Spinner, C.; Kobelt, A.; Eschenmoser, A. *Helv. Chim. Acta* **1991**, *74*, 697–716.
- (96) Jaun, B.; Pfaltz, A. *Chem. Commun.* **1986**, 1327–1329.
- (97) Capozzi, G.; Modena, G. In *The Thiol Group (1974)*; John Wiley & Sons, Ltd., 1974; pp. 785–839.
- (98) Stricks, W.; Frischmann, J. K.; Mueller, R. G. *J. Electrochem. Soc.* **1962**, *109*, 518.

- (99) Ragsdale, S. W. *J. Biol. Chem.* **2009**, *284*, 18571–18575.
- (100) Maroney, M. J. *Curr. Opin. Chem. Biol.* **1999**, *3*, 188–199.
- (101) Beyer, W.; Imlay, J.; Fridovich, I. *Prog. Nucleic Acid Res. Mol. Biol.* **1991**, *40*, 221–253.
- (102) Wallace, D. C. *Science* **1992**, *256*, 628–632.
- (103) Halliwell, B. In *Active Oxygen in Biochemistry SE - 7*; Valentine, J.; Foote, C.; Greenberg, A.; Liebman, J., Eds.; Structure Energetics and Reactivity in Chemistry Series (SEARCH series); Springer Netherlands: New York, 1995; Vol. 3, pp. 313–335.
- (104) McCord, J. M.; Fridovich, I. *J. Biol. Chem.* **1969**, *244*, 6049–6055.
- (105) McCord, J. M.; Keele, B. B.; Fridovich, I. *Proc. Natl. Acad. Sci. U. S. A.* **1971**, *68*, 1024–1027.
- (106) Tainer, J. A.; Getzoff, E. D.; Richardson, J. S.; Richardson, D. C. *Nature* **1983**, *306*, 284–287.
- (107) Youn, H. D.; Kim, E. J.; Roe, J. H.; Hah, Y. C.; Kang, S. O. *Biochem. J.* **1996**, *318*, 889–896.
- (108) Youn, H.; Youn, H.; Lee, J.; Yim, Y.; Lee, J. K.; Hah, Y. C.; Kang, S. *Arch. Biochem. Biophys.* **1996**, *334*, 341–348.
- (109) Eitinger, T. *J. Bacteriol.* **2004**, *186*, 7821–7825.
- (110) Methé, B. a; Nelson, K. E.; Deming, J. W.; Momen, B.; Melamud, E.; Zhang, X.; Moulton, J.; Madupu, R.; Nelson, W. C.; Dodson, R. J.; Brinkac, L. M.; Daugherty, S. C.; Durkin, A. S.; DeBoy, R. T.; Kolonay, J. F.; Sullivan, S. a; Zhou, L.; Davidsen, T. M.; Wu, M.; Huston, A. L.; Lewis, M.; Weaver, B.; Weidman, J. F.; Khouri, H.; Utterback, T. R.; Feldblyum, T. V; Fraser, C. M. *Proc. Natl. Acad. Sci. U. S. A.* **2005**, *102*, 10913–10918.
- (111) Dupont, C. L.; Neupane, K.; Shearer, J.; Palenik, B. *Environ. Microbiol.* **2008**, *10*, 1831–1843.
- (112) Wuerges, J.; Lee, J.-W.; Yim, Y.-I.; Yim, H.-S.; Kang, S.-O.; Djinnovic Carugo, K. *Proc. Natl. Acad. Sci. U. S. A.* **2004**, *101*, 8569–8574.

- (113) Szilagy, R. K.; Bryngelson, P. a; Maroney, M. J.; Hedman, B.; Hodgson, K. O.; Solomon, E. I. *J. Am. Chem. Soc.* **2004**, *126*, 3018–3019.
- (114) Fiedler, A. T.; Bryngelson, P. a; Maroney, M. J.; Brunold, T. C. *J. Am. Chem. Soc.* **2005**, *127*, 5449–5462.
- (115) Bryngelson, P. A.; Arobo, S. E.; Pinkham, J. L.; Cabelli, D. E.; Maroney, M. J. *J. Am. Chem. Soc.* **2004**, *126*, 460–461.
- (116) Meunier, B. *Biomimetic Oxidations Catalyzed by Transition Metal Complexes*; Imperial College Press: London, 2000.
- (117) Collman, J. P. *Inorg. Chem.* **1997**, *4*, 5145–5155.
- (118) Momenteau, M.; Reed, C. a. *Chem. Rev.* **1994**, *94*, 659–698.
- (119) Kim, E.; Helton, M. E.; Wasser, I. M.; Karlin, K. D.; Lu, S.; Huang, H.; Incarvito, C. D.; Rheingold, A. L.; Honecker, M.; Kaderli, S.; Zuberbu, A. D. *Proc. Natl. Acad. Sci. U. S. A.* **2003**, *100*, 3623–3628.
- (120) Decker, A.; Solomon, E. I. *Curr. Opin. Chem. Biol.* **2005**, *9*, 152–163.
- (121) Limberg, C. *Angew. Chemie* **2003**, *115*, 6112–6136.
- (122) Chemie, N.; Piera, J.; Bäckvall, J. *Angew. Chemie* **2008**, *120*, 3558–3576.
- (123) Suzuki, M. *Acc. Chem. Res.* **2007**, *40*, 609–617.
- (124) Yao, S.; Driess, M. *Acc. Chem. Res.* **2012**, *45*, 276–287.
- (125) Cramer, C. J.; Tolman, W. B. *Acc. Chem. Res.* **2007**, *40*, 601–608.
- (126) Yao, S.; Bill, E.; Milsman, C.; Wieghardt, K.; Driess, M. *Angew. Chemie* **2008**, *120*, 7218–7221.
- (127) Hikichi, S.; Yoshizawa, M.; Sasakura, Y.; Akita, M.; Moro-oka, Y. *J. Am. Chem. Soc.* **1998**, *120*, 10567–10568.
- (128) Kieber-Emmons, M. T.; Riordan, C. G. *Acc. Chem. Res.* **2007**, *40*, 618–625.
- (129) Shiren, K.; Ogo, S.; Fujinami, S.; Hayashi, H.; Suzuki, M.; Uehara, A.; Watanabe, Y.; Moro-oka, Y. *J. Am. Chem. Soc.* **2000**, *122*, 254–262.

- (130) Cho, J.; Furutachi, H.; Fujinami, S.; Suzuki, M. *Angew. Chemie* **2004**, *116*, 3362–3365.
- (131) Brown, E. J.; Duhme-Klair, A.-K.; Elliott, M. I.; Thomas-Oates, J. E.; Timmins, P. L.; Walton, P. H. *Angew. Chemie* **2005**, *117*, 1416–1419.
- (132) Wilke, G.; Schott, H.; Heimbach, P. *Angew. Chemie* **1967**, *79*, 62.
- (133) Otsuka, S.; Nakamura, A.; Tatsuno, Y. *J. Am. Chem. Soc.* **1969**, *191*, 6994–6999.
- (134) Matsumoto, M.; Nakatsu, K. *Acta Crystallogr.* **1975**, *B31*, 2711–2713.
- (135) Fujita, K.; Schenker, R.; Gu, W.; Brunold, T. C.; Cramer, S. P.; Riordan, C. G. *Inorg. Chem.* **2004**, *43*, 3324–3326.
- (136) Cho, J.; Sarangi, R.; Annaraj, J.; Kim, S. Y.; Kubo, M.; Ogura, T.; Solomon, E. I.; Nam, W. *Nat. Chem.* **2009**, *1*, 568–572.
- (137) Kieber-Emmons, M. T.; Annaraj, J.; Seo, M. S.; Van Heuvelen, K. M.; Tosha, T.; Kitagawa, T.; Brunold, T. C.; Nam, W.; Riordan, C. G. *J. Am. Chem. Soc.* **2006**, *128*, 14230–14231.
- (138) Geyer, C.; Dinjus, E.; Schindler, S. *Organometallics* **1998**, *17*, 98–103.
- (139) Geyer, C.; Schindler, S. *Organometallics* **1998**, *17*, 4400–4405.
- (140) Weiß, H. *Kinetische Untersuchungen der Reaktionen von Ni(0)-Komplexen mit ungesättigten Substraten*; Dissertation, Friedrich-Alexander-Universität Erlangen-Nürnberg, 2001.
- (141) Leibold, M. *Untersuchungen zur chemischen und elektronischen Kopplung von Kohlendioxid und Butadien an niedervalenten Nickel-Komplexen*; Dissertation, Friedrich-Alexander-Universität Erlangen-Nürnberg, 2003.
- (142) Römmling, L. *Untersuchungen zur Reaktivität von Ni(0)-Komplexen*; Diploma thesis, Justus-Liebig-Universität Giessen, 2005.
- (143) Henß, A. *Investigations on the reaction behaviour of copper and nickel complexes with N-Donor or olefin ligands*; Dissertation, Justus-Liebig-Universität Giessen, 2008.
- (144) Cho, J.; Sarangi, R.; Nam, W. *Acc. Chem. Res.* **2012**, *45*, 1321–1330.

- (145) Tolman, W. B. *Angew. Chemie* **2010**, *122*, 1034–1041.
- (146) Meijere, A. De; Kozhushkov, S. I.; Spaeth, T.; Zefirov, N. *J. Org. Chem.* **1993**, *58*, 502–505.
- (147) Kobrich, G.; Merkeli, D.; Thiem, K. W. *Chem. Ber.* **1972**, *105*, 1683–1693.
- (148) De Meijere, A.; Kozhushkov, S. I. *European J. Org. Chem.* **2000**, *2000*, 3809–3822.
- (149) Meijere, A. De; Kozhushkov, S. I.; Späth, T.; Seebach, M. Von; Löhr, S.; Nüske, H.; Pohlmann, T.; Es-Sayed, M.; Bräse, S. *Pure Appl. Chem.* **2000**, *72*, 1745–1756.
- (150) Binger, P.; Wedemann, P.; Kozhushkov, S. I.; Meijere, A. De. *European J. Org. Chem.* **1998**, 113–119.
- (151) De Meijere, A.; Kozhushkov, S. I.; Schill, H. *Chem. Rev.* **2006**, *106*, 4926–4996.
- (152) Emme, I.; Labahn, T.; de Meijere, A. *European J. Org. Chem.* **2006**, 399–404.
- (153) De Meijere, A.; Redlich, S.; Frank, D.; Magull, J.; Hofmeister, A.; Menzel, H.; König, B.; Svoboda, J. *Angew. Chemie* **2007**, *119*, 4658–4660.
- (154) Zhao, L.; de Meijere, A. *Adv. Synth. Catal.* **2006**, *348*, 2484–2492.
- (155) Foerstner, J.; Kozhushkov, S.; Binger, P.; Wedemann, P.; Noltemeyer, M.; Meijere, A. De; Butenschön, H. *Chem. Commun.* **1998**, 239–240.
- (156) Kozhushkov, S. I.; Foerstner, J.; Kakoschke, A.; Stellfeldt, D.; Yong, L.; Wartchow, R.; de Meijere, A.; Butenschön, H. *Chem. Eur. J.* **2006**, *12*, 5642–5647.
- (157) Hoyte, S. A. Platinum Complexes of Bicyclopropylidene and Related Ligands, Dissertation, Victory University of Wellington, 2014.
- (158) Keim, W.; Kowaldt, F. H.; Goddard, R.; Kruger, C. *Angew. Chemie* **1978**, *90*, 493.
- (159) Rappé, A. K.; Casewit, C. J.; Colwell, K. S.; III, W. A. G.; Skiff, W. M. *J. Am. Chem. Soc.* **1992**, *114*, 10024–10035.

- (160) Johnston, R.; Basolo, F.; Pearson, R. G. *Inorg. Chem.* **1971**, *10*, 247–251.
- (161) Yamamoto, T.; Yamamoto, A.; Ikeda, S. *J. Am. Chem. Soc.* **1971**, 3360–3364.
- (162) Thompson, J. S.; Whitney, J. F. *Inorg. Chem.* **1984**, *23*, 2813–2819.
- (163) Thompson, J. S.; Swiatek, R. M. *Inorg. Chem.* **1985**, *24*, 110–113.
- (164) Thompson, J. S.; Whitney, J. F. *J. Am. Chem. Soc.* **1983**, *105*, 5488–5490.
- (165) Thompson, J. S.; Harlow, R. L.; Whitney, J. F. *J. Am. Chem. Soc.* **1983**, *105*, 3522–3527.
- (166) Hideki, M.; Yamamoto, N.; Taga, T.; Machida, K. *J. Organomet. Chem.* **1987**, *322*, 121–129.
- (167) Munakata, M.; Kitagawa, S.; Kosome, S.; Asahara, A. *Inorg. Chem.* **1986**, *25*, 2622–2627.
- (168) Dakkouri, M.; Typke, V.; Bitschenauer, R. *Mol. Struct.* **1995**, *355*, 239–263.
- (169) Weitzer, M.; Schatz, M.; Hampel, F.; Heinemann, F. W.; Schindler, S. *J. Chem. Soc. Dalton Trans.* **2002**, 686–694.
- (170) Wu, A. www.freepatentsonline.com. Pat. - No. 5130458, 1992.
- (171) Mori, H.; Ikeda, K.; Nayaoka, I.; Hirayanagi, S.; Ikeyama, M.; Kiki, A. *Chem. Abstr.* **1971**, *74*, 3729.
- (172) Schwertfeger, H.; Fokin, A. a; Schreiner, P. R. *Angew. Chemie* **2008**, *120*, 1038–1053.
- (173) Fokina, N. a.; Tkachenko, B. a.; Merz, A.; Serafin, M.; Dahl, J. E. P.; Carlson, R. M. K.; Fokin, A. a; Schreiner, P. R. *European J. Org. Chem.* **2007**, *2007*, 4738–4745.
- (174) Landa, S.; Machacek, V. *Collect. Czech. Chem. Commun.* **1933**, *5*, 1–5.
- (175) Krishnamurthy, V. V; Shih, J. G.; Olah, G. A. *J. Org. Chem.* **1985**, *50*, 3005–3006.

- (176) Courtney, T.; Johnston, D. E.; McKervey, M. A.; Rooney, J. J. *J. Chem. Soc. Perkin Trans.* **1972**, *1*, 2691–2696.
- (177) Grund, T. M.; Schleyer, P. v. R. *Tetrahedron Lett.* **1973**, *22*, 1959–1962.
- (178) Munakata, M.; Kitagawa, S.; Shimono, H.; Hideki, M. *Inorg. Chem.* **1991**, *30*, 2610–2614.
- (179) Sheldrick, G. M. *Acta Crystallogr. Sect. A* **2008**, *64*, 112–122.
- (180) Dinjus, E.; Walther, D. *J. Organomet. Chem.* **1982**, *236*, 123–130.
- (181) Garber, T.; Van Wallendaël, S.; Rillema, D. P.; Kirk, M.; Hatfield, W. E.; Welch, J. H.; Singh, P. *Inorg. Chem.* **1990**, *29*, 2863–2868.
- (182) Mayer, W.; Wilke, G.; Benn, R.; Goddard, R.; Krüger, C. *Monatshefte für Chemie* **1985**, *116*, 879–888.
- (183) Holthausen, M. *Unpublished results*.
- (184) Seddon, E. J.; Yoo, J.; Folting, K.; Huffman, J. C.; Hendrickson, D. N.; Christou, G. *J. Chem. Soc. Dalt. Trans.* **2000**, *2*, 3640–3648.
- (185) Karmakar, T. K.; Aromí, G.; Ghosh, B. K.; Usman, a.; Fun, H.-K.; Mallah, T.; Behrens, U.; Solans, X.; Chandra, S. K. *J. Mater. Chem.* **2006**, *16*, 278.
- (186) Grant, C. M.; Stamper, B. J.; Knapp, M. J.; Folting, K.; Huffman, J. C.; Hendrickson, D. N.; Christou, G. *J. Chem. Soc. Dalt. Trans.* **1999**, 3399–3405.
- (187) Masood, M. A.; Sullivan, B. P.; Hodgson, D. J. *Inorg. Chem.* **1994**, *33*, 4611–4612.
- (188) Youinou, M.-T.; Ziessel, R.; Lehn, J.-M. *Inorg. Chem.* **1991**, *30*, 2144–2148.
- (189) Yao, Y.; Perkovic, M. W.; Rillema, D. P.; Woods, C. *Inorg. Chem.* **1992**, *31*, 3956–3962.
- (190) Lehn, J.; Ziessel, R. *Helv. Chim. Acta* **1988**, *71*, 1511–1516.
- (191) Dierks, H.; Dietrich, H. Z. *Z. Krist.* **1965**, *122*, 1–23.

- (192) Albinati, A.; Meille, S. V.; Carturan, G. *J. Organomet. Chem.* **1979**, *182*, 269–274.
- (193) Howard, J. A. K. *Acta Crystallogr. Sect. B* **1982**, *38*, 2896–2898.
- (194) Hamalainen, R.; Ahlgren, M.; Turpeinen, U.; Raikas, T. *Cryst. Struct. Commun.* **1979**, *8*, 75–80.
- (195) Burke, P. J.; Mcmillin, D. R.; Robinson, W. R. *Inorg. Chem.* **1980**, *19*, 1211–1214.
- (196) Healy, P. C.; Engelhardt, L. M.; Patrick, V. A.; White, A. H. *J. Chem. Soc. Dalt. Trans.* **1985**, 2541–2545.
- (197) Müller, S. *Synthese und Charakterisierung von Nickel-Komplexen mit olefinischen und makrozyklischen Liganden*; Bachelor thesis, Justus-Liebig-Universität Giessen, 2013.
- (198) Stein, S. E. In *NIST Chemistry WebBook, NIST Standard Reference Database Number 69*; Linstrom, P. J.; Mallard, W. G., Eds.; National Institute of Standards and Technology, Gaithersburg MD, <http://webbook.nist.gov>, 2014.
- (199) Lever, A. *Inorganic Electronic Spectroscopy*; Second Edi.; Elsevier: Amsterdam, 1997.
- (200) Kubas, G. J.; Monzyk, B.; Crumbliss, A. L. In *Inorganic Syntheses*; John Wiley & Sons, Inc., 1979; pp. 90–92.
- (201) Bourget-Merle, L.; Lappert, M. F.; Severn, J. R. *Chem. Rev.* **2002**, *102*, 3031–3066.
- (202) Holland, P. L.; Cundari, T. R.; Perez, L. L.; Eckert, N. A.; Lachicotte, R. *J. J. Am. Chem. Soc.* **2002**, *124*, 14416–14424.
- (203) Puiu, S. C.; Warren, T. H. *Organometallics* **2003**, *22*, 3974–3976.
- (204) Bai, G.; Wei, P.; Stephan, D. W. *Organometallics* **2005**, *24*, 5901–5908.
- (205) Pfirrmann, S.; Yao, S.; Ziemer, B.; Stösser, R.; Driess, M.; Limberg, C. *Organometallics* **2009**, *28*, 6855–6860.
- (206) Pfirrmann, S.; Limberg, C.; Herwig, C.; Stößer, R.; Ziemer, B. *Angew. Chemie* **2009**, *121*, 3407–3411.

- (207) Harrold, N. D.; Waterman, R.; Hillhouse, G. L.; Cundari, T. R. *J. Am. Chem. Soc.* **2009**, *131*, 12872–12873.
- (208) Barefield, E. K. *Inorg. Chem.* **1972**, *11*, 2273–2274.
- (209) Barefield, E. K.; Wagner, F. *Inorg. Chem.* **1973**, *12*, 2435 – 2439.
- (210) Crick, I. S.; Gable, R. W.; Hoskins, B. F.; Tregloan, P. A. *Inorganica Chim. Acta* **1986**, *111*, 35–38.
- (211) Moore, P.; Sachinidis, J.; Willey, G. R. *J. Chem. Soc., Chem. Commun.* **1983**, 522–523.
- (212) Herlinger, A. W.; Funk, E. H.; Chorak, R. F.; Siebert, J. W.; Roco, E. *Polyhedron* **1994**, *13*, 69–75.
- (213) Kunisch, H. K.; Brig; Zinstag, C. A. Preparation of diacetonitrile. 3,290,355, 1966.
- (214) Kieber-Emmons, M. T.; Schenker, R.; Yap, G. P. a; Brunold, T. C.; Riordan, C. G. *Angew. Chemie* **2004**, *116*, 6884–6886.
- (215) Ram, M. S.; Bakac, A.; Espenson, J. H. *Inorg. Chem.* **1986**, *25*, 3267–3272.
- (216) Ram, M. S.; Riordan, C. G.; Ostrander, R.; Rheingold, A. L. *Inorg. Chem.* **1995**, *34*, 5884–5892.
- (217) Hoppe, T.; Schaub, S.; Becker, J.; Würtele, C.; Schindler, S. *Angew. Chemie* **2013**, *125*, 904–907.
- (218) Hay, R. W.; Lawrance, G. A.; Curtis, N. F. *J.C.S Perkin Trans. I* **1975**, 591–593.
- (219) Jiang, L.; Feng, X.-L.; Lu, T.-B. *Cryst. Growth Des.* **2005**, *5*, 1469–1475.
- (220) Curtis, N. F.; Swann, D. A.; Waters, T. N. *J. Chem. Soc. Dalt. Trans.* **1973**, 1963–1974.

**Der Lebenslauf wurde aus der elektronischen
Version der Arbeit entfernt.**

**The curriculum vitae was removed from the
electronic version of the paper.**